

Soil erosion risk map for Swiss grasslands – A dynamic approach to model the spatio- temporal patterns of soil loss

Inauguraldissertation

zur

Erlangung der Würde eines Doktors der Philosophie

vorgelegt der

Philosophisch-Naturwissenschaftlichen Fakultät

der Universität Basel

von

Simon Schmidt

aus Deutschland

Basel, 2019

Originaldokument gespeichert auf dem Dokumentenserver der Universität Basel

edoc.unibas.ch



This work is licensed under the “Creative Commons Attribution-NonCommercial 4.0 International Public License” (CC BY-NC 4.0). The complete license may be reviewed here:
creativecommons.org/licenses/by-nc/4.0/legalcode

Genehmigt von der Philosophisch-Naturwissenschaftlichen Fakultät
auf Antrag von

Prof. Dr. Christine Alewell
Fakultätsverantwortliche

Dr. Julian Klaus
Korreferent

Basel, den 11. Dezember 2018

Dekan der Fakultät
Prof. Dr. Martin Spiess

Summary

Soil erosion by water on grassland does not attract the same attention like erosion on arable land as it is usually assumed that the closed vegetation cover prevents soil loss. However, the complex terrain and intensive pasture use of mountain grasslands can potentially induce high soil loss. With a share of 72% of the total agricultural area, grassland is one of the most dominant land use in Switzerland and therefore should not be neglected in topics concerning soil protection.

Previous soil erosion studies revealed that soil erosion rates in Switzerland are not constant over time but rather are highly dynamic within a year. Such seasonal variability is mainly caused by rainfall patterns and plant growth cycles. Hence, modeling of soil loss based on a seasonal resolution enables improved insights in the erosion dynamics within a year.

The present work aims to model soil erosion with a sub-annual resolution for Swiss grasslands. Thereby we will focus on the most dynamic soil erosion risk factors namely rainfall erosivity and land cover and management.

The soil erosion model itself relies on the Revised Universal Soil Loss Equation (RUSLE). Each of the erosion factors of the RUSLE (rainfall erosivity R, soil erodibility K, cover and management C, slope length L, slope steepness S, and support practices P) is modified according to the specific environmental conditions of Swiss grasslands. The factors R and C are the most variable factors within a year as they are directly related to the parameters rainfall intensity and plant growth cycle. Therefore, both factors are modeled on a monthly scale to capture the temporal variations of soil loss within the year. For flexibility and transparency reasons, we derived each factor separately with the most state-of-the-art data and methodology as each of the factor transmit information about its effect on the overall model. Support practices (P-factor) are not considered in the model as the parametrization of grassland management practices and their effect for erosion control is difficult due to a lack of data and studies.

Monthly estimates of the rainfall erosivity (R-factor) are based on 10-minutes rainfall data of 87 gauging stations distributed all over Switzerland. Subsequently, the monthly rainfall erosivity is interpolated with spatial covariates representing snow cover, precipitation, and topography. For the C-factor, the fraction of green vegetation cover (FGVC) was derived from the 0.25 m spatial resolution Swissimage orthophotos by a linear spectral unmixing technique. A temporal normalization of the spatial distribution of the FGVC combined with R-factor weighting results in spatial and temporal patterns of the C-factor. Soil erodibility (expressed as the K-factor of the RUSLE equation) was modeled with cubist regression and multilevel B-splines on a national scale based on a total of 199 Swiss and 1639 European Land Use/Cover Area frame statistical Survey (LUCAS) topsoil samples. The LS-factor was adopted to the steep alpine environment by limiting the slope length to 100 m and using a fitted S-factor of empirical slope steepness factors.

The mean monthly modeled R-factor for Switzerland is $96.5 \text{ MJ mm ha}^{-1} \text{ h}^{-1} \text{ month}^{-1}$. On average, rainfall erosivity is 25 times higher in August ($263.5 \text{ MJ mm ha}^{-1} \text{ h}^{-1} \text{ month}^{-1}$) than in January ($10.5 \text{ MJ mm ha}^{-1} \text{ h}^{-1} \text{ month}^{-1}$). In general, the winter has relatively low R-factor values (average of $14.7 \text{ MJ mm ha}^{-1} \text{ h}^{-1} \text{ month}^{-1}$). The mean monthly C-factor on Swiss grasslands is

0.012 with a maximum from May until September. The national average K-factor of Switzerland is $0.0327 \text{ t ha h ha}^{-1} \text{ MJ}^{-1} \text{ mm}^{-1}$. The LS-factor for Switzerland is relatively high (14.8) compared to other countries but is mainly driven by the complex topography of the Alps with its steep slopes.

The soil erosion modeling reveals distinct seasonal variations. July and August are identified to be the months with the highest soil loss rates ($1.25 \text{ t ha}^{-1} \text{ month}^{-1}$) by water on Swiss grasslands. Spatially, hotspots of soil erosion are in the Central Swiss Alps (parts of the cantons Fribourg, Bern, Obwalden, Nidwalden, St. Gallen, Appenzell Innerrhoden, and Appenzell Ausserrhoden) in summer. Winter is the season with the lowest risk of soil loss due to low rainfall erosivity on snow-covered ground. The average annual soil loss for Switzerland, expressed as the sum of all monthly erosion rates, is $4.55 \text{ t ha}^{-1} \text{ yr}^{-1}$.

The spatial rainfall erosivity patterns are heterogeneous in all months, but spatial differences are less pronounced in winter due to the low rainfall erosivity. The small-scale variability of rainfall erosivity is less distinct in all months as homogenous rainfall patterns usually cover larger regions controlled mainly by topography. However, the Swiss Alps are not equally affected by rainfall erosivity with a very low variability within a year in the western and eastern Alps. In contrast, the small-scale variability of the cover and management factor is higher in most of the months due to the impact of grassland land use. The average C-factor for Swiss grassland of 0.012 matches the commonly applied C-factor for grasslands (0.01) proposed in the literature. The Swiss K-factor is low to medium with a clear reduction under consideration of the surface stone cover. We expected a high LS-factor for Switzerland as steep slopes are frequently in the Swiss Alps.

The dominance of soil erosion risk on grasslands in summer is surprising as it is commonly assumed that the closed vegetation cover protects soils. Though, the individual consideration of all factors, especially of the R- and C-factor, reveal their strong effect and interaction within the erosion model. The average annual soil loss prediction for Swiss grassland exceeds the maximum tolerable soil loss of Switzerland ($2 \text{ t ha}^{-1} \text{ yr}^{-1}$; Schaub and Prasuhn, 1998) by a factor of 2. That modeling result highlights that soil erosion on grasslands is of high concern for the Swiss agricultural productivity and environmental protection of a large proportion of the Swiss territory.

Based on the increased temporal resolution of soil erosion predictions, spatial and temporal patterns of soil loss by water on Swiss grasslands can be captured. The simultaneous identification of spatial and temporal patterns of soil loss on Swiss grasslands makes a targeted soil erosion control feasible. The knowledge about where and when soil erosion occurs enables the implementation of selective erosion control measures specifically for time periods and regions with high susceptibility.

Developing a comprehensive soil erosion assessment on Swiss grassland that is comparable and connectable with available risk assessments such as the erosion risk map 2 for Swiss arable lands (Prasuhn et al., 2013) and the European Union's assessment RUSLE2015 (Panagos et al., 2015e) provides a national and even continental valuation of soil erosion risk. The soil erosion risk map can be seen as a prototype for other erosion modeling on grassland in the Alpine region.

Table of Contents

Summary	IV
Table of Contents.....	VI
List of Figures	X
List of Tables.....	XI
Nomenclature.....	XII
1 Introduction	13
1.1 Soil erosion as an environmental threat – from a global to local scale	13
1.2 Status quo of soil erosion in Switzerland	14
1.3 Soil erosion on Swiss grasslands.....	15
1.4 The objective of a nationwide soil erosion risk map for Switzerland	17
1.5 Modeling with RUSLE.....	19
1.6 Spatio-temporal dynamics of soil erosion	20
1.7 Objectives and outline of the thesis.....	21
2 Change of permanent grasslands extent (1996-2015) and national grassland dataset of Switzerland	24
Abstract.....	25
Specifications Table.....	26
2.1 Experimental design, materials and methods.....	27
2.2 Data.....	29
Acknowledgements.....	33
3 Regionalization of monthly rainfall erosivity patterns in Switzerland	34
Abstract.....	35
3.1 Introduction.....	36
3.2 Material and Methods	37
3.2.1 Rainfall erosivity (R-factor) calculation	37
3.2.2 Stations	38
3.2.3 Data and Covariates	39
3.2.4 Mapping the seasonal variability of rainfall erosivity in Switzerland	40

3.2.5 Cumulative daily R-factors.....	41
3.2.6 Monthly erosivity density	41
3.3 Results and Discussion	42
3.3.1 Monthly rainfall erosivity at the 87 Swiss gauging stations.....	42
3.3.2 Mapping of monthly rainfall erosivity and related uncertainties.....	43
3.3.3 Monthly rainfall erosivity maps for Switzerland.....	45
3.3.4 Cumulative daily rainfall erosivity	48
3.3.5 Monthly erosivity density	49
3.4 Conclusion and Outlook	51
Author contribution	52
Acknowledgements	52
4 Mapping spatio-temporal dynamics of the cover and management factor (C-factor) for grasslands in Switzerland.....	53
Abstract.....	54
Graphical Abstract.....	55
4.1 Introduction	56
4.2 Material and methods	58
4.2.1 Swiss grassland areas.....	58
4.2.2 Datasets for C-factor mapping.....	59
4.2.3 Concept of C-factor mapping for Swiss grasslands.....	60
4.2.4 Spatio-temporal mapping of grassland C-factors by considering soil loss ratios (SLRs) and rainfall erosivity (R-factor).....	65
4.3 Results and discussion	66
4.3.1. Spatial pattern of the fraction of green vegetation cover of Swiss grasslands	66
4.3.2. Temporal variation in the green vegetation cover of Swiss grasslands	69
4.3.3. Spatio-temporal patterns of the fraction of green vegetation cover of Swiss grasslands	70
4.3.4. Spatial and temporal hot-spots of C-factors on Swiss grasslands	72
4.4 Conclusion and outlook	77
Acknowledgement.....	78
Funding.....	78
5 Filling the European blank spot – Swiss soil erodibility assessment with topsoil samples.....	79
Abstract.....	80
5.1 Introduction	81

5.2 Material and methods.....	83
5.2.1 LUCAS topsoil sampling.....	83
5.2.2 Calculation of soil erodibility for the LUCAS topsoil samples.....	84
5.2.3 Mapping the K-factor for Switzerland.....	85
5.2.4 Extrapolation of soil erodibility for Switzerland by using data from EU countries.....	86
5.3 Results and discussion.....	86
5.3.1 Soil properties and erodibility of the LUCAS topsoil samples.....	86
5.3.2 Soil erodibility mapping.....	88
5.4 Conclusions.....	93
Acknowledgments.....	94
6 Modification of the RUSLE slope length and steepness factor (LS-factor) based on rainfall experiments at steep alpine grasslands.....	95
Abstract.....	96
Graphical Abstract.....	97
Specifications Table.....	97
6.1 Introduction.....	98
6.2 Method details.....	98
6.2.1 Existing approaches for S- and L-factor parametrization.....	98
6.2.2 Proposed adaption of the L-factor.....	100
6.2.3 Proposed adaption of the S-factor.....	102
6.3 The Swiss LS-factor map including the Alps.....	104
6.4 Quality assessment and method uncertainties.....	105
Acknowledgments.....	108
7 Monthly RUSLE soil erosion risk of Swiss grasslands.....	109
Abstract.....	110
7.1 Introduction.....	111
7.2 Material and Methods.....	112
7.2.1 Study area.....	112
7.2.2 Datasets.....	113
7.2.3 Mapping.....	114
7.3 Results and Discussion.....	116
7.3.1. Monthly soil erosion rates for Swiss grasslands.....	116
7.3.2. Comparison of dynamic and annual soil erosion rates.....	131
7.4.3. Soil loss rates and soil formation rates.....	132

7.4 Conclusions	132
7.5 Software.....	133
7.6 Geolocation information.....	133
Acknowledgement	133
Data availability statement	134
8 Final remarks and outlook.....	135
8.1 Innovations in the dynamic soil erosion risk mapping of Swiss grasslands	135
8.2 Mitigating soil erosion – Value of the Swiss erosion risk map for grasslands	137
8.3 Evaluation of the approach and future proceedings.....	139
Bibliography	143
APPENDIX.....	169
Saisonale und räumliche Variabilität der Niederschlagserosivität in der Schweiz.....	169
Abstract.....	170
Zusammenfassung	171
A.1. Einleitung.....	172
A.2. Material und Methoden.....	173
A.2.1. Berechnung der Niederschlagserosivität (R-Faktor)	173
A.2.2. Niederschlagsmessnetz	173
A.2.3. Datensätze und Kovariaten	174
A.2.4. Regionalisierung der monatlichen R-Faktoren für die Schweiz	174
A.2.5. Summenkurven der täglichen R-Faktoren	175
A.3. Ergebnisse und Diskussion	175
A.3.1. Monatliche R-Faktor-Karten der Schweiz.....	175
A.3.2. Summenkurven der täglichen Erosivität.....	178
A.4. Schlussfolgerungen.....	180
Danksagung	180
Supporting Information to Chapter 3.....	181
Supporting Information to Chapter 4.....	188
Acknowledgments	195
Curriculum Vitae	196

List of Figures

Fig. 1.1: Potential water erosion risk map (ERK2) of arable land in Switzerland	14
Fig. 1.2: Agricultural zoning in Switzerland	15
Fig. 1.3: Sheet erosion by water on Swiss grasslands	17
Fig. 1.4: Erosion risk map of the European Union.....	18
Fig. 1.5: Sections and chapters of the dissertation	22
Fig. 2.1: Flow chart for the processing of the refined Swiss national grassland map (2015)	28
Fig. 2.2: Refined Swiss national grassland map (spat. res. 300 m) of the year 2015.....	30
Fig. 2.3: Land use change of permanent grassland in Switzerland for 2015 related to 1996	32
Fig. 2.4: Fraction of permanent grassland from total area in Switzerland	33
Fig. 3.1: Biogeographic units and used gauging stations in Switzerland.....	38
Fig. 3.2: Mean monthly rainfall erosivity for all 87 Swiss stations.	42
Fig. 3.3: Monthly rainfall erosivity maps for Switzerland	45
Fig. 3.4: Seasonal rainfall erosivity maps for Switzerland.....	47
Fig. 3.5: Range map (maximum R_{mo} minus minimum R_{mo}) for Switzerland.....	48
Fig. 3.6: Cumulative daily rainfall erosivity proportion	49
Fig. 3.7: Monthly erosivity density (ED_{mo}) for Switzerland	50
Fig. 3.8: Mean monthly erosivity density (ED_{mo})	51
Fig. 4.1: Negative exponential relationship of the fraction of vegetation cover (FVC) and the soil loss ratio (SLR).....	61
Fig. 4.2: Processing workflow (rectangles) of the used and derived datasets	62
Fig. 4.3: Spatial patterns of the fraction of green vegetation cover ($FGVC_{spatial}$)	67
Fig. 4.4: RMSE of the calculated abundances based on LSU for Switzerland.	68
Fig. 4.5: Mean (2014 to 2016) $FGVC_{temporal}$ for Swiss grasslands	69
Fig. 4.6: Spatial pattern of the C-factor for grasslands in Switzerland for the base date DOY 181	71
Fig. 4.7: Spatio-temporal variation of C-factors of Swiss grasslands per season	73
Fig. 4.8: Monthly ratio maps of the annual rainfall erosivity (R-factor).....	74
Fig. 4.9: Seasonal distribution of national monthly R-factors ($MJ\ mm\ ha^{-1}\ h^{-1}\ month^{-1}$), soil loss ratios (SLR; %), and C-factors of Swiss grasslands.....	75
Fig. 4.10: Mean monthly C-factors of grasslands for different elevation zones	76
Fig. 5.1: Particle size distribution diagram of all 199 LUCAS topsoil samples	88
Fig. 5.2: (a) K-factor and (b) Kst-factor (including the effect of stone cover) maps	89
Fig. 5.3: Certainty map of observed and predicted K-factor values of Switzerland	90
Fig. 5.4: Difference of extrapolated K-factors (with no measured data from Switzerland) to the interpolated K-factors	92
Fig. 6.1: Different setups and preconditions of the rainfall simulation experiment.....	101
Fig. 6.2: Constraint flow accumulation grid with a maximal flow threshold of 100 m	102
Fig. 6.3: Review and behavior of different empirical S-factor functions and the fitted function for steep alpine environments (S_{alpine})	104
Fig. 6.4: LS_{alpine} -factor map (spatial resolution 2 m) for Switzerland	105
Fig. 6.5: Deviation in percentage of S_{alpine} to S_{cons}	106

Fig. 6.6: Deviation in percentage of S_{alpine} to S_{prog}	107
Fig. 6.7: LS-factor for the Swiss agricultural area embedded in the European Union's LS-factor map	108
Fig. 7.1: Topography of Switzerland including the Swiss Alps	113
Fig. 7.2: Flowchart of the seasonal erosion map of Swiss grassland using the erosion factors	116
Fig. 7.3: Spatiotemporal patterns of monthly soil erosion risk at Swiss grassland.....	118
Fig. 7.4: Comparison of the distribution of monthly soil loss rates for Swiss grasslands (dynamic) and a mean annual soil loss rate (annual)	131
Fig. 7.5: Influence of the temporal pattern of the monthly rainfall erosivity.....	132

List of Tables

Table 3.1: Datasets used as covariates for the spatiotemporal mapping of rainfall erosivity	39
Table 3.2: Regression equations and selected covariates for estimating mean monthly rainfall erosivity in Switzerland.	44
Table 3.3: Model efficiency by R^2 and E_{RMS} as well as omitted outliers and influential observations per month.	44
Table 3.4: Monthly national rainfall erosivity in $\text{MJ mm ha}^{-1} \text{ h}^{-1} \text{ month}^{-1}$	46
Table 4.1: Datasets used for C-factor modeling of Swiss grasslands.	59
Table 4.2: Mean national deviation of FGVC ($\text{FGVC}_{\text{deviation}}$) to the base date of DOY 181 (30 th of June) by $\text{FCover}_{300\text{m}}$	70
Table 4.3: Averaged seasonal $\text{FGVC}_{\text{spatio-temp}}$ and agricultural intensity (Federal Statistical Office Switzerland, 2017) of the year 2016 per Swiss Canton	71
Table 4.4: Mean C-factors of Swiss grasslands per month.	74
Table 5.1: List of covariates used in the cubist regression model for modeling the soil erodibility of Switzerland.....	85
Table 5.2: Mean values for soil properties.....	87
Table 6.1: Review of selected S-factors (S).....	99
Table 6.2: Rainfall simulation measurements at the two study sites on steep alpine slopes in Switzerland.....	102
Table 7.1: Overview of RUSLE factor maps used for the soil erosion risk mapping of Swiss grasslands.....	114
Table 7.2: Erosion factors for the monthly soil erosion modelling of Swiss grassland.....	115
Table 7.3: Monthly ($\text{t ha}^{-1} \text{ month}^{-1}$) and annual ($\text{t ha}^{-1} \text{ yr}^{-1}$) soil erosion risk averaged for the Swiss grassland area.....	117

Nomenclature

C	cover and management
CR	cubist regression
DSM	digital soil mapping
ERK2	potential erosion risk map for arable lands
ERK _{Berg}	erosion risk map for mountain zones III, IV and summering grazing zones
ERK _{Grünland}	erosion risk map for Swiss grasslands
FGVC	fraction of green vegetation cover
FOAG	Federal Office for Agriculture
FOEN	Federal Office for the Environment
GIS	geographic information system
GLM	generalized linear model
IDW	inverse distance weighted
K	soil erodibility
L	slope length
LASSO	least absolute shrinkage and selection operator
LOOCV	leave-one-out cross-validation
LS	slope length and slope steepness
LUCAS	Land Use/Cover Area frame statistical Survey
MBS	multilevel B-splines
MNF	minimum noise fraction
NDVI	normalized difference vegetation index
P	support practices
PG	permanent grassland
PPI	pixel purity index
R	rainfall erosivity
RUSLE	revised universal soil loss equation
S	slope steepness
SLR	soil loss ratio
soil erosion	<i>abbreviation for soil erosion by water</i>
SwissAlti3D	Swiss digital elevation model
SwissTLM3D	Swiss topographic landscape model
TG	temporal grassland
USLE	universal soil loss equation

CHAPTER 1

Introduction

1.1 Soil erosion as an environmental threat – from a global to local scale

Soil erosion is one of the main causes of soil degradation worldwide (WBGU, 1994; Pimentel, 2000). Numerous global environmental threats (e.g. overexploitation, land abandonment, agricultural intensification) are linked to soil erosion as a triggering process.

Erosion is the „process involved when the soil or rock formation is loosened and carried away by the agents of wind, water, freeze and thaw or biological activities” (Chesworth, 2008). Soil erosion can be seen as a natural process that shaped the landscapes and produces fertile soils. However, the natural process transformed to human-induced erosion with the accelerated removal of vegetation and intensification in land cultivation (Lal, 2001) and a historical peak in Europe in the first half of the fourteenth century caused by frequently extreme precipitation events and intense land use (Dotterweich, 2013).

Currently, a global land surface of 6.1% is affected by severe soil erosion that exceeds a global tolerable soil loss threshold of $10 \text{ t ha}^{-1} \text{ yr}^{-1}$ (Borrelli et al., 2017). The annual amount of global soil loss by water was estimated to be 35.9 billion tons for the year 2012 (Borrelli et al., 2017). Such high soil loss rates are not only of major concern for the health of the environment but provoke high monetary loss for the agriculture sector. In the European Union, the cost of agricultural productivity loss induced by water erosion is about 1.25 billion Euros per year (Panagos et al., 2018). In Switzerland, the estimated costs of direct and indirect consequences of soil erosion on arable land are 49.3 million Euro per year (Ledermann, 2012). A study by Mosimann et al. (1991) reported exposure of 20% of all arable land to soil erosion in Switzerland. However, soil erosion in Switzerland is not exclusively a threat on arable land. Grassland measurements of soil loss identified severe soil loss rates at disturbed hotspots up to $30 \text{ t ha}^{-1} \text{ yr}^{-1}$ (Meusburger et al., 2012; Alewell et al., 2015a).

Different scales and levels of soil erosion regulation demonstrate that soil erosion is not only of local concern. In the European Union, the controlling of soil erosion is regulated by the Cross Compliance regulation (Council of the European Union, 2009) by advising to protect soil through appropriate soil erosion measures. Since 1998, soil erosion is also regulated by different laws in Switzerland (Verordnung über Belastungen des Bodens VBBö; Verordnung über die Direktzahlungen an die Landwirtschaft DZV; Gewässerschutzverordnung GSchV; Verordnung

über Sömmerungsbeiträge SöBV; Swiss Federal Council, 1998a; 1998b; 1998c; 1998d). For a transnational erosion control in the Alps, legal guidelines to combat soil erosion are compiled in the soil conservation protocol of the Alpine Convention (Badura et al., 2018).

1.2 Status quo of soil erosion in Switzerland

In Switzerland, since the 1950s, soil erosion by water has increased under arable land due to an intensification of agriculture (Weissshaidinger and Leser, 2006). Many measurements and experiments were conducted in the Swiss midlands to quantify the soil loss and assess the erosion risk (Mosimann et al., 1990; Mosimann et al., 1991; Prasuhn, 2010). Furthermore, one of the longest (20 years) European long-term measurement sequences on the loss of sediments from fields exists in Switzerland (Prasuhn, 2011; Prasuhn, 2012; Prasuhn, 2017). Since many years, the Swiss public authorities provide guidelines to the landowners to prevent soil erosion (Mosimann and Rüttimann, 2000; AGRIDEA, 2007). In addition to these guidelines, a potential erosion risk map with a 2 m spatial resolution (ERK2) was introduced in 2011 to serve as a tool for localizing, quantifying, and awareness raising of soil erosion (Fig. 1.1; Gisler et al., 2011; Prasuhn et al., 2013). However, the map is restricted to agricultural zones which are dominated by arable farming. These agricultural zones are defined as valley zone, hilly zone, mountain zone I, and mountain zone II (Fig. 1.2).

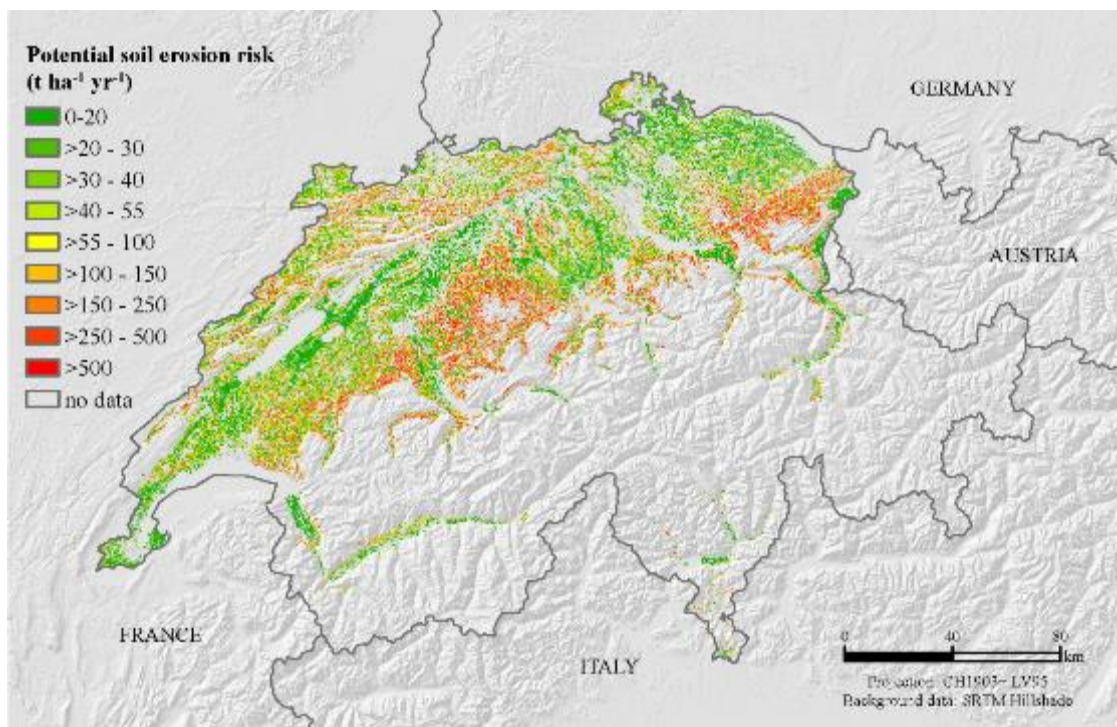


Fig. 1.1: Potential water erosion risk map (ERK2) of arable land in Switzerland, classified according to Prasuhn et al. (2013) (data: Federal Office for Agriculture, 2010)

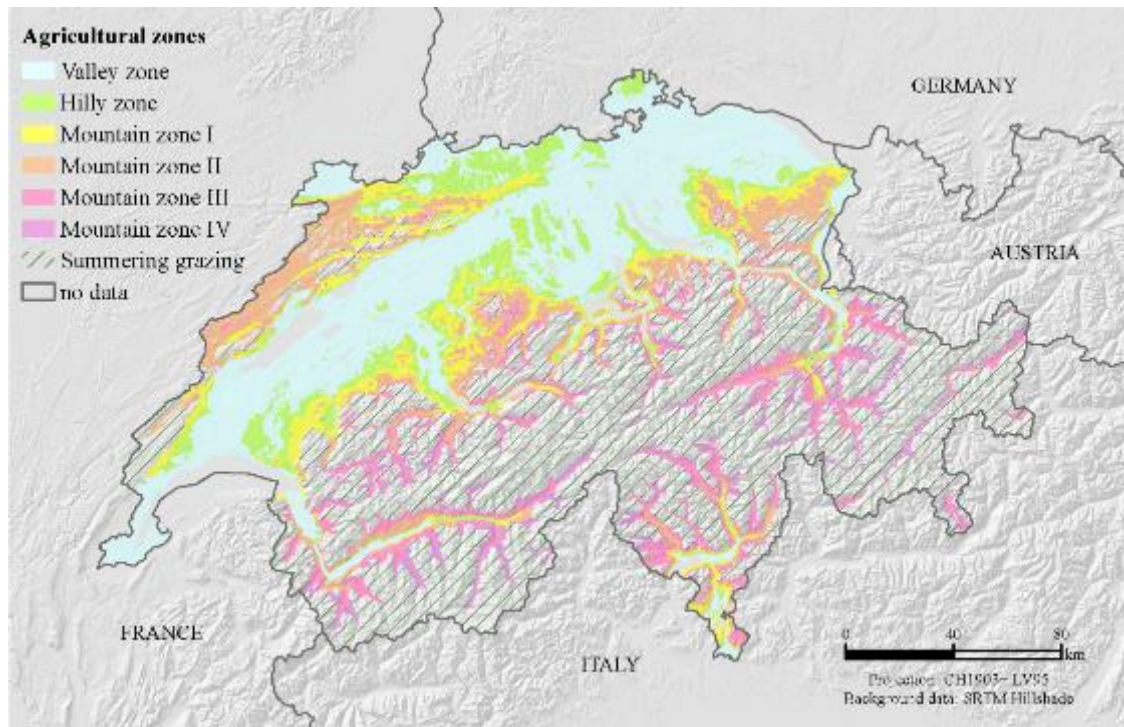


Fig. 1.2: Agricultural zoning in Switzerland (data: Federal Office for Agriculture, 1997)

Often, soils covered by grassland are assumed to be protected against soil loss by dense vegetation cover. However, many experiments and measurements on grasslands confirm that soil erosion is not only a concern on arable land (Martin et al., 2010; Konz et al., 2012; Schindler Wildhaber et al., 2012; Alewell et al., 2014) especially if the protecting vegetation cover of grasslands is disturbed. In 2007 and 2012, two national workshops on “Soil Erosion in the Alps” were held in Switzerland (Meusburger and Alewell, 2014) raising the awareness of soil erosion as a potential threat in grasslands.

1.3 Soil erosion on Swiss grasslands

Grasslands are the predominant land use type of Swiss agricultural areas (72%) with an extent of 28% of the national area (Bötsch, 2004; Jeangros and Thomet, 2004). They exist likewise in the valley/hilly zone and the mountain zone. About 46% of all grasslands are designated as alpine grassland and are the common land use type at elevations above 1500 m a.s.l. (Hotz and Weibel, 2005). Therefore, a large area of grassland is covered by snow in the winter. The typical melt-out day at elevations between 1560 and 2545 m a.s.l. is around May 27th (Jonas et al., 2008; Fontana et al., 2008). Humans have been managing the alpine soils for about 5000 years (Bätzing, 2015). Grasslands in Switzerland have been mainly used as meadows for fodder production and as pastures for livestock farming. Today, grasslands in the valleys are generally used for hay production and mountain grasslands are used for livestock grazing (Meusburger and Alewell, 2014).

Soil mobilization processes on grasslands are notably different in winter than in summer due to the winter snow cover. In winter, the effect of snow (e.g. snow gliding, avalanches) causes the loosening of soil material that is displaced by the melting snow in spring (Ceaglio et al.,

2012; Meusbürger et al., 2014; Stanchi et al., 2014;). The erosional impacts of wind and biological activities on Swiss grasslands are yet not studied in detail. However, considerably soil erosion by water is observable and measurable on Swiss grasslands (Fig. 1.3). The most present forms of water erosion on grasslands is sheet erosion. Rill erosion is occasionally visible on steep or sparsely vegetated slopes. Gully erosion is so far seldom observed (Strunk, 2003). Next to water erosion, landslides are a dominant gravity process that causes relocation of soil material on grasslands (Wilde et al., 2018). In this study, we will focus on soil erosion by water because intrinsically different models are needed to study mass movements and soil displacement by sheet erosion.

As a natural effect, grasslands are prone to water erosion triggered by natural conditions like rainfall intensity, soil (in)stability, and topography. The triggering processes of soil erosion on grassland, with particular emphasis on alpine grasslands, are usually different from those on arable lands as grassland soils are often less developed, and more exposed to extremes (snow, intense rainfall). Additionally, soil mobilization on grassland is accelerated by the specific influence of grassland cultivation and management such as selective grazing, overgrazing, or cattle trails. Like for arable soils, an intensification of the land use of grasslands on lower slopes can be observed in the last 50 years (Jeangros and Thomet, 2004; Alewell et al., 2008). For reasons of workload reduction, a transition from remote pastures to more accessible pastures is perceptible (Hotz and Weibel, 2005). The latter land use change caused a partial abandonment of remote grasslands with an overall reduction of grazing area (from 14.8% in 1954 to 11.2% in 2005 of the total Swiss territory) but simultaneously increased stocking rates and animal weight (Troxler et al., 2004). The total number of livestock units increased by 3.2% from 1962 to 2004 with a particular focus on heavy grazing cattle (Troxler et al., 2004). Since 1955, the number of sheep and cattle in the Urseren Valley experienced a sixfold respectively twofold increase accompanying by a reduction of grazing area (Meusbürger and Alewell, 2008). Degraded soil structure by the trampling of livestock, disturbed vegetation composition due to selective eating, and prolonged grazing periods are favoring the susceptibility of soils to be eroded. A comprehensive overview of the soil erosion problems in the Swiss Alps is provided by Meusbürger and Alewell (2014).



Fig. 1.3: Sheet erosion by water on Swiss grasslands (Val Piora, Ticino, Switzerland) as a combined effect of natural triggering factors and land use

1.4 The objective of a nationwide soil erosion risk map for Switzerland

The soil loss by water on arable lands in Switzerland is already predicted by various modeling and mapping studies (e.g. Friedli, 2006; Chisholm, 2008; Ledermann et al., 2010). As a lumped outcome of the lessons learned by these works, the first comprehensive and spatially high resolution potential erosion risk map (ERK2) for arable lands on plot scale was financed by the Federal Office for Agriculture (FOAG; see chapter 1.2; Gisler et al., 2010). Initially, the map is based on the Modified Universal Soil Loss Equation 1987 (MUSLE87; Hensel and Bork, 1988) and implemented in ESRI ArcView 3.x (extension AVErosion 1.0; Schäuble, 1999). In the meanwhile, most of the input datasets of the ERK2 are substituted by newer versions and the software is outdated. Therefore, the FOAG financed an upgrade of the existing ERK2 to implement the latest data and transfer the model to a more modern software. The primary interest of the project is to quantify the potential soil erosion risk for arable land on a plot scale. In a second project, information about crops and crop rotation are implemented in a user tool to calculate the actual soil erosion risk for fields with available data.

Later, in 2015, a soil erosion risk map for the European Union was published by the Joint Research Centre (JRC) of the European Union (Fig. 1.4; Panagos et al., 2015e). That map provides an overview of the spatial patterns of water erosion for 28 countries of Europe. However, as Switzerland is no member of the EU, Switzerland appears as a blank spot within the modeled neighboring countries. A qualitative map of the soil erosion risk in the Alps was

published in 2009 (Bosco et al., 2009) but this map is relatively coarse and is not suitable as a management instrument in Switzerland due to missing effective soil loss rates.

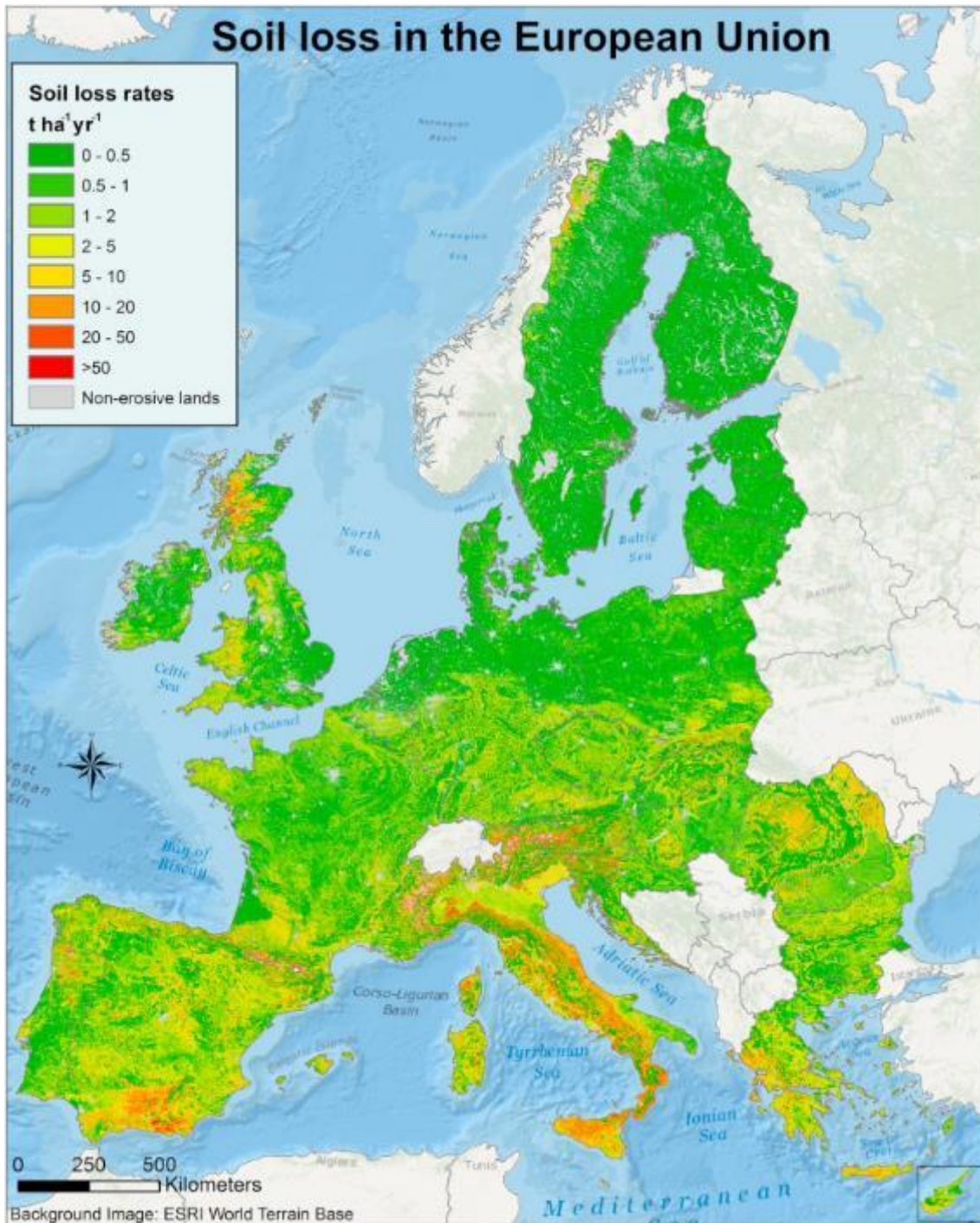


Fig. 1.4: Erosion risk map of the European Union with Switzerland appearing as a blank spot (Panagos et al., 2015e)

Since many years, the working group “environmental geoscience” of the University of Basel is measuring, modeling, and observing soil erosion on grassland in different study areas of the Swiss Alps (e.g. Bänninger et al., 2006; Alewell and Imhof, 2008; Alewell et al., 2008; Konz et

al., 2010; Meusbürger et al., 2010a; Meusbürger et al., 2010b; Konz et al., 2012; Meusbürger et al., 2012; Schindler Wildhaber et al., 2012; Alewell et al., 2014; Arata et al., 2016). As the terrain in the grasslands of the Swiss Alps is complex, comprehensive field surveys are often impeded. Meusbürger (2010) stated that “in high relief regions, with rugged topography, a more detailed scale is needed.” To assess also remote and difficultly accessible grasslands in Switzerland, the sound geodatabase of Switzerland can serve as an appropriate solution. With the recent development of geoinformation tools and the improvement of resolution of geodata, a national assessment of the soil erosion risk on grassland on a detailed scale (100 m to 500 m, monthly) is now feasible. Switzerland is among the countries with the best geoinformation data availability, mainly provided by the Federal Office of Topography (Swisstopo) (e.g. SwissAlti 3D, Swissimage FCIR/RGB/RS, swissTLM 3D). Furthermore, the advancements in remote sensing over the last decades expand the versatile database. Recently, Swiss authorities also participated in the pan-European data sampling campaign as part of the Land Use/Cover Area frame statistical Survey (LUCAS) with more than 22000 grassland and forest samples all over Europe (Orgiazzi et al., 2018).

To consider soil erosion in the rest of the Swiss agriculture area, namely the grasslands, and to fill the blank spot within the European assessment, another research project was financed by the Federal Office for the Environment (FOEN) in Switzerland to result in the first erosion risk map of grasslands (ERK_{Grünland}) in Switzerland. This dissertation presents the research outcomes of that research project.

It was agreed in several meetings of the responsible persons of FOAG and FOEN that both erosion risk maps (the updated ERK2 and the ERK_{Grünland}) should be combinable to a national soil erosion risk map of the total agricultural area (including arable land and grassland) of Switzerland. Therefore, the used methodologies, approaches and dataset were regularly exchanged between the projects. A dissertation about the project of the FOAG is in preparation by P. Bircher.

1.5 Modeling with RUSLE

The present soil erosion risk map for Swiss grasslands is modeled with the Universal Soil Loss Equation (USLE) and its revised version (RUSLE) (Wischmeier and Smith, 1965; 1978; Renard et al., 1997; Foster et al., 2008). A variety of models were tested and examined earlier for Switzerland like WEPP, LISEM, PESERA, USPED, Erosion3D, and RUSLE (Alewell et al., 2008; Konz Hohwieler, 2010; Meusbürger et al., 2010b; Meusbürger and Alewell, 2014). The evaluation of the models showed that RUSLE is the most robust model for large-scale modeling of Swiss grasslands because most of the other models have a much larger data demand and were less sensitive to the fraction of vegetation cover, which is one of the main risk factors for soil erosion on grassland. The RUSLE factors are broken down into sub-factors to permit more flexibility and an improved capturing of the small-scale processes in erosion dynamics. As such, RUSLE uses basic process-based erosion science to complement the empirical basis. In addition to that, the choice of the appropriate soil erosion model always depends on the available datasets for the study area, the spatial and temporal scale of the model application, and the

necessary type of information to be obtained (Meusburger and Alewell, 2014; Borrelli et al., 2017).

In the estimation of soil loss with USLE/RUSLE, the soil erosion related factors of rainfall erosivity (R) and soil erodibility (K) are corrected by information about the vegetation cover (cover and management C), topography (slope length L and slope steepness S) and erosion-protection measures (P). The combination of all factors result in the following equation of USLE/RUSLE:

$$A = R * K * C * L * S * P \quad (1.1)$$

Where A is the total soil loss in $t \text{ ha}^{-1} \text{ yr}^{-1}$.

The individual calculation of each erosion factor is of significant advantage compared to black-box-models, as the single factors transmit information itself, enable transparency and verifiability. Each erosion factor can be adjusted and evaluated on its own. That adjustment of each factor is of relevance for modifying the erosion model to the specific conditions of (alpine) grasslands.

Initially, the USLE was developed based on more than 10000 plot-years at 49 locations in the US with a plot length $\leq 122\text{m}$ and a slope gradient between 3% and 18% (Wischmeier and Smith, 1978). These data were related to a standardized unit plot of 22.1 m length and 9% slope steepness with specific management (regularly tilled fallow, slope vertical tillage) (Renard et al., 1997).

Already in 1993, Risse et al. (1993) pointed out that “USLE is the most widely used of all soil erosion models.” A keyword search for the term “Universal Soil Loss Equation”, “USLE”, “Revised Universal Soil Loss Equation”, and “RUSLE” by Borrelli et al. (2017) resulted in 1118 publications for the period of 2003 to 2016 with rapid growth during the end of that period. Publications with other soil erosion model keywords are by far less popular (243 results for SWAT, AGNPS, Watem/Sedem, EPIC and 254 results for WEPP, LISEM, EUROSEM, and PESERA). The vast request for soil erosion models was also demonstrated at the “1st Erosion Modelling Workshop” in 2017 at the JRC in Ispra with more than 80 presentations about soil erosion models and participants from 25 countries (<https://esdac.jrc.ec.europa.eu/themes/erosion-modelling-workshop>). Still, USLE/RUSLE was the most presented model during that workshop. Two follow-up erosion modeling workshops were held in 2017 in Seoul and 2018 in Rio de Janeiro.

1.6 Spatio-temporal dynamics of soil erosion

Initially, USLE/RUSLE was developed to predict long-term average annual soil loss (Wischmeier and Smith, 1978) usually expressed in $t \text{ ha}^{-1} \text{ yr}^{-1}$. However, investigations on soil erosion over the last decades indicate that soil erosion rates are not distributed equally over a year. Instead, soil erosion is process driven by a few extreme events within a year. The soil loss of such triggering extreme events is averaged to a whole year. Therefore, the early criticism by Hawkins (1985) of not considering the time and spatial variations in site properties is comprehensible. Nowadays, the annual approaches can be complemented by sub-annual erosion assessments with higher temporal resolutions owing to the advances in data and measuring

quality. Quantifying soil loss on a seasonal, monthly, weekly or even daily time-scale helps to better understand the underlying erosion processes.

Furthermore, a finer temporal resolution reduces errors in soil loss predictions (Alexandridis et al., 2015). Wischmeier and Smith (1965) propose a monthly temporal resolution to be appropriate for soil erosion modeling. This recommendation was affirmed four decades later by Panagos et al. (2012a), Panagos et al. (2016a), Karydas and Panagos (2016), and Karydas and Panagos (2017).

The factors C and R of the USLE/RUSLE are highly dynamic with a clear annual cycle (Wischmeier and Smith, 1978; Renard and Freimund, 1994; Vrieling, 2006; Vrieling et al., 2014; Möller et al., 2017) in contrast to the rather constant RUSLE-factors K, L, and S (Panagos et al., 2012a; Alexandridis et al., 2015) which are only variable on a long-term scale (e.g. change in soil permeability due to freeze-thaw/weathering processes, landscape change due to erosion or landslides, introduction of protection measures) and therefore not recognized on a sub-annual scale (Wang et al., 2001). Especially for grassland, a clear natural growth cycle, periodical hay cutting, or periodical grazing within a year is evident and influence the C-factor. Likewise, the weather is changing over time, the rainfall erosivity R is not constant. Meusbürger et al. (2012) already proved the presence of a strong seasonality of rainfall erosivity in Switzerland.

The original USLE/RUSLE equation of Eq. 1.1 can be modified to a sub-annual soil erosion equation by considering the dynamics of the factors R and C in the respective temporal resolution. We followed the recommendation of a monthly resolution. The USLE/RUSLE equation is thus transformed to:

$$A_{\text{month}} = R_{\text{month}} * K * C_{\text{month}} * L * S * P \quad (1.2)$$

Where A_{month} is the quantification of soil loss in $\text{t ha}^{-1} \text{ month}^{-1}$. R_{month} and C_{month} are the R- and C-factors with a monthly resolution.

Such multi-temporal and spatial approaches to assess the riskiest periods and areas for soil erosion by water are realized on a continental/national level, e.g. for Africa, Brazil (Vrieling et al., 2008; 2014), and Albania (Grazhdani and Shumka, 2007). Time-dependent assessments of soil loss are relevant to support policymakers and farmers to implement soil protection measures more organized. These spatio-temporal assessments are decisive for an accurate soil erosion risk assessment and relevant for gaining knowledge about where and when soil erosion is endangering soils simultaneously (Panagos et al., 2014c; Ballabio et al., 2017; Möller et al., 2017).

1.7 Objectives and outline of the thesis

So far, neither a dynamic soil erosion risk assessment in Switzerland nor a mapping of the soil erosion risk by water exists for Swiss grassland. To fill that soil erosion gap for Switzerland and to fill the blank spot in European assessments, we adopted the USLE/RUSLE to the specific environmental conditions of Swiss grasslands and used state-of-the-art high resolution data to quantify the soil erosion risk on a monthly scale. Different geoinformation and statistical

approaches, remote sensing techniques, and sampling methods were used for deriving maps of the soil erosion risk by water on grasslands.

The overall aim of the thesis is to model the soil loss for Swiss grassland at a monthly temporal resolution. For that purpose, (i) the national grassland extend of Switzerland has to be defined, (ii) the rainfall erosivity and (iii) the cover and management factor are modeled on a monthly scale, (iv) the soil erodibility database is extended to the Swiss Alps, and (v) the suitability of different slope length and slope steepness factors for alpine environments is verified.

The thesis is subdivided into four sections (Fig. 1.5). The first section (chapter 2) presents a Swiss grassland map of the year 2015, which serves as the mask layer for defining the extent of grasslands in Switzerland. Chapters 3 and 4 are assessing the dynamic erosion factors rainfall erosivity (R) and cover and management factor (C) of the USLE/RUSLE which are based on regression-kriging and linear spectral unmixing, respectively. The assessments of the rather static factors soil erodibility (K), slope length (L) and slope steepness (S) are the content of chapters 5 and 6. The spatial patterns of soil erodibility are assessed with a total of 1837 subsoil samples in Switzerland and neighboring countries. L- and S-factors rest on a modification of 12 empirical S-factors and rainfall simulations on Swiss grasslands. The P-factor (support practices) is not investigated for Swiss grasslands due to a lack of spatial information on grazing management and their effect on soil loss. The dynamic factors, as well as the static factors, are multiplied according to Eq. 1.2 to twelve monthly erosion risk maps by water on Swiss grasslands which are presented in the synthesis chapter 7. This chapter also provides an overview of used datasets and methods for each of the factors.

SOIL EROSION RISK MAP ON SWISS GRASSLANDS

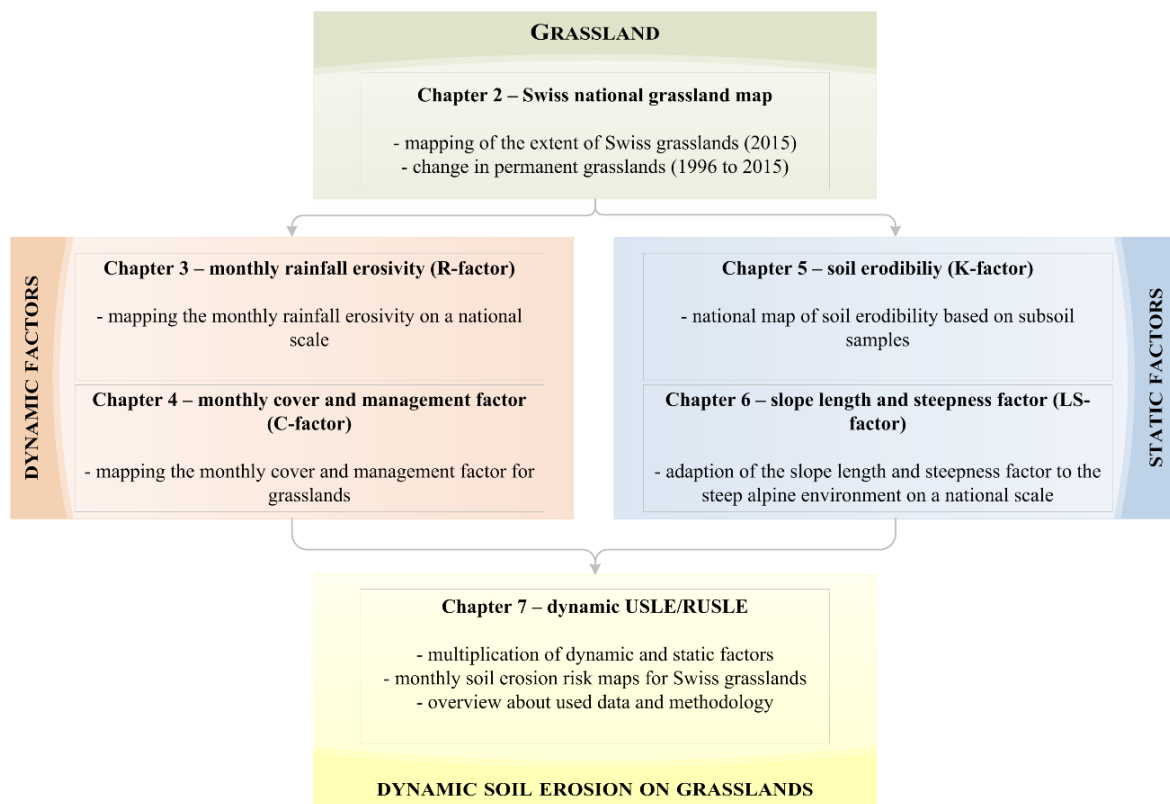


Fig. 1.5: Sections and chapters of the dissertation

The factor maps of R, K, L, and S are elaborated on a Swiss national scale. The extent of the C-factor map is limited to grassland as the underlying processes of the cover and management factor are principally different from those on arable land.

For readability reasons, the authors decided to truncate the term “soil erosion by water” to “soil erosion”, as the main subject of that dissertation is water erosion otherwise it will be referred accordingly.

The final erosion maps as presented in this dissertation are the output of the research project originally entitled “Soil Erosion Risk Modeling in the Alps – ERKBerg as a Prototype of ERK2 for mountain zones III, IV and summering grazing zones”, financed by the FOEN (chapter 1.4). The project title was later modified to only cover grasslands (see the title of the dissertation). The corresponding erosion risk map for grasslands is abbreviated to ERK_{Grünland}. The aggregation of the erosion risk map of grasslands with the erosion risk map of arable land is not part of this thesis.

CHAPTER 2

Change of permanent grasslands extent (1996-2015) and national grassland dataset of Switzerland

This chapter is published in Data in Brief as:

Simon Schmidt¹, Christine Alewell¹, Katrin Meusburger^{1,2}: Change of permanent grasslands extent (1996-2015) and national grassland dataset of Switzerland, Data in Brief, 20, 1992-1998, 10.1016/j.dib.2018.09.039, 2018.

¹Environmental Geosciences, University Basel, Bernoullistrasse 30, CH-4056 Basel, Switzerland

²Swiss Federal Institute for Forest, Snow and Landscape Research WSL, Zürcherstrasse 111, CH-8903 Birmensdorf, Switzerland

Abstract

So far, neither a grassland map, temporal analysis of the conversion of permanent grassland (PG) to other land uses nor the differentiation of permanent and temporal grassland exists for Switzerland. For the first time in Switzerland, we present a Swiss national grassland map for the year 2015 capturing the extent of both, permanent and temporal grasslands (here called grasslands) by intersecting the information of three datasets. We blended the high temporal resolution Climate Change Initiative (CCI) Land Cover of 2015 (processed by the European Space Agency (ESA)), with the high spatial resolution Swiss topographical landscape model “SwissTLM3D” and the landscape model “vector25” both provided by Swisstopo. The final data presents the spatial patterns and the national extent of Swiss grasslands. Furthermore, the recently published (April 2017) CCI Land Cover dataset allow extracting the extent of grasslands for 24 years (1992-2015) with a coarse spatial resolution of 300 m. We used the time series data of the grassland extent to produce annual PG maps from 1996 to 2015. That data enables the identification of the development of grassland extent over two decades. The Swiss national grassland map is used for investigating the spatio-temporal patterns of the soil erosion risk of Swiss grasslands (see Mapping spatio-temporal dynamics of the cover and management factor (C-factor) for grasslands in Switzerland, DOI 10.1016/j.rse.2018.04.008; Schmidt et al., 2018b).

Keywords: land use change, land cover classification, time series, change detection, soil erosion, alpine environment, C-factor, CCI Land Cover

Value of the data:

- The data provide a first national map of the extent of Swiss grasslands which might not only be an important baseline data for ecological studies but also for multiple disciplines, e.g., alpine research, soil sciences, geosciences, agronomy, hydrology.
- Modelers and GIS-users are provided with a grassland map (2015) to distinct grasslands from other land use classes (e.g., arable land, forest).
- The separation of temporal and permanent grassland is feasible and of high relevance for ecological, geobotanical, biodiversity and soil research to interpret specific species composition and indicator for soil properties.
- The capturing of the conversion of permanent grassland from 1996 to 2015 is a valuable resource for future policy decision making.

Specifications Table

Subject area	<i>Ecology</i>
More specific subject area	<i>Grassland mapping and land use change</i>
Type of data	<i>Figures (maps)</i>
How data was acquired	<i>Data were derived from Climate Change Initiative (CCI) Land Cover (Arino and Ramoino, 2017; Bontemps et al., 2015) and Swisstopo (Swisstopo, 2017a; Swisstopo, 2007). Data were processed for 2015 and an annual resolution for Switzerland for the years 1992/1996 to 2015</i>
Data format	<i>processed and analyzed data is available as Raster format (GeoTIFF) and Polygons (Shapefile)</i>
Experimental factors	<i>Details provided by the European Space Agency (ESA)</i>
Experimental features	<i>Grassland maps were extracted from the global CCI Land Cover (Arino and Ramoino, 2017; Bontemps et al., 2015) and clipped for Switzerland. Two Swiss landscape models (Swisstopo, 2017a; Swisstopo, 2007) were used for the refinement of the grassland extent by clipping with additional topographical and land use information. Permanent grasslands and their change were derived by sets of five successive grassland maps.</i>
Data source location	<i>Switzerland</i>
Data accessibility	<i>The data are available with this article.</i>
Related research	<i>Schmidt, S., Alewell, C., & Meusburger, K. (2018). Mapping spatio-temporal dynamics of the cover and management factor (C-factor) for grasslands in Switzerland. Remote Sensing of Environment, 211, 89–104. doi:10.1016/j.rse.2018.04.008.</i>

2.1 Experimental design, materials and methods

In 2017, the European Space Agency published annual globally available CCI Land Cover Maps (v2.0.7) including grassland for 24 consecutive years (1992-2015) with a spatial resolution of 300 m. We extracted the grasslands for all 24 years and clipped them to the Swiss national border (Swisstopo, 2017a). The spatial resolution of 300 m represents a single class value of an area of 300 m x 300 m of the ground. Based on this data source we derived two grassland products: (i) the Swiss national grassland map for the year 2015 and (ii) the temporal change of permanent grassland areas in Switzerland from 1996 to 2015.

(i) We refined the extracted grassland class for the Swiss national grassland map of the year 2015 as they entail some generalization which affects primarily small landscape elements (e.g., streets, buildings) and other land use classes. For instance, small elements are not recorded as an individual class but assigned as grassland. The high resolution landscape models (geometric accuracy of 0.2 m to 8 m; SwissTLM3D; Swisstopo, 2017a, vector25; Swisstopo, 2007) of Switzerland increase the accuracy of the CCI Land Cover grassland map of 2015 by a clipping procedure due to its fine distinction of these landscape elements and land use classes. A flow chart of the processing is presented in Fig. 2.1. The landscape models contain a class (“Z_Uebrig”) which represents remaining primary areas such as grassland, arable land and so on which are not part of any other class and presented on a combined class level. That class is used for clipping to improve the accuracy of the CCI Land Cover maps of grassland. A grid cell remains grassland if a CCI Land Cover grassland grid cell matches with the Z_Uebrig polygon otherwise it is masked and a bad classification assumed due to the cell size. Furthermore, the buildings and streets (after buffering according to the mean street body width) were masked from the grassland map. Thereby, the accuracy of the map is increased, and misclassified landscape elements and land use classes are extracted.

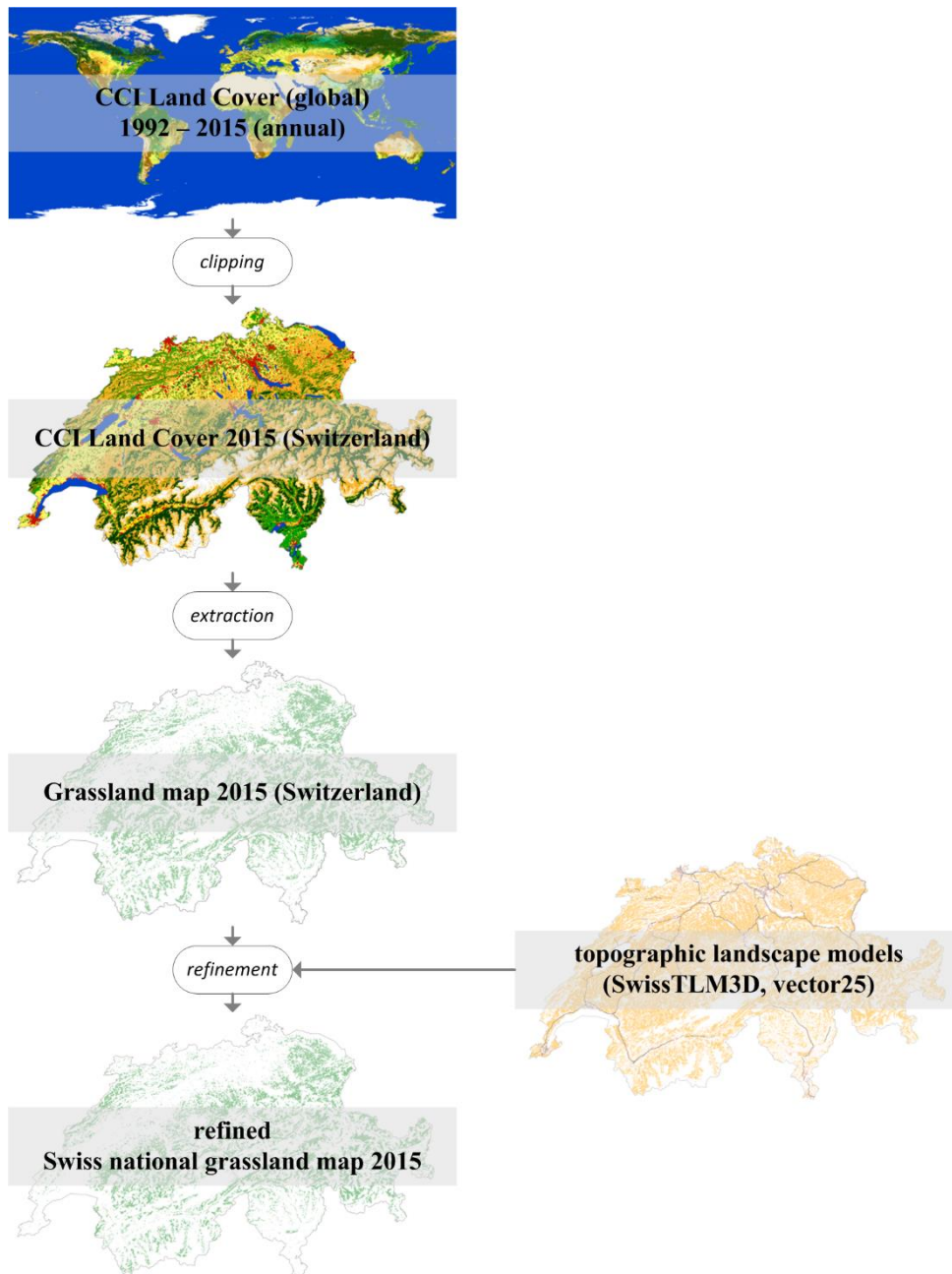


Fig. 2.1: Flow chart for the processing of the refined Swiss national grassland map (2015)

High spatial resolution digital orthophotos (0.25 m, SwissImage RGB, Swisstopo, 2010) were used for validating the grassland map of Switzerland. A total of 1000 random points were set for a pseudo ground control within the here generated grassland map. These points are visual and statistical evaluated according to their real land use type.

(ii) The availability of grassland time series enables the extraction of PG from 1996 to 2015. Following the definition Smit et al. (2008), we defined all grid cells as PG which represented grasslands in a succession of five years. PG maps could not be improved by clipping with the topographic landscape models (compare Fig. 2.2) owing to the lack of historical data of SwissTLM3D and vector25 (Swisstopo, 2017a; Swisstopo, 2007). However, the investigation of

the proportional change in PG is also feasible with the moderate-resolution of the CCI Land Cover grassland maps.

2.2 Data

The presented map (Fig. 2.2) represents the extent of total grassland (no separation between temporal (TG) and permanent grasslands (PG)) for Switzerland for the year 2015. The comparison between the presented grassland map with digital orthophotos for 1000 random points reveals a mapping accuracy of grassland by 82.1%. The remaining of non-matching points (7.6%) is bedrock which is usually socialized with grassland. The remaining misclassified points correspond to 3.9% of forest areas, 2% of asphalted areas (e.g. streets), and 4.4% undefined land use types. The main cause for the mismatch is the coarse resolution of the grassland map pixels.

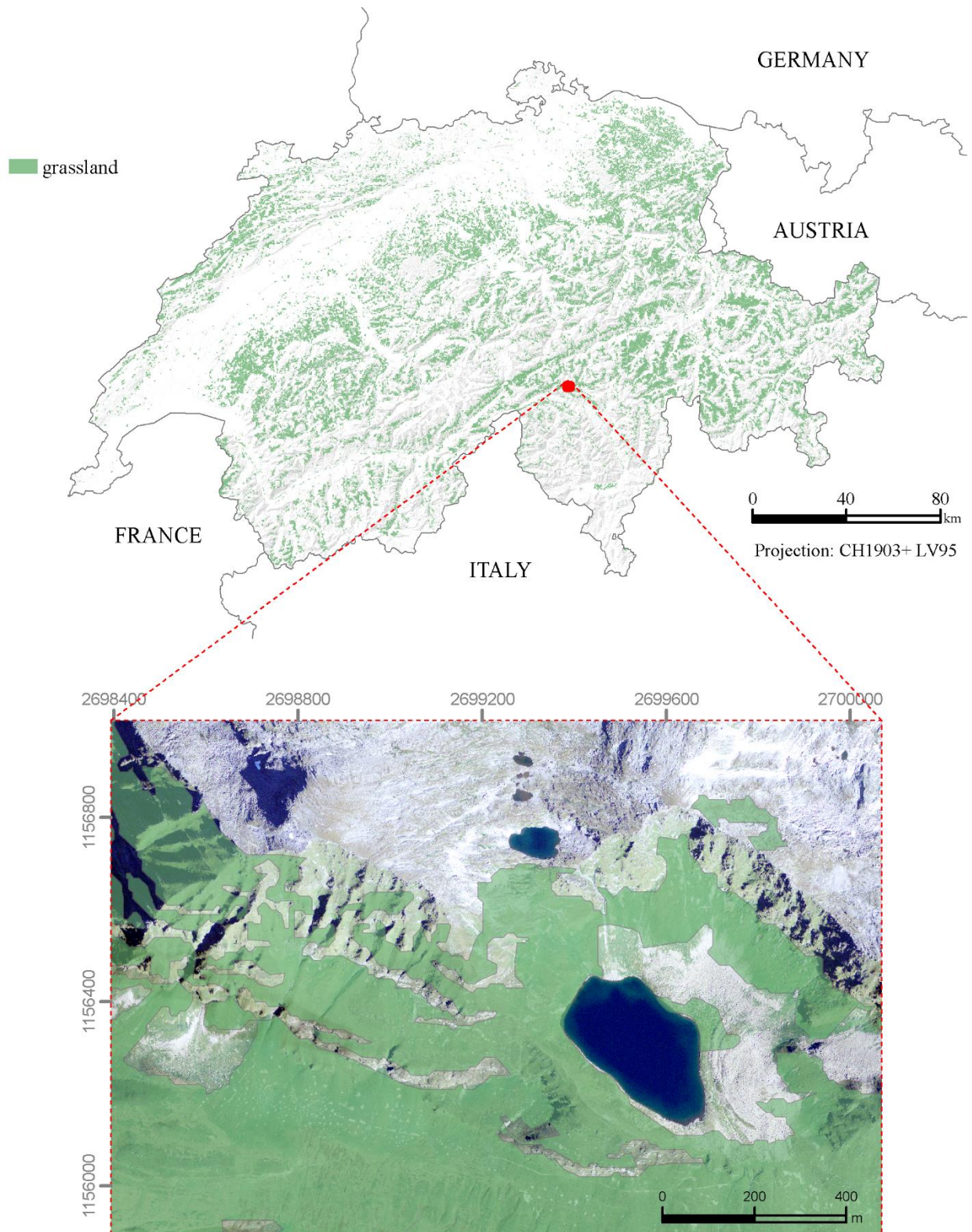


Fig. 2.2: Refined Swiss national grassland map (spat. res. 300 m) of the year 2015. Temporal and permanent grassland is not distinguished here.

According to the Food and Agricultural Organization (FAO) definition, grassland is defined as “ground covered by vegetation dominated by grasses, with little or no tree cover” (Suttie and Reynolds, 2005). In contrast to TG, PG is not part of the crop rotation for a minimum of five successive years (Smit et al., 2008). An overall gain (2.1%) of PG in 2015 compared to 1996 can be assessed (Fig. 2.3). About 0.4% of PG was converted to other land use units in the same comparative period. The PG time series over 20 years (1996-2015) shows a slight but continuously increasing trend from 1998 onwards (Fig. 2.4). The PG maps of the two decades are provided as enclosed data with this article. Soil properties vary with grassland type due to plowing and cultivation of TG. Therefore, the data, particularly when linked to agrarian development, planning, or soil degradation threats, are also a valuable resource for soil scientists. The Swiss national grassland map of 2015 (Fig. 2.2) was originally developed for investigating the spatio-temporal patterns of soil erosion risk on Swiss grasslands (Schmidt et al., 2018b).

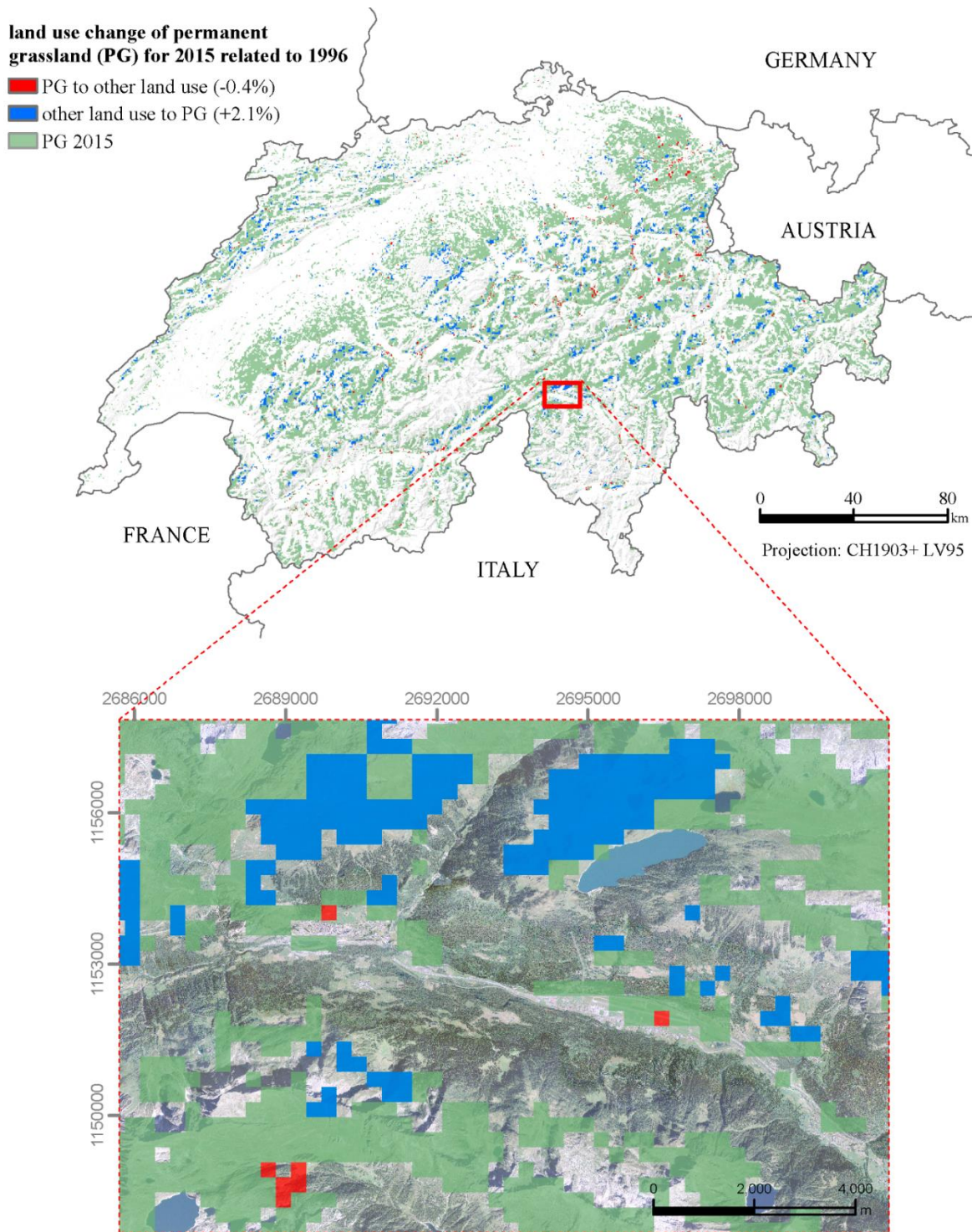


Fig. 2.3: Land use change of permanent grassland in Switzerland for 2015 related to 1996 (spat. res. 300 m)

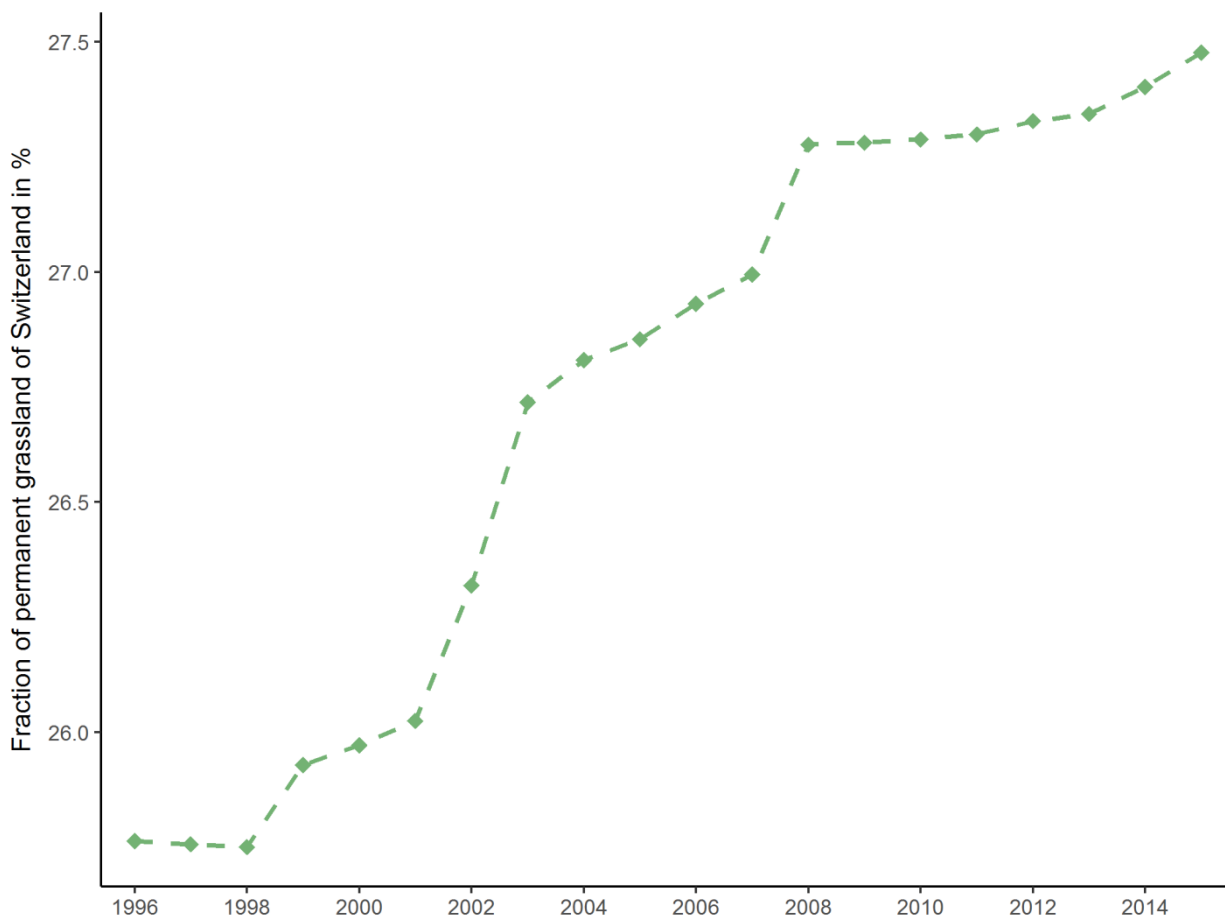


Fig. 2.4: Fraction of permanent grassland from total area in Switzerland from 1996 to 2015 in percentages

Acknowledgements

This work was supported by the Swiss Federal Office for the Environment (FOEN) (grant numbers N° N222-0350 and N° P182-1535). The authors would like to thank the data providers, namely European Space Agency and Swisstopo for making their data available. The authors would like to thank two anonymous referees for their valuable comments and suggestions to improve the quality of the paper.

CHAPTER 3

Regionalization of monthly rainfall erosivity patterns in Switzerland

This chapter is published in Hydrology and Earth System Sciences as:

Simon Schmidt¹, Christine Alewell¹, Panos Panagos², and Katrin Meusburger¹:
Regionalization of Monthly Rainfall Erosivity Patterns in Switzerland, *Hydrol. Earth Syst. Sci.*, 20, 4359-4373, doi.org/10.5194/hess-20-4359-2016, 2016.

¹Environmental Geosciences, University Basel, Bernoullistrasse 30, CH-4056 Basel, Switzerland

²European Commission, Joint Research Centre, Institute for Environment and Sustainability, Via E. Fermi 2749, I-21027 Ispra, Italy

Abstract

One major controlling factor of water erosion is rainfall erosivity, which is quantified as the product of total storm energy and a maximum 30 min intensity (I_{30}). Rainfall erosivity is often expressed as R-factor in soil erosion risk models like the Universal Soil Loss Equation (USLE) and its revised version (RUSLE). As rainfall erosivity is closely correlated with rainfall amount and intensity, the rainfall erosivity of Switzerland can be expected to have a regional characteristic and seasonal dynamic throughout the year. This intra-annual variability was mapped by a monthly modeling approach to assess simultaneously spatial and monthly patterns of rainfall erosivity. So far only national seasonal means and regional annual means exist for Switzerland. We used a network of 87 precipitation gauging stations with a 10-minute temporal resolution to calculate long-term monthly mean R-factors. Stepwise generalized linear regression (GLM) and leave-one-out cross-validation (LOOCV) were used to select spatial covariates which explain the spatial and temporal patterns of the R-factor for each month across Switzerland. The monthly R-factor is mapped by summarizing the predicted R-factor of the regression equation and the corresponding residues of the regression, which are interpolated by ordinary kriging (regression-kriging). As spatial covariates, a variety of precipitation indicator data has been included such as snow depths, a combination product of hourly precipitation measurements and radar observations (CombiPrecip), daily Alpine precipitation (EURO4M-APGD), and monthly precipitation sums (RhiresM). Topographic parameters (elevation, slope) were also significant explanatory variables for single months. The comparison of the 12 monthly rainfall erosivity maps showed a distinct seasonality with the highest rainfall erosivity in summer (June, July, and August) influenced by intense rainfall events. Winter months have the lowest rainfall erosivity. A proportion of 62% of the total annual rainfall erosivity is identified within four months only (June to September). The highest erosion risk can be expected in July where not only rainfall erosivity but also erosivity density is high. In addition to the intra-annual temporal regime, a spatial variability of this seasonality was detectable between different regions of Switzerland. The assessment of the dynamic behavior of the R-factor is valuable for the identification of susceptible seasons and regions.

3.1 Introduction

Rainfall has direct impacts on soil mobilization by processes like rapid wetting or splash and runoff effects and is, therefore, one of the main driving forces of water erosion. The R-factor, as one of the five soil erosion risk factors (rainfall erosivity, soil erodibility, slope steepness and length, cover management, and support practices) of the Revised Universal Soil Loss Equation (RUSLE) (Renard et al., 1997; Foster et al., 2008) expresses the impact of rainfall on soils in the form of rainfall erosivity. The RUSLE is widely used for calculating soil loss, but each of the five factors also has an essential message on its own. For instance, besides being an important driving factor of soil erosion, the R-factor can also be used to draw conclusion about soil vulnerability, flood hazard, natural hazards, or probability of droughts (Panagos et al., 2015a).

Soil erosion by water is a major environmental issue in Switzerland, which has been measured (Konz et al., 2012; Alewell et al., 2014), mapped (Mosimann et al., 1990; Prasuhn, 2011; Prasuhn, 2012), and modeled (Gisler et al., 2011; Prasuhn et al., 2013) extensively. In Switzerland, since the 1950s, soil erosion by water has increased under arable land (Weisshaidinger and Leser, 2006) as well as in mountain grasslands (Meusburger and Alewell, 2008). Mosimann et al. (1991) assessed a quantity of up to 20% of all cultivated land in Switzerland to be affected by soil erosion. The costs of soil erosion for Switzerland's arable land were estimated to be about 53 million CHF yr⁻¹ (US \$55.2 million yr⁻¹; Ledermann, 2012). Increasing trends of water erosion are predicted for Switzerland under future climate change due to more frequent and heavy rainfall during winter (Fuhrer et al., 2006). Trends towards increasing rainfall erosivity are already observable in the months of May to October (Meusburger et al., 2012).

Previously published studies on rainfall erosivity in Switzerland focused on national seasonal means (Panagos et al., 2015a) or regional annual means (Friedli, 2006; Gisler et al., 2011; Meusburger et al., 2012; Prasuhn et al., 2013). Since Switzerland has a high spatial climate variability (humid continental to oceanic climate; Köppen, 1936), seasonal and temporal variations of the weather are consequential. As such, these spatiotemporal climate variations can be expected to influence patterns in the rainfall erosivity. Spatial and temporal patterns of R-factors have not yet been established and mapped for Switzerland although Meusburger et al. (2012) already showed the presence of a strong seasonality of the rainfall erosivity for stations clustered at different elevation classes in Switzerland. So far the lack of significant spatial covariates impeded the mapping of intra-annual rainfall erosivity patterns. The availability of hourly radar rainfall observations for Switzerland (CombiPrecip data; Sideris et al., 2014) might offer a new possibility for the modeling of rainfall erosivity maps for individual months. These spatiotemporal patterns are decisive in combination with spatiotemporal patterns of vegetation cover in order to allow for an accurate soil erosion risk assessment and relevant for a monthly and seasonal management of agriculture practices and hazard controls. A rather static approach, which aggregates either regional or temporal R-factors such as those presented by Meusburger et al. (2012), is not suitable to model the dynamic soil erosion risk on a seasonal scale. Furthermore, the impact of precipitation on rainfall erosivity can be assessed by determining the monthly erosivity density.

Here, we aim to assess the spatiotemporal variability of rainfall erosivity in Switzerland by

- (i) extending the network of gauging stations from Meusburger et al. (2012);
- (ii) producing monthly R-factor maps based on high-resolution spatial covariates using a regression-kriging approach;

- (iii) evaluating the spatiotemporal patterns of the seasonal R-factor dynamics;
- (iv) determining the spatiotemporal erosivity density.

3.2 Material and Methods

3.2.1 Rainfall erosivity (R-factor) calculation

The rainfall erosivity expressed as R-factor in RUSLE is the summation of the total storm energy (E) of an erosive rainfall event times its corresponding maximum intensity over a time span of 30-minutes (I_{30}) within a certain time period (Brown and Foster, 1987). We used the erosive rainfall event thresholds defined by Renard et al. (1997), which were modified by Meusburger et al. (2012). The unit rainfall energy (e_r) ($\text{MJ ha}^{-1} \text{mm}^{-1}$) for each time interval is expressed as the intensity of rainfall (i_r) (mm h^{-1}) during that time interval. It is calculated by Brown and Foster (1987) as

$$e_r = 0.29[1 - 0.72 \exp(-0.05i_r)] \quad (3.1)$$

The erosive rainfall event erosivity (EI_{30}) ($\text{MJ mm ha}^{-1} \text{h}^{-1}$) is a product of the unit rainfall energy (e_r) (Eq. 3.1) and its maximum rainfall amount within a 30-minutes interval (according to Wischmeier and Smith, 1978):

$$EI_{30} = (\sum_{r=1}^k e_r v_r) I_{30} \quad (3.2)$$

where v_r is the rainfall volume (mm) during a time unit r and I_{30} is the maximum rainfall intensity within 30-minutes of the event (mm h^{-1}).

The monthly rainfall erosivity (R_{mo}) ($\text{MJ mm ha}^{-1} \text{h}^{-1} \text{month}^{-1}$) is the mean of the accumulated event erosivity (EI_{30}) (Eq. 3.2) within a month:

$$R_{mo} = \frac{1}{n} \sum_{j=1}^n \sum_{k=1}^{m_j} (EI_{30})_k \quad (3.3)$$

where n is the recorded number of years with the number of erosive events (m_j) within a certain month j . k is the index of a single event with its corresponding event erosivity.

The event rainfall erosivity was calculated for each station by applying the algorithm of Meusburger et al. (2012) (<http://esdac.jrc.ec.europa.eu/themes/r-factor-switzerland-version-2012>). The event rainfall erosivity was averaged by months to a long-term monthly mean R-factor (R_{mo}). Originally, the 30-minute maximum rainfall rate (I_{30}) is obtained by breakpoint precipitation data, which is recorded in intervals of fixed rainfall rates instead of fixed time intervals (Wischmeier and Smith, 1978; Hollinger et al., 2002). As stations recording breakpoints are rare in Switzerland, we used records with a fixed time interval of 10-minutes. Using small time intervals better represents breakpoint data and records the intensity more realistic. Longer intervals might underestimate rainfall intensity (Porto, 2016; Panagos et al., 2016a). For time intervals shorter than 15 minutes Porto (2016) reported an overestimation compared to the commonly used (EI_{30})₁₅ (15-minutes interval) and proposed a mean conversion factor of 0.97 for all investigated stations in southern Italy. This rather small deviation can

mainly be explained by the fact that the maximum intensity of the 10-minute record is upscaled to the whole 30-minute increment. To avoid this bias our algorithm uses a 30-minute moving average to identify the maximum I_{30} and as such resembles the original approach of Wischmeier and Smith (1978) to obtain the I_{30} from “successive increments of essentially uniform intensity” (Wischmeier and Smith, 1978). As we are working with the same 10-minute measuring interval at all 87 stations, no conversion factor was applied to homogenize the data (cf. Agnese et al., 2006; Porto, 2016; Panagos et al., 2016a). Usually, snow, snowmelt, and rainfall on frozen soil are not assessed in the R-factor (Renard et al., 1997). Thus, a temperature threshold of 0°C was set to obtain only rainfall and exclude snow water equivalents, which are subject to uncertainty in rainfall erosivity assessments (Leek and Olsen, 2000). Temperature data were measured simultaneous to precipitation (for 71 stations) or were directly derived (for 16 stations) from the closest stations (within a distance of less than 20 km) at similar elevation with an hourly resolution. We assumed only minor variation in temperature within that distance at a similar elevation level.

Besides neglecting snow, we did not consider rainfall as hail, which mainly occurs during summer in Switzerland (Nisi et al., 2016; Punge and Kunz, 2016). Although, Hurni (1978) investigated the impact of hail on rainfall erosivity for single plots in Switzerland and concluded that a water equivalent amount of hail exceeds the one of rainfall, hail erosivity has not yet been considered for this study.

3.2.2 Stations

We extended the gauging station network of Meusburger et al. (2012) (10-minute measuring intervals) by 23% from 71 to an updated dataset of 87 stations (Fig. 3.1) and upgraded stations by a longer time series if available.

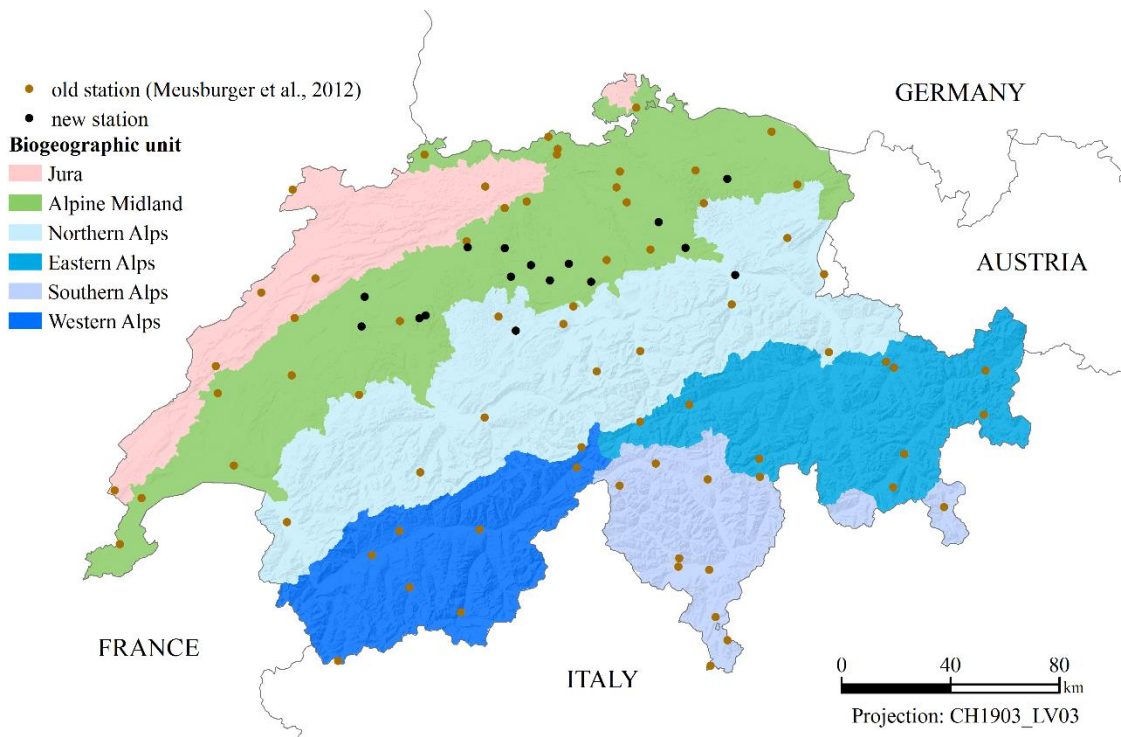


Fig. 3.1: Biogeographic units and used gauging stations in Switzerland.

The stations are well distributed and were subject to a quality control (Begert et al., 2005; Nogler, 2012). The additional 16 stations were previously investigated for rainfall erosivity by Nogler (2012). The mean density of one gauging station is 474.5 km². The average distance of one station to all others is 113.6 km by a minimum distance to the closest station of 13.2 km and a maximum distance of two stations by 324.6 km. A majority of 72% of all stations (63) have recorded data of at least 22 yr. The mean length of observations is 19.5 yr and thus meet the proposed minimum timescale requirements for rainfall erosivity calculations of a 15-year measuring period (Foster et al., 2008).

3.2.3 Data and Covariates

The high intra-annual variability of rainfall erosivity was already discussed in Meusburger et al. (2012), but not spatiotemporally mapped. The monthly erosivity mapping in a country with a high proportion of remote Alpine areas requests a variety of erosivity influencing covariates. High temporal information on snow cover and snow water equivalents, high spatiotemporal information on rainfall and high spatial information on topography are acquired as covariates (Table 3.1) for the monthly erosivity maps since rainfall erosivity is mainly controlled by precipitation and relief parameters (Meusburger et al., 2012; Panagos et al., 2015a; Panagos et al., 2016b). All spatial covariates have a much higher resolution (spatial and temporal) than datasets used in previous R-factor studies for Europe (Panagos et al., 2015a; 2016a) and Switzerland (Meusburger et al., 2012), and therefore the R-factor mapping is feasible at a higher spatial and temporal precision.

Table 3.1: Datasets used as covariates for the spatiotemporal mapping of rainfall erosivity.

dataset	derived information	temporal resolution	spatial resolution	measuring period	source	information
Total snow depth	long-term monthly snow depth	hourly	58 stations	1988 – 2010	MeteoSwiss	-
CombiPrecip	long-term monthly mean rainfall amount from measured and radar data	hourly	1 km	2005 – 2015	MeteoSwiss	Sideris et al., 2014
EURO4M-APGD	long-term mean daily precipitation per month	monthly	5 km	1971 – 2008	MeteoSwiss	Isotta et al., 2014
RhiresM	long-term mean monthly precipitation sums	monthly	1 km	1961 – 2015	MeteoSwiss	MeteoSwiss, 2013
SwissAlti3D	elevation, slope, aspect	-	2 m	-	SwissTopo	-

The long-term snow depth (derived from mean monthly snow depth by MeteoSwiss) on a monthly resolution was used as an approximation for snow. The monthly point data of snow depth were regionalized by inverse distance weighting. Hourly Swiss CombiPrecip data (geostatistical combination of rain gauge measurements at 150 automatic stations and three C band radar observations; Sideris et al., 2014) were aggregated and averaged to a long-term monthly mean. Long-term mean daily precipitation per month was calculated based on the daily

values of Alpine precipitation in EURO4M-APGD (Isotta et al., 2014). Averaging the monthly spatial precipitation of RhiresM (MeteoSwiss, 2013) over the years leads to long-term monthly mean precipitation sums. The variables elevation, slope, and aspect are retrieved from a 2 m digital terrain model (SwissAlti3D) for Switzerland.

3.2.4 Mapping the seasonal variability of rainfall erosivity in Switzerland

Hanel et al. (2016) and Angulo-Martínez and Beguería (2009) tested different interpolation methods for Czech Republic (Hanel et al., 2016) and the Ebro Basin in Spain (Angulo-Martínez and Beguería, 2009). Both studies could confirm that a combination of regression and residual kriging (regression-kriging) is among the most suitable methods to interpolate rainfall erosivity. We also used regression-kriging (Hengl et al., 2004; Hengl, 2007; Hengl et al., 2007) to map the monthly variability of rainfall erosivity in Switzerland. The regression-kriging approach employed on the monthly mean rainfall erosivity for each of the 87 stations (R_{mo}). In a first step a generalized linear regression (GLM) (Gotway and Stroup, 1997) is used to establish a regression between R_{mo} and the high-resolution covariates. The GLM relates the rainfall erosivity (target variables) to the covariates (Table 3.1) and predicts rainfall erosivity at the same scale as covariates are available (Odeh et al., 1995; McBratney et al., 2000). In a second step the residuals of the GLM are interpolated by an ordinary global kriging (McBratney et al., 2000; Hengl et al., 2004). Finally, the predicted rainfall erosivity by the GLM is summarized with the residuals map (established by the kriging procedure). The combination of interpolated R_{mo} with the spatial variation of its residuals enables the quantification of the standard error related to the erosivity mapping.

Besides the standard error maps, leave-one-out cross-validation (LOOCV) was used as a second quality check of the mapping procedure (Efron and Tibshirani, 1997). However, data splitting reduces the training observations and doesn't show the same results by repetition due to bias and randomness (Steyerberg, 2009; Harrell, Jr., 2015). In contrast, LOOCV avoids a resampling bias since it omits only one observation from the dataset per run and estimates the model from the remaining $n-1$ observations. It yields the same regression coefficients by repetition due its reproducibility (James and Witten, 2015). In contrast, data split reduces the training observations and doesn't show the same coefficients due to randomness (Steyerberg, 2009; Harrell, Jr., 2015). To compensate for the low validation subset, the process was repeated 100 times.

A log transformation of R_{mo} resulted in a normal distribution of the data. The suitability of each covariate for the GLM was determined by an automated stepwise feature selection process according to the Akaike information criterion (AIC). The α -to-enter significance level for covariate selection was set to 0.1 (Kutner et al., 2005; Gupta and Guttman, 2013). We also tested least absolute shrinkage and selection operator (LASSO) as an alternative feature selection method to the stepwise GLM, but it was less transparent for evaluation and showed inappropriate residual diagnostics (systematic error). Both, the LOOCV stepwise regression, as well as LASSO, were performed in the R-package "caret" (v6.0-68). Outliers (Bonferroni-adjusted outlier test) and influential observations (Cook's distance) were omitted in the stepwise GLM.

The goodness-of-fit of the model was described by the coefficient of determination (R^2), the root mean square error (E_{RMS}), and the deviance. Regression diagnostics to evaluate the model

included normality, non-constant error variance (homoscedasticity), multicollinearity (variance inflation factor, vif), and autocorrelation.

In all, 12 monthly maps of the long-term mean R_{mo} were derived by applying the regression equation with the covariates and their corresponding coefficients according to the individual monthly regression equation. The residuals of each months' stepwise GLM were interpolated by an ordinary global kriging with a stable variogram model and added to the R_{mo} maps in ESRI ArcGIS (v10.2.2.) afterwards.

Each monthly map is subject to an individual GLM. Therefore, a subset of individual covariates explains rainfall erosivity for each month separately. An averaging of 3-monthly maps leads to long-term seasonal mean R-factor (R_{seas}) maps for Switzerland with high spatial resolution. In addition, the sum of all 12 maps results in an updated (compared to Meusbürger et al., 2012) long-term annual mean R-factor (R_{year}) map.

3.2.5 Cumulative daily R-factors

The averaged cumulative percentage of R-factor within a year is obtained and grouped by Swiss biogeographic regions (Gonseth et al., 2001). The biogeographic regions were selected because they show distinct differences in climate, soils, elevation, steepness, and geographic location. The cumulative curve of rainfall erosivity enables the extraction of the annual share of rainfall erosivity on a daily scale and is required for the calculation of RUSLE C-factors. C-factors are based on the product of the soil loss ratio (for a specific time of the year and a specific crop) and the cumulative percentage of rainfall erosivity of distinct days of the year (Wischmeier and Smith, 1978; Schwertmann et al., 1987; Renard et al., 1997). Therefore, all recorded rainfall events of a certain station within an individual biogeographic unit and at a specified day in the year are averaged over the measuring period and with the other stations of the region on a long-term mean daily level. That calculation of C-factors requires the percentage of the total annual rainfall erosivity of distinct days of the year, which can be derived by that procedure.

3.2.6 Monthly erosivity density

Monthly erosivity density (ED_{mo}) ($MJ\ ha^{-1}\ h^{-1}$) is calculated by the ratio of the long-term R_{mo} ($MJ\ mm\ ha^{-1}\ h^{-1}\ month^{-1}$) (neglecting snow) to mean monthly precipitation amount (P_{mo}) ($mm\ month^{-1}$) (including snow) according to the equation proposed by Foster et al. (2008):

$$ED_{mo} = \frac{R_{mo}}{P_{mo}} \quad (3.4)$$

Small values (<1) of ED_{mo} indicate that the influence of monthly precipitation on the monthly rainfall erosivity is mainly driven by its amount. On the other hand, high values of ED_{mo} show that relative to the absolute rainfall amount a high kinetic energy of rainfall was observed (e.g., strong storm events; Panagos et al., 2016b). The highest soil erosion risk is expected for areas where rainfall erosivity is high but related to a few intense rainfall events (high values of ED_{mo}). As such, ED_{mo} can reflect the temporal variability of rainfall intensity (Dabney et al., 2011) and can indicate how precipitation (short duration events with high intensities or high amounts of rainfall) controls the seasonality of rainfall. ED_{mo} was calculated using i) the erosivity (R_{mo87}) and monthly precipitation sums (P_{mo87}) of each station (ED_{mo87}) and ii) the 12 interpolated monthly rainfall erosivity maps R_{mo} and RhiresM as the monthly

precipitation dataset (ED_{mo}). RhiresM is an already available precipitation dataset of MeteoSwiss that includes most of the 87 gauging stations. For the spatial mapping of monthly erosivity density, the interpolated monthly datasets R_{mo} and RhiresM were chosen since an interpolation of ED_{mo87} would require additional interpolation methods and spatial covariates, which are explanatory for the monthly erosivity density. Additionally, a performed interpolation might still modify the ED_{mo87} in accordance to the values at neighboring stations. According to Dabney et al. (2012), erosivity density is relatively independent of elevation up to a height of 3000 m a.s.l.. In Switzerland, only the station Piz Corvatsch (COV) exceeds that threshold of height.

3.3 Results and Discussion

3.3.1 Monthly rainfall erosivity at the 87 Swiss gauging stations

R_{mo} data averaged for all investigated stations show a bell-shaped curve over the 12 months (Fig. 3.2) with an increasing trend starting from February ($17.3 \text{ MJ mm ha}^{-1} \text{ h}^{-1} \text{ month}^{-1}$) to a maximum in July ($289 \text{ MJ mm ha}^{-1} \text{ h}^{-1} \text{ month}^{-1}$). The mean R_{mo} is $112 \text{ MJ mm ha}^{-1} \text{ h}^{-1} \text{ month}^{-1}$. The meteorological season winter (Dec-Jan-Feb) has the lowest mean R_{mo} ($33 \text{ MJ mm ha}^{-1} \text{ h}^{-1} \text{ month}^{-1}$), followed by spring (Mar-Apr-May; $68 \text{ MJ mm ha}^{-1} \text{ h}^{-1} \text{ month}^{-1}$), fall (Sep-Oct-Nov; $92 \text{ MJ mm ha}^{-1} \text{ h}^{-1} \text{ month}^{-1}$), and summer (Jun-Jul-Aug; $257 \text{ MJ mm ha}^{-1} \text{ h}^{-1} \text{ month}^{-1}$). Most of the monthly R-factors (96%) of the lowest 10% of all monthly values are part of the period between November and April, whereas 97% of the highest 10% are monthly rainfall erosivity in the period from May to October.

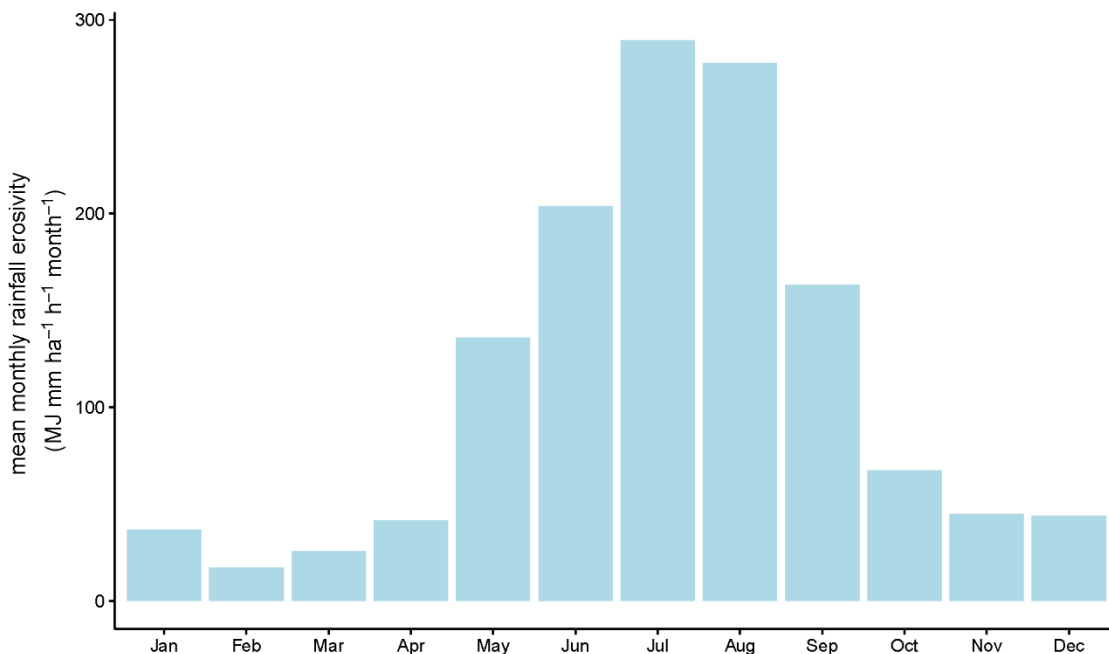


Fig. 3.2: Mean monthly rainfall erosivity for all 87 Swiss stations.

The “Monthly Rainfall Erosivity” for Europe by Panagos et al. (2016a) and the national observations of Mosimann et al. (1990) for a single station in Switzerland (Bern, Swiss midland) comply with the present calculations with the highest rainfall erosivity for the season from June/July to August. The Swiss monthly rainfall erosivity in the European assessment (Panagos et al., 2016a) are on average by $3 \text{ MJ mm ha}^{-1} \text{ h}^{-1} \text{ month}^{-1}$ smaller (after rescaling with the calibration factors from 30 to 10 minutes). That discrepancy by 5% mainly arises due to the different numbers and time series of gauging stations (87 vs. 71).

Seasonality of R_{mo} on a continental scale is observed for Europe (Panagos et al., 2016a) and Africa (Vrieling et al., 2014), on a national scale for Brazil (da Silva, 2004), Cabo Verde (Mannaerts and Gabriels, 2000), Chile (Bonilla and Vidal, 2011), Denmark (Leek and Olsen, 2000), El Salvador (da Silva et al., 2011), Greece (Panagos et al., 2016b), Iran (Sadeghi et al., 2011; Sadeghi and Hazbavi, 2015; Sadeghi and Tavangar, 2015), Italy (Diodato, 2005; Borrelli et al., 2016), New Zealand (Klik et al., 2015), South Korea (Lee and Won, 2013), and inter alia for the regions of Australia (Yang et al., 2015; Yang and Yu, 2015), Belgium (Verstraeten et al., 2006), Brazil (da Silva et al., 2013), Cabo Verde (Sanchez-Moreno et al., 2014), China (Jing et al., 2009; Zhu et al., 2011; Wang et al., 2013b; Zhao et al., 2015; Lai et al., 2016), England and Wales (Davison et al., 2005), Ethiopia (Meshesha et al., 2015), Japan (Lacey et al., 2015), the Himalayas (Ma et al., 2014), Italy (Terranova and Gariano, 2015), South Korea (Arnhold et al., 2014), Malaysia (Shamshad et al., 2008), Poland (Banasik and Górski, 1993; Banasik et al., 2001), Slovenia (Petkovšek and Mikoš, 2004; Mikoš et al., 2006), Spain (Renschler et al., 1999; Angulo-Martínez and Beguería, 2009), Turkey (Özşahin, 2014), and the USA (Wilkes and Sawada, 2005). However, the timing of the maximum and minimum erosivity varies considerably. Some of the above-mentioned studies show highest values in fall and winter (e.g., Greece), the highest values in March and the lowest values in July (e.g., Iran), or the highest values in January and the lowest values in July (e.g., Australia). The seasonal R_{mo} in Italy and Greece have lower ranges (209 and $121 \text{ MJ mm ha}^{-1} \text{ h}^{-1} \text{ month}^{-1}$ compared to $272 \text{ MJ mm ha}^{-1} \text{ h}^{-1} \text{ month}^{-1}$ in Switzerland), and the peak of the R-factor is shifted from July to September for Italy and to November for Greece.

3.3.2 Mapping of monthly rainfall erosivity and related uncertainties

All covariates – aspect excluded – were significant (p-value < 0.1) within the stepwise regressions for at least one month to explain R_{mo} (Table 3.2). For each month, an individual selection of covariates was achieved by the stepwise GLM. The higher the ratio of the null deviance to the residual deviance, the better the model fits by including the covariates. The residual deviance is lower than the null deviance in all 12 investigated months. Monthly model efficiency and omitted influential outliers to increase the model's goodness of fit are summarized in Table 3.3. The monthly observations of R_{mo} at the 87 locations (exclusive outliers) as well as the residuals are normally distributed after the log-transformation. A non-constant error (homoscedasticity), multicollinearity and non-autocorrelation were determined for all observations of the 12 months. H_0 , which tests that all error variances are equally, was accepted by the Breusch-Pagan-test in all cases and confirms homoscedasticity. Regression diagnostics further show a $\text{vif} < 4$ for each month. Therefore, we could not identify collinear data. According to a Durbin-Watson-test, the Swiss R_{mo} -dataset is not autocorrelated.

Model efficiency, averaged over all 12 months has a mean R^2 of 0.51 and a mean ERMS of $93.27 \text{ MJ mm ha}^{-1} \text{ h}^{-1} \text{ month}^{-1}$. Among that period, R^2 varies between 0.10 (Nov) and 0.66

(July). ERMS ranges from 6.98 to 330.16 MJ mm ha⁻¹ h⁻¹ month⁻¹ within a year. Regression functions for November and December are most uncertain with lowest R² and highest ERMS. The low R² are arising due to the generally low rainfall erosivity in winter that is mainly caused by lower rainfall amounts and higher amounts of snow (neglected in this study), which make it more challenging to predict R. The same constrain was observed in a study for Greece where the lowest R² was observed for the month with lowest rainfall erosivity (Panagos et al., 2016b). Even though, the spatial erosivity prediction for the winter month related to high uncertainties, the latter will have little effects on soil erosion assessment since rainfall erosivity has the lowest impact on soils in winter.

Table 3.2: Regression equations and selected covariates for estimating mean monthly rainfall erosivity in Switzerland.

Month	Regression equation
January	$R_{Jan} = 2.101 - 4.150 \cdot \text{CombiPrecip}_{Jan} - 0.006 \cdot \text{Snow depth}_{Jan} + 0.017 \cdot \text{Rhires}_{Jan} - 0.001 \cdot \text{Elevation}$
February	$R_{Feb} = 2.702 - 13.812 \cdot \text{CombiPrecip}_{Feb} - 0.007 \cdot \text{Snow depth}_{Feb} + 0.019 \cdot \text{Rhires}_{Feb} + 0.211 \cdot \text{Alpine Precip}_{Feb} - 0.001 \cdot \text{Elevation}$
March	$R_{Mar} = 2.534 - 7.735 \cdot \text{CombiPrecip}_{Mar} - 0.006 \cdot \text{Snow depth}_{Mar} + 0.018 \cdot \text{Rhires}_{Mar} + 0.170 \cdot \text{Alpine Precip}_{Mar} - 0.001 \cdot \text{Elevation}$
April	$R_{Apr} = 2.330 - 3.319 \cdot \text{CombiPrecip}_{Apr} - 0.008 \cdot \text{Snow depth}_{Apr} + 0.023 \cdot \text{Rhires}_{Apr} - 0.001 \cdot \text{Elevation} - 0.019 \cdot \text{Slope}$
May	$R_{May} = 2.965 + 2.072 \cdot \text{CombiPrecip}_{May} - 0.002 \cdot \text{Snow depth}_{May} + 0.015 \cdot \text{Rhires}_{May} - 0.001 \cdot \text{Elevation}$
June	$R_{Jun} = 3.890 + 0.014 \cdot \text{Rhires}_{Jun} - 0.001 \cdot \text{Elevation}$
July	$R_{Jul} = 3.926 + 5.710 \cdot \text{CombiPrecip}_{Jul} + 0.251 \cdot \text{Alpine Precip}_{Jul} - 0.001 \cdot \text{Elevation}$
August	$R_{Aug} = 3.627 + 0.010 \cdot \text{Rhires}_{Aug} + 0.194 \cdot \text{Alpine Precip}_{Aug} - 0.001 \cdot \text{Elevation}$
September	$R_{Sep} = 2.760 + 2.243 \cdot \text{CombiPrecip}_{Sep} + 0.539 \cdot \text{Alpine Precip}_{Sep} - 0.001 \cdot \text{Elevation}$
October	$R_{Oct} = 2.753 + 0.0161 \cdot \text{Rhires}_{Oct} - 0.001 \cdot \text{Elevation}$
November	$R_{Nov} = 2.665 + 3.787 \cdot \text{CombiPrecip}_{Nov} - 0.034 \cdot \text{Snow depth}_{Nov} + 0.166 \cdot \text{Alpine Precip}_{Nov}$
December	$R_{Dec} = 2.437 + 0.013 \cdot \text{Rhires}_{Dec} - 0.001 \cdot \text{Elevation}$

Table 3.3: Model efficiency by R² and E_{RMS} as well as omitted outliers and influential observations per month.

Month	Excl. outlier stations	R ²	E _{RMS} (MJ mm ha ⁻¹ h ⁻¹ month ⁻¹)	Null Deviance	Res. deviance
January	Mathod	0.52	6.98	70.36	20.65
February	Monte Generoso, Napf, Saetis	0.53	12.96	79.28	31.82
March	Col du Grand St-Bernard, Saetis	0.49	13.10	61.45	21.84
April	Col du Grand St-Bernard, Saetis, Weissfluhjoch	0.65	21.01	63.69	15.90
May	Davos, Col du Grand St-Bernard	0.60	73.39	56.28	16.83
June	Col du Grand St-Bernard	0.58	126.03	51.61	19.31
July	Monte Generoso, Col du Grand St-Bernard, Stabio	0.66	138.77	38.58	11.57
August	Col du Grand St-Bernard, Stabio	0.47	330.16	50.47	21.75
September	Col du Grand St-Bernard, Stabio	0.64	81.91	61.23	16.27
October	Piz Corvatsch, Col du Grand St-Bernard, Stabio	0.62	81.60	37.86	12.07
November	Piz Corvatsch, Col du Grand St-Bernard, Saetis	0.10	55.72	58.85	47.22
December	Col du Grand St-Bernard	0.26	177.65	73.90	50.66

After adding the kriging interpolation of the residuals to the regionalization of monthly R-factors (based on the stepwise GLM), R² are increased in all months. As such, the regression-kriging improves the prediction of R-factors especially for months with low R² as in the case for November and December. The ranges of the stable variograms exceed the minimum distance

(approx. 13.2 km) of neighboring stations in all months. The average prediction error of all 12 months is -0.0055. The used stable semivariogram models are represented by 12 lag classes. Common patterns of increasing standard deviations with distances from gauging stations are recognizable in the standard deviation maps.

3.3.3 Monthly rainfall erosivity maps for Switzerland

Regionalized temporal patterns of modeled R_{mo} show a distinct seasonality with national means being the lowest in January ($10.5 \text{ MJ mm ha}^{-1} \text{ h}^{-1} \text{ month}^{-1}$) and the highest in August ($263.5 \text{ MJ mm ha}^{-1} \text{ h}^{-1} \text{ month}^{-1}$) (Table 3.4 and Fig. 3.3). Fig. 3.3 represents R_{mo} on a stretch between 0 and $200 \text{ MJ mm ha}^{-1} \text{ h}^{-1} \text{ month}^{-1}$ for a better spatial comparison of the color schemes although the R-factors are higher than $200 \text{ MJ mm ha}^{-1} \text{ h}^{-1} \text{ month}^{-1}$ in summer (cf. Table 3.4). Winter is the season (Fig. 3.4) with the lowest rainfall erosivity. The highest R_{mo} peak in summer is consistent with the map of extreme point rainfall of 1h duration (100-year return period; Spreafico and Weingartner, 2005), where the strong influence of extreme rainfall events on rainfall erosivity is indicated. Meusburger et al. (2012) already pointed to the relationship of thunderstorm activity to annual rainfall erosivity. The thunderstorm season in Switzerland lasts from late spring (May) to early fall (September). Thunderstorms are at least partly responsible for the high values of rainfall erosivity in summer. Starting from early fall (September), a decreasing trend of R_{mo} is noticeable all over Switzerland.

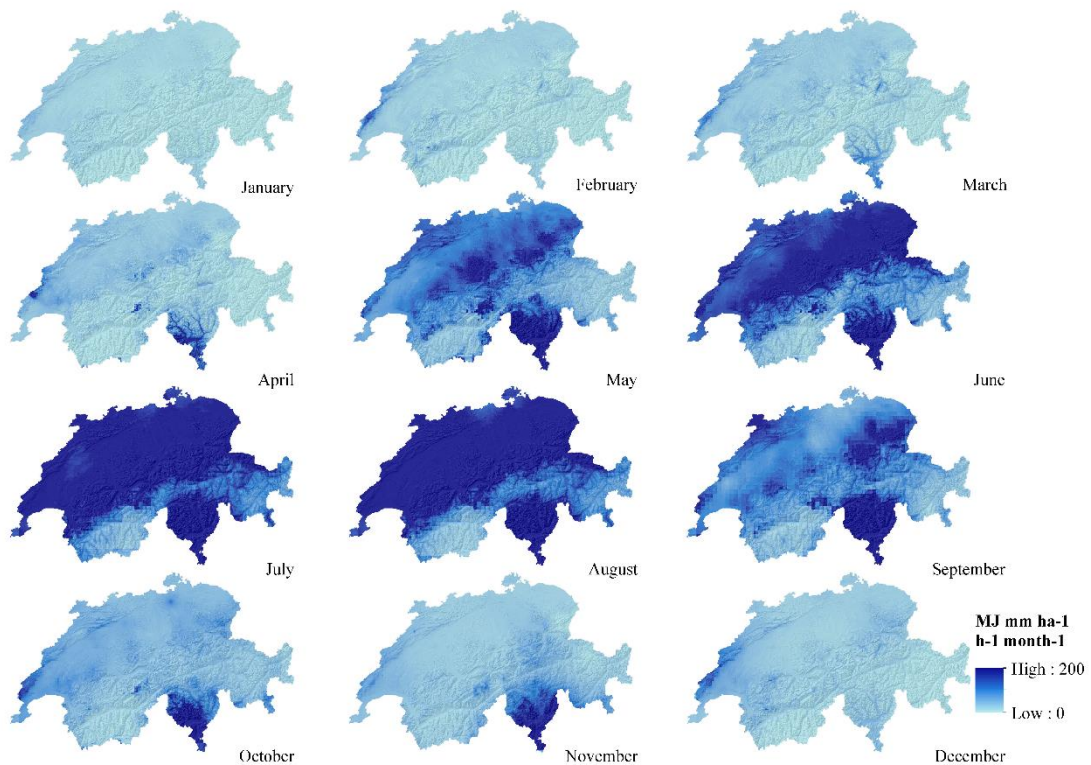


Fig. 3.3: Monthly rainfall erosivity maps for Switzerland (equal stretch from 0 to $200 \text{ MJ mm ha}^{-1} \text{ h}^{-1} \text{ month}^{-1}$) derived by regression-kriging.

Averaged months are aggregated to representative seasons (R_{seas}) to identify spatial differences (Fig. 3.4). Spatially, mean winter rainfall erosivity show the highest values in the

Jura Mountains, western and eastern parts of the northern Alps and the southern Alps (canton Ticino). High winter rainfall erosivity can be explained by rainfall resulting from low-pressure areas in northern Europe and weather fronts moved by northwesterly winds. These fronts are uplifted at the Jura Mountains which results in orographic rainfall. In spring, the northern and the southern Alps become more affected by high rainfall erosivity. The spatial variability of rainfall erosivity in spring in the southern Alps (canton Ticino) corresponds to the airflow from the south and the onset of the thunderstorm season in that region, which causes intense rainfall. High rainfall erosivity is persistent from spring to fall in the southern Alps. The generally high summer R-factors in the southern Alps, the Jura Mountains, and the northern Alpine foothill are driven by thunderstorms (van Delden, 2001; Perroud and Bader, 2013; Nisi et al., 2016; Punge and Kunz, 2016) and particularly in the southern Alps by high intense rainfall originating from orographic uplifts (Schwarb et al., 2001; Perroud and Bader, 2013). The cantons of Valais and Grisons remain with relatively low rainfall erosivity among all seasons due to lower convection and thereby lower rainfall erosivity in summer.

Table 3.4: Monthly national rainfall erosivity in $\text{MJ mm ha}^{-1} \text{h}^{-1} \text{month}^{-1}$.

Month	Minima	Maxima	Mean
January	0.2	71.3	10.5
February	0.0	247.3	13.5
March	0.0	179.0	20.1
April	0.2	1014.4	28.8
May	8.3	1717.8	120.2
June	3.6	1262.1	174.8
July	12.6	1481.1	255.4
August	8.3	1994.9	263.5
September	6.8	6107.9	147.7
October	5.7	977.0	57.0
November	4.9	357.1	41.6
December	1.3	234.4	24.9

The degree of maximal variation at a certain location in a year (expressed as the difference between minimum and maximum monthly rainfall erosivity of all 12 months; Fig. 3.5) indicates the highest intra-annual range (up to $6086 \text{ MJ mm ha}^{-1} \text{h}^{-1} \text{month}^{-1}$) in the canton Ticino in the southern Alps. Furthermore the northern Alps, Swiss midland and Jura Mountains show a high erosivity variation within a year. The eastern and western Alps have lowest ranges in accordance with their relatively low rainfall erosivity among in a year. While the range map displays the absolute values of variation, the coefficient of variation map (ratio of standard deviation to the mean of all 12 months; Fig. S3.1) indicates the relative degree of erosivity variation (in percent) at a certain location in a year. According to this map, the highest variation of up to 207% can be observed in the eastern Alps (canton Grisons) where monthly rainfall erosivity is low and standard deviation is high. In the Muamba catchment in Brazil, high seasonal variations are also observed in regions with relatively low rainfall erosivity (da Silva et al., 2013).

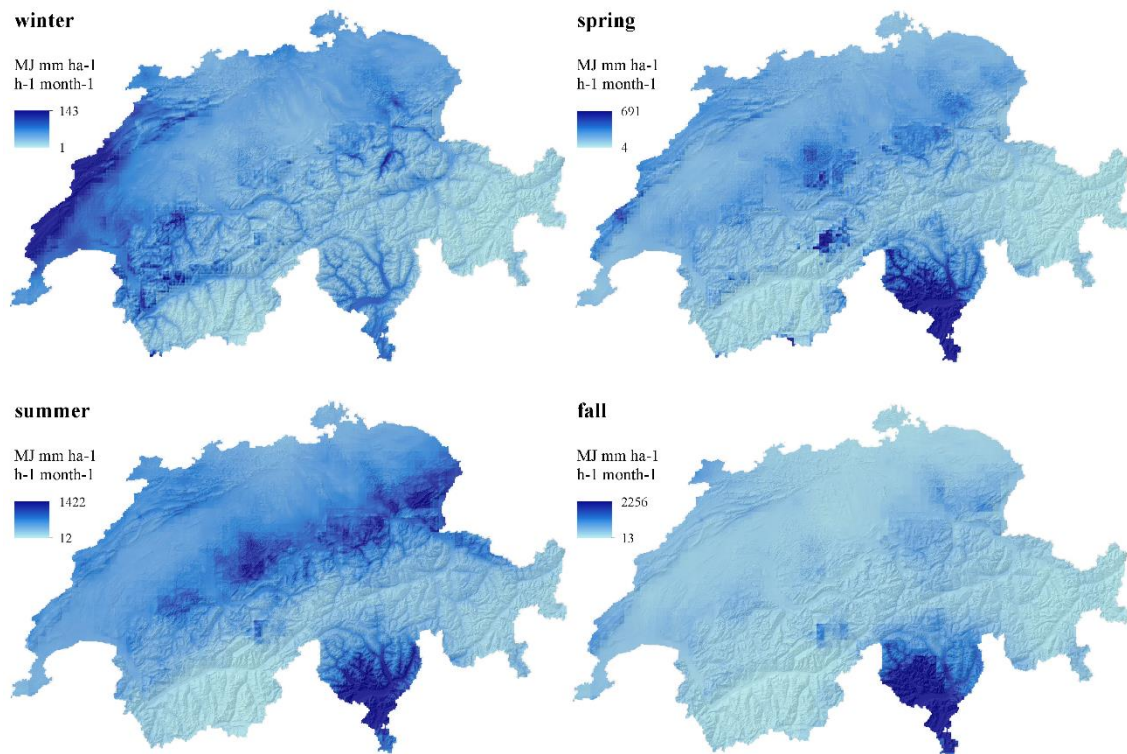


Fig. 3.4: Seasonal rainfall erosivity maps for Switzerland derived by regression-kriging. The following months were averaged to derive seasonal maps: winter (December–February), spring (March–May), summer (June–August), fall (September–November).

Compared to the rainfall erosivity evaluation by Meusburger et al. (2012) on an annual scale, the observed mean R_{year} and spatial patterns only changed slightly due to the extended station network and higher resolution spatial covariates (aggregated by all 12 monthly R-factor maps). Improvements of the new map are the extended network of gauging stations, the cross-validation of the regression-kriging approach, and the inclusion of new high spatiotemporal covariates in order to increase the spatial resolution of the maps.

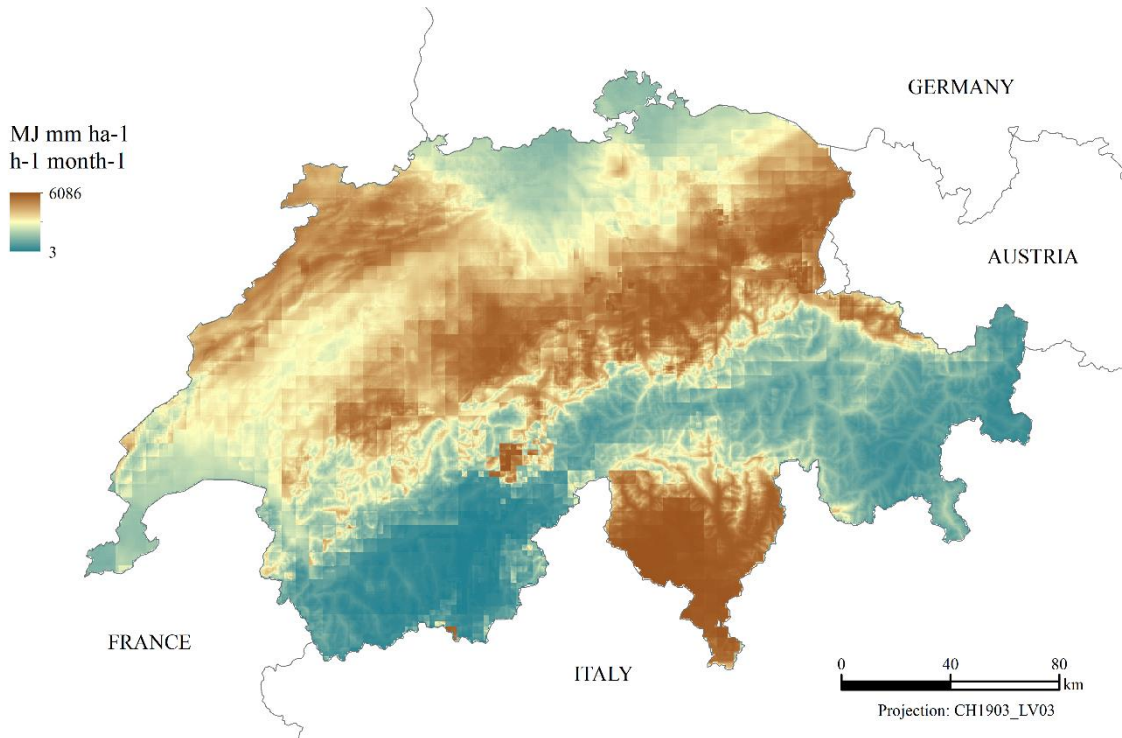


Fig. 3.5: Range map (maximum R_{mo} minus minimum R_{mo}) for Switzerland showing the variability of rainfall erosivity in a year.

3.3.4 Cumulative daily rainfall erosivity

Generally, the steepest slopes of the cumulative rainfall erosivity curve for Switzerland can be noticed from June to September with a share of 62% of the total annual rainfall erosivity within these 4 months (Fig. 3.6). That proportion complies with the cumulative sum of southwest Slovenia (63,2%; Petkovšek and Mikoš, 2004) and exceeds the average share for Europe of 53% (Panagos et al., 2016a) during the same period. A much larger proportion (90%) of cumulative percentage of daily rainfall erosivity was observed for Bavaria (Schwertmann et al., 1987) and eastern Poland (78%; Banasik and Górski, 1993). Mosimann et al. (1990) showed in a single-station approach (Bern, Swiss midland) that a proportion of 80% of the total annual erosivity occurs in the period from April to September, which complies with the national share (resulting from the multi-station (87) calculation) of 77% during the same period of a year.

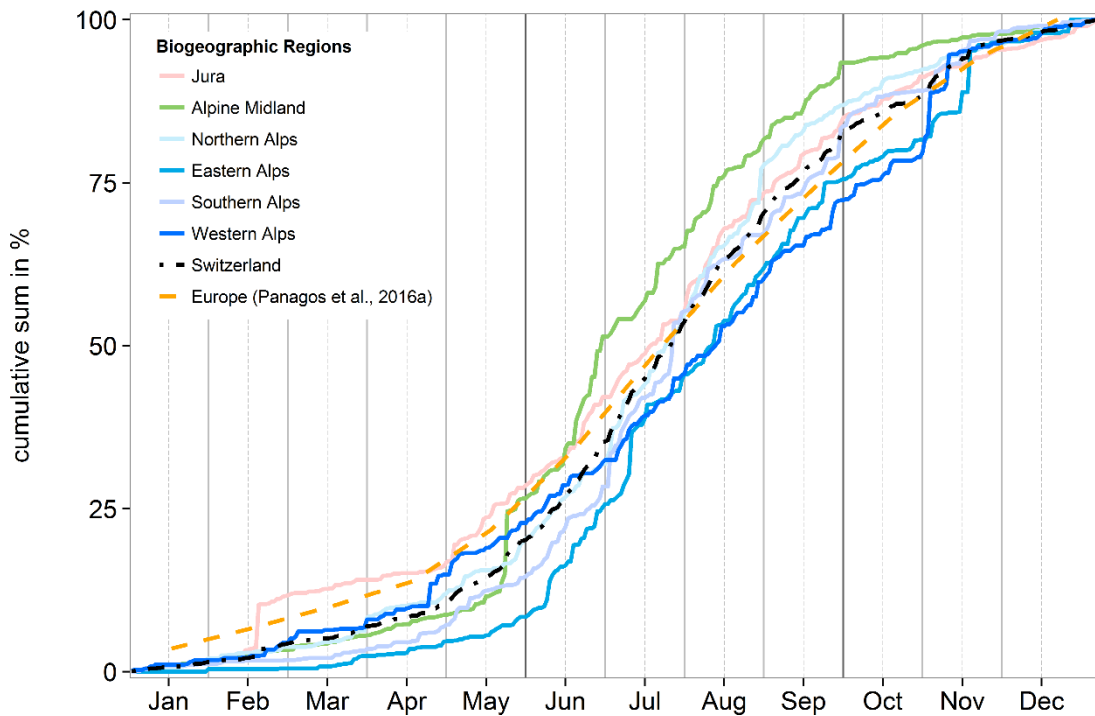


Fig. 3.6: Cumulative daily rainfall erosivity proportion for Swiss biogeographic units, Switzerland and monthly rainfall erosivity for Europe (linear smoothed, European data from Panagos et al., 2016a).

All biogeographic units in Switzerland have similar trends of the cumulative daily rainfall erosivity. However, a Wilcoxon signed rank showed that all pairs of the sum curves of biogeographic regions have significant differences (significance level 0.05). The highest proportions (from Jun to Sep) and, therefore, steepest slopes can be identified for the southern Alps with a share of 70% of the total sum. This high percentage of rainfall erosivity within a short period of time (4 months) is likely to have a large impact on the soil erosion susceptibility since it may coincide with the lowest (after harvesting of crops, carrots, etc.) and most unstable vegetation cover (after late sowing) (Hartwig and Ammon, 2002; Wellinger et al., 2006; Torriani et al., 2007; Prasuhn, 2011). Furthermore, fully grown pre-harvest field crops (e.g. cereals, maize) might suffer by bend over of corn stalks due to high intensity storms. In addition, water saturated conditions which are usual in May and September/October, make soils even more erodible. Highly susceptible soils in summer may also be expected in areas where forest fires occurred in spring and soils are uncovered by vegetation (which is the case especially for Ticino) (Marxer, 2003). The combination of the monthly rainfall erosivity maps with dynamic monthly C-factors might enable a monthly soil erosion risk assessment for Switzerland.

3.3.5 Monthly erosivity density

Erosivity density (expressed as ratios of R to P) can be used to distinguish between high rainfall erosivity that is mainly influenced by high rainfall amounts and those that are influenced by relatively low rainfall amounts but highly intense rainfalls. That distinction helps to evaluate the potential consequences of rainfall erosivity for each month. The ED_{mo} maps (Fig. 3.7) show

that the influence of rainfall intensity on rainfall erosivity also underlies seasonal and spatial variations.

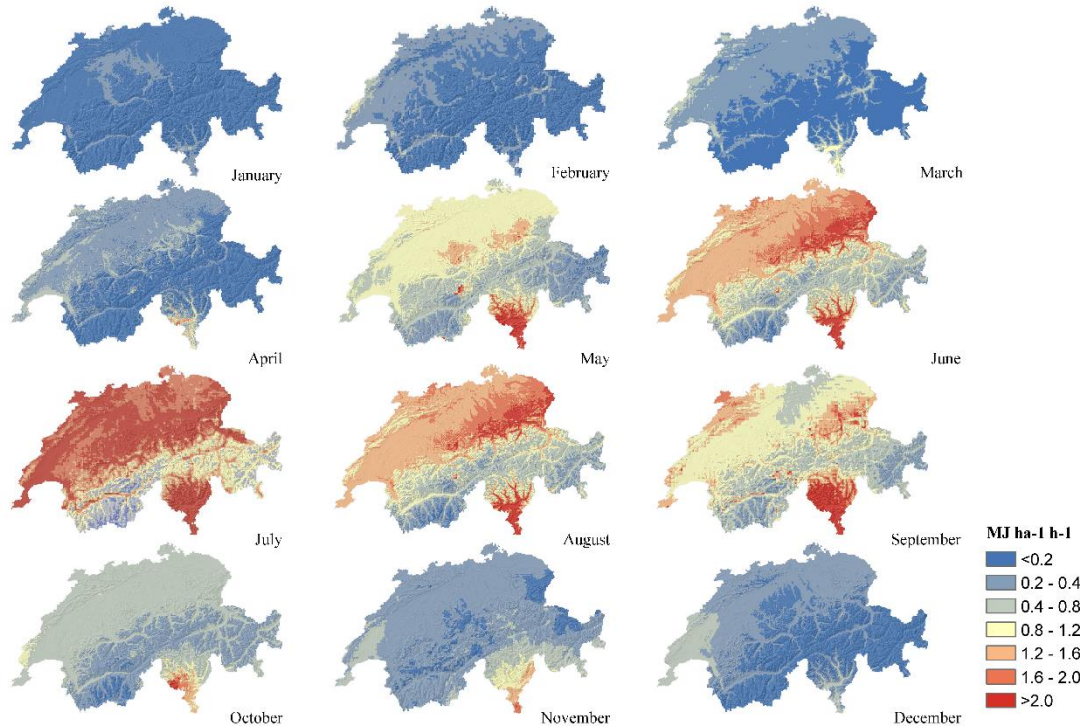


Fig. 3.7: Monthly erosivity density (ED_{mo}) for Switzerland as ratio of monthly rainfall erosivity (R_{mo}) to monthly precipitation amount (P_{mo} based on RhiresM).

Interpolated and spatially averaged ED_{mo} in winter is lower than $1 \text{ MJ ha}^{-1} \text{ h}^{-1}$ (Fig. 3.7) for Switzerland. Therefore, rainfall intensity is not the driving factor for rainfall erosivity in these months, where low rainfall erosivity meets high rainfall amounts. The relatively high R_{mo} in the Jura Mountains is therefore mainly driven by large amounts of rainfall instead of high intensity rains. Interpolated and spatially averaged ED_{mo} has a maximum for Switzerland in July ($1.8 \text{ MJ ha}^{-1} \text{ h}^{-1}$), which results from a relatively low rainfall amount indicating that rainfall erosivity is mainly controlled by high intensified events. Intense summer rainfall has its maximum in the regions of Jura, Swiss midland, northern Alpine foothill, and southern Alps. In these regions, R_{mo} is high accompanied by relatively low precipitation amounts. As such, the erosivity risk is at its highest in the year, especially when soils are dry during periods of rare but high rainfall intensities, and therefore, infiltration is reduced due to crusts.

The distribution of the Swiss mean ED_{mo} (Fig. 3.8) is bell-shaped as is also the case for investigated stations in the USA, Italy and Austria (Foster et al., 2008; Dabney et al., 2012; Borrelli et al., 2016; Panagos et al., 2016a). The monthly erosivity density of the neighboring country, Austria, complies with the Swiss values with minor variability. Greece, Italy, and the stations of the USA are characterized by higher ED_{mo} values than in Switzerland. Nonetheless, the conclusion Panagos et al. (2016b) drew for Greece is also generally valid for Switzerland; i.e., “rainfall erosivity is not solely dependent on the amount of precipitation” is also generally valid for Switzerland.

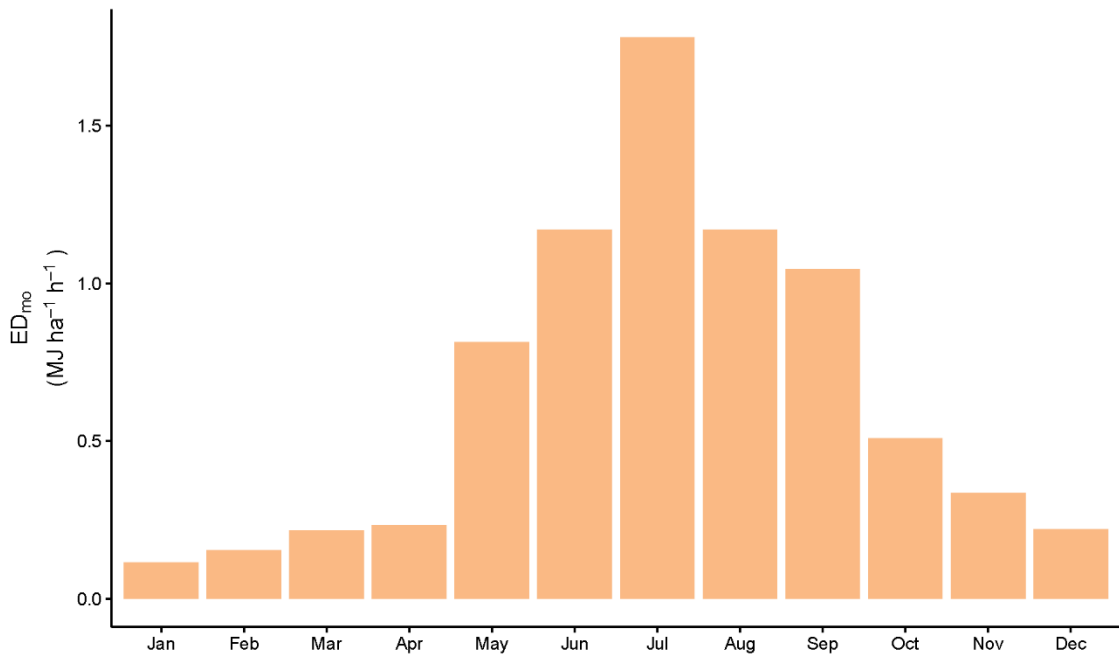


Fig. 3.8: Mean monthly erosivity density (ED_{mo}) as ratios of R_{mo} (interpolated erosivity maps based on regression-kriging) to P_{mo} (precipitation sums from RhiresM) for Switzerland.

In addition to the ED_{mo} maps, ED_{mo87} at the 87 stations (Table S3.1) were calculated. ED_{mo87} show generally higher values than ED_{mo} calculated from the interpolated raster maps, since the interpolated R-factors are smoothed and adapted according to the surrounding values. This fact is also visible in Fig. S3.2, where the relationship of absolute R-factors at the 87 stations (R_{mo87}) and the interpolated R-factors at the 87 stations (extracted after the interpolation with regression-kriging; $R_{\text{regression-kriging}}$) is presented.

3.4 Conclusion and Outlook

The main aim of the current study was to investigate the seasonal and regional variability of rainfall erosivity in Switzerland. A crucial advancement of the present research was to identify spatial and temporal windows of high erosivity. Through spatial-temporal mapping, it was possible to determine regions that are hardly affected by rainfall erosivity, such as Grisons and Valais, and it was also possible to determine those that are only affected in a certain months, such as the Jura Mountains. The spatiotemporal variability of rainfall erosivity of Switzerland enables the controlled and time-dependent management of agriculture (like crop selection, time-dependent sowing) and droughts, ecosystem services evaluation, as well as for seasonal and regional hazard prediction (e.g., flood risk control, landslide susceptibility mapping). Rainfall erosivity based on high erosivity density has more severe impacts on soils, agriculture, droughts, and hazards in summer than in winter due the high impact of intense rainfalls.

In contrast to previous studies for Switzerland, which were either limited spatially (to a few stations) or temporally (to annual), we were able to produce 12 monthly spatiotemporal R-factor maps. The maps are based on high-resolution covariates in combination with an extended database of 87 automated gauging stations recording in 10 min intervals, showing

simultaneously spatial and temporal variations of R-factors. Regression-kriging based on high-resolution covariates was a successful method for most of the months (mean $R^2=0.51$, $E_{RMS}=93.27 \text{ MJ mm ha}^{-1} \text{ h}^{-1} \text{ month}^{-1}$). It was used to map the long-term monthly mean R-factors based on an extended database of rain-gauging stations. The spatiotemporal mapping of rainfall erosivity and erosivity density revealed that intense rainfall events in August trigger the highest national monthly mean rainfall erosivity value ($263.5 \text{ MJ mm ha}^{-1} \text{ h}^{-1} \text{ month}^{-1}$). In particular the regions of Jura, Swiss midland, northern Alpine foothill, and Ticino in the southern Alps show pronounced rainfall erosivity during that month. The months June to September have a total share of 62% of the total annual rainfall erosivity in Switzerland.

The current data highlight that rainfall erosivity has a very high variability within a year. These trends of seasonality vary between regions and consequently support that a dynamic soil erosion and natural hazard risk assessment is crucial. The combination of the temporally varying RUSLE factors (R- and C-factor) will lead to a more realistic and time-dependent estimation of soil erosion within a year, which is valuable for the identification of more susceptible seasons and regions. A mapping of the seasonality of the C-factor for a subsequent synthesis to a dynamic soil erosion risk assessment for Switzerland is envisaged in a later study.

The findings of this study have a number of important implications for soil conservation planning. Based on the knowledge of the variability of rainfall erosivity, agronomists can introduce selective erosion control measures, a change in crop or crop rotation to weaken of the rainfalls impact on soils and vegetation by increasing soil cover or stabilizing topsoil during these susceptible months. As such, a targeted erosion control for Switzerland not only reduces the direct costs of erosion by mitigation but also shrinks the costs for the implementation of control measures to a requested minimum.

Author contribution

S. Schmidt, K. Meusburger and C. Alewell analysed the data; S. Schmidt, K. Meusburger, C. Alewell, and P. Panagos wrote the paper.

Acknowledgements

The research has been funded by the Swiss Federal Office for the Environment (FOEN) (project N° N222-0350). We would like to thank MeteoSwiss, SwissTopo, and the cantons Lucerne, Berne, and St. Gallen for providing the datasets.

CHAPTER 4

Mapping spatio-temporal dynamics of the cover and management factor (C-factor) for grasslands in Switzerland

This chapter is published in Remote Sensing of Environment as:

Simon Schmidt¹, Christine Alewell¹, Katrin Meusburger^{1,2}: Mapping Spatio-Temporal Dynamics of the Cover and Management Factor (C-Factor) for Grasslands in Switzerland, *Remote Sens. Env.*, 211, 89-104, doi.org/10.1016/j.rse.2018.04.008, 2018.

¹Environmental Geosciences, University Basel, Bernoullistrasse 30, CH-4056 Basel, Switzerland

²Swiss Federal Institute for Forest, Snow and Landscape Research WSL, Zürcherstrasse 111, CH-8903 Birmensdorf, Switzerland

Abstract

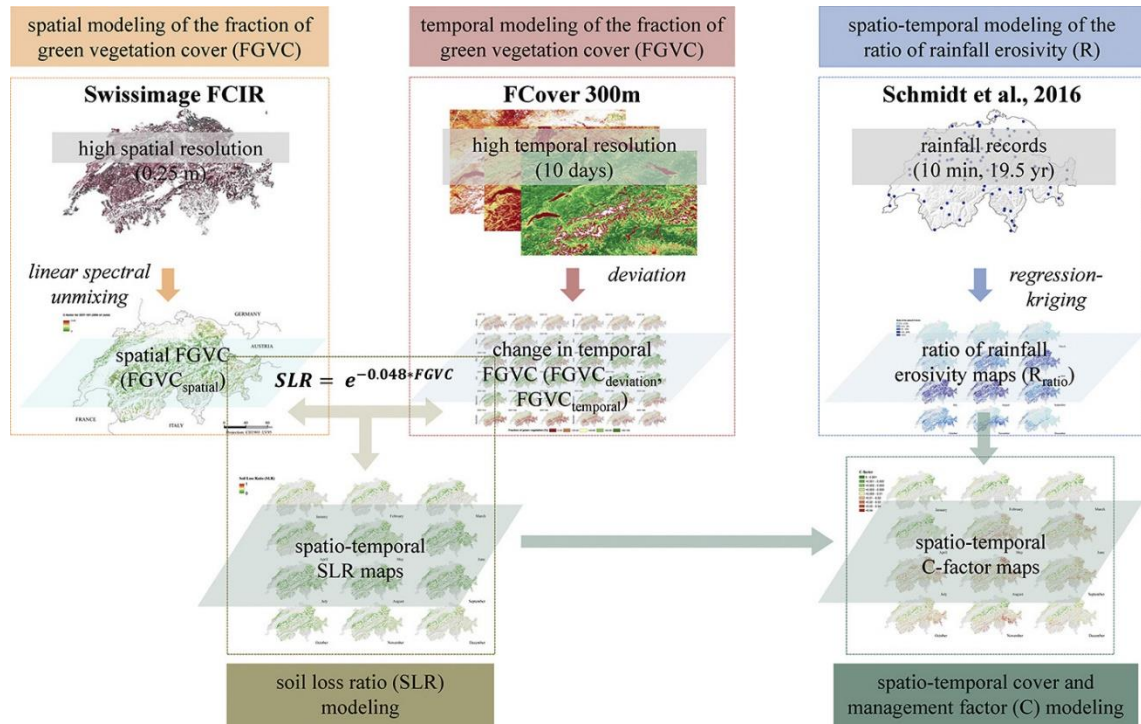
The decrease in vegetation cover is one of the main triggering factors for soil erosion of grasslands. Within the Revised Universal Soil Loss Equation (RUSLE), a model commonly used to describe soil erosion, the vegetation cover for grassland is expressed in the cover and management factor (C-factor). The site-specific C-factor is a combination of the relative erosion susceptibility of a particular plant development stage (here expressed as soil loss ratio SLR) and the corresponding rainfall pattern (here expressed as R-factor ratio). Thus, for grasslands the fraction of green vegetation cover (FGVC) determines the SLRs. Although Switzerland is a country dominated by grassland with high percentages of mountainous regions and evidence for high erosion rates of grassland exists, soil erosion risk modeling of grasslands and especially of mountainous grasslands in Switzerland is restricted to a few studies. Here, we present a spatio-temporal approach to assess the dynamics of the C-factor for Swiss grasslands and to identify erosion prone regions and seasons simultaneously. We combine different satellite data, aerial data, and derivative products like Climate Change Initiative (CCI) Land Cover, Swissimage false-color infrared (Swissimage FCIR), PROBA-V Fraction of green Vegetation Cover (FCover300m), and MODIS Vegetation Indices 16-Day L3 Global (MOD13Q1) for the FGVC mapping of grasslands. In the spatial mapping, the FGVC is extracted from Swissimage FCIR (spat. res. 2 m) by linear spectral unmixing (LSU). The spatially derived results are then fused with the 10-day deviations of temporal FGVC derived by FCover300m. Following the original RUSLE approach, the combined FGVC are transformed to SLRs and weighted with high spatio-temporal resolved ratios of R-factors to result in spatio-temporal C-factors for Swiss grasslands. The annual average C-factor of all Swiss grasslands is 0.012. Seasonal and regional patterns (low C in winter, high C in summer, dependency on elevation) are recognizable in the spatio-temporal mapping approach. They are mainly explicable by the R-factor distribution within a year. Knowledge about the spatio-temporal dynamic of erosion triggering factors is of high interest for agronomists who can introduce areal and time specific selective erosion control measures and thereby reduce the direct costs of mitigation as well as erosion measures.

Keywords: Monthly soil erosion modeling, Soil loss ratio SLR, R-factor, RUSLE, Vegetation dynamics, Swissimage, MODIS MOD13Q1, FCover, CCI land cover

Highlights:

- C-factor as a product of soil loss ratio SLR weighted by rainfall erosivity ratio.
- Annual C-factor (2014–2016) for Swiss grasslands: 0.012 (monthly range 0.003–0.025)
- Grassland C-factors show high seasonality and dependency on the elevation level. Highest C-factors within a year from May until September.

Graphical Abstract



4.1 Introduction

Among all soil erosion risk factors in USLE-type (Universal Soil Loss Equation) and USLE based soil erosion models (e.g., RUSLE Revised Universal Soil Loss Equation), the cover and management factor namely C-factor is the one most sensitive as it follows plant growth and rainfall dynamics (Wischmeier and Smith, 1978; Nearing et al., 2005). The C-factor represents the effect of cropping and management practices on soil erosion rates by water (Renard et al., 1997). The factor can be expressed as a combination of crop and plant systems, management, and rainfall pattern (Wischmeier and Smith, 1978). Following the USLE-original approach (Wischmeier and Smith, 1978; Schwertmann et al., 1987), a site-and time-specific C-factor is derived by the ratio of soil losses (soil loss ratio SLR) of a particular crop stage period (for arable land) or plant development stage (for grassland) weighted by its corresponding fraction of rainfall erosivity (R-factor ratio; Renard et al., 1997). Thus, the rainfall erosivity is considered twice in the RUSLE: as R-factor and as a weighting factor of the C-factor (Schwertmann et al., 1987). Alternatively, SLRs are a multiplication of sub-factors (previous land use, canopy cover, surface cover, surface roughness, soil moisture; Renard et al., 1997). C-factor values are equaling 1 for bare soil of the reference plot and reach a minimum in forests (C-factor = 0.0001; Wischmeier and Smith, 1978). The C-factor is the most adjustable factor by land use management (Durán Zuazo and Rodríguez Pleguezuelo, 2008; Maetens et al., 2012; Biddoccu et al., 2014; Eshel et al., 2015; Biddoccu et al., 2016) with the highest amplitude of spatial and temporal variation among all the RUSLE factors (Zhang et al., 2011; Estrada-Carmona et al., 2016). Thus, the factor can easily alter by a change of policy and farming strategies (McCool et al., 1995; Panagos et al., 2015e). An alteration of the support practice factor (P) (e.g., introducing of stone walls, grass margins, contour farming, terracing) often requires higher financial investments and soil conservation subsidies (Panagos et al., 2015c; 2015d). Other important soil erosion risk factors such as rainfall erosivity (R), soil erodibility (K) and topography (LS) are mainly determined by natural conditions and are relatively more independent from anthropogenic interventions.

SLRs of grassland are preferably determined by vegetation cover fraction in contrast to arable land where plant type and/or rotation is the influencing factor (Schindler Wildhaber et al., 2012). The fractional vegetation cover is one of the most critical factors in soil erosion modeling as it describes a negatively exponential or negatively linear relationship (according to the different types of vegetation) to soil erosion (McCool et al., 1995; Puigdefábregas, 2005; Vrieling et al., 2008). A dense vegetation cover protects the soil against the raindrop splash effect (Schwertmann et al., 1987), causes a stabilization of the soil structure by plant roots (Jury and Horton, 2004; Pohl et al., 2009), enriches soils by soil organic carbon, leads to soil aggregation (Lugato et al., 2014), reduces runoff flow velocity (Bochet et al., 2006), and thus mitigates the susceptibility to soil loss (Durán Zuazo and Rodríguez Pleguezuelo, 2008; Zhou et al., 2008; Wang et al., 2009; Butt et al., 2010; Sun et al., 2013). As such, grassland cover has a high protective function for soils (Martin et al., 2010; Schindler Wildhaber et al., 2012). However, due to disturbance (García-Ruiz et al., 2015; Merz et al., 2009; Meusburger and Alewell, 2014; Sutter, 2007; Sutter and Keller, 2009; Panagos et al., 2014b), harsh climate and snow processes (Ceaglio et al., 2012; Meusburger et al., 2014), the vegetation cover can be disturbed and the consequent soil losses might be substantial. If vegetation cover is partially (66% fractional vegetation cover, Felix and Johannes, 1995) or nearly completely reduced (Frankenberg et al., 1995), erosion rates are considerably higher ($4.4 \text{ t ha}^{-1} \text{ yr}^{-1}$ and $20 \text{ t ha}^{-1} \text{ yr}^{-1}$,

respectively). Switzerland is a country dominated by grassland (Jeangros and Thomet, 2004). Nonetheless, up to now, soil erosion risk modeling is mainly restricted to arable land although evidence for high erosion rates of grasslands exists (Alewell et al., 2009; Martin et al., 2010; Meusbürger et al., 2010a; 2010b; 2014; Konz et al., 2012; Meusbürger and Alewell, 2014; Alewell et al., 2014).

Commonly, remote sensing approaches to determine the C-factors (Vrieling, 2006; Zhang et al., 2011; Panagos et al., 2014b) are not calculating SLRs but frequently assess the C-factor directly without weighting SLRs with the intra-annual distribution of rainfall erosivity to assess C-factors in the original sense of (R)USLE. Remote sensing methods for C-factor determination are often based on vegetation indices like the Normalized Difference Vegetation Index (NDVI). NDVIs are directly transformed to C-factors by a linear (de Jong et al., 1998) or exponential regression (van der Knijff et al., 2000) or related to field observations (Karaburun, 2010; Vatandaşlar and Yavuz, 2017). NDVI based C-factor modeling also exists for determining the C-factor for mountainous grasslands (regions of Korea, Lee and Won, 2012; China, Zhang and Li, 2015; Kyrgyzstan, Kulikov et al., 2016; Turkey, Vatandaşlar and Yavuz, 2017). However, drawbacks of that technique are its uncertainty due to the poor correlation with vegetation attributions, the soil reflectance, and the changing vitality of plants (de Jong, 1994; Vrieling, 2006; Asis and Omasa, 2007; Montandon and Small, 2008; Meusbürger et al., 2010a; Grauso et al., 2015; Panagos et al., 2015c). As an alternative to NDVI-based approaches, spectral unmixing can estimate the fractional abundance of green vegetation (here called the fraction of green vegetation cover FGVC) and bare soils/ bedrock simultaneously (Paringit and Nadaoka, 2003; Guerschman et al., 2009) which are related to C-factors after including rainfall erosivity (Yang, 2014). Spectral unmixing techniques (e.g., linear spectral unmixing LSU) are used in many erosion studies to determine C-factors over the last years (Hill et al., 1995; Ma et al., 2003; Lu et al., 2004; Asis and Omasa, 2007; Asis et al., 2008; de Jong and Epema, 2010; Meusbürger et al., 2010a; 2010b). An advantage of spectral unmixing compared to traditional hard classification methods is the decomposition of mixed pixels in its corresponding component fractions rather than assigning them to a unique single class (Foody, 2006). Under consideration of the NDVI-related disadvantages, Asis and Omasa (2007), Asis et al. (2008) and Yang (2014) perform a comparative analysis of C-factors, derived from NDVI- and LSU-approaches, which result in better results for LSU. A relationship between C-factor and canopy cover fraction can be observed in various studies. Zhang et al. (2003) and Gao et al. (2012) determine an exponential decrease of the C-factor with an increase in canopy cover of grasslands. Wischmeier and Smith (1978) also observed a negatively exponential relationship of decreasing C-factors with increasing coverage in their empirical experiments on the USLE plots.

The (R)USLE factors C and R are highly dynamic with a clear annual cycle (Wischmeier and Smith, 1978; Renard and Freimund, 1994; Vrieling, 2006; Vrieling et al., 2014; Möller et al., 2017) in contrast to the rather constant RUSLE-factors K and LS (Panagos et al., 2012a; Alexandridis et al., 2015). The status of grasslands is diversified within a year owing to the natural growth cycle, periodical cutting of hay, or pasture farming (Wiegand et al., 2008). Despite, this spatio-temporal variability of the C-factor for grasslands, it is often parameterized without accounting for the spatial variability within a land cover unit (Ozcan et al., 2008; Bosco et al., 2009; Efthimiou, 2016; Mancino et al., 2016) nor for the temporal variations (Wang et al., 2002). Hawkins (1985) stated already that “the complications of time and spatial variations in site properties are usually not considered” by applying the USLE. Alexandridis et al. (2015)

conclude that a dynamic approach focusing on C-factors for the four seasons or 12 months of a year might help to reduce errors in the annual soil loss compared to a single annual C-factor. Vrieling et al. (2008, 2014) follow a multi-temporal and spatial approach to assess the riskiest erosion periods of the year for Brazil and Africa. López-Vicente et al. (2008) capture erosive periods among a year for a study area in the mountains of the Central Spanish Pyrenees by a dynamic approach on a monthly scale. Such time-dependent assessments of soil loss are relevant to support policy makers and farmers to protect the soil more targeted like it was done by López-Vicente et al. (2008). Panagos et al. (2012, 2016) and Karydas and Panagos (2016, 2017) propose a monthly time-step to be appropriate for soil erosion modeling. The same resolution was already proposed by Wischmeier and Smith (1965). Grazhdani and Shumka (2007) modeled the soil erosion rate for Albania on a monthly scale. A combination of both spatially and temporally varying R- and C-factors lead to a more dynamic soil erosion risk assessment and simultaneously allows the identification of susceptible seasons and regions (Panagos et al., 2014b; Ballabio et al., 2017; Möller et al., 2017). As it is shown in Meusburger et al. (2012), Schmidt et al. (2016), and Ballabio et al. (2017), the R-factor of Switzerland also has a high intra-annual variability with clear regional patterns.

So far, most of the existing national C-Factor maps either do not include grassland areas (Friedli, 2006; Alexandridis et al., 2015), do not consider the temporal variations of vegetation cover and management (Friedli, 2006; Bosco et al., 2009; Panagos et al., 2015c), nor taking rainfall erosivity for C-factor calculation into account. An assessment following the original approach by Wischmeier and Smith (1978) to derive C-factor maps with a high spatio-temporal resolution based on SLRs and spatio-temporal R-factor ratios does not yet exist on a national scale. We aim to (i) determine the fractional vegetation cover with a linear spectral unmixing of orthophotos (2 m spatial resolution), and (ii) quantify the temporal change of vegetation fraction (10 days temporal resolution) to (iii) assess the spatial and temporal patterns of the C-factor based on SLRs and high-spatio-temporal R-factor ratios.

4.2 Material and methods

4.2.1 Swiss grassland areas

Switzerland is a country with a high heterogeneity of climatic, topographic and edaphic conditions. Hills and mountains cover more than one-third of the state. The Swiss elevation ranges can be clustered in elevation zones (in m a.s.l. modified after Ellenberg et al., 2010: Colline zone <800; Montane >800-1800; Subalpine >1800–2300; Alpine >2300–2700; Subnival >2700–3100; Nival >3100), which are typical for the plant development in the Swiss Alps. Owing to these natural conditions, permanent grassland is the predominant land use in about 28% of the territory of Switzerland with a share of 72% of the total agricultural area (Bötsch, 2004; Jeangros and Thomet, 2004; Schmidt et al., 2018a). Grassland is the prevailing land use type at elevations above 1500 m a.s.l. (Hotz and Weibel, 2005). Almost half (46%) of the grassland area is therefore designated as alpine grassland (Hotz and Weibel, 2005). Alpine soils have been managed by humans for about 500 years already, but an intensification of the usage and management of grasslands can be observed since the last 50 years (Jeangros and Thomet, 2004; Bätzing, 2015; Alewell et al., 2008). Changes in grassland cover are expected due to land use and climate change.

4.2.2 Datasets for C-factor mapping

We subdivided the datasets of the C-factor mapping approach into data for the spatial and for the temporal assessment. In the spatial modeling approach, we used a high spatial resolution false-color infrared orthophoto (0.25 to 0.50 m; G R NIR) mosaicked of a set of 3432 tiles. This orthophoto mosaic called Swissimage FCIR (Swisstopo, 2010) is recorded with a Leica ADS80 airborne digital sensor, containing the channels green (533–587 nm), red (604–664 nm) and near-infrared (833–920 nm). The production process of Swissimage FCIR is based on an along-track scanning from east to west that generates stripes of aerial photos during each flight. The scheduling of the flights of the used version of Swissimage FCIR was in the years 2012, 2013, 2014 and 2015 between the months March and September. In the preprocessing step, the aerial photos have undergone a georeferencing, orthorectification, mosaicking, and clipping to tiles of 4375 m × 3000 m by Swisstopo. We reduced the file size (original file size 1.17 Gigabytes per tile) and the spatial resolution by resampling to 2 m for a more straightforward data handling.

The temporal variations of grassland cover in Switzerland are derived from time series of 10-day fractions of the green vegetation cover (FCover300m, spatial resolution 300 m; Smets et al., 2017) as a product from PROBA-V. The FGVC is expressed in percentages from 0% (no vegetation cover) to 100% (full vegetation cover). PROBA-V is a satellite with an assembled vegetation (V) instrument to image the global land surface vegetation regularly (Blair, 2013).

A long-term recording sequence (2005–2015) of 16-day vegetation indices (MOD13Q1, spatial resolution 250 m; Didan et al., 2015) of the Moderate Resolution Imaging Spectroradiometer (MODIS) is used as supplementary data. Based on MOD13Q1, we determine the day of the year (DOY) with the highest NDVI values to be used as an indicator date for a maximum in plant growth (Leilei et al., 2014). This information is relevant for normalizing different recording periods of the Swissimage to the date of the peak growing period. A data accuracy modification was applied for MOD13Q1. Not processed or filled data, marginal data, and cloudy grid cells were substituted either by the preceding or succeeding good data or snow/ice data. With this routine, unreliable pixels were adjusted by the temporally closest reliable values.

Table 4.1: Datasets used for C-factor modeling of Swiss grasslands.

dataset	derived information	resolution	source
Swissimage FCIR	spatial distribution of FGVC ^a	0.25 m spatial resolution, spectral bands NIR, R, G	Swisstopo, 2010
FCover300m	temporal variation of FGVC ^a	10-day temporal resolution (2014 to 2016)	Smets et al., 2017
MOD13Q1	DOY ^b with maximum NDVI	16-day temporal resolution (2005 to 2015)	Didan et al., 2015
Swiss National Grassland Map	extent of Swiss grasslands of 2015	300 m spatial resolution, improved with swissTLM3D and vector25	Schmidt et al., 2018a
CCI Land Cover	dynamic long-term snow occurrence	500 m spatial resolution, annual resolution (1992 to 2015)	Arino and Ramoino, 2017
SwissAlti3D	digital elevation model	2 m spatial resolution	Swisstopo, 2018a

Rainfall erosivity	Rainfall erosivity of Swiss grasslands	100 m spatial resolution, based on 87 rainfall stations	Schmidt et al., 2016
--------------------	--	---	----------------------

^aFGVC Fraction of Green Vegetation Cover

^bDOY Day of the Year.

We used the Swiss National Grassland Map of the year 2015 (Schmidt et al., 2018a) for clipping the previously mentioned datasets to the grassland extent. Further, the dynamics of the long-term snow occurrence in Switzerland (Fig. S5.1) are derived from the Climate Change Initiative (CCI) Land Cover provided by the European Space Agency (ESA) (Arino and Ramoino, 2017). Elevation zones are extracted from the Swiss digital elevation model (SwissAlti3D, Swisstopo, 2018a). An overview of all used datasets is provided in Table 4.1. Data processing was done in ENVI 5.3., ESRI ArcGIS 10.3.1., and GDAL 2.1.3.

4.2.3 Concept of C-factor mapping for Swiss grasslands

Firstly, we derived the spatial pattern of Fraction of Green Vegetation Cover ($FGVC_{\text{spatial}}$) by LSU from the high spatial resolution Swissimage FCIR (chapter 4.2.3.1). Secondly, we used FCover300m to estimate the temporal changes in the FGVC ($FGVC_{\text{temporal}}$; chapter 4.2.3.2). Both approaches, the high spatial and the high temporal one are combined (Chen et al., 2015; Zhang and Li, 2015) via a normalizing procedure to result in a set of monthly FGVC maps for Switzerland (chapter 4.2.3.3). This procedure involves the normalization of the orthophoto mosaic Swissimage FCIR with the temporal variations in vegetation cover of FCover300m to a given base date. The normalized high spatial and temporal $FGVC_{\text{spatio-temp}}$ maps of Swiss grasslands were then converted to SLR maps. The relationship of SLR and the fraction of vegetation cover (FVC) is based on measured data in alpine grasslands by Martin et al. (2010) and Schindler Wildhaber et al. (2012). SLRs were derived from the measured sediment yield for the given FVC classes proportional to an uncovered soil surface (SLR 100%; Schwertmann et al., 1987). SLR and FVC describe an exponential relationship (Eq. 4.1, Fig. 4.1). The SLRs are multiplied by the corresponding proportion of rainfall erosivity (R_{ratio}) to result in the C-factor according to the original approach by Wischmeier and Smith (1978) and Schwertmann et al. (1987). Monthly R_{ratio} for Swiss grasslands with a spatial resolution of 100 m can be obtained from Schmidt et al. (2016). The processing workflow and manipulation of data is visualized in Fig. 4.2.

$$SLR = e^{-0.048 \cdot FVC} \quad \text{and} \quad FVC \approx FGVC \quad (4.1)$$

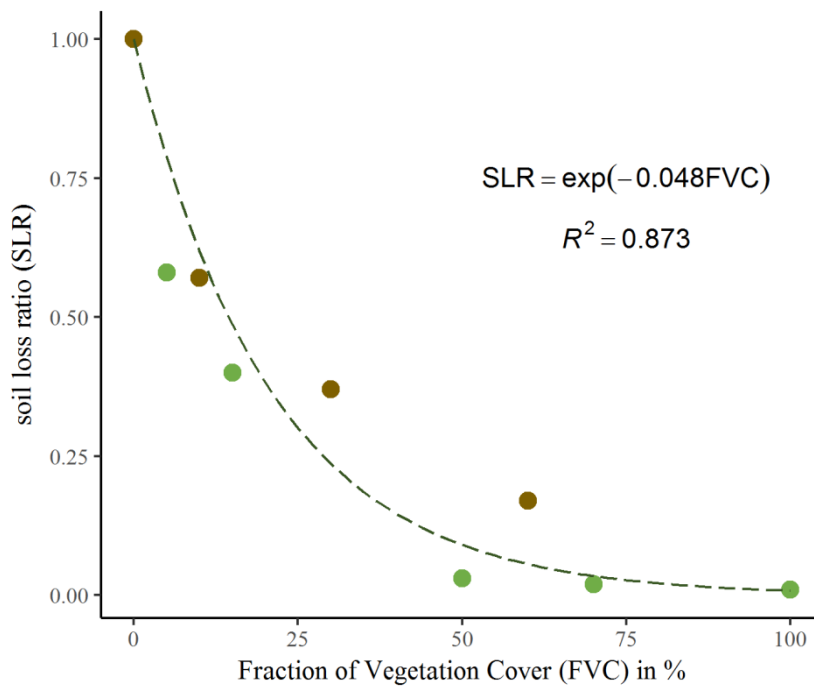


Fig. 4.1: Negative exponential relationship of the fraction of vegetation cover (FVC) and the soil loss ratio (SLR). The relationship of FVC and SLR results from rainfall simulations by Martin et al. (2010) (brown dots) and Schindler Wildhaber et al. (2012) (green dots).

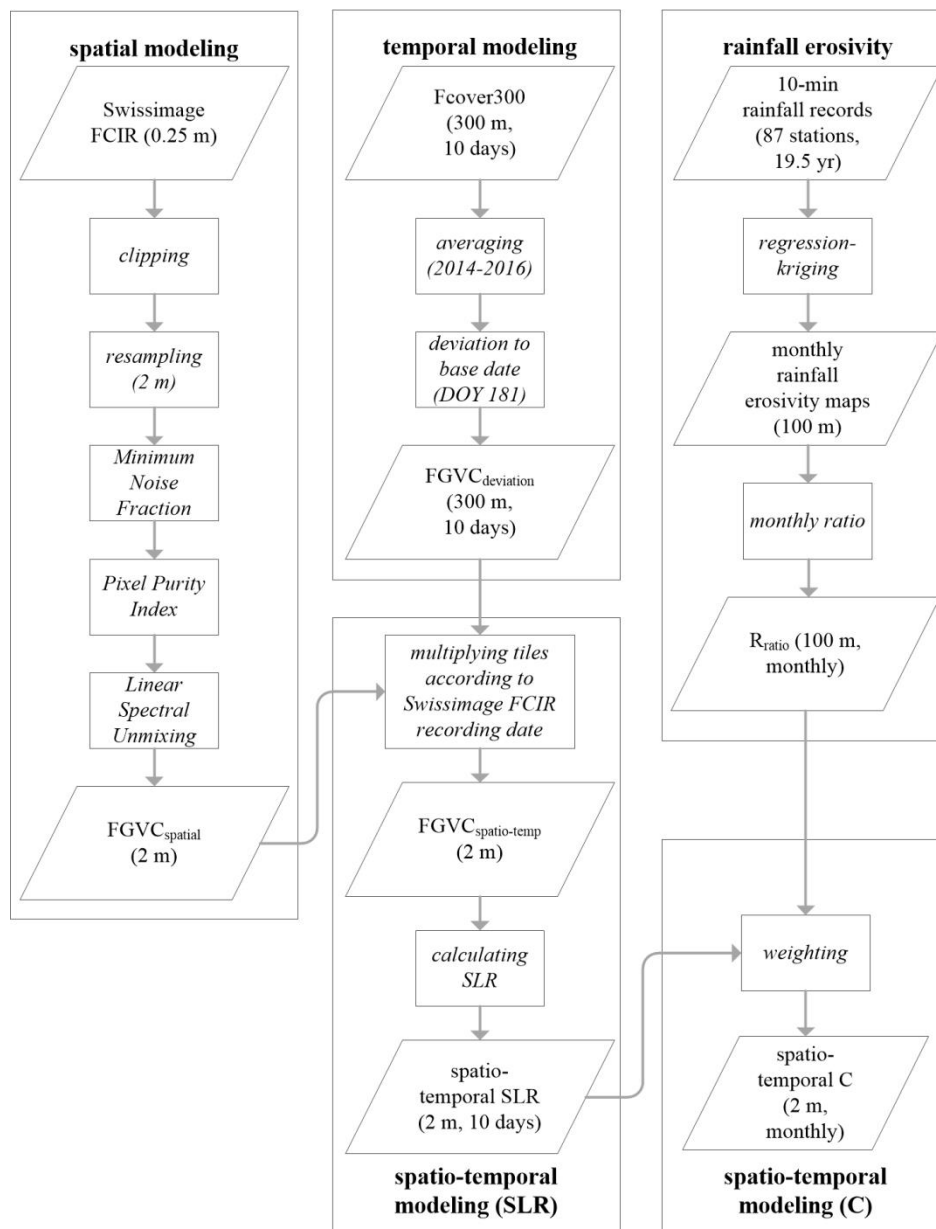


Fig. 4.2: Processing workflow (rectangles) of the used and derived datasets (parallelograms; detailed description of the datasets see Table 4.1) to result in spatio-temporal C-factors of Swiss grasslands.

4.2.3.1 Spatial modeling of fraction of green vegetation cover (FGVC_{spatial}) by linear spectral unmixing

Spectral unmixing assumes that the spectrum measured by a sensor and represented as a mixed pixel is a combination of the spectra of components within the instantaneous field of view. As such, the reflectance of a mixed pixel is a mixture of distinct spectra (Roberts et al., 1993; Gilabert, 2000; Heidari Mozaffar et al., 2008). In spectral unmixing techniques, the mixed pixel is decomposed into a collection of endmembers and a set of fractional abundances according to the endmembers (Keshava and Mustard, 2002). The image endmembers, also called pure pixels, are at the vertices of the image simplex in an n-dimensional space (Smith et al., 1985). Pixels defined as endmembers are relatively unmixed with other endmember signals

(Rogge et al., 2007). Among the spectral mixture methods, the LSU is by far the most common type (Asis and Omasa, 2007). LSU assumes that the incoming radiation only interacts with a single component of surface and is represented in a mixed pixel without multiple scattering between different components (van der Meer and Jong, 2010). Although this is a crucial assumption, the effects of intimate association between the components have been found to be relatively minor (Kerdiles and Grondona, 1995). LSU is expressed as the spectral reflectance (R_i) of the mixed pixel in band i as followed (Smith et al., 1990; Hill et al., 1995; Asis et al., 2008):

$$\mathbf{R}_i = \sum_{j=1}^n \mathbf{f}_j \mathbf{r}_{ij} + \boldsymbol{\varepsilon}_i \quad \text{and} \quad \sum_{j=1}^n \mathbf{f}_j = \mathbf{1} \quad (4.2)$$

where j is the number of endmembers, f_j the fraction of the pixel area covered by the endmember j , r_{ij} itself is the reflectance of the endmember j in band i and ε_i the residual error in band i . In the present case, the sum of all fractions (f_j) is constrained to a value of 1 (100%; Heinz and Chein-I-Chang, 2001). A root-mean-square-error (RMSE) of the residuals for each pixel indicates the error between the measured and the modeled spectra whereas M is the total number of bands (Roberts et al., 1999; Dennison and Roberts, 2003; Bachmann, 2007):

$$\text{RMSE} = \sqrt{\frac{\sum_{j=1}^M (\varepsilon_i)^2}{M}} = \sqrt{\frac{\sum_{j=1}^M (b_i - b_i^*)^2}{M}} \quad (4.3)$$

b_i is the measured and b_i^* is the modeled signal of all the bands M . A small RMSE indicates that endmembers are appropriately selected, and its number is sufficient (Mather and Koch, 2011). LSU of QuickBird data was already applied with reasonable results for deriving vegetation parameters for an alpine grassland catchment in Switzerland ($R^2 = 0.85$ in relation to ground truth measurements; Meusburger et al., 2010a). However, QuickBird data is too cost intensive and heterogeneous for a national assessment and therefore rather applicable for catchment studies like it was done by Meusburger et al. (2010a, 2010b). Guerschman et al. (2009) use the hyperspectral EO-1 Hyperion in combination with MODIS data to result in a higher variety of endmembers with a spatial resolution of 1000 m. However, that spatial resolution of fractional cover is relatively coarse to explain the spatial patterns of the FGVC, SLRs and C-factors.

In the present study, orthophotos (Swissimage FCIR) with a national coverage and resampled resolution of 2 m (resampled from 0.25 m to 0.5 m) were used. The spatial assessment for deriving $\text{FGVC}_{\text{spatial}}$ (see Fig. 4.2) is based on all three bands of the Swissimage FCIR. ENVI 5.2 provides a Pixel Purity Index tool (PPI) to automatically identify the most spectrally pure pixels of the image, designated to be the mixing endmembers (Pal et al., 2011; RSI Research Systems, 2004). PPI works with an iterative process by counting the number of times a pixel is registered as extreme pixel for each run. Pixels that appear to be extreme most often are then endmembers (González et al., 2010). We performed 10.000 iterations with a threshold value of 2.5 and identified a maximum of 100.000 pure pixels. The application of LSU can result in $n + 1$ endmembers where n is the number of bands (Phillips et al., 2005). PPI based on the three bands (G, R, and NIR) of Swissimage FCIR and determined the following endmembers namely i) vegetation, ii) bedrock, bare soil, asphalt, and iii) shade. These endmembers are the typical groups of endmembers which are distributed all over the grassland

areas in the country (Roberts et al., 1993; Adams et al., 1995; Theseira et al., 2003; Meusburger et al., 2010a). Although the spectrum of water is relatively pure, water was not selected as an endmember since it is occurring only locally (Adams et al., 1995).

Swissimage FCIR has undergone a Minimum Noise Fraction (MNF) rotation before the selection of purest pixel and unmixing (Green et al., 1988). The MNF rotation is a two-step principle component analysis and used to determine the inherent dimensionality of the image data, to improve the signal-to-noise ratio and reduce the processing time (Boardman and Kruse, 1994; Nascimento and Dias, 2005). MNF can improve the quality of the resulting abundance maps by a decorrelation of the bands (van der Meer and de Jong, 2000). Furthermore, since the spectra are neither purposed to be linked to laboratory and field reflectance spectra nor to be meant for temporal approaches, a transformation of encoded-radiances in digital numbers (DN) was not required in this study (Adams et al., 1995; van der Meer, 2002).

A well-known problem of FGVC mapping is its underestimation due to the presence of dry vegetation (Meusburger et al., 2010a; 2010b). This problem can either be addressed by long-wave spectral bands in hyperspectral sensors at the expense of spatial resolution (Guerschman et al. 2009) or by a calibration of the approach. As we aim to explain the spatio-temporal dynamics in soil erosion for Switzerland, we decided to preserve the high spatial resolution of our dataset (Swissimage FCIR) and followed the second option by using 1000 calibration points ($FGVC_{cal}$) to calibrate the $FGVC_{spatial}$ (based on the LSU) and to identify potential biases in the automated assignment of vegetation abundances. These points are randomly set for grassland areas. The $FGVC_{cal}$ is estimated user-driven for each point based on the 0.25 m resolved Swissimage FCIR and RGB. Besides that, the types of vegetation (photosynthetic and non-photosynthetic grassland, clipped grass, forest) or non-vegetation (shade, asphalt), slope degree and exposition are recorded. Although the calibration procedure assesses dry vegetation, it is not to be differentiated from bare soil in the LSU approach. Thus, the endmember of bare soil includes e.g. non-photosynthetic grassland. Thereby, the unmixed vegetation cover can be calibrated by the biases of dry vegetation. The density of optimization points is 37 km², corresponding to one optimization point for each 6 to 6 km on average. An acquisition of ground truth data with a representative distribution in the field is hardly feasible on a national scale.

4.2.3.2 Temporal mapping of fraction of green vegetation cover ($FGVC_{temporal}$ and $FGVC_{deviation}$)

Temporal variations of the fraction of green vegetation cover ($FGVC_{temporal}$) are provided within the FCover300m dataset. We averaged three files of the same date by the years 2014 to 2016 to a short-term mean fraction of green vegetation ($FGVC_{temporal}$; see Fig. 4.2; Smets et al., 2017). Each of the three years of FCover300m is represented by a set of 36 files (108 files in total) in a 10-day resolution from 10th of January to 31st of December. The deviation of $FGVC_{temporal}$ to a base date is determined on a per pixel scale ($FGVC_{deviation}$) to be used for normalizing the $FGVC_{spatial}$ in the following chapter 4.2.3.3. The processing of the FCover300m data is done within the Copernicus program where FCover is derived from the leaf area index and further canopy structural variables (Smets et al., 2017). Concerning its computation, FCover300m is more robust than classical vegetation indexes like NDVI which has stronger dependencies on geometry and illumination of surface cover (Weiss et al., 2000; Fontana et al., 2008).

A series of 253 NDVI datasets from 2005 to 2015 of the MOD13Q1 (Didan et al., 2015) were used for determining this respective base date as mean peak growing season indicated by the maximum NDVI within a year (Leilei et al., 2014). Fontana et al. (2008) demonstrate that the relationship between plant growth records in alpine grasslands and NDVI is quite remarkable. Busetto et al. (2010) use a time series from 2005 to 2007 of MOD13Q1 to determine the start and the end of the growing season of larches in the alpine region. For more robust results we averaged all ten years by each specific recording date to derive a mean NDVI per recording date for Switzerland. A correction of snow cover like it was done by Busetto et al. (2010) was neglected in the study as we are only focusing on the assessment of the peak growing season and not on minimum NDVI. The maximum NDVI of all the averaged datasets was selected for each cell and the corresponding DOY assigned to the associated cell. If a cell contained a no data value, it was skipped and the averaging done over the cells of the remaining year(s).

4.2.3.3. Merging of spatial and temporal fraction of green vegetation cover ($FGVC_{spatio-temp}$)

As Swissimage is a mosaic of tiles recorded at heterogeneous dates, the vegetation cover can be assumed to be different between tiles according to its recording date. We used a normalizing process to make all tiles comparable. Therefore, the $FGVC_{spatial}$ are normalized to a base date. The spatial results, as well as the temporal results, are meant for being combined to spatio-temporal $FGVC_{spatio-temp}$ of grasslands (see Fig. 4.2). First of all, we extracted the recording dates of each along-track scanning stripe, and spatially joined the dates with the 3432 image tiles. In cases of multiple recording dates, we used the mode to extract the most common date. Tiles with same recording dates were aggregated to a multiple tile mask (Fig. S4.2) and later used to clip the $FGVC_{spatial}$ according to their recording dates.

Each $FGVC_{spatial}$ tileset of a specific DOY i can be normalized to that base date by weighting it with the relative change of the $FGVC_{deviation}$ to the same base date as expressed in Eq. 4.4:

$$FGVC_{norm\ i} = (FGVC_{spatial\ i} * FGVC_{deviation\ i}) + FGVC_{spatial\ i} \quad (4.4)$$

Thus, tiles recorded early in the season where the plant growth can be assumed to be low are weighed by a greater $FGVC_{deviation}$ factor compared to an image tile recorded close to the base date.

All $FGVC_{norm}$ are merged to a new raster which represents a national map of FGVC at the defined base date. The normalized composite raster of the base date can then be recalculated to other dates.

4.2.4 Spatio-temporal mapping of grassland C-factors by considering soil loss ratios (SLRs) and rainfall erosivity (R-factor)

Originating from the $FGVC_{spatio-temp}$, the SLR can be calculated with the relationship proposed in Eq. 5.1. SLRs express the ratio of soil loss of an area with a certain plant development relative to an uncovered surface (Renard et al., 1997). The SLRs are weighted with the ratio of the total annual rainfall erosivity (R_{ratio}) of the same period to result in the C-factor. The R_{ratio} can be derived from monthly R-factor maps which exist with a high spatial resolution (100 m) for Switzerland (Schmidt et al., 2016). Monthly rainfall erosivity maps (100 m spatial resolution) for Switzerland are generated by regression-kriging of 10-min rainfall records at 87

automated gauging stations (19.5 yrs. measuring sequences) and with the use of up to five spatial covariates. The 12 maps have a mean R^2 of 0.51 and a mean RMSE of $93.27 \text{ MJ mm ha}^{-1} \text{ h}^{-1} \text{ month}^{-1}$ with highest uncertainties in winter due to generally low rainfall erosivity. The authors have discussed the variability of monthly R-factors for Switzerland in detail. R_{ratio} can be assessed by calculating the monthly fraction of R-factor of the sum of all 12 maps. For the present purpose of Swiss grasslands, the monthly national maps of the R-factor are clipped to the extent of the improved Swiss National Grassland Map (Schmidt et al., 2018a). The R_{ratio} maps are multiplied with the SLR maps for grassland to result in monthly C-factor maps with a high spatial resolution. For each month we averaged the three corresponding FGVC_{spatio-temp} maps to monthly FGVC maps to comply with the temporal resolution of the R-factor maps.

4.3 Results and discussion

4.3.1. Spatial pattern of the fraction of green vegetation cover of Swiss grasslands

The optimized LSU of the Swissimage FCIR enables the differentiation of the $FGVC_{\text{spatial}}$ as well as the fractions for bare soil and bedrock. Spatial patterns of $FGVC_{\text{spatial}}$ are visualized on a national scale as well on a local level (Fig. 4.3). Such an analysis of the degree of fractional vegetation cover is of high relevance when categorizing land use for potential hot spots of erosion since it is more likely that an erosion process starts from the uncovered or bare soil.

The dimensionality of the Swissimage FCIR stays unchanged after noise segregation by MNF. The estimated ranges of $FGVC_{\text{spatial}}$ had 0.56% outliers outside the LSU constrained range of 0 to 1 (100%), which indicates that one or more of the endmembers chosen for the analysis is probably not well-characterized or that additional endmembers might be missing (RSI Research Systems, 2004). These outliers were omitted. They predominantly consisted of constructed environments (buildings, streets) that could not be masked in the grassland areas (Schmidt et al., 2018a). The RMSE of the LSU for Switzerland is 22.6%. Higher uncertainties generally occur in the valleys of the Alpine foothill (Fig. 4.4). One reason for the high RMSE is the incorrect separation of grassland from arable land due to the coarse resolution (300 m) of the grassland map based on CCI Land Cover.

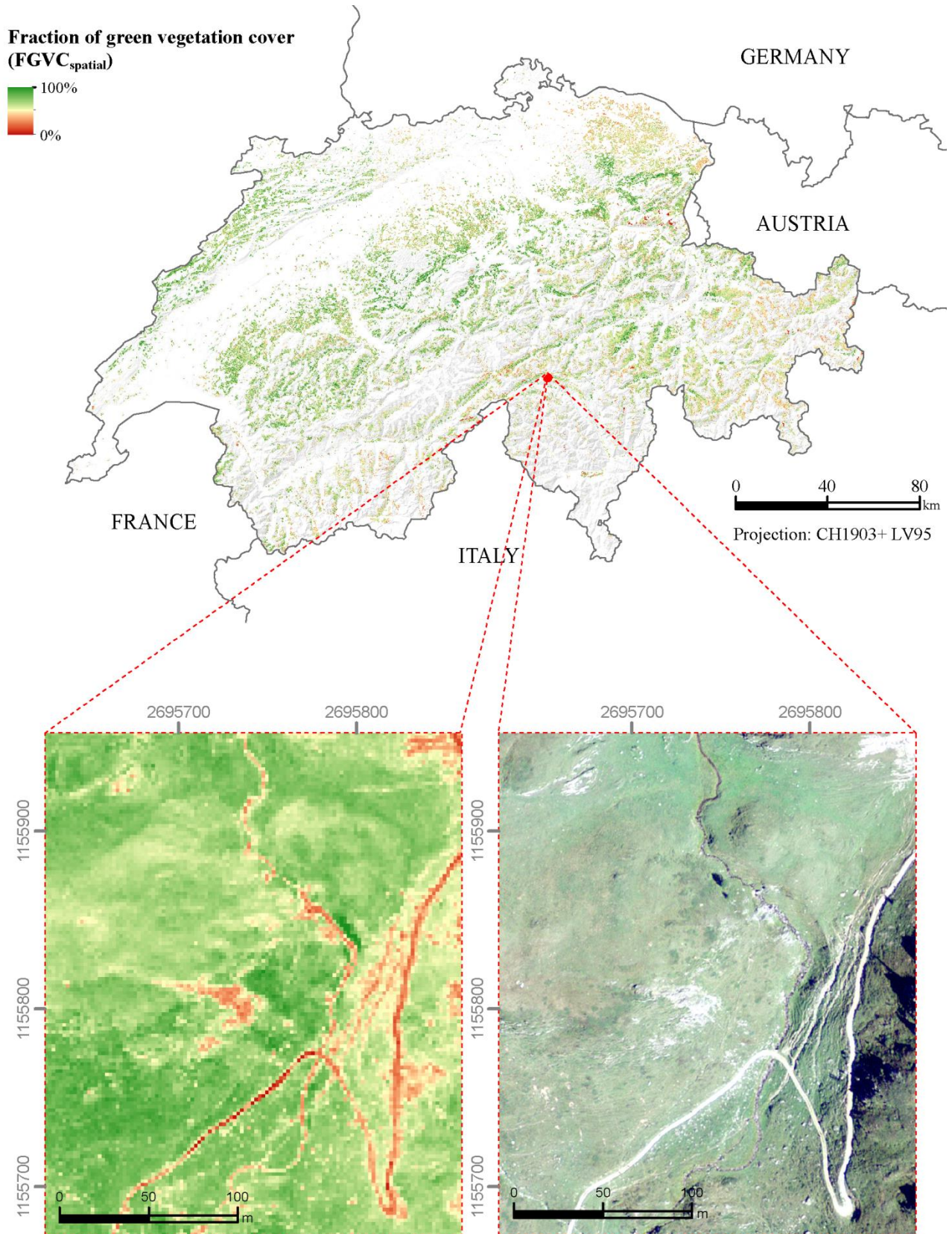


Fig. 4.3: Spatial patterns of the fraction of green vegetation cover (FGVC_{spatial}) and the orthophoto Swissimage RGB (bottom right) on different scales. The FGVC_{spatial} is presented on

a national and a local scale (spat. resolution 2 m). The Swissimage RGB (spat. resolution 0.25 m) represents the landscape on the local level.

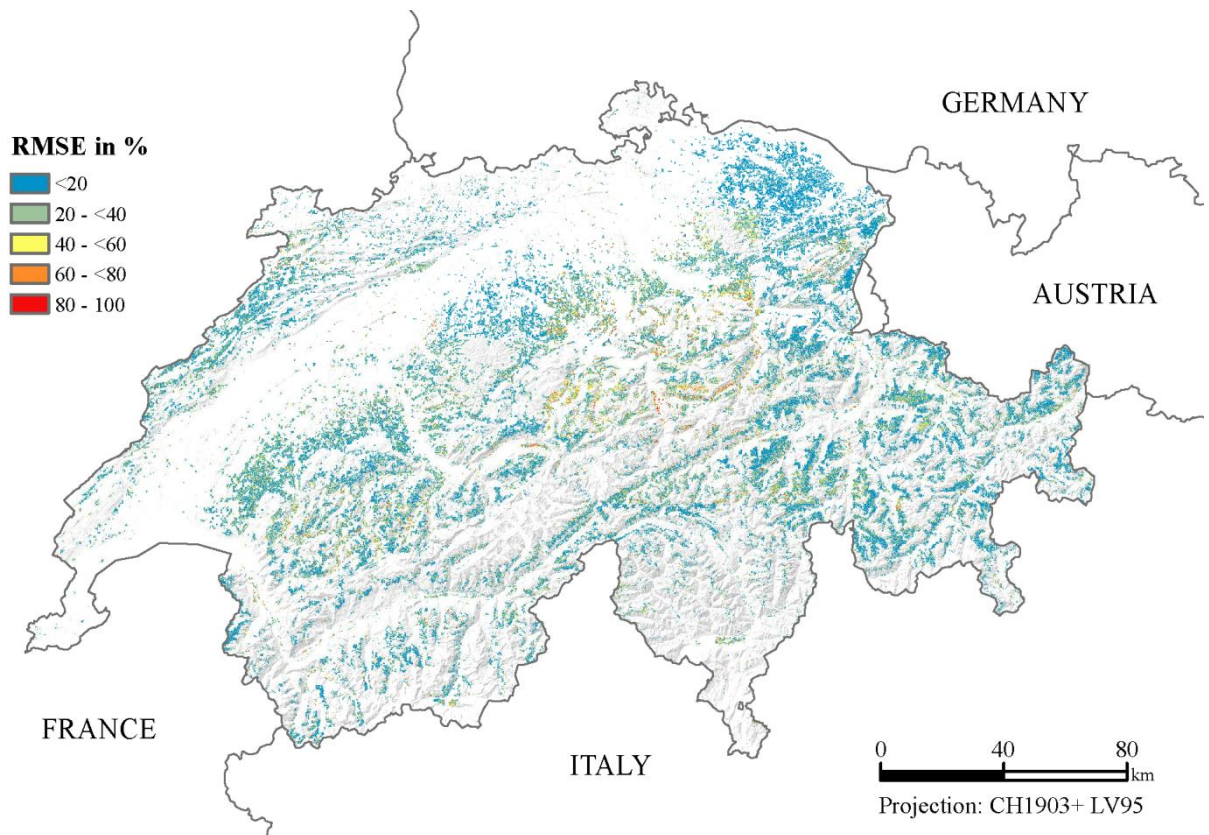


Fig. 4.4: RMSE of the calculated abundances based on LSU for Switzerland.

The mean FGVC of the 1000 calibration points ($FGVC_{cal}$; 61%) identifies a systematic underestimation of the mean $FGVC_{spatial}$ (39%) by 22% which is close to the mean RMSE. The highest discrepancy between $FGVC_{cal}$ and $FGVC_{spatial}$ mainly arises by an erroneous classification of non-photosynthetic vegetation (33% deviation), shades and artifacts (42% deviation), and forested areas (46% deviation). The segregation of non-photosynthetic vegetation and bare soil is impeded due to the very similar spectral characteristics. Shaded areas and artifacts disrupt the spectral signal of vegetation cover which is visually detectable but automatically assigned with a very low degree of coverage. The pattern of discrepancy between $FGVC_{cal}$ and $FGVC_{spatial}$ show a strong dependency to slope exposition. Highest deviations up to 34% are present at northern exposed slopes. All $FGVC_{spatial}$ were calibrated by adding the amount of mean underestimation to each grid cell. Subsequently, we used the calibrated $FGVC_{spatial}$ for all further calculations. The accuracy of the LSU approach could be increased with a more accurate grassland map and a higher number of spectral bands as it was already discussed in Meusburger et al. (2010a). A new orthophoto of Switzerland (Swissimage RS; Swisstopo, 2017b) with four spectral bands (NIR, R, G, B) is about to be released in 2020. Such an increase in bands could result in an additional endmember and might improve the LSU.

4.3.2. Temporal variation in the green vegetation cover of Swiss grasslands

The annual distribution of the mean $FGVC_{temporal}$ for Swiss grasslands visualizes the seasonal dynamic of grasslands with periods of dormancy and growing (Fig. 4.5). Higher $FGVC_{temporal}$ lasts until the end of October (approx. DOY 304) in lower elevations (Colline and Montane zone) of northern Switzerland. According to $FCover300m$, an $FGVC_{temporal}$ below 40% is present for most of the Swiss grasslands from December to February. The annual distribution of the $FGVC_{temporal}$ is comprehensive and complies with the typical expectable grassland plant growth cycle (Fontana et al., 2008; Filippa et al., 2015; Inoue et al., 2015). The lack of $FCover300m$ data mainly covers the northern latitudes of Switzerland. According to the high solar altitude in summer, missing values are relatively rare during that season. Winter records are comprised of a higher number of no data values due to snow cover (especially in the Nival zone), sun path and cloudiness (Camacho, 2016). Thus, erosion in winter continues to be a blank spot, because we can neither observe changes in $FGVC$ below the snow cover (which will affect the SLR and C-factor) nor assess the erosivity induced by snow movement and snowmelt (which will affect the R-factor) (Ceaglio et al., 2012; Meusbürger et al., 2014; Stanchi et al., 2014). We excluded no data pixels (indicating snow) from the dataset if they are presented in all the three averaged years. The $FCover300m$ still is in demonstration mode and has only undergone a validation over Europe yet (Camacho, 2016). Therefore, uncertainty could be introduced in the absolute fraction of green vegetation cover. Nevertheless, as all the 10-day data are assessed identically, the relative deviation of the values can be deemed correctly.

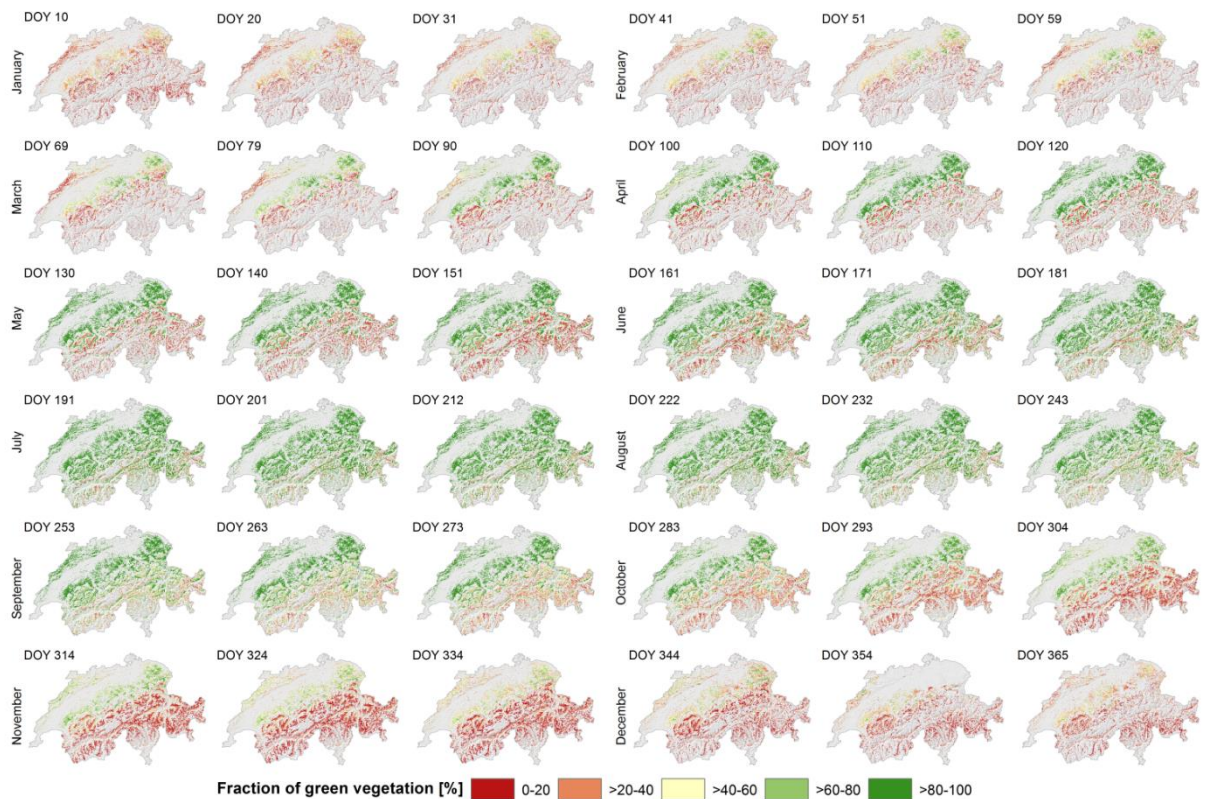


Fig. 4.5: Mean (2014 to 2016) $FGVC_{temporal}$ for Swiss grasslands. Mean $FGVC_{temporal}$ are derived and averaged from $FCover300m$ from 2014 to 2016 (DOY = day of the year).

Table 4.2: Mean national deviation of FGVC (FGVC_{deviation}) to the base date of DOY 181 (30th of June) by FCover300m

DOY ^a	Date	FGVC _{deviation} relative to DOY ^a 181 in %	DOY ^a	Date	FGVC _{deviation} relative to DOY ^a 181 in %
10	Jan 10	-57	191	Jul 10	2
20	Jan 20	-58	201	Jul 20	3
31	Jan 31	-55	212	Jul 31	3
41	Feb 10	-53	222	Aug 10	3
51	Feb 20	-51	232	Aug 20	1
59	Feb 28	-50	243	Aug 31	-2
69	Mar 10	-49	253	Sep 10	-6
79	Mar 20	-44	263	Sep 20	-9
90	Mar 31	-39	273	Sep 30	-14
100	Apr 10	-31	283	Oct 10	-20
110	Apr 20	-25	293	Oct 20	-45
120	Apr 30	-24	304	Oct 31	-34
130	May 10	-22	314	Nov 10	-40
140	May 20	-20	324	Nov 20	-45
151	May 31	-17	334	Nov 30	-48
161	Jun 10	-10	344	Dec 10	-53
171	Jun 20	-5	354	Dec 20	-56
181	Jun 30	0	365	Dec 31	-56

^aDOY Day of the Year.

Based on the MOD13Q1 data, the long-term (2005 to 2015) maximum NDVI of the most considerable proportion of pixels is DOY 177 (26th of June, Fig. S4.3). We used the 30th of June (DOY 181) as the base date as this date has a high temporal proximity to the maximum NDVI of our analysis. This is in agreement with Jonas et al. (2008) who proposed the 6th of July as the mean date of the maximum height of grassland cover for elevations between 1560 and 2545 m a.s.l.. According to model results by Garonna et al. (2014), the growing season in the alpine zone starts at DOY 118 and lasts until DOY 266. The FGVC_{deviation} in relation to DOY 181 marks a positive trend from DOY 181 to DOY 232 which determines the peak growing season for the national grassland area (Table 4.2). The minimal FGVC in relation to DOY 181 is met on DOY 20 with a reduction of 58% in green vegetation cover.

4.3.3. Spatio-temporal patterns of the fraction of green vegetation cover of Swiss grasslands

The mean FGVC_{spatio-temp} of Swiss grasslands on DOY 181 (30th of June; Fig. 4.6) is 60%. Grasslands next to the border of Austria (Cantons Appenzell and St. Gallen) have the lowest FGVC_{spatio-temp}. These Cantons (see a map of Swiss cantons in Fig. S4.4) are fully dominated by meadows and alpine pastures (Table 4.3; Federal Statistical Office Switzerland, 2017, 2017). As the management of these grasslands is very intense (grazing, fodder), the FGVC_{spatio-temp} is comparatively low. Intense grazing causes a significant limitation in grass growth (Bilotta et al., 2007, 2007; Mayer et al., 2009) which results in a degradation of vegetation cover (Yong-Zhong et al., 2005). These regions have one of the highest mean livestock unit (1.7 per ha; Table 4.3) and mean share of grazing livestock farming (78.8%). Hence, most of the areas in the region are already mowed at the 30th of June (typical mowing period for St. Gallen is DOY 166 to DOY 196; Zwingli, 2017). The whole Switzerland experienced a land use intensification of grassland

over the last decades. It is apparent by an increase in stocking rates (~50% increase of sheep numbers during 40 years) and an alteration in grazing systems (permanent shepherding replaced by uncontrolled grazing, Troxler et al., 2004).

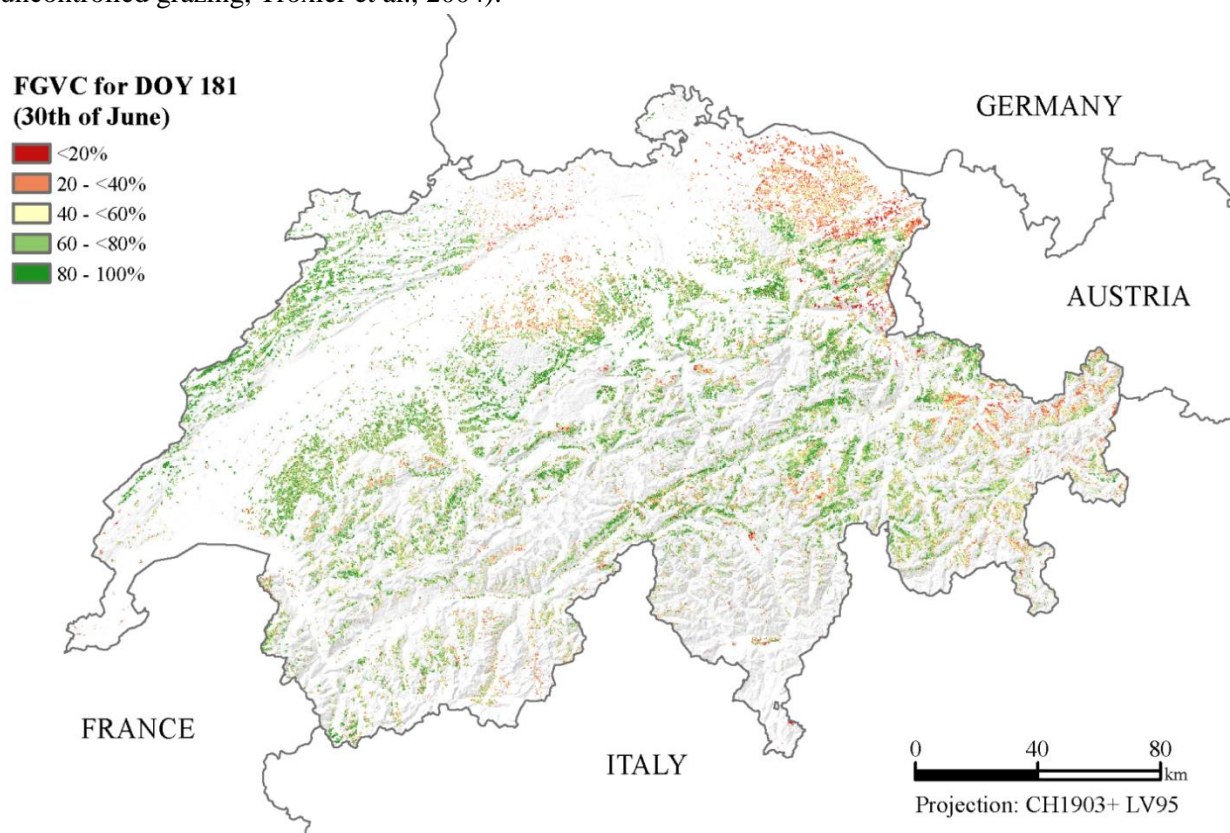


Fig. 4.6: Spatial pattern of the C-factor for grasslands in Switzerland for the base date DOY 181 (30th of June; spatial res. 2 m).

Table 4.3: Averaged seasonal FGVC_{spatio-temp} and agricultural intensity (Federal Statistical Office Switzerland, 2017) of the year 2016 per Swiss Canton

Canton	short name	FGVC _{spatio-temp} (%)					livestock unit (per hectare)	grain farming ^a (%)	grazing livestock farming ^b (%)
		annual	winter	spring	summer	fall			
Aargau	AG	44.5	30.6	50.2	55.0	40.6	1.2	24.1	37.2
Appenzell Ausserrhoden	AR	28.7	16.8	29.6	37.5	28.3	1.5	0.1	85.8
Appenzell Innerrhoden	AI	46.6	29.7	45.5	61.7	45.3	1.9	0	78.5
Basel-Landschaft	BL	40.6	27.0	45.1	51.7	36.7	1	15.7	46.0
Bern	BE	50.0	27.7	46.1	70.4	46.8	1.3	12.9	64.4
Fribourg	FR	51.7	32.0	54.2	68.4	50.8	1.4	16.9	55.7
Glarus	GL	48.4	20.5	34.0	72.4	40.7	1.3	0.1	95.4
Graubünden	GR	43.0	21.2	28.1	60.6	36.3	0.9	1.7	77.0
Jura	JU	58.3	35.1	61.3	77.7	56.2	1	15.1	65.0
Lucerne	LU	52.2	36.1	56.6	65.7	49.7	2.1	9.7	56.3
Neuchâtel	NE	58.2	29.3	56.5	79.9	58.7	0.9	8.3	63.4
Nidwalden	NW	47.9	26.9	44.8	69.5	43.2	1.7	0	88.3
Obwalden	OW	48.2	26.0	39.1	69.6	42.8	1.8	0	88.9

Mapping spatio-temporal dynamics of the cover and management factor (C-factor) for grasslands in Switzerland

Schaffhausen	SH	50.1	32.3	55.5	65.2	42.6	0.8	33.9	14.5
Schwyz	SZ	49.4	27.6	46.0	68.5	45.8	1.4	0.4	86.5
Solothurn	SO	50.7	30.4	54.5	67.2	47.5	1.1	18	53.1
St. Gallen	SG	43.7	25.5	40.9	58.4	40.6	1.7	1.9	72.4
Thurgau	TG	30.7	21.5	33.4	37.5	29.1	1.7	17.5	38.4
Ticino	TI	46.5	24.5	29.1	63.7	40.6	0.8	4.6	40.2
Uri	UR	48.7	21.1	31.1	68.3	40.8	1.2	0	92.0
Valais	VS	45.3	22.0	30.9	61.6	38.6	0.7	2.7	40.3
Vaud	VD	49.5	25.0	45.4	71.8	47.1	0.8	28.3	24.5
Zug	ZG	55.7	32.6	60.0	73.4	54.2	1.7	5.7	70.6
Zürich	ZH	50.6	30.7	55.1	65.4	48.8	1	19.2	40.3

^aof the total agricultural land.

^bof total farming.

4.3.4. Spatial and temporal hot-spots of C-factors on Swiss grasslands

The monthly maps (Fig. S4.5) are averaged to seasonal maps of C-factors for grasslands (Fig. 3.7). They represent the high temporal and spatial variability of the C-factors for grasslands throughout a year. According to the modeling results, relative high C-factors in winter can only be observed in the Jura mountain at the border to France and the western Alps. These patterns are mainly controlled by the ratio of the annual rainfall erosivity (R_{ratio} ; Fig. 4.8). The whole alpine range experiences increased values in spring. The distribution of C-factors in summer for Swiss grasslands is relative diffuse with a spatial cluster in the north-eastern region of Switzerland (Cantons Appenzell and St. Gallen) which is a result by the low FGVC due to intense grassland land use (see chapter 4.3.3.3) and the high rainfall erosivity. Absolute C-factors are decreasing in fall but with regional pattern of high C-factors at the southern and eastern Alps. The minimum C-factors within a year are covering the lowland areas of Switzerland in winter. Maximum C-factors are observable in the previously mentioned region of the Cantons Appenzell and St. Gallen (close to the border of Austria) in summer.

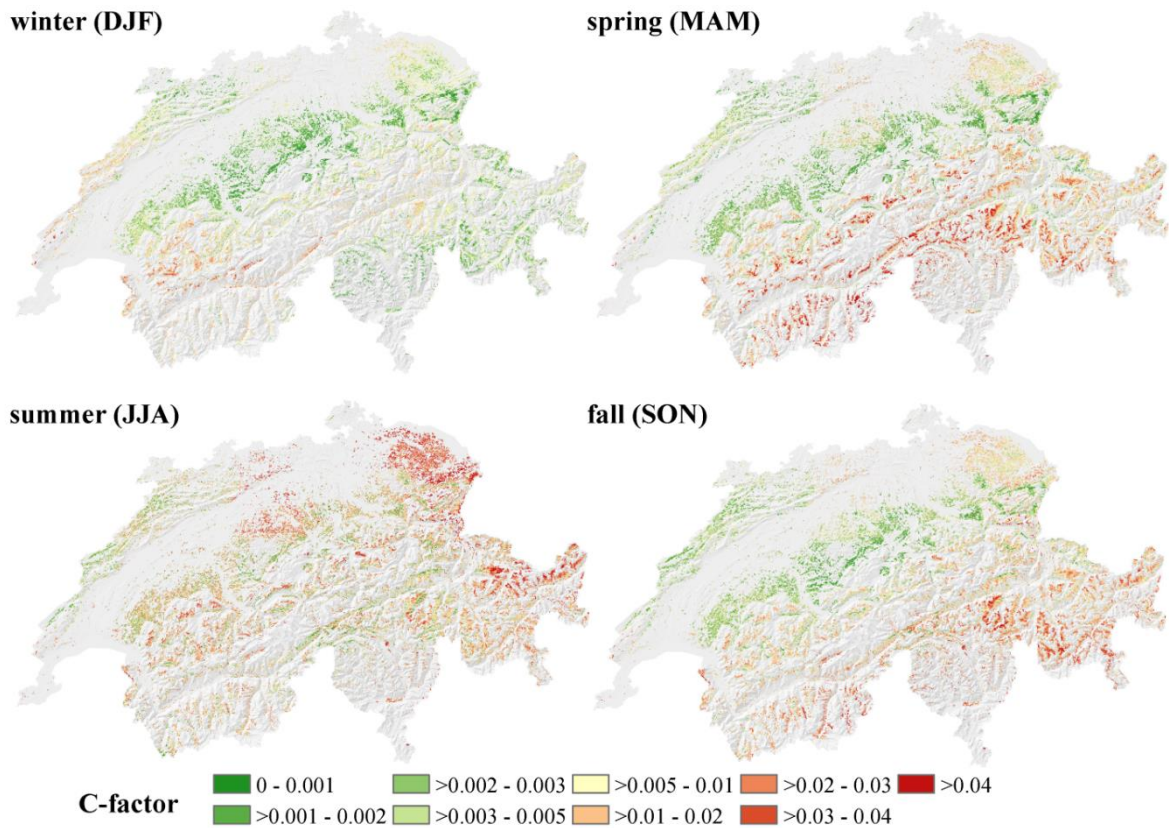


Fig. 4.7: Spatio-temporal variation of C-factors of Swiss grasslands per season (spar. res. 100 m). C-factors are a product of soil loss ratios and weighted rainfall erosivity ratios. The seasonal C-factors are an average of three monthly C-factor maps.

The mean annual C-factor for Switzerland is 0.012 (Table 4.4). Lowest mean C-factors of Swiss grasslands can be observed in January (0.003), highest in the summer months July (0.024) and August (0.025) (Fig. 4.9). The maximum C-factor in August is about 8 times higher than the minimum C-factor in January. The trend marks an abrupt increase of C-factors from April to August with a decrease in its low winter values. The natural plant growth cycle determines the annual trend of FGVC. As the C-factor is not solely related to FGVC but further a product of SLR and weighted R-factor ratios, the trend of the C-factor is influenced by the regional and temporal rainfall erosivity pattern.

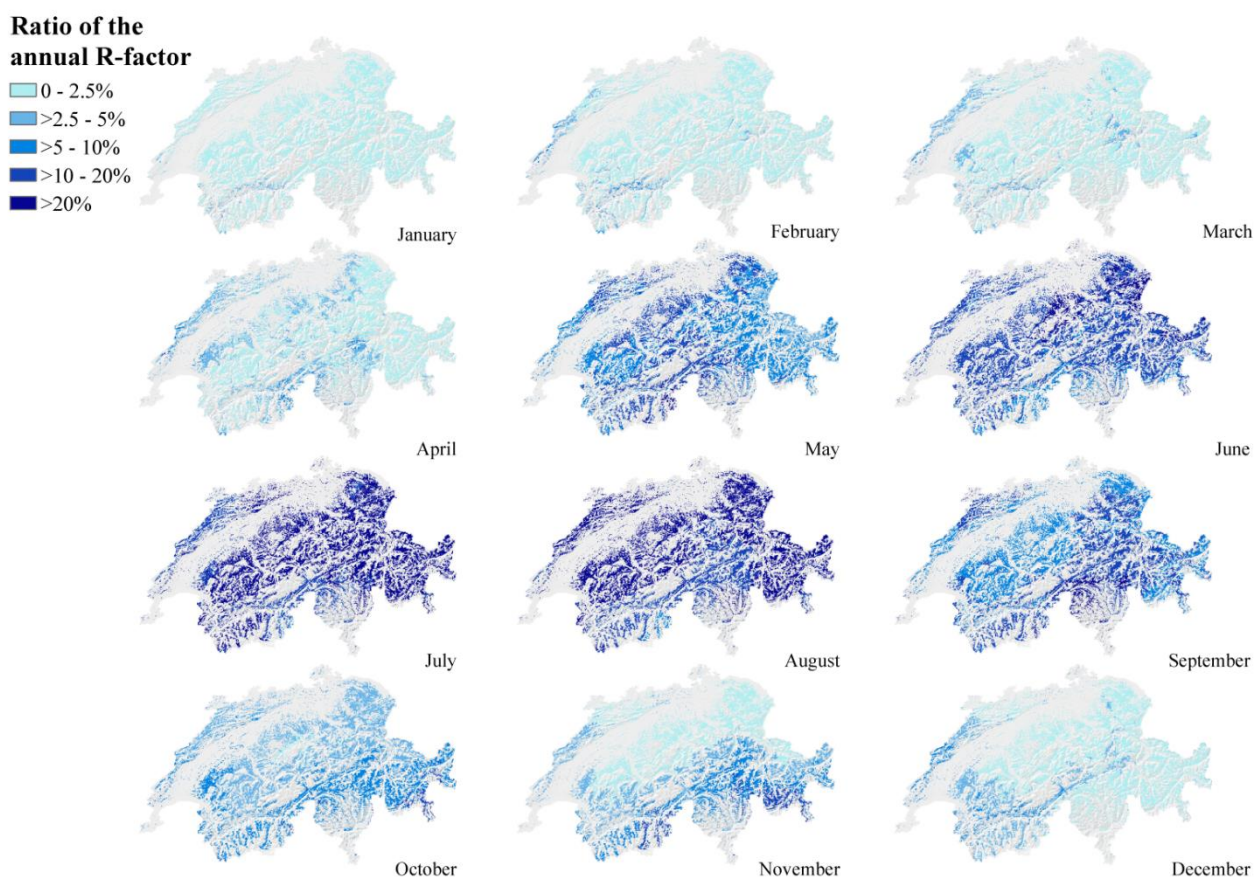


Fig. 4.8: Monthly ratio maps of the annual rainfall erosivity (R-factor) of Swiss grasslands. Monthly R-factor ratios are the fraction of R-factor related to the total annual R-factor sum. Rainfall erosivity maps of Switzerland are based on Schmidt et al. (2016).

Table 4.4: Mean C-factors of Swiss grasslands per month.

month	mean C-factor of Swiss grasslands
January	0.003
February	0.004
March	0.005
April	0.005
May	0.018
June	0.016
July	0.024
August	0.025
September	0.015
October	0.012
November	0.013
December	0.008
Ø	0.012

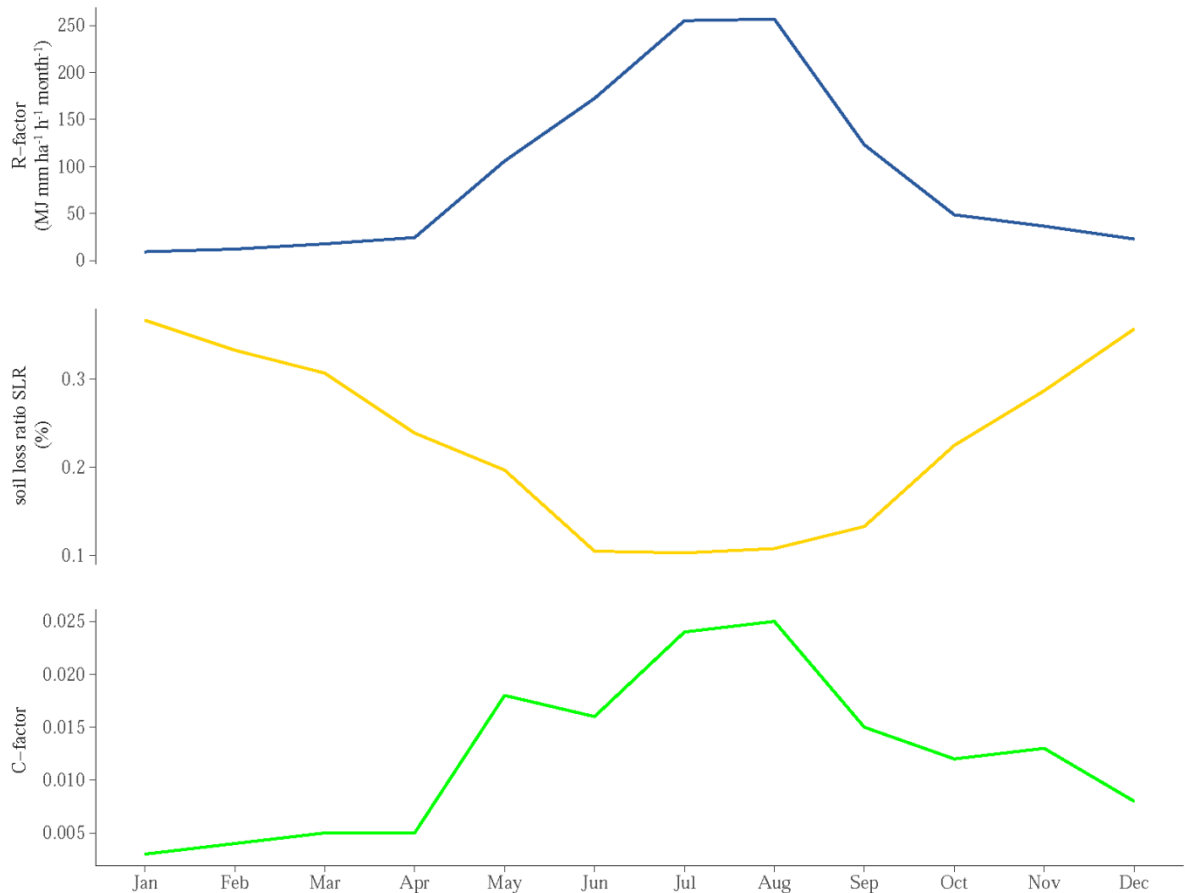


Fig. 4.9: Seasonal distribution of national monthly R-factors ($\text{MJ mm ha}^{-1} \text{h}^{-1} \text{month}^{-1}$), soil loss ratios (SLR; %), and C-factors of Swiss grasslands. C-factors are a product of soil loss ratios and weighted rainfall erosivity ratios.

The rainfall erosivity, as well as the FGVC, is controlled by elevation level (Fig. 4.10). The C-factors per month and elevation zone follow typical patterns. Highest C-factors can be observed in the Alpine zone. The Subalpine, Alpine and Subnival zone show more than one peak with highest C-factors. The Colline and Montane zone have only one maximum in August. The C-factors in all elevation zones are lowest in the winter months January and February. FGVC in winter is low due to the reduced plant growth. The here excluded presence of snow cover in winter results in a delay of increasing FGVC with elevation after melt-out. The typical melt-out at elevations between 1560 and 2545 m a.s.l. is recorded by Jonas et al. (2008) and Fontana et al. (2008) at DOY 147. Large areas of Switzerland show a snow occurrence in winter (Fig. S4.1). Protection of grassland soils by plant cover is relatively low in winter but simultaneously affected by only very low rainfall erosivity. However, the tremendous impact of snow gliding on exposed soil surfaces during winter might be a crucial impact (Meusburger et al., 2014). Although the fraction of vegetation cover is increasing in summer for all the grasslands, the weighting with the R_{ratio} causes a high C-factor. As discussed in Schmidt et al. (2016), a significant fraction of the annual rainfall erosivity is within the time window between June and September. The predominantly glaciated Nival zone (>3100 m a.s.l.) could not be considered due to a small proportion of grassland areas (0.6% of the zone).

Cantons in the east of Switzerland (Fig. S4.6) have slightly higher C-factors in the month May to December which is also related to the differences elevation level (mean elevation of eastern cantons 1122 m a.s.l., western cantons 865 m a.s.l.) and different ratios of R-factors. The elevation patterns become also visible by comparing the northern and southern cantons (mean elevation 928 m a.s.l. and 1795 m a.s.l., respectively). The capturing of the relationship between C-factor and elevation zone meets our expectations and confirms the plausibility of the input parameters and modeling approach. Bosco et al. (2009) already observed a relationship of C-factors and elevation level based on literature values.

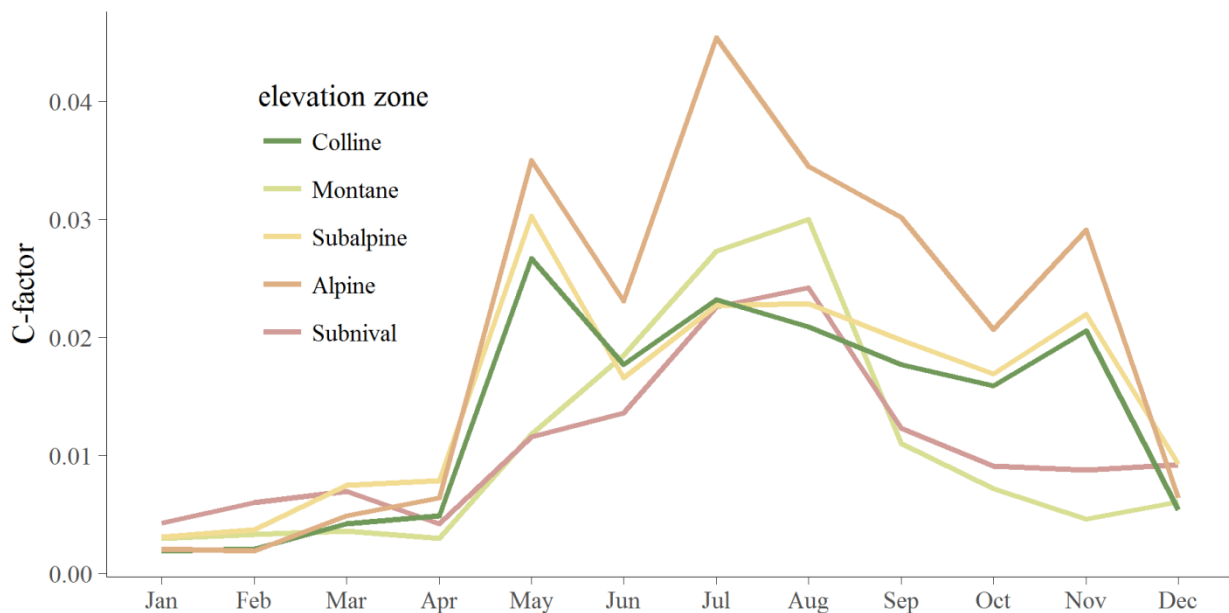


Fig. 4.10: Mean monthly C-factors of grasslands for different elevation zones in Switzerland.

Kulikov et al. (2016) studied the temporal variations of C-factors of Kyrgyz mountain grasslands. They observed decreasing C-factors from April (immediately after snowmelt) to June in both of their study areas. They assess the months April and May with the highest potential soil loss owing to high C-factors with simultaneous high rainfall erosivity. A soil erosion assessment for a watershed in Brazil (de Carvalho et al., 2014) reveals highest soil loss in the rainy season where rainfall erosivity is high and the C-factor low. Another combination of dynamic R- and C-factors, done by Panagos et al. (2014a) for Crete in Greece, assesses March as a month with high rainfall erosivity and low fractional vegetation cover. Thus, it is important for C-factor assessment to consider the relative timing of peak C- and peak R-Factor.

Panagos et al. (2015c) derived C-factors for grasslands for the 28 European Union member states from FCover300m and ranges of literature values. Their results present a mean European grassland C-factor of 0.0435 which is about 3.5 times higher than the one for Switzerland. However, C-factors in Mediterranean regions, which are included in the mean European C-factor, are substantially higher than ones in Central Europe. The surrounding countries of Switzerland have mean national values between 0.0345 (Austria) to 0.0421 (Germany). Switzerland's nationwide C-factor for grasslands (0.012) is 70% lower than the mean of the four neighboring countries (0.0396). A different seasonal trend and lower values compared to Panagos et al. (2015c) and Kulikov et al. (2016) can be explained by the different methods to compute C-factors and the neglecting of the rainfall erosivity.

Extensive pasture systems might have a positive effect on a dense vegetation cover. Furthermore, rotation grazing systems or reduced stocking rates supports the development of a better-closed vegetation cover (Troxler et al., 2004). The exclusion (e.g., by fencing) of susceptible soils or spots with a reduced growth period due to a late melt-out could effectively prevent soils from being mobilized. The regeneration time of a degraded sward will take many years, and as long as then the soil surface remains uncovered, it will be fragile and highly prone to an expansion of soil degradation in the form of erosion.

The study of the dynamic soil erosion is of high importance as growing seasons in the European Alps are about to be extended under futures changing climates and shortened snow-cover periods (Defila and Clot, 2001; Studer et al., 2005; Bänninger et al., 2006; Fontana et al., 2008; Frei et al., 2017). A long-term effect of the prolonged growing season for alpine plants would be the favoring of higher and faster-growing plants with enhanced biomass production. More biomass production increases the vegetation cover and lowers the C-factor in summer (Rammig et al., 2010). Simultaneously, the warmer climate and heavy precipitation events during fall and winter will result in higher R-factors (after snowmelt; Fuhrer et al., 2006; Rajczak et al., 2013; Rajczak and Schär, 2017). Sparsely covered soils in late fall (before snow cover) and early spring are then more susceptible to erosion by water. A significant increase and intensification in the cold-season precipitation is already observable for Switzerland (Widmann and Schär, 1997; Schmidli et al., 2002; Schmidli and Frei, 2005).

4.4 Conclusion and outlook

We derived Swiss C-factor maps of grasslands from soil loss ratios weighted with R-factor ratios in using the most state-of-the-art remote sensing products for Switzerland (e.g., national orthophoto with an original spatial resolution of 0.25m (Swissimage FCIR) and a 10-day time series of fractional green vegetation cover (FGVC, FCover300m)). The assessment enables the nationwide quantification of the C-factor of grasslands in its dynamic throughout a year. C-factors are much higher in winter than in summer due to the relation to rainfall erosivity ratio and show the expected dependency on elevation gradient. The mean annual C-factor of Swiss grasslands is 0.012 which complies with the C-factor of October. An improved spectral resolution will be available with the future Swissimage RS product which might increase the accuracy and quality of the linear spectral unmixing results. However, the present results can help to implement soil conservation strategies of an adopted land use management. The identification of regions in Switzerland and periods of the year with high C-factors in combination with the dynamic R-factors might help agronomists to introduce selective mitigation strategies for erosion control of Swiss grasslands. The mitigation potential of soil erosion particularly relies on the C-factor since the R-factor is climate driven and not directly to be altered by human interventions. The utilized grassland areas of Switzerland are of particular interest since grazing might degrade soil functions and stability and has an impact on soil cover. Grazing in alpine environments usually takes place during the most susceptible season. As sediment yield is reduced to a minimum under closed vegetation cover, priority should be on keeping the vegetation coverage of grassland high. The FGVC can be increased, and thus the C-factor lowered by avoiding grazing on highly susceptible grassland or at least by paying more attention to the choice of the grazing animal species and stocking numbers/ diversity. To capture

the spread of degraded surfaces, the automated identification and classification of bare soil spots with a higher spectral resolution is envisaged for future studies. Beyond the current state of C-factors, the models can be linked to land use and climate scenarios to get an idea of future impacts of soil erosion. As we demonstrated the usefulness and applicability of the C-factor and its relation to the R-factor, this study also highlights the advantages of USLE-type modeling. Individual computation and assessment of every single factor result in a high transparency and verifiability of USLE-based erosion models. Each individual factor does not only have the advantage to be adjusted and evaluated on its own but also deliver valuable conclusions for other environmental issues.

Acknowledgement

This work was supported by the Swiss Federal Office for the Environment (FOEN) (grant numbers N° N222-0350 and N° P182-1535). The authors would like to thank all data providers, namely Swisstopo, Copernicus Global Land Services, European Space Agency (ESA), and National Aeronautics and Space Administration (NASA) for making their data available. Furthermore, we would like to thank the anonymous reviewers for their valuable comments and suggestions to improve the quality of the paper.

Funding

This work was supported by the Swiss Federal Office for the Environment (FOEN) (grant numbers N° N222-0350 and N° P182-1535).

CHAPTER 5

Filling the European blank spot – Swiss soil erodibility assessment with topsoil samples

This chapter is published in Journal of Plant Nutrition and Soil Science as:

Simon Schmidt¹, Cristiano Ballabio², Christine Alewell¹, Panos Panagos², Katrin Meusburger^{1,3}: Filling the European blank spot – Swiss soil erodibility assessment based on topsoil samples, J. Plant Nutr. Soil Sci., doi.org/10.1002/jpln.201800128, 2018.

¹Environmental Geosciences, University Basel, Bernoullistrasse 30, CH-4056 Basel, Switzerland

²European Commission, Joint Research Centre, Sustainable Resources Directorate, Via E. Fermi 2749, I-21027 Ispra, Italy

³Swiss Federal Institute for Forest, Snow and Landscape Research WSL, Zürcherstrasse 111, CH-8903 Birmensdorf, Switzerland

Abstract

Soil erodibility, commonly expressed as the K-factor in USLE-type erosion models, is a crucial parameter for determining soil loss rates. However, a national soil erodibility map based on measured soil properties did so far not exist for Switzerland. As an EU non-member state, Switzerland was not included in previous soil mapping programs such as the Land Use/Cover Area frame Survey (LUCAS). However, in 2015 Switzerland joined the LUCAS soil sampling program and extended the topsoil sampling to mountainous regions higher 1500 m a.s.l. for the first time in Europe. Based on this soil property dataset we developed a K-factor map for Switzerland to close the gap in soil erodibility mapping in Central Europe. The K-factor calculation is based on a nomograph that relates soil erodibility to data of soil texture, organic matter content, soil structure and permeability. We used 160 Swiss LUCAS topsoil samples below 1500 m a.s.l. and added in an additional campaign 39 samples above 1500 m a.s.l. In order to allow for a smooth interpolation in context of the neighboring regions, additional 1638 LUCAS samples of adjacent countries were considered. Point calculations of K-factors were spatially interpolated by Cubist Regression and Multilevel B-Splines. Environmental features (vegetation index, reflectance data, terrain and location features) that explain the spatial distribution of soil erodibility were included as covariates. The Cubist Regression approach performed well with an RMSE of $0.0048 \text{ t ha h ha}^{-1} \text{ MJ}^{-1} \text{ mm}^{-1}$. Mean soil erodibility for Switzerland was calculated as $0.0327 \text{ t ha h ha}^{-1} \text{ MJ}^{-1} \text{ mm}^{-1}$ with a standard deviation of $0.0044 \text{ t ha h ha}^{-1} \text{ MJ}^{-1} \text{ mm}^{-1}$. The incorporation of stone cover reduces soil erodibility by 8.2%. The proposed Swiss erodibility map based on measured soil data including mountain soils was compared to an extrapolated map without measured soil data, the latter overestimating erodibility in mountain regions (by 6.3%) and underestimating in valleys (by 2.5%). The K-factor map is of high relevance not only for the soil erosion risk of Switzerland with a particular emphasis on the mountainous regions but also has an intrinsic value of its own for specific land use decisions, soil and land suitability and soil protection.

Keywords: RUSLE, soil erosion, LUCAS, erodibility, cubist regression, soil properties, digital soil mapping

5.1 Introduction

The productive capacity of the soil is the most important resource for human food supply (Morgan, 2006; Borrelli et al., 2017). However, depletion in productive capacity and an increase of soil erosion rates are progressing with the growth of population and agricultural intensification (Brown, 1981; Pimentel et al., 1995; Lal, 2001; Yang et al., 2003; Dotterweich, 2013). On global arable lands, soils are not in equilibrium as soil loss rates exceed the tolerable soil loss (FAO, 2015). Among the physical parameters influencing soil erosion (soil physical, chemical, and biological properties, climate conditions, landscape characteristics; Verheijen et al., 2009) the susceptibility of soil is controlled by soil properties that restrain the detachment of soil particles, and affect infiltration, permeability, and water capacity (Wischmeier and Smith, 1965). The susceptibility of a soil to erode is commonly called soil erodibility. It is assessed as the K-factor in the Universal Soil Loss Equation (USLE; Wischmeier and Smith, 1965) and its revised versions (RUSLE; Renard et al., 1997) which compute soil erosion by a multiplication of the rainfall erosivity R, cover and management C, slope length and steepness LS, and support practices P (Wischmeier and Smith, 1978). Experimentally, the K-factor is the average annual soil loss (A) per rainfall erosivity unit (R) measured for the standard conditions of the unit plot (Wischmeier and Smith, 1978):

$$K = \frac{A}{R} \quad (5.1)$$

In a rather practical context, it can be seen as a value to describe the annual average of the total soil and soil profile reactions in relation to substantial water erosion processes like detachment and transport (Renard et al., 2010). Information about soil erodibility is preferable to be assessed by long-term measurements on natural plots (Renard et al., 2010). A relationship of soil erodibility and particle size distribution was assessed by Wischmeier (1971) for soils in the USA and expressed in a nomograph. That nomograph was developed to estimate soil erodibility from readily available soil property data and standard profile descriptions as field measurements of K are time-consuming and demand at least 3 (up to 10) years of measurement to determine values (Foster et al., 2008). Later, Wischmeier and Smith (1978) developed an equation that rests on the nomograph based on rainfall simulations data from 55 soils in the US (see equation 5.2; (Renard and Ferreira, 1993)). This equation is the most used and cited function to calculate soil erodibility from ready-to-use soil data (Borrelli et al., 2017). Alternative equations for particular soil types (e.g., high clayey, volcanic, mollisol) were developed but these are not of necessity for Swiss conditions (Wang et al., 2013a). Auerswald et al. (2014) developed a K-factor equation based on German soil survey data. Their equation fully emulated the nomograph of Wischmeier and Smith (1978) beyond the limitations of 70% silt, soil erodibility less than 0.02 t ha h ha⁻¹ MJ⁻¹ mm⁻¹, 4% soil organic matter, and exclusion of rock fragments. However, the equation is not yet widely tested (applied in 5 publications) and considered as “far from perfect in many cases” (Auerswald et al., 2014). To ensure a continental comparability of Swiss soil erodibility, we decided to use the equation of Wischmeier and Smith (1978) which was earlier applied for European countries (see below; Panagos et al., 2014c).

Determining the soil properties of the equation of Wischmeier and Smith (1978) includes topsoil texture (sand, very fine sand, silt, and clay content), soil organic matter, soil structure and soil permeability (Wischmeier et al., 1971). However, as the latter parameters are also

difficult to measure and regarding the demand on large-scale models and assessments, alternative methods to cover the spatial distribution of soil information are needed (Diek et al., 2016; 2017; Wang et al., 2016a). Still the majority of these alternatives follow the nomograph or equation of Wischmeier et al. (1971) and Wischmeier and Smith (1978) to model soil erodibility with soil properties derived by remote sensing (Wang et al., 2016b; Ostovari et al., 2017) or digital soil mapping (DSM) techniques (Bahrawi et al., 2016; Ganasri and Ramesh, 2016; Iaaich et al., 2016).

For Switzerland, previous studies have used a variety of polygon-based soil property and soil suitability maps of different scales to estimate the soil erodibility based on the parameter classes of texture, stone, and organic matter content (Prasuhn et al., 2010; 2013). Unfortunately, high- and medium-resolution soil maps (up to 1:50000) are heterogeneous and do only cover 25% of the Swiss national area. With the recent demand of national spatial soil data, DSM evolved as an appropriate method to complement the conventional soil survey methods (McBratney et al., 2003) that are often biased especially for Switzerland with its high percentage of remote mountain areas with low accessibility (Nussbaum et al., 2014; 2017; 2018). The principle of DSM considers that similar environmental conditions cause the formation of similar soil and soil properties (Hudson, 1992).

Often, soil survey input data sources of the DSM maps originate from non-uniform soil databases, which make the results often incomparable, although underlying equations and methodologies are identical. Topsoil surveys (0-20 cm) in the framework of the Land Use/Cover Area frame Survey (LUCAS; Tóth et al., 2013) allowed the establishment of a homogenous soil database across 23 EU member states. Panagos et al. (2012b) presented a K-factor map as a first homogenized product of the database. Later, the underlying spatial prediction methodology was improved (Cubist Regression and Multilevel B-Splines), the number of soil samples increased and the number of countries enlarged (25 EU member states; Panagos et al., 2014c). The past two sampling campaigns of LUCAS (2009-2012 and 2015) cover a total of more than 22000 soil samples (Orgiazzi et al., 2018). As Switzerland was not part of the first LUCAS sampling (2009), an extrapolation of soil erodibility for Switzerland without Swiss soil samples was realized based on topsoil data of other EU countries (map uploaded at the European Soil Data Centre ESDAC; Panagos et al., 2012c). However, this extrapolated soil erodibility is associated with high uncertainties and was therefore not published in a peer-review journal. In 2015, Switzerland joined the LUCAS program and 199 samples were collected. For the first time also soil samples from mountain areas above 1500 m a.s.l. were included ($n = 39$).

Although the presence of seasonal effects on the K-Factor (mainly triggered by freeze-thaw processes) is discussed in the literature (Renard et al., 1991; Renard and Ferreira, 1993; Renard et al., 1997; Bryan, 2000), we decided not to model soil erodibility on a seasonal scale. Kinnell (2010) reviewed different approaches to assess the seasonality of the K-factor. However, none of these approaches include the hardly measurable influencing interactions and effects (e.g., climate influences and seasonality of freeze-thaw, compaction by life stock trampling, human management activities) simultaneously for a proper process-oriented modeling (Leitinger et al., 2010; Piñeiro et al., 2010; Vannoppen et al., 2015). Furthermore, the divergence of seasonal K-factors to an annual K-factor is poorly discussed in the literature (e.g., Wall et al., 1988). In the RUSLE2 User's Reference Guide (Foster et al., 2008) it is even stated that no statistical evidence exists for an inconsistency of soil erodibility over time. Rather, the rainfall erosivity

(Schmidt et al., 2016) and the cover and management factor (Schmidt et al., 2018b) can be seen as highly dynamic erosion factors with an intra-annual variation.

The aim of the present study is to assess the spatial and temporal patterns of soil erodibility of Switzerland by (i) mapping K-factors based on Swiss LUCAS data. Additionally, (ii) differences between the interpolation and extrapolation to produce a national soil erodibility map are evaluated. With the mapping of soil erodibility based on soil samples, we aim to improve the prediction of the existing extrapolated soil erodibility map.

5.2 Material and methods

5.2.1 LUCAS topsoil sampling

A dataset of 199 soil samples from the LUCAS topsoil sampling was used to obtain a soil erodibility map of Switzerland. The LUCAS topsoil sampling is a standardized procedure with one aliquot out of five mixed subsamples for each sampled location. A recent review about LUCAS is provided by Orgiazzi et al. (2018). All samples were air-dried and analyzed for particle size distribution (according to the USDA classification) and soil organic carbon content in a single ISO-certified laboratory. The laboratory analysis are explained in detail by Orgiazzi et al. (2018). 160 soil samples of Switzerland cover grasslands and forests at elevations less than 1500 m a.s.l. (sample distribution of 12.7 km x 12.7 km), 39 samples were taken at the same land use units in the Alpine region above 1500 m a.s.l. (20.6 km x 20.6 km) (named as Alpine samples throughout the study). The total Swiss sample set spans over elevations from 287 m a.s.l. to 2337 m a.s.l. It covers all biogeographic regions (Jura, Alpine Midland, and Northern/Southern/Western/Eastern Alps) of Switzerland and has a mean point density of one per 207 km² what equals an average distribution of one sample within a grid of 14.4 km x 14.4 km (Fig. 5.3). That sample spread of Switzerland corresponds to the mean spread across the 25 EU Member States of the 2009-2012 sampling (14 km x 14 km; Panagos et al., 2013). The Alpine samples were selected following a stratified random sampling to make sampling in remote areas possible. As a logistical stratum we selected sampling points at grassland locations above 1500 m a.s.l. by the criteria of accessibility (max. distance of 200 m to the next street accessible with 4-wheel drive). We tried to manually cover the natural strata exposition (south, north) and geological units (consolidated and unconsolidated sediment, igneous rock, metamorphic rock) which are related to the soil formation but are not homogeneously assessed by a random sampling approach. We assume that differently exposed soils experienced another degree of solar radiation (Yimer et al., 2006) and soil texture varies with geological units (Jenny, 1941). After assigning the strata, the 39 samples were randomly distributed (in ESRI ArcGIS) proportional to the strata units to cover each combination of exposition and geology. Additionally, 1638 samples of the surrounding countries Germany, Austria, Slovenia, Italy, and France were used to delineate a better prediction for the spatial interpolation (see below). These data were already part of the European soil erodibility mapping (Panagos et al., 2014c). Additionally, the European Soil Database (King et al., 1994) provides information for the soil structure of the LUCAS samples.

5.2.2 Calculation of soil erodibility for the LUCAS topsoil samples

The soil erodibility (K) equation by Wischmeier and Smith (1978) includes the following soil properties: particle size distribution in percent (very fine sand m_{vfs} [0.05-0.1 mm], silt m_{silt} [0.002-0.05 mm], and clay m_{clay} [<0.002 mm] content), the organic matter content OM in percent, the soil structure class s and the permeability class p . According to their empirical experiments, Wischmeier and Smith (1978) propose to calculate the soil erodibility as the following function whereby K is expressed in $t\ ha\ h\ ha^{-1}\ MJ^{-1}\ mm^{-1}$ according to the International System of units (Foster et al., 1981):

$$K = [(2.1 * 10^{-4} * M^{1.14} * (12 - OM) + 3.25 * (s - 2) + 2.5 * (p - 3))/100] * 0.1317 \quad (5.2)$$

Where M is the textural factor composed of $(m_{silt} + m_{vfs}) * (100 - m_{clay})$.

The particle size distribution is analytically determined. Textural classes are set according to USDA (1951). Soil structure is defined as the overall architecture of soils and the assembling of individual texture components like sand, silt, and clay and its combination to aggregates (Chesworth, 2008). It can be derived by a pedotransfer function including the land use class and soil name proposed by van Rast et al. (1995). Soil structure is classified into four classes (humic, poor, normal or good). Soil permeability is the soils capacity to transmit water and can be assessed by the soil texture classes (permeability classes 0 to 4) (USDA, 1983; Chesworth, 2008). The used tables to extract soil structure s and soil permeability p can be found in Panagos et al. (2014c). The soil erodibility equation underlies three restrictions: silt content $>70\%$ is set to 70% , organic matter content $>4\%$ is set to 4% , and the very fine sand fraction is estimated as 20% of the total sand fraction (Panagos et al., 2014c). Only 1 out of 199 of all Swiss samples (0.5%) has a silt fraction greater 70% and was adjusted to that threshold. Assets and drawbacks of the organic content limitation are already discussed (Panagos et al., 2014c). The fine sand fraction was approximated to 20% of the total sand fraction (Panagos et al., 2014c). A particle size analysis of a subset of the Swiss samples ($n=38$) including very fine sand (26% of total sand) confirmed that an estimated ratio of 20% is appropriate for European soils.

Additionally, we calculated the K-factor for all 199 Swiss LUCAS topsoil samples based on another K-factor equation proposed by Römken et al. (1997) which takes only the soil texture into consideration and neglects the soil organic matter content, the soil structure, and the soil permeability. The information on soil texture is transformed by the geometric mean particle diameter equation by Shirazi and Boersma (1984).

As discussed in the literature (Poesen et al., 1994; Figueiredo and Poesen, 1998; Panagos et al., 2014c; Bosco et al., 2015), the positive effects of the stone cover on reducing soil erosion are not negligible. That impact can be incorporated into the soil erodibility calculation by using a correction factor S_t for the relative decrease in sediment yield. That correction factor is multiplied with the K-factor and calculated as following (Poesen et al., 1994):

$$S_t = e^{-0.04*(R_c-10)} \quad (5.3)$$

Where R_c is the percentage of stone cover (stoniness). It was estimated (classes: 0-10%, ≥ 10 -25%, ≥ 25 -50%, $\geq 50\%$; Eurostat, 2009) during the LUCAS topsoil sampling for each location (Panagos et al., 2014c).

The soil erodibility K and soil erodibility incorporating the stoniness correction factor K_{st} were calculated for a total of 1837 LUCAS topsoil samples (including data from bordering countries in addition to the 199 Swiss samples) following the equations 5.2 and 5.3.

5.2.3 Mapping the K-factor for Switzerland

In the present study we used vegetation indices (Normalized Difference Vegetation Index NDVI, Enhanced Vegetation Index EVI) of the Moderate Resolution Imaging Spectroradiometer (MODIS) data MOD13Q1 (Didan et al., 2015), reflectance data from MODIS, terrain features (elevation, slope, base level of streams, altitude above channel base level, and multi-resolution index of valley bottom flatness) derived from the Shuttle Radar Topography Mission (SRTM) Digital Elevation Model (Farr et al., 2007), and latitude and longitude as covariates. A list of covariates can be found in Table 5.1 and in Panagos et al. (2014c). These covariates are already identified as the most important for predicting soil erodibility in the European Union. In order to be reproducible, consistent, and comparable we used the same predictive variables and resolutions for Switzerland as were used for the European Union.

Table 5.1: List of covariates used in the cubist regression model for modeling the soil erodibility of Switzerland

covariate group	covariate	spatial resolution	data source
vegetation index	Normalized Difference Vegetation Index NDVI, Enhanced Vegetation Index EVI	250 m	Moderate Resolution Imaging Spectroradiometer (MODIS) MOD13Q1 (Didan et al., 2015)
MODIS raw band data	Band 1,2,3,7	250 m	MODIS (Didan et al., 2015)
terrain features	elevation, slope, base level of streams, altitude above channel base level, multi-resolution index of valley bottom flatness	25 m	Shuttle Radar Topography Mission (SRTM) (Farr et al., 2007)
location parameter	latitude, longitude	-	-

We used Cubist Regression (CR) (Quinlan, 1992; 1993) to spatially predict the K-factors for Switzerland including the above-mentioned covariates. CR is a tree model that uses recursive partitioning to subset the dataset into finer rule-based sub-datasets. These rules cluster data with relatively homogeneous characteristics. As long as a condition is identified to be false, the model proceeds with the next rule until it meets a true condition. As soon as a situation matches a condition, an individual linear regression model is fit for the data partition. A specific set of covariates that predict best is automatically chosen for each subset of an individual regression equation (Ballabio et al., 2017). It can be seen as a model tree with linear regression models at its terminal leaves. As such, CR allocates a series of local linear regression models and results in an overall combined non-linear function. Furthermore, it makes use of the previous linear regression to smooth and adjust the prediction (prevent underprediction, reduce overfitting). The selection of covariates and combination of regressions increase the estimation accuracy. After the CR, the residuals are interpolated with Multilevel B-Splines (MBS) (Lee and Won, 2013). MBS interpolate scattered points to generate a smooth surface as well as the best fit of these

points. The method used a hierarchy of control lattices to generate a series of functions, whose sum approaches the desired approximation function. A bootstrapped cross-validation (Efron and Gong, 1983) (100 repetitions) with randomly selected samples and a one out of ten replacement of the main dataset was used to fit the model. The K_{st} -factor, incorporating the effect of stoniness, was also modeled by CR and MBS. The modeling was performed in R (v 3.4.2) with the packages ‘cubist’ and ‘MBA’. Terrain features were extracted in SAGA GIS (v 6.0.0) (Conrad et al., 2015) and visualization was realized in ESRI ArcGIS (v 10.3.1).

The K-and K_{st} -factor values are the base for the DSM. We extended the database across the Swiss border to increase population size for the statistical regressions, to better predict particularly the border areas of Switzerland and the special features of the high Alpine soils erodibility where the sample number is limited.

The performance of the interpolation is evaluated with the standardized measure of certainty f based on the standard deviation s of the estimated variable V (McBratney et al., 2003) and calculated as follows:

$$f = 1 - \min\left(\frac{2s}{V}, 1\right) \quad (5.4)$$

A low certainty is expressed by 0 (0%) and high certainty by 1 (100%).

5.2.4 Extrapolation of soil erodibility for Switzerland by using data from EU countries

Extrapolated K-factor maps for European countries (from the EU28 assessment; Panagos et al., 2013) not being part of the previous LUCAS campaigns are already provided via the European Soil Data Centre (ESDAC, 2018; Panagos et al., 2012c) due to a number of requests from non-EU users. The extrapolated map of Switzerland used the same covariates and methodology but is not supported by measured data. A comparison of the extrapolated map with the herein processed interpolated K-factor map of Switzerland evaluates the necessity for soil input data into the DSM process.

5.3 Results and discussion

5.3.1 Soil properties and erodibility of the LUCAS topsoil samples

The calculations of the K factor from the analysis of the 199 Swiss LUCAS topsoil samples in the laboratory show an average soil erodibility of $0.0334 \text{ t ha h ha}^{-1} \text{ MJ}^{-1} \text{ mm}^{-1}$ (Table 5.2) with a range from $0.0180 \text{ t ha h ha}^{-1} \text{ MJ}^{-1} \text{ mm}^{-1}$ (lowest susceptibility of Swiss soils to be eroded) to $0.0611 \text{ t ha h ha}^{-1} \text{ MJ}^{-1} \text{ mm}^{-1}$ (highest susceptibility of Swiss soils to be eroded). 83% (166) of all samples have K-factor values between $0.0250 \text{ t ha h ha}^{-1} \text{ MJ}^{-1} \text{ mm}^{-1}$ and $0.0400 \text{ t ha h ha}^{-1} \text{ MJ}^{-1} \text{ mm}^{-1}$. The K-factor increases as the samples are getting siltier (Spearman correlation coefficient $r_s=0.397$). Silt content varies between 16% and 73%. The mean fraction of very fine sand is 6.4% (range from 1.2% to 16.4%). A higher content of the sand fraction is very weakly correlated with a reduction of the K-value ($r_s=-0.078$). The mean clay content of all 199 samples is 17.7% (range from 2.0% to 40.0%). All samples are rich in organic matter content with a mean proportion of 3.3%. Erodiability is slightly reduced by a higher content of organic matter ($r_s=-0.265$). However, in general, Wischmeier and Mannering (1969) could not identify a clear

correlation between organic matter and soil erodibility as particle size distribution is overruling a possible influence.

Soil structure class has a relatively low variability in Switzerland. Only 1% of soil structure is classified outside class 1 or 2. The permeability class with the highest frequency is 3 (moderate). Soils with higher permeability have a higher infiltration capacity and reduce runoff. In a first approach, we considered a pedotransfer function to predict the soil permeability instead of deriving soil permeability from soil texture classes. As such, a subset of undisturbed topsoil samples of 11 Alpine locations with three replicates were measured in the laboratory according to the corresponding saturated hydraulic conductivity. Results indicated that the permeability was driven by secondary pores and not at all related to the primary porosity. That fact impedes the prediction and led us back to the original approach of Panagos et al. (2014c).

The 39 Alpine samples are rich in sand content and can be classified as loamy soils. The mean soil texture of the remaining 160 Swiss samples is silty loam. Most of the Swiss samples are either classified to the texture class loam or silty loam (Fig. 5.1). The mean soil erodibility of samples above 1500 m a.s.l. is smaller than the mean of locations below 1500 m a.s.l. (0.0320 versus 0.0338 t ha h ha⁻¹ MJ⁻¹ mm⁻¹, respectively), although a decreasing trend of clay content ($r_s=-0.172$) with height and a slightly increasing trend of very fine sand and organic matter ($r_s=0.151$, resp. $r_s=0.159$) with height (from 287 m a.s.l. to 2337 m a.s.l. of 199 samples) is observed. Spatial trends by latitude exist for clay and sand. Clay content increases ($r_s=0.545$) and sand content decreases ($r_s=-0.476$) from South to North. This relation of latitude and soil properties is mainly influenced by the terrain contrasts between southern and northern Switzerland. No correlation exists between soil properties and longitude. We expected no relationship between soil properties and longitude as the terrain contrasts are heterogeneous and do not follow any obvious gradient. However, due to the correlation of soil properties and latitude we decided to use spatial coordinates as a predictor for the K-factor modeling in the following chapter.

Table 5.2: Mean values for soil properties

measured soil properties	samples		Switzerland
	<1500 m a.s.l.	>1500 m a.s.l.	
number of samples n	160	39	199
sand (%)	29.2	42.6	31.8
very fine sand m_{vfs} (%)	5.8	8.5	6.4
silt m_{silt} (%)	51.3	47.1	50.5
clay m_{clay} (%)	19.5	10.4	17.7
textural factor M	4588.3	4965.4	4662.2
organic matter OM (%)	5.3	5.9	5.4
soil structure class s *	1	1	1
permeability class p *	3	3	3
soil erodibility K (t ha h ha ⁻¹ MJ ⁻¹ mm ⁻¹)	0.0338	0.0320	0.0334

*mode value

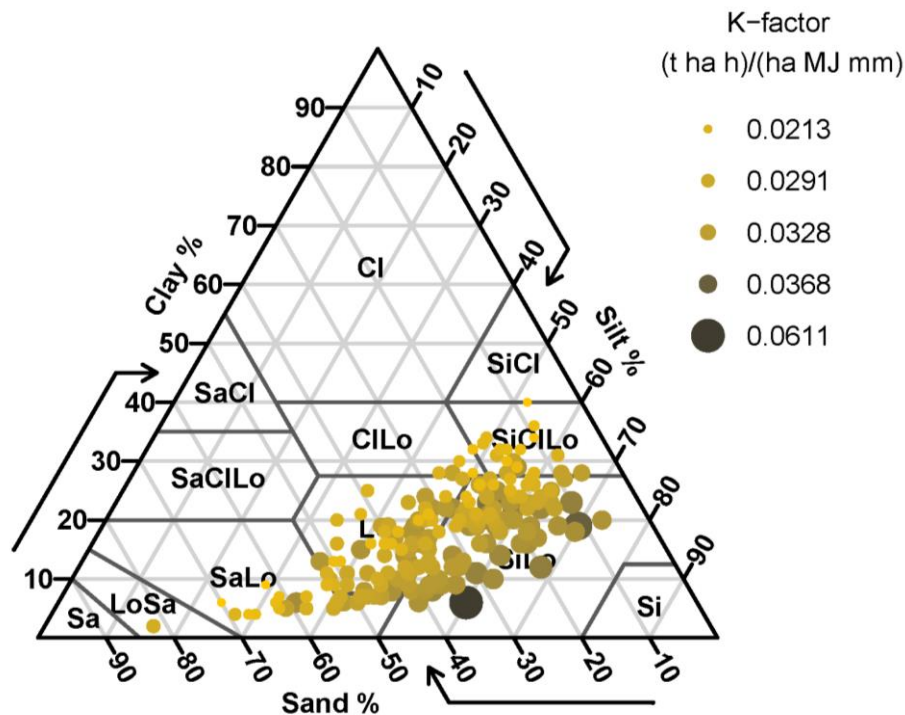


Fig. 5.1: Particle size distribution diagram of all 199 LUCAS topsoil samples according to the USDA soil texture classification proportional to the K-factor (quantile classification)

The soil erodibility calculation based on Römken et al. (1997) revealed a slightly different K-factor of $0.0371 \text{ t ha h ha}^{-1} \text{ MJ}^{-1} \text{ mm}^{-1}$. However, we decided to use the nomograph based equation as it is recommended by Renard et al. (1997) as long as measured soil parameters are not limited and measured in the USDA soil texture classification.

5.3.2 Soil erodibility mapping

5.3.2.1 National soil erodibility map based on LUCAS topsoil samples

The mean spatially predicted soil erodibility for Switzerland is $0.0327 \pm 0.0044 \text{ t ha h ha}^{-1} \text{ MJ}^{-1} \text{ mm}^{-1}$. The histogram represents a bell-shaped curve with varying K-factors from 0.0143 to $0.0517 \text{ t ha h ha}^{-1} \text{ MJ}^{-1} \text{ mm}^{-1}$. Lowest values are in the Alpine valleys and highest in the top elevated regions of the Swiss Alps. The map has a spatial resolution of 500 m (Fig. 5.2, note that urban areas and lakes have been removed from the resulting Swiss K-factor map). The RMSE at all the 199 locations of predicted and measured samples is $0.0048 \text{ t ha h ha}^{-1} \text{ MJ}^{-1} \text{ mm}^{-1}$. The standardized measure of certainty f is 87% for the predicted K values (Fig. 5.3). The distribution of certainties of predicted and observed K-factors is heterogeneous without any apparent distribution. The RMSE of all 1836 samples used for the spatial prediction (Switzerland incl. adjacent countries) is $0.0064 \text{ t ha h ha}^{-1} \text{ MJ}^{-1} \text{ mm}^{-1}$ with a mean predicted K of $0.0328 \text{ t ha h ha}^{-1} \text{ MJ}^{-1} \text{ mm}^{-1}$ and a f of 82%.

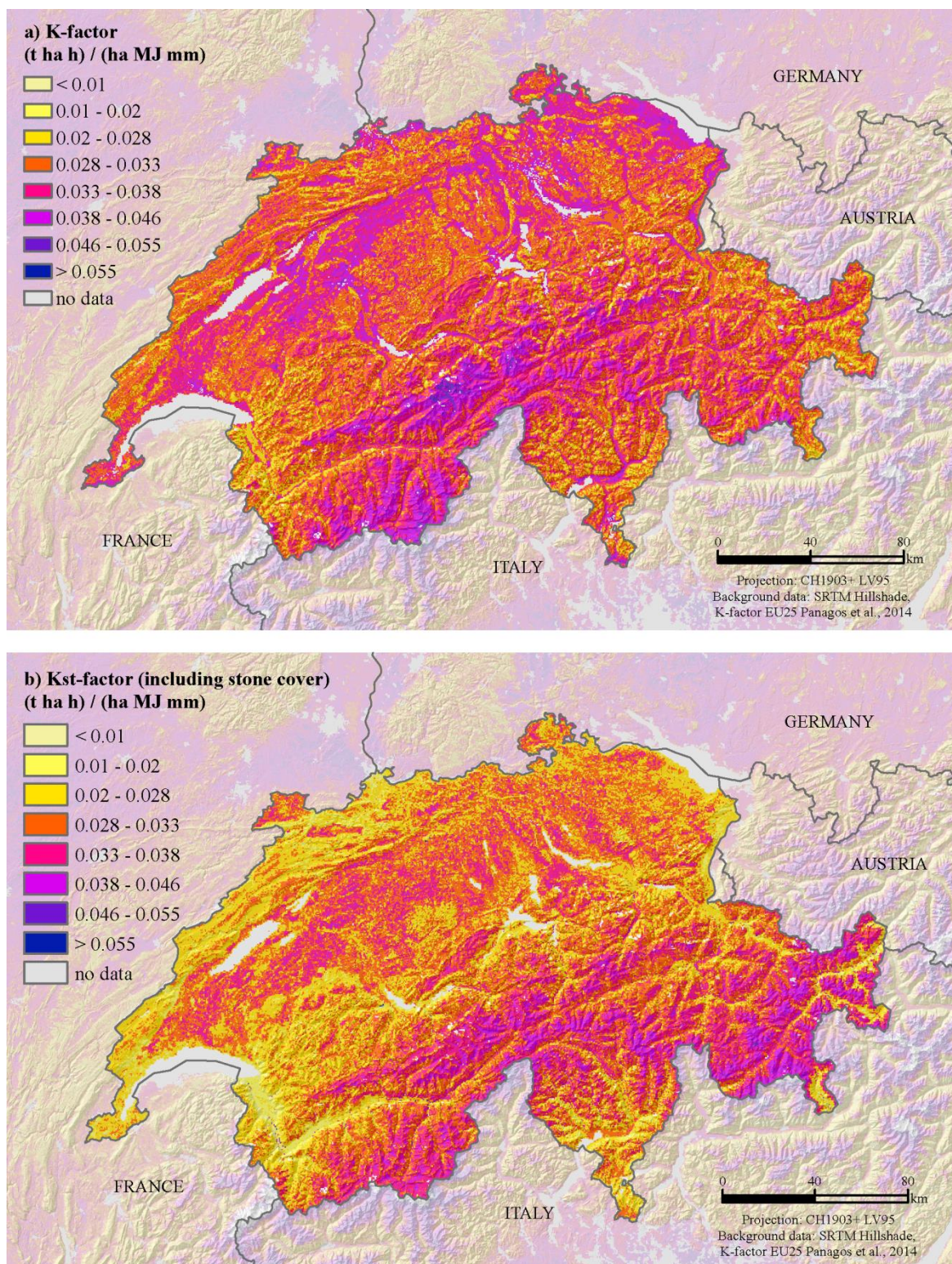


Fig. 5.2: (a) K-factor and (b) Kst-factor (including the effect of stone cover) maps of Switzerland.

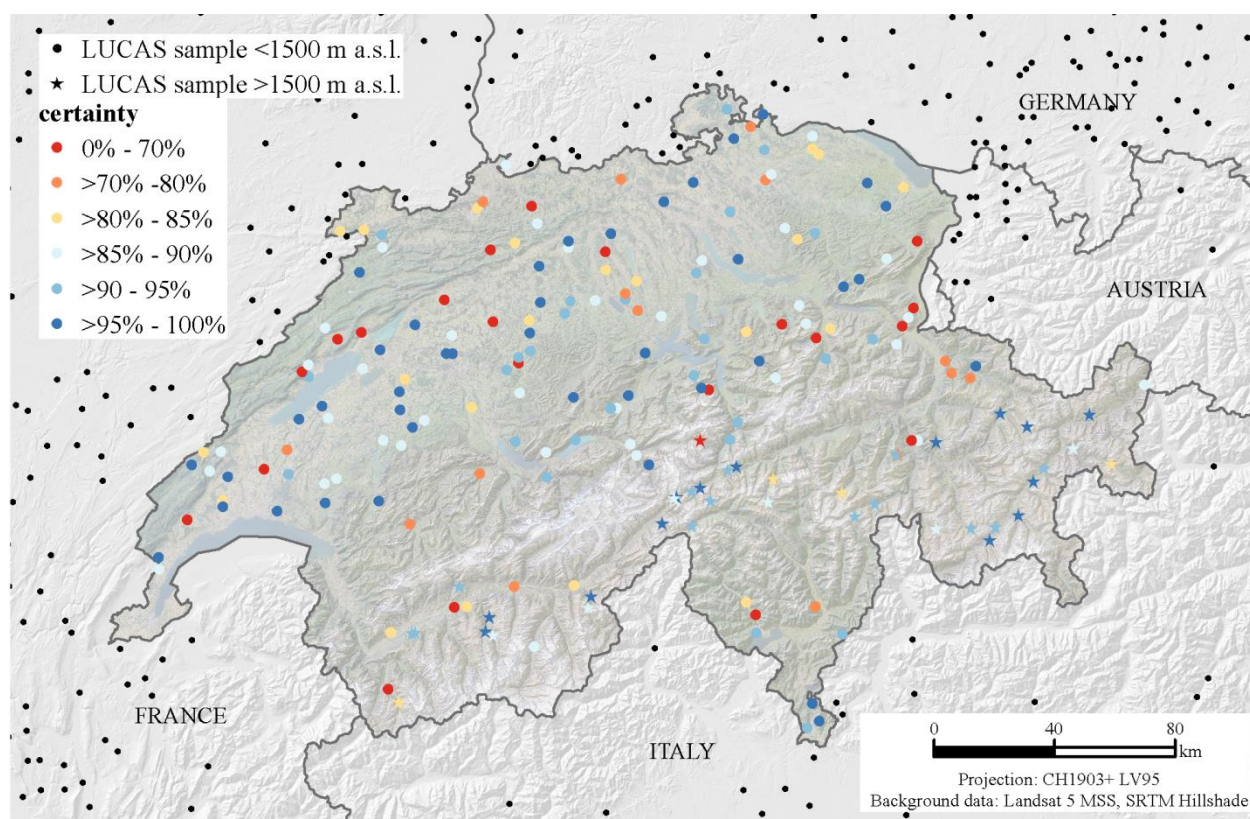


Fig. 5.3: Certainty map of observed and predicted K-factor values of Switzerland in percentage (0% low certainty; 100% very high certainty) and distribution of LUCAS samples. Certainty is calculated according to equation 5.4. Black dots in the surrounding of Switzerland represent a subset ($n=261$) of the additional used 1638 LUCAS samples.

Advantages of CR are its capacity to work for non-linear relationships and its interpretability. It diminishes overfitting due to its partitioning and rule-based routines (Malone et al., 2017). Cubist is among the best performing prediction methods compared to 17 others (e.g., random forest, neural net, linear regression) (Kuhn and Johnson, 2013). MBS has a high performance in terms of computing speed and automatic optimization of the parameters. It was preferred over kriging, as kriging is heavily dependent on the variogram estimation, which can be problematic especially in computing the empirical variogram. The choice of binning distance, maximum range, and other parameters can drastically change the final outcome. Moreover, kriging makes several assumptions about data distribution that are often not met in practice.

Vegetation indices, reflectance data, terrain features and spatial coordinates were used as covariates. The relative importance of the used covariates is already discussed (Panagos et al., 2014c). A direct relationship between the K-factor and hillslope features could be proved for mountainous areas of Southern Italy (Colombo et al., 2010). Kulikov et al. (2017) used terrain features (e.g., slope degree and curvature, elevation) next to Landsat band ratios as covariates to spatially model K-factors in Kyrgyzstan. According to a review by McBratney et al. (2003), the key sources of environmental covariates for predicting soil properties were either relief (80%) and/ or auxiliary soil property (35%) data. Additionally, spatial coordinates appear to be serving as a meaningful predicting factor in DSM. They include spatial relationships which are not expressed in any other environmental variable (McBratney et al., 2003). Usually, parent

material can be seen as a suitable covariate for soil erodibility as a relationship of the geological parent material and soil texture is often assumed (André and Anderson, 1961). However, our analysis on Alpine soils showed no significant correlation of geological bedrock and soil texture due to the homogeneous glacial till coverage (Blume et al., 2016) and the sampling only of topsoils.

Comparison of modeled K-factors for Switzerland and the surrounding countries reveal a mean of soil erodibility close to the averages of Austria ($0.0321 \text{ t ha h ha}^{-1} \text{ MJ}^{-1} \text{ mm}^{-1}$), Germany ($0.0334 \text{ t ha h ha}^{-1} \text{ MJ}^{-1} \text{ mm}^{-1}$), and Italy ($0.0322 \text{ t ha h ha}^{-1} \text{ MJ}^{-1} \text{ mm}^{-1}$). The K-factor of Slovenia is slightly lower ($0.0313 \text{ t ha h ha}^{-1} \text{ MJ}^{-1} \text{ mm}^{-1}$) with highest values in the karst zone (Prus et al., 2015). One exception is met by the comparison to France where the K-factor is higher ($0.0356 \text{ t ha h ha}^{-1} \text{ MJ}^{-1} \text{ mm}^{-1}$). The higher values in France might arise out of the high proportion of erodible loess plateaus in Northern France.

The average K-factors have a slightly positive altitudinal gradient (with the exception of the colline zone <800 m a.s.l.). K-factors are increasing from $0.0308 \text{ t ha h ha}^{-1} \text{ MJ}^{-1} \text{ mm}^{-1}$ in the montane zone (800-1800 m a.s.l.) to a maximum of $0.0404 \text{ t ha h ha}^{-1} \text{ MJ}^{-1} \text{ mm}^{-1}$ in the nival zone (>3100 m a.s.l.). Willen (1965) could identify a doubling of erodibility at elevation ranges of 2160 m a.s.l. compared to 600 m a.s.l. in California.

The incorporation of the stoniness cover reduces the spatially predicted mean K-factor of Switzerland by 8.2% (to $0.0297 \text{ t ha h ha}^{-1} \text{ MJ}^{-1} \text{ mm}^{-1}$ with a standard deviation of $0.0054 \text{ t ha h ha}^{-1} \text{ MJ}^{-1} \text{ mm}^{-1}$) (Fig. 5.2). This reduction is similar to the influence of stoniness in reducing K-factors in neighboring central European countries (Austria, Germany, and Slovenia). The RMSE ($0.0054 \text{ t ha h ha}^{-1} \text{ MJ}^{-1} \text{ mm}^{-1}$) is slightly higher, *f* is lower (83%) than those of the soil erodibility neglecting the stoniness effect. The strongest effect of stoniness to the soil erodibility is visible in the region close to the French border (Jura mountain range) and the northern Alpine foothill (Fig. 5.2). The reduction due to stone cover is smaller than the average reduction of the K-Factor at the European scale (15%; Panagos et al., 2014c). The latter might be explained by the relatively lower effect of stoniness in the high alpine regions of Switzerland compared to lowlands: The average K-factor in the Swiss lower regions (<1500 m a.s.l.) is reduced by 12.2%, in the Swiss Alpine region (>1500 m a.s.l.) only by 1.8%.

As auxiliary soil data, we considered datasets from Swiss federal agencies (e.g., NABODAT, Rehbein et al., 2017) and cantonal soil data. In these particular cases, we had to deal with inconsistencies owing to different soil sampling methods, sampling periods, laboratory analysis, clustered data, incomplete spatial coverage, and missing parameters. Thus, the tested local data could not be used to improve the model result.

5.3.2.2 Comparison with extrapolated mapping of soil erodibility at the European scale

The comparison of the extrapolated (EU map; no measured data for Switzerland available; Panagos et al., 2014c) and the interpolated map (including measured data from Switzerland, this study) with identical methods (CR, MBS) and covariates results in similar average K-factor values for Switzerland ($0.0327 \text{ t ha h ha}^{-1} \text{ MJ}^{-1} \text{ mm}^{-1}$ vs. $0.0333 \text{ t ha h ha}^{-1} \text{ MJ}^{-1} \text{ mm}^{-1}$). The mean deviation of extrapolated and interpolated average values is -1.2%. The mean is relatively balanced by considering under- and overestimation simultaneously. However, the spatial patterns, mainly caused by the addition of the measured Alpine samples that had not been integrated into the LUCAS before, expose some systematic deviations (Fig. 5.4).

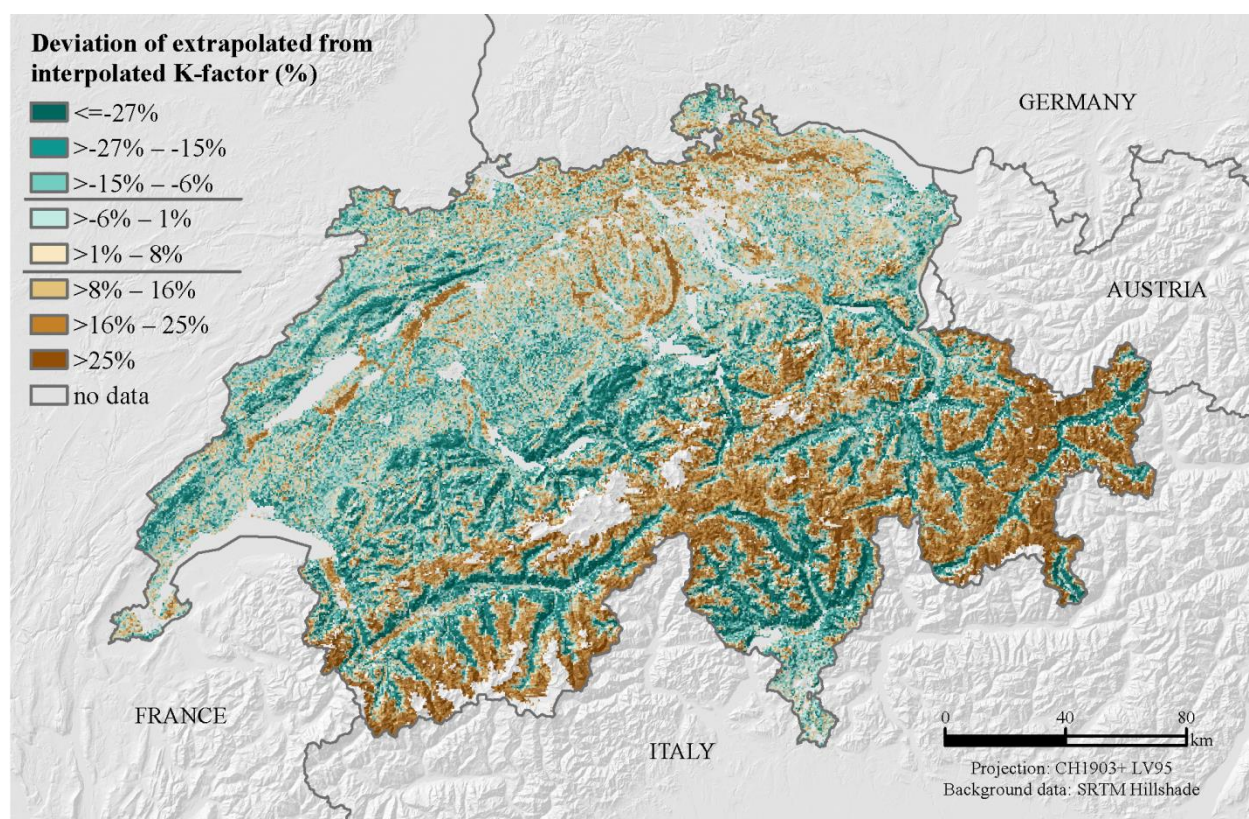


Fig. 5.4: Difference of extrapolated K-factors (with no measured data from Switzerland) to the interpolated K-factors (based on 199 additional LUCAS topsoil samples in Switzerland) in percentages. Map classes are classified according to quantiles.

The difference map shows an overestimation of K-factors in the top Alpine region and an underestimation in the valleys and Northern/Southern Alpine foothills by the extrapolated EU map compared to the interpolated map of this study. The highest overestimation can be found in the eastern Alps (Canton Grisons). The differences between extrapolation and interpolation of soil erodibility are relatively small in the lower relief Swiss midland in the north of the Alps, because these areas seem to be well represented by the non-Swiss LUCAS dataset. Regions with a small deviation (-6% to 8%) from the interpolated K-factor map have an average elevation of 272 m a.s.l.. The extrapolation is based on LUCAS topsoil samples of the surrounding EU countries and the sampling campaign was limited up to heights of 1500 m a.s.l.. This means that alpine samples were not considered in the extrapolation at all. Thus, neglecting of mountainous soils might provoke high uncertainties with a general trend of overestimating K-factors in the mountains. In contrast, even though lower regions like the Alpine valleys are included in the sampling of other countries were obviously nevertheless difficult to predict, most likely owing to the complex relief situations in Europe.

We calculated the local mean soil losses on a polygon scale over 100 random municipalities to evaluate the influence of an under-/or overestimate on the overall soil erosion risk assessment. The municipalities were derived from a total of 2382 Swiss municipalities of the dataset SwissBOUNDARIES3D (Swisstopo, 2018b). They are randomly distributed in Switzerland and are differently-sized (from 1.2 km² to 149.2 km²). We used the annual R-, annual C-, and the LS-factor to multiply them once with the interpolated and once with the extrapolated annual K-factor of Switzerland. Results of the 100 municipalities showed a

tendency of the extrapolated K-factors to overestimate soil loss by 6.3% and underestimate soil loss by 2.5% in the Alpine region (>1500 m a.s.l.) and lower regions (<1500 m a.s.l.), respectively.

5.4 Conclusions

The soil data of the Swiss soil erodibility mapping originates from the first LUCAS sampling campaign including samples above 1500 m a.s.l.. For the first time, the K-factor based on measured topsoil samples is presented on a national scale in Switzerland. We modeled the spatial distribution of soil erodibility for Switzerland with Cubist Regression and Multilevel B-Splines under consideration of environmental covariates. An incorporation of the stoniness into the K-factor cover causes a mean reduction of 12.2% in the lower regions (<1500 m a.s.l.) and 1.8% in the Alpine regions (>1500 m a.s.l.). A comparison of the K-factors interpolated with 199 measured LUCAS topsoil samples in Switzerland (including n=39 >1500m a.s.l.) and extrapolated values based only on soil samples of the neighboring countries <1500m a.s.l. of previous LUCAS campaigns not considering Switzerland, resulted in surprisingly consistent average values, but indicated considerable spatial deviations mostly at high elevations and in Alpine valleys. The analysis demonstrates that regions with high elevation contrasts but no measured soil data tend to be over- or underestimated. A well-distributed sampling network, extended even to high elevation regions, increased the mapping accuracy compared to an extrapolated approach without measured soil samples within the predicted area. Our results suggest that the soil erodibility in other Alpine countries might also be under-/ overestimated due to a lack of topsoil samples on mountainous regions. A sampling of mountainous regions as was done in this study in Switzerland should be envisaged in future campaigns of Alpine countries to reduce that uncertainty in soil erodibility and in soil loss assessments.

By modeling the K-factor of Switzerland we were able to fill the Swiss blank spot in the European soil erodibility map and make the Swiss values comparable to other European countries. However, caused by the number of samples and spatial resolution, the map should be used as an overview, indicating trends and regional differences within Switzerland or to neighboring countries and not as a detailed map for local studies. The mapping approach could be further improved by additional topsoil data and spatial high resolution covariates (e.g. NABODAT, Rehbein et al., 2017; SwissAlti3D, Swisstopo, 2018a). Unfortunately, most of the existing Swiss topsoil datasets do not have a national coverage and a harmonization of several datasets is impeded by various data owners, different sampling campaigns and applied sampling and analytical methodologies. It would be conceivable to use these clustered data (e.g., NABODAT data, Rehbein et al., 2017) in addition to high resolution predictors to model soil erodibility for specific regions of Switzerland with a high sampling density (e.g., for Swiss midland). The calculation of the soil erodibility for the blank spot of Switzerland on the map has not only an added value for European soil erosion risk assessments but deliver further valuable information on a continental scale for other environmental and soil related issues like site-specific land use decisions, soil and land suitability, and soil protection including agro-economic considerations.

Acknowledgments

This work was supported by the Swiss Federal Office for the Environment (FOEN) (grant numbers N° N222-0350 and N° P182-1535). We like to thank Agroscope and R.G. Meuli for the participation in the LUCAS and the allowance to use the data. Furthermore, we thank O. Fernández-Ugalde for preparing the existing LUCAS data. The authors would like to thank F. Bracher and J. Maissen for their experiments in the laboratory. We thank J. Moeys, M. Kuhn, and A. Finley et al. for providing the R packages ‘soiltexture’, ‘cubist’, and ‘MBA’.

CHAPTER 6

Modification of the RUSLE slope length and steepness factor (LS-factor) based on rainfall experiments at steep alpine grasslands

This chapter is published in MethodsX as:

Simon Schmidt¹, Simon Tresch^{2,3,4}, Katrin Meusburger⁵: Modification of the RUSLE slope length and steepness factor (LS-factor) based on rainfall experiments at steep alpine grasslands, *MethodsX*, 6, 219-229, doi.org/10.1016/j.mex.2019.01.004, 2019.

¹Environmental Geosciences, University of Basel, Bernoullistrasse 30, CH-4056 Basel, Switzerland

²Department of Soil Sciences, Research Institute of Organic Agriculture (FiBL), Ackerstrasse 113, CH-5070 Frick, Switzerland

³Functional Ecology Laboratory, Institute of Biology, University of Neuchâtel, Rue Emile-Argand 11, CH- 2000 Neuchâtel, Switzerland

⁴Biodiversity and Conservation Biology, Swiss Federal Institute for Forest, Snow and Landscape Research (WSL), Zürcherstrasse 111, CH-8903 Birmensdorf, Switzerland

⁵Forest Soils and Biogeochemistry, Swiss Federal Institute for Forest, Snow and Landscape Research (WSL), Zürcherstrasse 111, CH-8903 Birmensdorf, Switzerland

Abstract

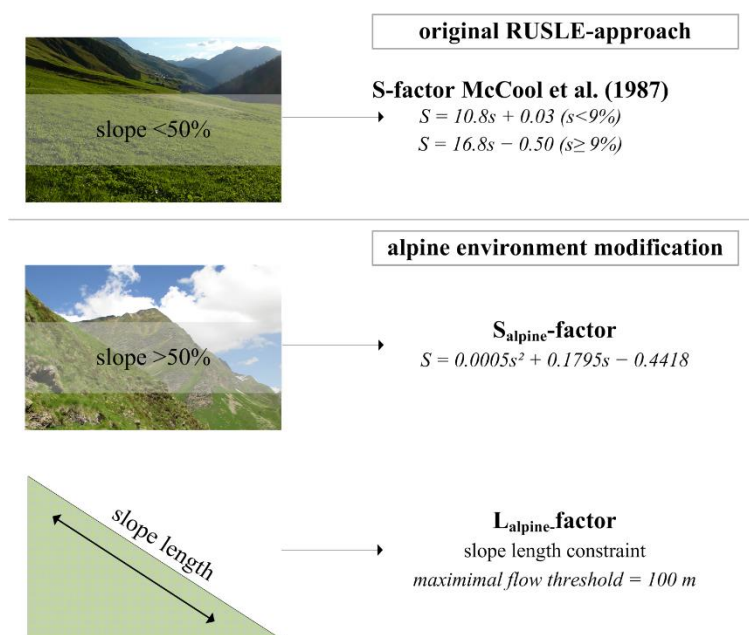
The slope length and slope steepness factor (LS-factor) is one of five factors of the Universal Soil Loss Equation (USLE) and its revised version (RUSLE) describing the influence of topography on soil erosion risk. The LS-factor was originally developed for slopes less than 50% inclination and has not been tested for steeper slopes. To overcome this limitation, we adapted both factors slope length L and slope steepness S for conditions experimentally observed at Swiss alpine grasslands. For the new L -factor (L_{alpine}), a maximal flow path threshold, corresponding to 100 m, was implemented to take into account short runoff flow paths and rapid infiltration that has been observed in our experiments. For the S -factor, a fitted quadratic polynomial function (S_{alpine}) has been established, compiling the most extensive empirical studies. As a model evaluation, uncertainty intervals are presented for this modified S -factor. We observed that uncertainty increases with slope gradient. In summary, the proposed modification of the LS-factor to alpine environments enables an improved prediction of soil erosion risk including steep slopes.

Keywords: Revised Universal Soil Loss Equation, Erosion modeling, Switzerland, Terrain features, Maximal, Flow length

Highlights:

- Empirical experiments (rainfall simulation, sediment measurements) were conducted on Swiss alpine grasslands to assess the maximal flow length and slope steepness factor (S -factor).
- Flow accumulation is limited to a maximal flow threshold (100 m) at which overland runoff is realistic in alpine grassland.
- Slope steepness factor is modified by a fitted S -factor equation from existing empirical S -factor functions.

Graphical Abstract



Specifications Table

Subject area	<i>Environmental Science</i>
More specific subject area	<i>Soil erosion modeling</i>
Method name	<ul style="list-style-type: none"> - L_{alpine} - S_{alpine} - LS_{alpine}
Name and reference of original method	<p>USLE LS-factor: Wischmeier, W.H., & Smith, D.D. (1978). Predicting rainfall erosion losses. Washington.</p> <p>S-factor: McCool, D.K., Brown, L.C., Foster, G.R., Mutchler, C.K., & Meyer, L.D. (1987). Revised Slope Steepness Factor for the Universal Soil Loss Equation. Transactions of the ASAE, 30, 1387–1396. doi:10.13031/2013.30576.</p> <p>S-factor: Smith, D.D., & Whitt, D. (1948). Estimating soil losses from field areas. Agricultural Engineering, 29, 394–396.</p>
Resource availability	<ul style="list-style-type: none"> - SAGA GIS (http://www.saga-gis.org; Conrad et al., 2015) - RSAGA (https://cran.r-project.org/web/packages/RSAGA/index.html; Brenning et al., 2018)

6.1 Introduction

The slope length factor L and slope steepness factor S , often lumped together as the topographic factor LS . The LS -factor is one of the factors (R rainfall erosivity, C cover and management factor, K soil erodibility, P support practices) of the Universal Soil Loss Equation (USLE) and its revised version (RUSLE) (Renard et al., 1991; Wischmeier and Smith, 1978). LS is a factor that describes the influence of the topography to the soil erosion risk by considering the length of a slope and the influence of surface runoff which can be active on eroding soil material before it infiltrates or continuous as interflow. Furthermore, it includes the steepness of a slope as runoff on steeper slopes has a higher gravity and therefore is more relevant for erosion.

With the availability of Digital Elevation Models the calculation of LS -factors in GIS environments was made possible even for large-scale erosion modeling approaches. Winchell et al. (2008) revealed a reasonable agreement of GIS-based LS -factor and field measured LS -factors of the US Natural Resource Inventory database for the Mississippi Catchment.

Originally, the LS -factor was assessed on a 9% steep slope with a length of 22.13 m (72.6 feet) (Wischmeier and Smith, 1978). Owing to its empirical character, LS -factors are usually limited to a maximum slope angle of 50% (26.6°) (McCool et al., 1987; Liu et al., 2000). As Switzerland is a country with a high elevation gradient from 192 m a.s.l. to 4633 m a.s.l. (mean elevation 1288 m a.s.l.) and a mean slope gradient of up to 36% (20°), a not negligible fraction of slopes (4.7%) exceeds the limitation of 50%. Yet, no uniform equation to assess the LS -factor for steep slopes like in the alpine environment of Switzerland was presented to the scientific community. Only a few studies are dealing with LS -factors on steep slopes (e.g., Liu et al., 2000). For example, slopes >50% were disregarded in the most recent European Union's LS -factor map by Panagos et al. (2015b).

To overcome that limitation in LS -factor modeling on steep slopes, we (i) limited the potential flow path length to a maximal flow and (ii) choose the most representative equation for Swiss steep slopes.

6.2 Method details

6.2.1 Existing approaches for S- and L-factor parametrization

The LS -factor is a product of the slope length (L -) and the slope steepness (S -factor). The most widely used slope length factor represents the ratio of observed soil loss related to the soil loss of a standardized plot (22.13 m). Originally, Wischmeier and Smith (1978) defined the L -factor as Eq. 6.1:

$$L = \left(\frac{\lambda}{22.13} \right)^m \quad (6.1)$$

where λ represents the length of the slope in meters and m the different slope steepness. Later, Eq. 6.2 was adapted for the RUSLE-approach to better describe soil loss with increasing slope steepness. Desmet and Govers (1996) transformed the original L -factor (Eq. 6.1) into a

GIS-approach (Eq. 6.2) considering the flow accumulation and adding a ratio of rill to interrill erosion (Eq. 6.3):

$$L_{i,j} = \frac{(A_{i,j-in} + D^2)^{m+1} - A_{i,j-in}^{m+1}}{D^{m+2} * X_{i,j}^m * 22.13^m} \quad (6.2)$$

where $A_{i,j-in}$ is the flow accumulation in m^2 at the inlet of a grid cell (i,j). D is the grid cell size in m and $X_{i,j}$ equals to $\sin a_{i,j} + \cos a_{i,j}$ where $a_{i,j}$ is the aspect of the grid cell (i,j). The coefficient m (Eq. 6.3) represents the ratio of rill and interrill erosion and is calculated by the β -value (Eq. 6.4):

$$m = \frac{\beta}{\beta+1} \quad (6.3)$$

With a range between 0 (ratio of rill to interrill erosion close to 0) and 1.

$$\beta = \frac{\frac{\sin \theta}{0.0896}}{[0.56+3*(\sin \theta)^{0.8}]} \quad (6.4)$$

Where θ is the slope angle in degrees.

For the S-factor, most often the empiric function proposed by McCool et al. (1987) is used to determine the slope steepness factor in the Revised Universal Soil Loss Equation (RUSLE). McCool et al. (1987) differentiate the relation between soil loss and slope steepness in radians (s) with two functions. One for slopes with an inclination less than 9% and the other greater or equal 9%. The functions are as follows:

$$S = 10.8s + 0.03 \quad \text{for slope steepness in percent} < 9\% \quad (6.5)$$

$$S = 16.8s - 0.50 \quad \text{for slope steepness in percent} \geq 9\% \quad (6.6)$$

The S-factor after McCool et al. (1987) is particular recommended for areas with low summer rainfall amounts (Auerswald, 1986). Many other empirical S-factors were developed since the 1940s (Table 6.1) but all S-factors have in common that empirical evidence and thus validity is limited to slope gradients less than 50%.

Table 6.1: Review of selected S-factors (S)

Source	function	Description
Zingg (1940)	$S = \left(\frac{S}{9}\right)^{1.4}$	s = slope steepness in percent
Musgrave (1947)	$S = \left(\frac{S}{9}\right)^{1.35}$	s = slope steepness in percent
Smith and Whitt (1948)	$S = 0.025 + 0.052s^{\frac{4}{3}}$	s = slope steepness in percent
Smith (1958)	$S = 0.00650s^2 + 0.0453s + 0.065$	s = slope steepness in percent
Smith (1958)	$S = 0.044 + 0.10s - 0.00073s^2$	s = slope steepness in percent

Wischmeier and Smith (1978)	$S = 65.4\sin\theta^2 + 4.56\sin\theta + 0.0654$	θ = slope steepness in radians
McCool et al. (1987)	$S = \left(\frac{\sin\theta}{0.00896}\right)^{0.6}$	θ = slope steepness in radians
Foster (1982)	$S = 3(\sin\theta)^{0.8} + 0.56$	θ = slope steepness in radians
McCool et al. (1987)	$S = 16.8\sin\theta - 0.5$	θ = slope steepness in radians
McCool et al. (1987)	$S = 10.8\sin\theta + 0.03$	θ = slope steepness in radians
Nearing (1997)	$S = -1.5 + \frac{17}{1 + e^{2.3-6.1\sin\theta}}$	θ = slope steepness in radians
Liu et al. (2000)	$S = 21.91\sin\theta - 0.96$	θ = slope steepness in radians
S_{alpine} present study	$S = 0.0005s^2 + 0.1795s - 0.4418$	s = slope steepness in percent

6.2.2 Proposed adaption of the L-factor

Often, GIS modeled potential flow path length on slopes, expressed as flow accumulation in a GIS-environment, is driven by gravity and generally not limited (Orlandini et al., 2012). In particular cases, these potential flow path lengths can reach many kilometers and enormous runoff volumes. The flow accumulation can be constrained by streets or houses as ending points of the potential flow paths as discussed by Winchell et al. (2008).

In 2016, we conducted 19 different rainfall simulation experiments on south facing slopes in an alpine environment (Val Piora, Switzerland) with different conditions regarding soil moisture (dry, moist), steepness (36° to 82°), and vegetation (low, medium, full vegetation cover) to observe the flow path lengths. The rainfall simulations were realized with an Eijkelkamp mini rainfall simulator (type M1.09.06.E, Eijkelkamp, NL; Figure 6.1) for erosion tests with a rainfall intensity of 640 mm/h and an energy of 4 J mm⁻¹ m⁻². This rainfall energy is comparable with the average rainfall energy of Val Piora (station Piotta; 5.6 J mm⁻¹ m⁻²; MeteoSwiss, 2018a). Regardless of the conditions, our observations revealed short surface flow path lengths at the scale of meters with a rapid infiltration into shallow alpine soils. Our measurements and observations show, that potential flow paths without considering infiltration is not realistic for alpine environments and thus, requesting a maximal flow threshold for the estimation of the slope length factor L. McCool et al. (1997) and Winchell et al. (2008) limited the slope length to a maximal threshold of 333m (1000 feet) as longer slope length appear only occasionally. According to McCool et al. (1997), the usual threshold in many cases is 121 m (400 feet). As a compromise of their suggestion and our observed short flow path lengths in the Swiss Alps, we decided to limit the maximal flow length to 100 m.



Fig. 6.1: Different setups and preconditions of the rainfall simulation experiment on steep slopes in Val Piora, Ticino, Switzerland

The threshold is implemented as a condition either directly in SAGA GIS or in RSAGA after creating the flow accumulation grid:

$$A_{\text{alpine } i,j-\text{in}} = \text{ifelse}(A_{i,j-\text{in}} > \text{thresh}, \text{thresh}, A_{i,j-\text{in}}) \quad (6.7)$$

where $A_{\text{alpine } i,j-\text{in}}$ is the constraint flow accumulation in m^2 at the inlet of a grid cell (i,j) considering a threshold value *thresh*. That constraint flow accumulation value is inserted into the L-factor equation for the alpine environment (Eq. 6.8):

$$L_{\text{alpine } ij} = \frac{(A_{\text{alpine } i,j-\text{in}} + D^2)^{m+1} - A_{\text{alpine } i,j-\text{in}}^{m+1}}{D^{m+2} * X_{ij}^m * 22.13^m} \quad (6.8)$$

Likewise to Eq. 6.2, D is the grid cell size in m and $X_{i,j}$ equals to $\sin a_{i,j} + \cos a_{i,j}$ where $a_{i,j}$ is the aspect of the grid cell (i,j). The coefficient m is the ratio of rill (β -value) to interrill erosion according to the above mentioned Eq. 6.3 and 6.4.

For our calculation of L-factor using a 2 m resolution Digital Elevation Model, the maximal flow length of 100 m, corresponds to a threshold of 50 cells multiplied by the cell size of 2 m (Fig. 6.2).

Additionally, maximal flow path length was constrained by a field block cadaster. The cadaster defines hydrological units of continuous agricultural land, that are separated by landscape elements acting as flow boundaries (e.g., forests, streets, urban areas, water bodies, or ditches) following the approach of Winchell et al. (2008).

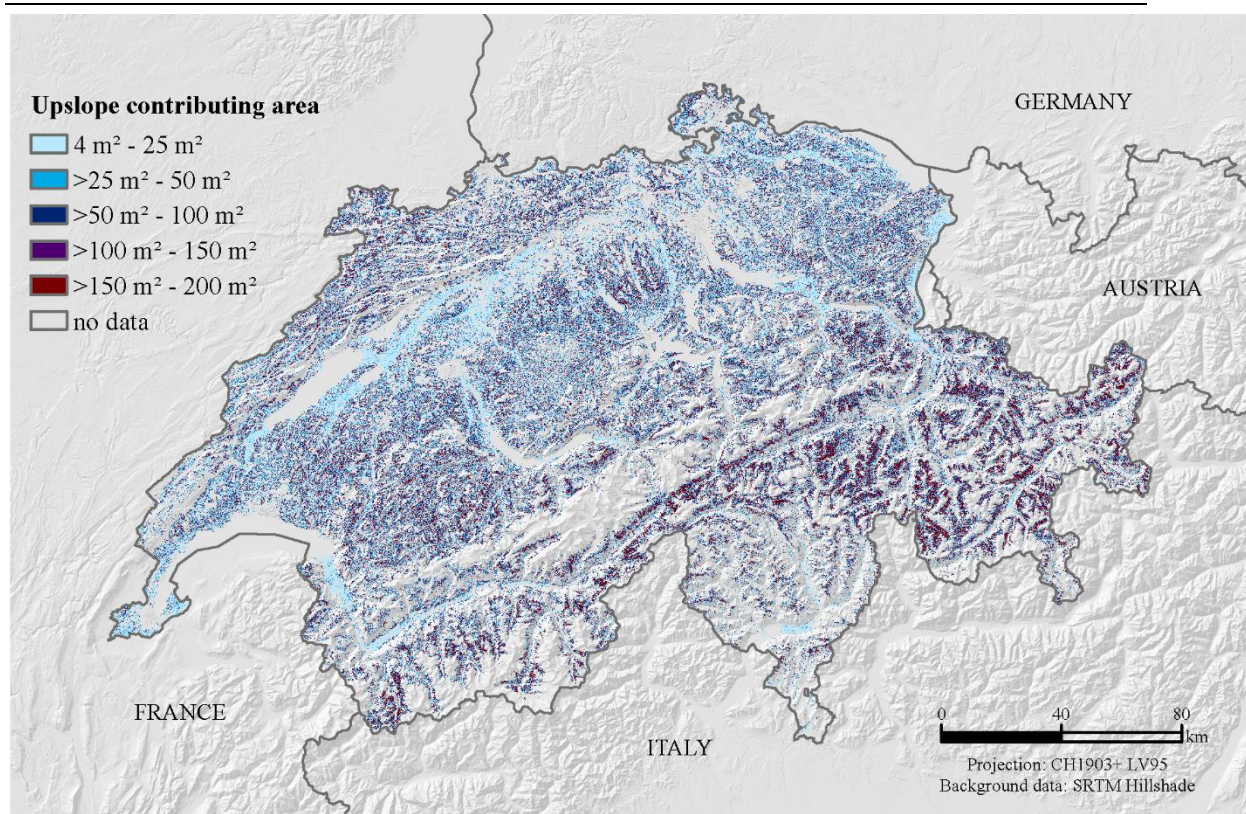


Fig. 6.2: Constraint flow accumulation grid with a maximal flow threshold of 100 m

6.2.3 Proposed adaption of the S-factor

In 2014, we conducted a total of 16 rainfall simulations on alpine slopes to assess the soil loss rates related to different slope inclinations (Table 6.2; Tresch, 2014). The experiments were conducted at a north and south facing slope both with grassland cover in the mountains of the Urseren Valley, Switzerland. At each slope two transects were selected with slope gradient ranging from 20-90%. We used a field hybrid rainfall simulator modified after Schindler Wildhaber et al. (2012) with an intensity of 60 mm h⁻¹, which is comparable to a high rainfall event in this area.

Table 6.2: Rainfall simulation measurements at the two study sites on steep alpine slopes in Switzerland under consideration of different inclinations and vegetation cover

N°	inclination (°)	vegetation cover (%)	measured sediment rate (t ha ⁻¹ yr ⁻¹)	normalized ^a sediment rate (t ha ⁻¹ yr ⁻¹)	normalized ^a sediment rate without outliers (t ha ⁻¹ yr ⁻¹)
1	17	23	13.8	8.5	8.5
2	22	33	0.6	0.7	0.7
3	11	27	0.0	0.0	0.0
4	27	41	1.2	1.6	1.6
5	31	35	0.2	0.2	0.2
6	35	34	6.8	5.6	5.6
7	42	53	9.4	19.0	19.0
8	39	26	31.0	17.4	17.4

Modification of the RUSLE slope length and steepness factor (LS-factor) based on rainfall experiments at steep alpine grasslands

9	11	33	0.6	0.7	0.7
10	17	36	1.4	1.8	1.8
11	22	47	1.3	2.0	2.0
12	27	33	34.3	40.6	
13	31	63	26.1	111.3	
14	35	38	11.1	13.1	13.1
15	39	34	40.2	26.0	26.0
16	42	40	75.4	69.8	

^aby C-factor with 35% vegetation cover, L-factor of 1.2, and K-factor of 0.031

The experimental sites showed small variation in vegetation cover, soil erodibility, and slope length (due to the effect of slope angle), therefore all experimental plots were normalized to average values of the respective factors. S-factors were fitted to observed soil loss versus sine of the slope angle using an exponential, power, and polynomial equation to the original dataset with all observation and a dataset excluding one outlier (N° 13), and three outliers (N° 12, 13, 16). The nine regression lines yield R² estimates between 0.18 and 0.70, but differ largely with increasing slope steepness. This range of S-factors with increasing steepness is comparable to previous developed empirical S-factor equations (Table 6.1, Fig. 6.1). Therefore, we decided that a fitted function (S_{alpine} in Table 6.1, Fig. 6.1) complying the most important S-factors from the literature would be most suitable to describe the soil loss behavior at steep slopes. The aggregated S function and is a quadratic polynomic function with progressive growth (Eq. 6.9):

$$S_{\text{alpine}} = 0.0005s^2 + 0.7956s - 0.4418 \quad (6.9)$$

Where s is the slope steepness in percent.

S_{alpine} is very close to the empirical normalized function proposed by Musgrave (1947) for a slope steepness of 9%.

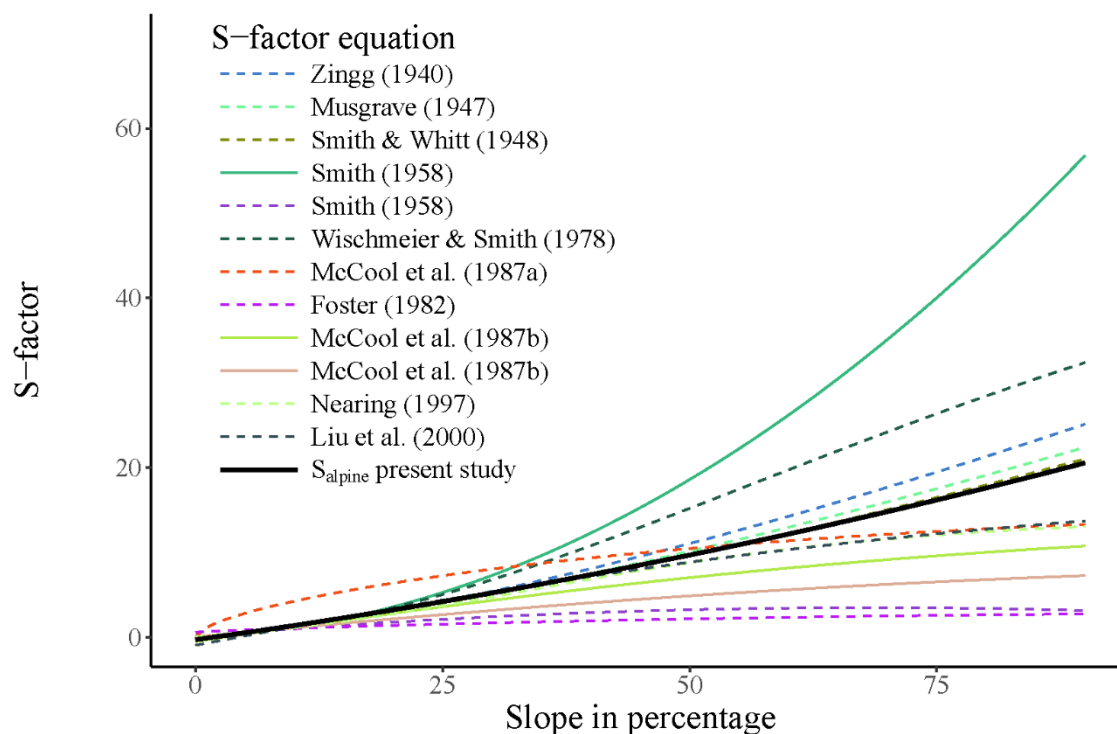


Fig. 6.3: Review and behavior of different empirical S-factor functions and the fitted function for steep alpine environments (S_{alpine})

6.3 The Swiss LS-factor map including the Alps

The resulting modeled mean LS_{alpine} -factor of Switzerland is 14.8. The LS-factor increases with elevation gradient from a mean of 7.0 in the zone <1500 m a.s.l. to 30.4 in the zone >1500 m a.s.l.. A cluster of highest mean LS-factors can be found across the Alps (Fig. 6.4). The lowest mean LS-factors are in the Swiss lowlands. South-western facing slopes have higher LS-factors (17.6) compared to plain surfaces (0.04) and north facing slopes (12.5).

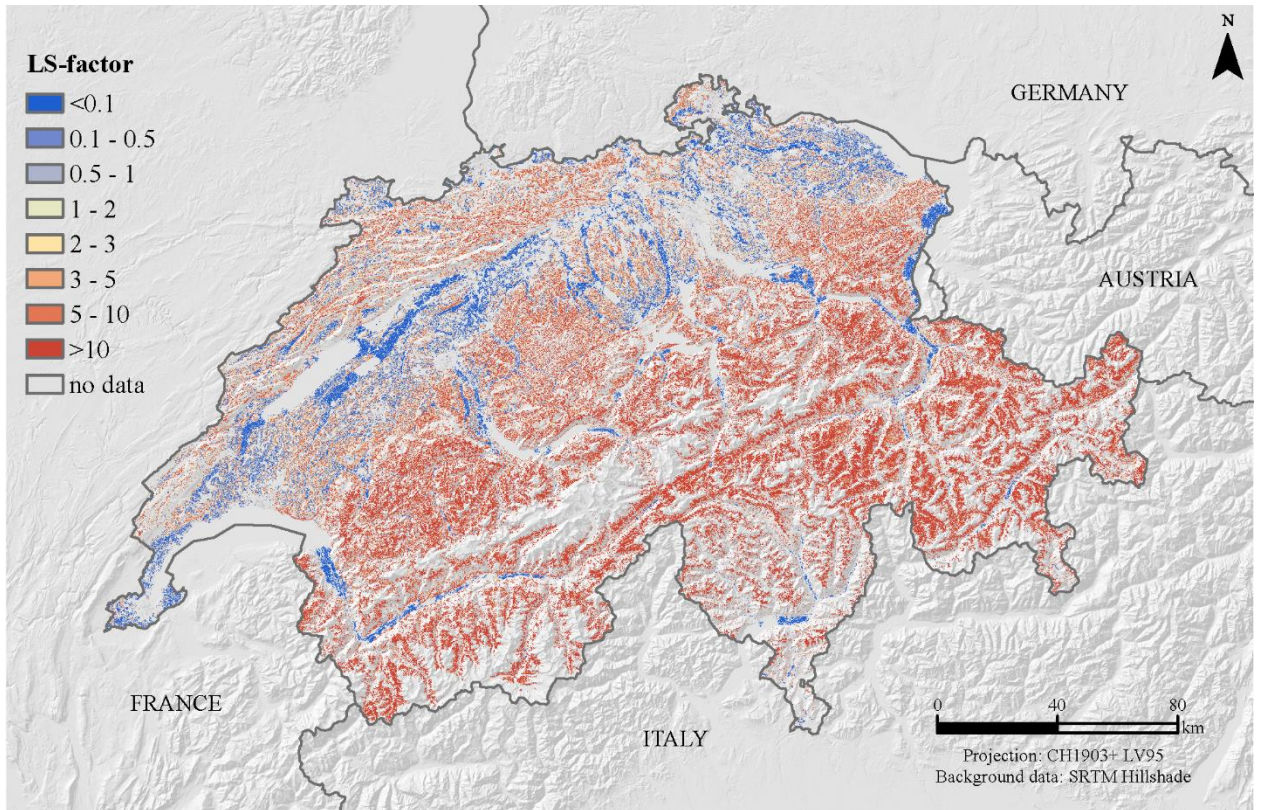


Fig. 6.4: LS_{alpine} -factor map (spatial resolution 2 m) for Switzerland derived by the digital elevation model SwissAlti3D

6.4 Quality assessment and method uncertainties

The original LS-factor has its origin in empirical field experiments and is developed for a maximum slope steepness of 50%. Validation of existing equations for slopes that are steeper than 50% is a challenge. However, while previous studies at inclinations $>25\%$ with approximately 20 plot measurements (Kilinc and Richardson, 1973, 24 plots; Liu et al., 1994, 19 plots; Liu et al., 2000, 9 plots; Merz et al., 2009, 22 plots; Schindler Wildhaber et al., 2012, 6 plots) were successful in delineating and S-factor equation, in our case the variability of the data impeded a unique solution of the S-factor equation. To account for this high variability and still existing uncertainty, the way forward is to include the variability in the LS-factor calculation.

We investigated the deviation in percentage of our proposed S_{alpine} to a conservative function and a rather progressive function. The conservative function (S_{cons}) is based on the translated and scaled sine functions of Eq. 6.5 and 6.6 by McCool et al. (1987) with a proportional and slightly digressive growth. The progressive function (S_{prog}) is a quadratic polynomial function according to Smith and Whitt (1948) with a progressive growth, but a higher coefficient than the here presented fitted function S_{alpine} (Eq. 6.10) for S_{alpine} .

$$S_{\text{prog}} = 0.00650s^2 + 0.0453s + 0.065 \quad (6.10)$$

Where s is the slope steepness in percent.

Low uncertainty has a deviation close to 0%. Higher percentages equals to a higher deviation of $S_{\text{cons/prog}}$ to S_{alpine} .

The deviation of S_{alpine} to S_{cons} shows higher deviations in areas with less slope gradients (parts of Swiss midland) (Fig. 6.5). The steep slope areas in the Alps have deviations of 25% to 50%. Both functions, S_{alpine} and S_{cons} predict the steep alpine environment in a comparable way. The deviation of the progressive S-factor (S_{prog}) and S_{alpine} diverge much more in the Alps whereas the equations are rather fitting in flatter regions (Fig. 6.6). A sharp edge of low divergence to high divergence is marked by the northern Alpine foothill with increasing slope gradients.

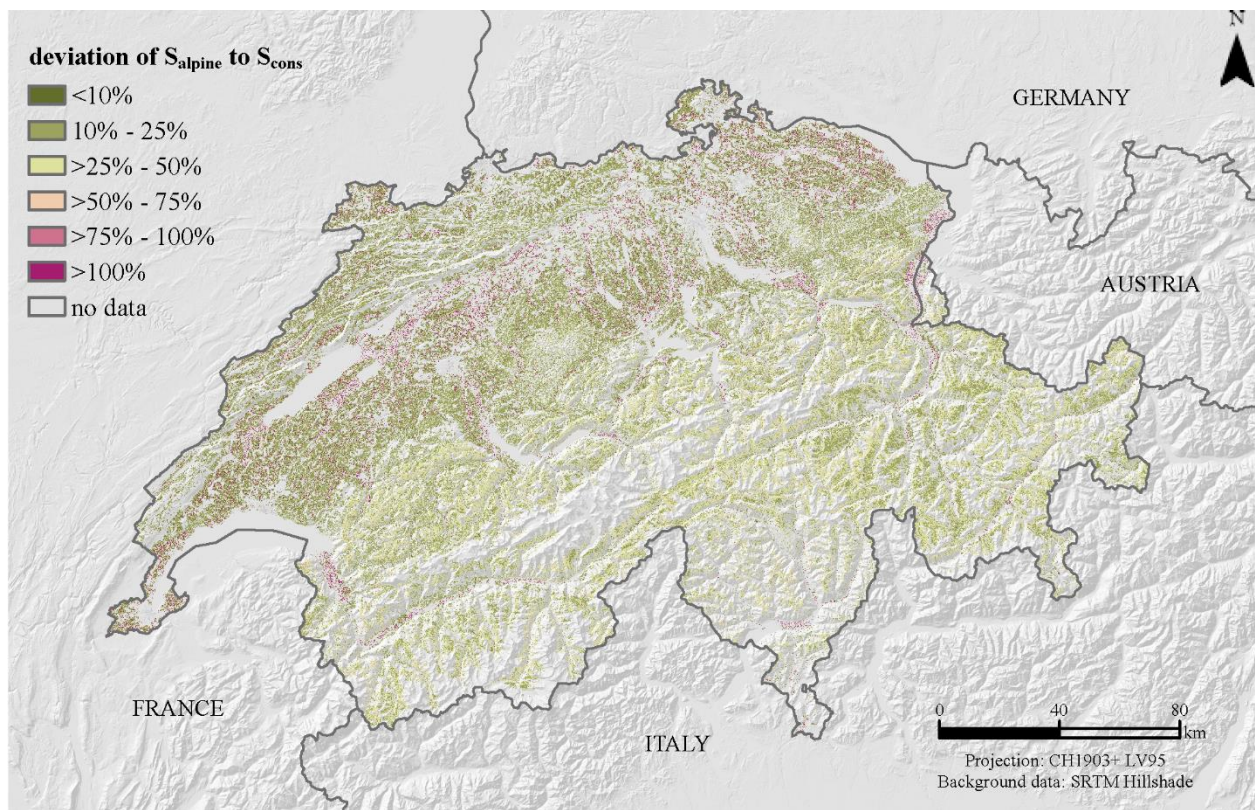


Fig. 6.5: Deviation in percentage of S_{alpine} to S_{cons} as an indicator of quality for the proposed S_{alpine} -factor. S_{alpine} is a lumped S-factor of a total of 12 empiric S-factor equations of the literature (Eq. 6.9). It can be seen as an approximation to the high slope gradients in alpine environments. S_{cons} complies with the proposed S-factor of McCool et al. (1987) (Eq. 6.5, 6.6). The deviation is presented in percentage.

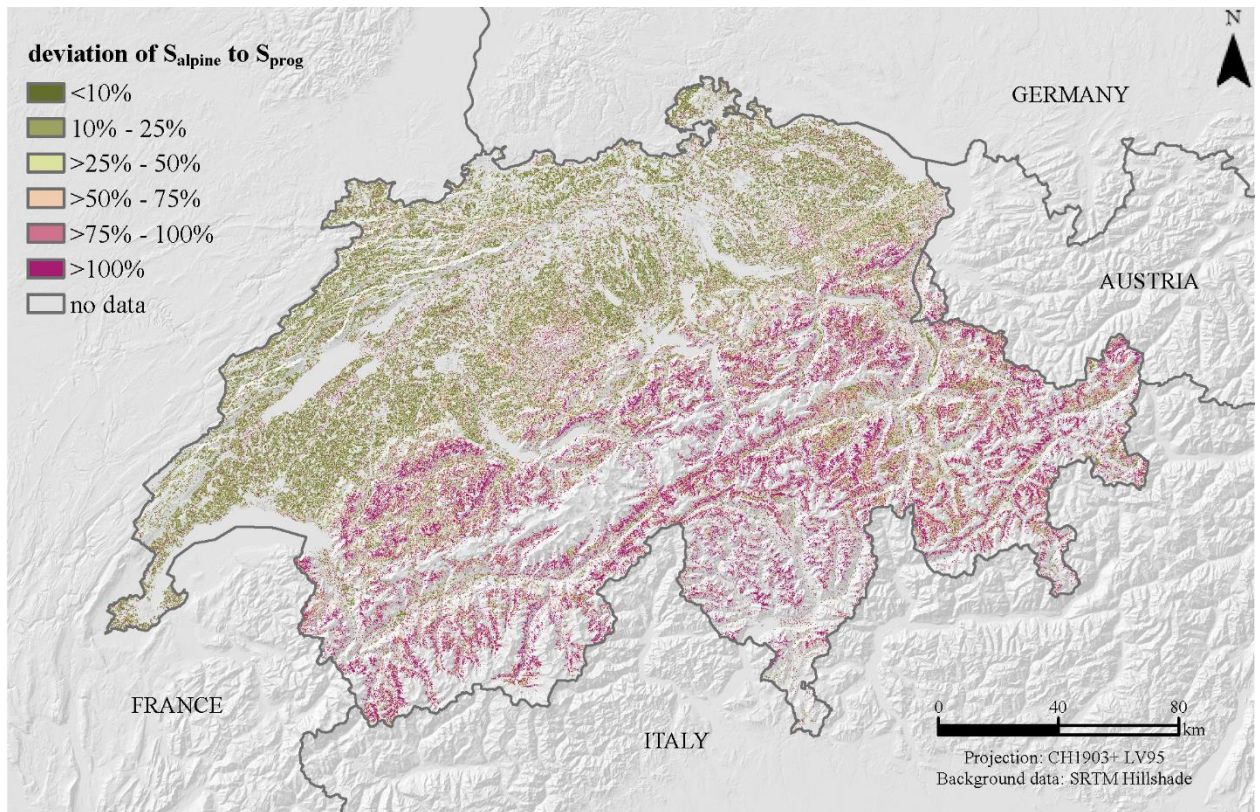


Fig. 6.6: Deviation in percentage of S_{alpine} to S_{prog} as an indicator of quality for the proposed S_{alpine} -factor. S_{alpine} is a lumped S-factor of a total of 12 empiric S-factor equations of the literature (Eq. 6.9). It can be seen as an approximation to the high slope gradients in alpine environments. S_{prog} complies with the proposed S-factor of Smith and Whitt (1948) (Eq. 6.10). The deviation is presented in percentage.

This relationship of deviation and slope gradient is not surprising as the uncertainty of many equations rises with slope steepness (cf. Fig. 6.1). García-Ruiz et al. (2015) identified an increasing trend of uncertainty for 624 measured erosion rates and slope gradients across the world for slope steepness $>11^\circ$.

The LS-Factor map of the Swiss agricultural land use unit is visually compatible with the LS-factor maps of the European Union provided by Panagos et al. (2015b) (Fig. 6.7). In contrast to the modeling of the total country area by Panagos et al. (2015b) we constrained the LS-factor to agricultural soils incl. grasslands using a field cadaster. The main differences are found on steeper slopes $>50\%$, which have been excluded in the European approach. Furthermore, the European map relies on the conservative equations 5 and 6 by McCool et al. (1987). Additionally, different spatial resolutions of Digital Elevation Models (2 m versus 25 m) are influencing the slope and aspect mapping and thus the LS-factor (Chang and Tsai, 1991; Ramli et al., 2006; Zhu et al., 2016).

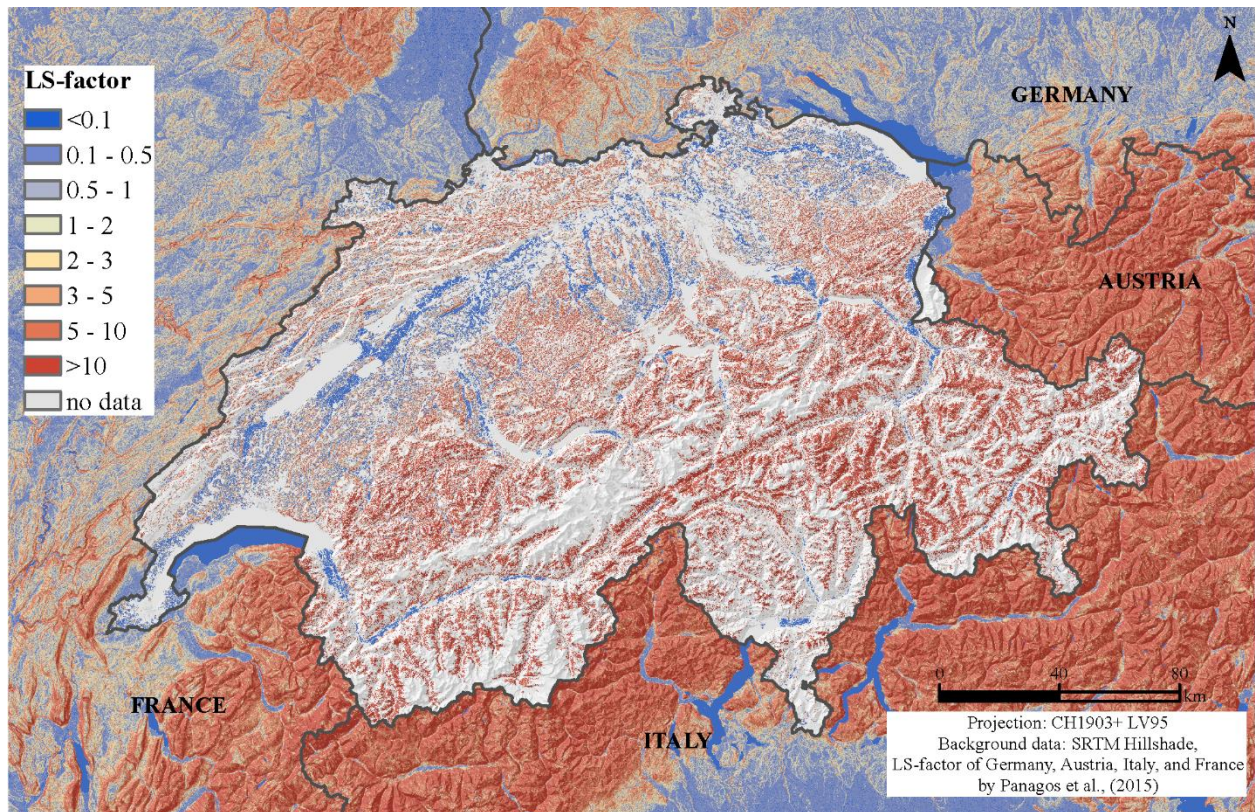


Fig. 6.7: LS-factor for the Swiss agricultural area embedded in the European Union's LS-factor map (for total country area) by Panagos et al. (2015b)

It should be considered that the number of rainfall experiments for the L-factor ($n=19$) and the S-factor ($n=16$) is short and limited only to grasslands which are the predominant land use at Swiss alpine slopes (Schmidt et al., 2018a). Rainfall simulations in alpine environments are difficult to conduct due to the harsh terrain and climate conditions. Often, the temporal period for measurements is limited by the late melt out of snow cover and the short vegetation period (Schmidt et al., 2018b). To better model the S-factor for steep alpine slopes further measurements (e.g., rainfall simulation experiments) are needed to constrain S-factor assessment for steep slopes.

Acknowledgments

This work was supported by the Swiss Federal Office for the Environment (FOEN) (grant numbers N° N222-0350 and N° P182-1535). The authors would like to thank Christine Alewell for the methodological support and Pascal Bircher for the advice in data handling with SAGA GIS/RSAGA and the upgrade of the existing field block cadaster of Switzerland. Our thank goes to M. Schulthess, C. Keller, N. Bongni, S. Rothenbühler, and A. Aeschbach for the support in the field and the footage. The authors thank Swisstopo for making their data available for this research. The authors would like to thank two anonymous referees for their valuable comments and suggestions to improve the quality of the paper.

CHAPTER 7

Monthly RUSLE soil erosion risk of Swiss grasslands

This chapter is published in Journal of Maps as:

Simon Schmidt¹, Christine Alewell¹, Katrin Meusburger^{1,2}: Monthly RUSLE soil erosion risk of Swiss grasslands, Journal of Maps, 15 (2), 247-256, doi.org/10.1080/17445647.2019.1585980, 2019.

¹Environmental Geosciences, University of Basel, Bernoullistrasse 30, CH-4056 Basel, Switzerland

²Forest Soils and Biogeochemistry, Swiss Federal Institute for Forest, Snow and Landscape Research (WSL), Zürcherstrasse 111, CH-8903 Birmensdorf, Switzerland

Abstract

This study presents the first mapping of soil erosion risk modelling based on the Revised Universal Soil Loss Equation (RUSLE) at a sub-annual (monthly) temporal resolution and national scale (100 m spatial resolution). The monthly maps show highest water erosion rates on Swiss grasslands in August ($1.25 \text{ t ha}^{-1} \text{ month}^{-1}$). In summer, the mean monthly soil loss by water erosion is 48 times higher than the mean soil loss in winter. Considering the annual average fraction of green vegetation cover of 54%, the predicted soil erosion rate for the Swiss national grassland area would add up to a total eroded soil mass of 5.26 Mt yr^{-1} . The RUSLE application with an intact 100% vegetation cover would largely reduce the soil loss to an average annual rate of $0.14 \text{ t ha}^{-1} \text{ year}^{-1}$. These findings clearly highlight the importance to consider and maintain the current status of the vegetation cover for soil erosion prediction and soil conservation, respectively.

Keywords: Soil loss, modelling, revised universal soil loss equation, Switzerland

7.1 Introduction

Soil erosion is a serious threat to soils worldwide. Currently, 6.1% of the global land surface is affected by severe soil erosion that exceeds a global tolerable soil loss threshold of $10 \text{ t ha}^{-1} \text{ yr}^{-1}$ (Borrelli et al., 2017). The annual global soil loss by water is estimated to be 35.9 billion tons for the year 2012 (Borrelli et al., 2017). The cost induced by soil erosion for the European Union is about 1.25 billion Euros per year (Panagos et al., 2018). Soil erosion control could not only reduce these costs for agriculture but could also protect the valuable soil resource (Kuhlman et al., 2010; Panagos et al., 2016c). Some protection measures (e.g. fencing of risk zones) could be even more efficient if they were implemented by spatial and temporal targeting of specific areas during the riskiest seasons of a year (Troxler et al., 2004). So far, soil erosion by water in Switzerland is modelled on an annual basis despite known temporal variations of soil loss (Prasuhn et al., 2013) and rainfall erosivity (Meusburger et al., 2012; Schmidt et al., 2016). Simultaneous identification of both, risky areas and risky seasons is urgently needed. Recently, Borrelli et al. (2018) stated that the lateral carbon transfer from erosion in noncroplands on a global scale “may play a more important role than previously assumed” because too little is known about erosion on grasslands and their impact on erosion rates is thus usually underestimated. The same knowledge gap also exists for Switzerland. However, soil loss has been observed and measured in many small scale studies by different techniques (e.g. by rainfall simulation experiments, plot experiments, tracing techniques, modelling; Martin et al., 2010; Meusburger et al., 2010b; Konz et al., 2012; Schindler Wildhaber et al., 2012; Alewell et al., 2014) and was identified to be severe at disturbed hotspots ($> 3 \text{ t ha}^{-1} \text{ yr}^{-1}$, Meusburger et al., 2010b; Alewell et al., 2015a). Since grassland areas are the dominant agricultural land use unit in Switzerland (Hotz and Weibel, 2005) they should be included in Swiss soil erosion risk maps. The common assumption of nearly zero soil loss on grasslands by the protective characteristics of the closed vegetation cover should be reconsidered, as about 6.5% of the land surface is covered by grassland (based on global CCI Land Cover 2015 data; Arino and Ramoino, 2017) with a high percentage of the grassland having low and/or damaged vegetation cover (Meusburger et al., 2010a; Gallo et al., 2001).

With the recent development of geoinformation tools and the improved quality and availability of geodata, a national assessment of the soil erosion risk for Swiss grassland is now feasible.

One of the most commonly used erosion models for modelling soil loss is the Universal Soil Loss Equation (USLE; Wischmeier and Smith, 1978) and its revised version (RUSLE; Renard et al., 1991). These empirical models are based on a multiplication of single erosion risk factors (rainfall erosivity R, soil erodibility K, cover and management C, slope length and steepness LS, support practices P).

A high intra-annual variability can generally be expected for R and C, as these factors are related mainly to the natural temporal variability of precipitation and plant growth (Renard et al., 1997). The temporal variation of the K-factor is discussed by Kinnell (2010). However, temporal changes of the K-factor are rather expected for a multi-annual scale (Wang et al., 2001). The factors LS and P are relatively static as long as no natural (e.g. landslides) or human-induced changes (e.g. implementation of new protection measures) occur (Panagos et al., 2012a). Thus, modelling of the variable R and C factors at a sub-annual scale is essential to increase the explanatory power of soil erosion prediction. Wischmeier and Smith (1965) propose a monthly temporal resolution to be appropriate for soil erosion modelling. This

recommendation was affirmed four decades later by Panagos et al. (2016c) and Karydas and Panagos (2016). Quantifying soil loss on a seasonal, monthly, weekly or even daily time-scale helps to improve our mechanistic understanding and allows for targeted protection measures. The recent availability of high temporal resolution spatial datasets (Alexandridis et al., 2015) enables a high temporal resolution of rainfall erosivity and of the cover and management factor. Several studies across the world use at least daily rainfall records to calculate the R-factor (e.g. Angulo-Martínez and Beguería, 2009; Ma et al., 2014) and model the R-factor on a seasonal (Nunes et al., 2016) or monthly scale (Ballabio et al., 2017). The modelling of monthly C-factors is presented by Yang (2014) for New South Wales, Australia with a spatial resolution of 500 m and Alexandridis et al. (2015) for Northern Greece aggregated on a catchment scale. Soil loss by water was modelled with monthly resolution by Evrard et al. (2007) and Inoubli et al. (2017) for selected catchments in Belgium and Tunisia. However, so far spatiotemporal large-scale soil erosion maps are relatively rare. National monthly soil erosion maps can only be found for Albania (Grazhdani and Shumka, 2007) and Mauritius (Nigel and Rughooputh, 2010).

The objective of the present study is to (i) quantify the monthly rates of soil loss of Swiss grasslands and (ii) delineate the spatial and temporal patterns of soil erosion risk.

7.2 Material and Methods

7.2.1 Study area

Switzerland has high climatic contrasts owing to variations in topography (from 192 m a.s.l. to 4633 m a.s.l.) (Fig. 7.1). The long-term (1981-2010) mean precipitation in Switzerland (measured at 418 stations; MeteoSwiss, 2018c) is 1299 mm following the humid continental to oceanic climate zone with highest rainfall in summer and lowest in winter. The typical melt-out date for alpine elevation ranges is in the late spring (DOY 147, 27th of May) (Jonas et al., 2008). This late melt-out in the Alps shortens the plant growth period in higher elevations. Soils of Switzerland are dominated by Cambisols (King et al., 1994). Switzerland can be subdivided into five main geological units: the Alps mainly dominated by granite, the Jurassic, a young fold mountains of limestone, the partly flat, partly hilly Swiss Midland (between Jura and Alps) and of minor spatial extend are the Po Valley at the southernmost tip of Ticino (Southern Alps), and the Upper Rhine Plain around Basel.

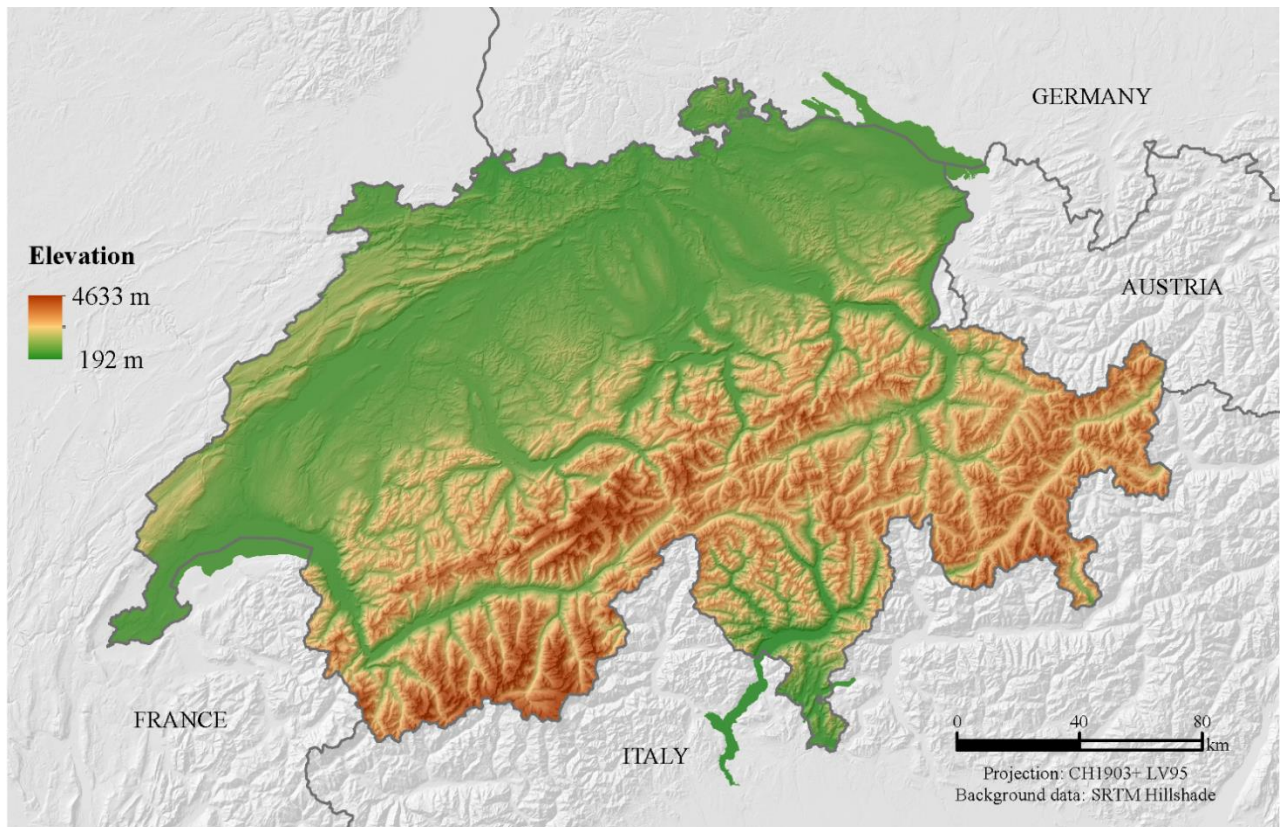


Fig. 7.1: Topography of Switzerland including the Swiss Alps (data source: SwissAlti3D, 2 m spatial resolution)

Mapping of the seasonality of soil erosion by water was undertaken for the national grassland area of Switzerland, which covers to about 28% (11.559.800 ha) of the Swiss national territory and accounts for 72% of the total agricultural area (Bötsch, 2004; Jeangros and Thomet, 2004). Grassland areas are distributed widely with a major extent in the Alps (Hotz and Weibel, 2005). They are usually used as pastures or hayfields for fodder production. Alpine grasslands are commonly covered by snow in winter. Permanent grassland areas, which are not being part of the crop rotation for a minimum of five successive years, have slowly but steadily increased over the last two decades in Switzerland (Schmidt et al., 2018a).

7.2.2 Datasets

To depict the grassland extent of Switzerland, the grassland class in the global Climate Change Initiative (CCI) Land Cover dataset was used and refined with topographic models of Switzerland (Schmidt et al., 2018a). That grassland map serves as the mask for modelling soil erosion by water on Swiss grasslands.

Each of the RUSLE-factors (excluding the P factor) was calculated separately and adapted to the specific environmental conditions of Swiss grasslands. The generation of the RUSLE factor maps (rainfall erosivity, Schmidt et al., 2016; soil erodibility, Schmidt et al., 2018c; cover and management, Schmidt et al., 2018b; slope length and steepness, Schmidt et al., 2019) is explained in detail in the individual sections and in Table 7.1.

Table 7.1: Overview of RUSLE factor maps used for the soil erosion risk mapping of Swiss grasslands

Erosion factor	Dataset	Derived variable	Data source
Rainfall erosivity R	Rainfall station data	Long-term rainfall measurements at 87 stations	MeteoSwiss, 2018b
	Snow depth	Monthly snow depth	MeteoSwiss, 2018b
	CombiPrecip	Rainfall amount (measured and radar)	Sideris et al., 2014
	EURO4M-APGD	Daily precipitation per month	Isotta et al., 2014
	RhiresM	Monthly precipitation sums	MeteoSwiss, 2013
	SwissAlti3D	Elevation, slope, aspect	Swisstopo, 2018a
Soil erodibility K	LUCAS topsoil	199 Swiss and 1638 European topsoil samples	Orgiazzi et al., 2018
	MODIS13Q1	NDVI, Enhanced Vegetation Index EVI, Raw bands	Didan et al., 2015
	EU-DEM	Elevation, slope, base level of streams, altitude above channel base level, multi-resolution index of valley bottom flatness	Farr et al., 2007
	Location parameter	Latitude, longitude	-
Cover and management C	Swissimage FCIR	Spatial distribution of the fraction of green vegetation cover	Swisstopo, 2010
	FCover300m	Temporal distribution of the fraction of green vegetation cover	Smets et al., 2017
	MOD13Q1	NDVI	Didan et al., 2015
	CCI land cover	Dynamic long-term snow occurrence	Arino and Ramoino, 2017
Slope length L	SwissAlti3D	Upslope contributing area	Swisstopo, 2018a
Slope steepness S	SwissAlti3D	Slope	Swisstopo, 2018a

The high-resolution spatial datasets of the Swiss Federal Offices (e.g. SwissAlti3D Digital Elevation Model 2 m spatial resolution, SwissImage Orthophoto 0.25 m spatial resolution) are among the most detailed in Europe. They allow modelling of the spatiotemporal patterns of soil erosion for Swiss grassland in combination with temporal datasets (e.g. Rainfall measurement 10 minutes temporal resolution, Copernicus FCover 10 day temporal resolution).

7.2.3 Mapping

All (R)USLE-factors are multiplied according to the following equation by Wischmeier and Smith (1965) and Renard et al. (1997):

$$A = R * K * C * L * S * P \quad (7.1)$$

where A is usually the soil loss in $t \text{ ha}^{-1} \text{ yr}^{-1}$. The equation can be modified to a monthly soil erosion equation by including a monthly temporal resolution of the dynamic factors R and C (Schmidt et al., 2016; 2018b):

$$A_{\text{month}} = R_{\text{month}} * K * C_{\text{month}} * L * S * P \quad (7.2)$$

where A_{month} is the quantification of soil loss in $t \text{ ha}^{-1} \text{ month}^{-1}$.

The R-factor was regionalized on a monthly scale by regression-kriging with 87 automated gauging stations, serving as dependent variable and high resolution spatial and temporal covariates, serving as independent variables (Table 7.1). Dynamics in the cover and management factor for Swiss grasslands were assessed by a linear spectral unmixing of high spatial resolution orthophotos and normalized by temporal variations of the fraction of green vegetation cover. The potential soil loss of a specific plant development stage expressed as soil loss ratio (SLR), was then weighted by the rainfall erosivity ratio to generate in monthly C-factor maps (Table 7.2).

Table 7.2: Erosion factors for the monthly soil erosion modelling of Swiss grassland

Erosion factor	Method description	Spatial resolution	Temporal resolution	Factor source
Rainfall erosivity R	Regression-kriging	100 m	Monthly	Schmidt et al., 2016
Soil erodibility K	Cubist regression	500 m	-	Schmidt et al., 2018c
Cover and management C	Linear spectral unmixing	100 m	Monthly	Schmidt et al., 2018b
Slope length L	Upslope contributing area with maximal flow threshold	2 m	-	Schmidt et al., 2019
Slope steepness S	Modification of S-factor for alpine environments (S_{alpine})	2 m	-	Schmidt et al., 2019

Soil erodibility on a national scale is a result of a cubist regression and multilevel B-splines of a total of 1837 Land Use/Cover Area Survey (LUCAS) topsoil samples (Orgiazzi et al., 2018) and independent variables (Table 7.1). Finally, the L and S factors were adapted to the complex alpine topography (Table 7.2). Slope length were originally constrained to a maximal flow threshold of 100 m to account for the whole agricultural area in Switzerland (Schmidt et al., 2019). However, flow measurements in the Swiss alpine grasslands revealed short flow length less than 2 m due to high surface roughness and infiltration capacity. These observations lead to the assumption that the influence of the L-factor is minimal. In future, more empirical data is needed to support this assumption. Therefore, an L-factor of 1 is used for predicting the soil loss of Swiss grasslands to comply with field observations. Slope steepness was predicted by a mean equation (S_{alpine}) of a total of 12 empirical S-factor equations. The regionalization of the support practice factor was difficult to obtain for Swiss grasslands because of a lack of spatial information on grazing management and its effect on soil loss. Thus, the P-factor was set to 1 (not influential) for this study, even though the authors are aware of the substantial variation of management and its effect on soil loss (e.g. stocking numbers and rotation frequency of livestock as well as watering places, fencing, and herding).

The multiplication of all RUSLE factors (according to Eq. 7.2) provides monthly soil erosion risk maps for Swiss grasslands (Fig. 7.2). Note that while the K-factor (Schmidt et al., 2018c), R-factor (Schmidt et al., 2016), and LS-factor (Schmidt et al., 2019) are available for the whole of Switzerland, the C-factor (Schmidt et al., 2018b) is limited to the grassland areas of Switzerland (Schmidt et al., 2018a) and thus presets the extent of the erosion modelling.

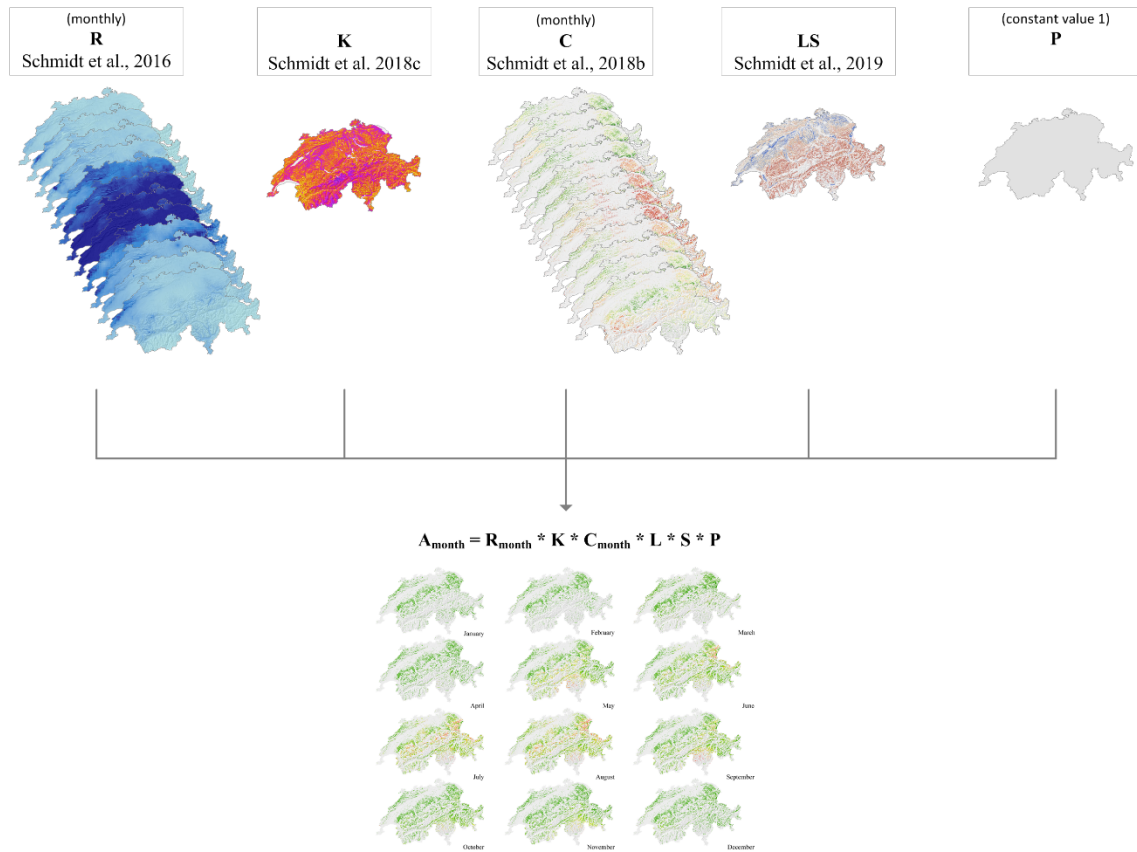


Fig. 7.2: Flowchart of the seasonal erosion map of Swiss grassland using the erosion factors

The maps were visually interpreted regarding their spatial and temporal patterns of soil erosion risk. In addition, descriptive statistics for all twelve monthly erosion maps were calculated.

The maps were evaluated by a sensitivity analysis of the dynamic and annual soil loss rates. Such a sensitivity analysis contrasts the differences between dynamic and static erosion factors. For the non-dynamic assessment, the mean monthly R- and C-factor maps over a year were multiplied with the annual factors K, LS and P.

7.3 Results and Discussion

7.3.1. Monthly soil erosion rates for Swiss grasslands

Spatially, the grasslands in the Alps are more prone to soil erosion in most of the months than those in the Swiss lowlands, owing to the influence of topography on the RUSLE model (please note that due to regional snow cover, the predicted area is considerably reduced in winter). Given an intact 100% vegetation cover the annual sum of soil loss as cumulative sum of monthly soil losses is $0.14 \text{ t ha}^{-1} \text{ yr}^{-1}$. However, considering the actual fraction of green vegetation cover (average annual FGVC = 54% mapped for the period 2014 to 2016 based on FCover300m, Smets et al., 2017) the annual sum of soil loss as cumulative sum of the monthly soil losses rises up to $4.55 \text{ t ha}^{-1} \text{ yr}^{-1}$. The latter is significant, as the mean annual value for Europe including arable lands was calculated as $2.5 \text{ t ha}^{-1} \text{ yr}^{-1}$ (Panagos et al., 2015e), and

exemplifies the potential vulnerability of Swiss grassland soils to soil erosion if the vegetation cover is disturbed or removed. Moreover, this clearly highlights the sensitivity of RUSLE based models to the status of vegetation cover that should be more carefully observed in future studies.

The calculation of soil loss risk by water erosion at monthly temporal resolution allows the identification of summer as the main erosive season of Swiss grasslands. The combined effect of R- and C-factor (Meusburger et al., 2012; Schmidt et al., 2016; 2018b) is amplifying the erosion risk in summer. For Swiss grassland, July and August have the highest monthly risk of soil erosion by water ($1.25 \text{ t ha}^{-1} \text{ month}^{-1}$, Table 7.3, Fig. 7.3). In contrast, for all winter months, a relatively low soil erosion by water risk (winter average $0.02 \text{ t ha}^{-1} \text{ month}^{-1}$) was predicted (Table 3, Fig. 3) because of low rainfall erosivity (due to snow fall/ snow cover). However, processes like snow gliding and avalanches or even snow melt are not included in the present model and need to be considered separately (Ceaglio et al., 2012; Meusburger et al., 2014 ; Stanchi et al., 2014). The mean monthly soil loss due to water erosion for summer is 48 times higher than the mean soil loss in winter, 6 times higher than in spring and 3 times higher than in autumn (see Schmidt et al., 2018b).

Table 7.3: Monthly ($\text{t ha}^{-1} \text{ month}^{-1}$) and annual ($\text{t ha}^{-1} \text{ yr}^{-1}$) soil erosion risk averaged for the Swiss grassland area with a constraint of the maximal flow length to $<1 \text{ m}$ according to observations (L-factor equals 1). Minimum soil erosion rate is $0 \text{ t ha}^{-1} \text{ month}^{-1}$ (no soil erosion) in all month.

Month	Mean soil erosion risk ($\text{t ha}^{-1} \text{ month}^{-1}$)	Maximum soil erosion risk ($\text{t ha}^{-1} \text{ month}^{-1}$)	Standard deviation ($\text{t ha}^{-1} \text{ month}^{-1}$)
January	0.01	0.43	0.02
February	0.01	2.40	0.05
March	0.02	4.19	0.06
April	0.02	6.23	0.10
May	0.47	35.17	1.24
June	0.56	103.03	2.11
July	1.25	128.85	3.73
August	1.25	218.75	3.84
September	0.61	662.91	5.86
October	0.15	170.84	1.14
November	0.17	17.84	0.47
December	0.04	5.00	0.11
Ø	0.38	112.97	1.56
Σ ($\text{t ha}^{-1} \text{ yr}^{-1}$)	4.55	1355.62	18.71

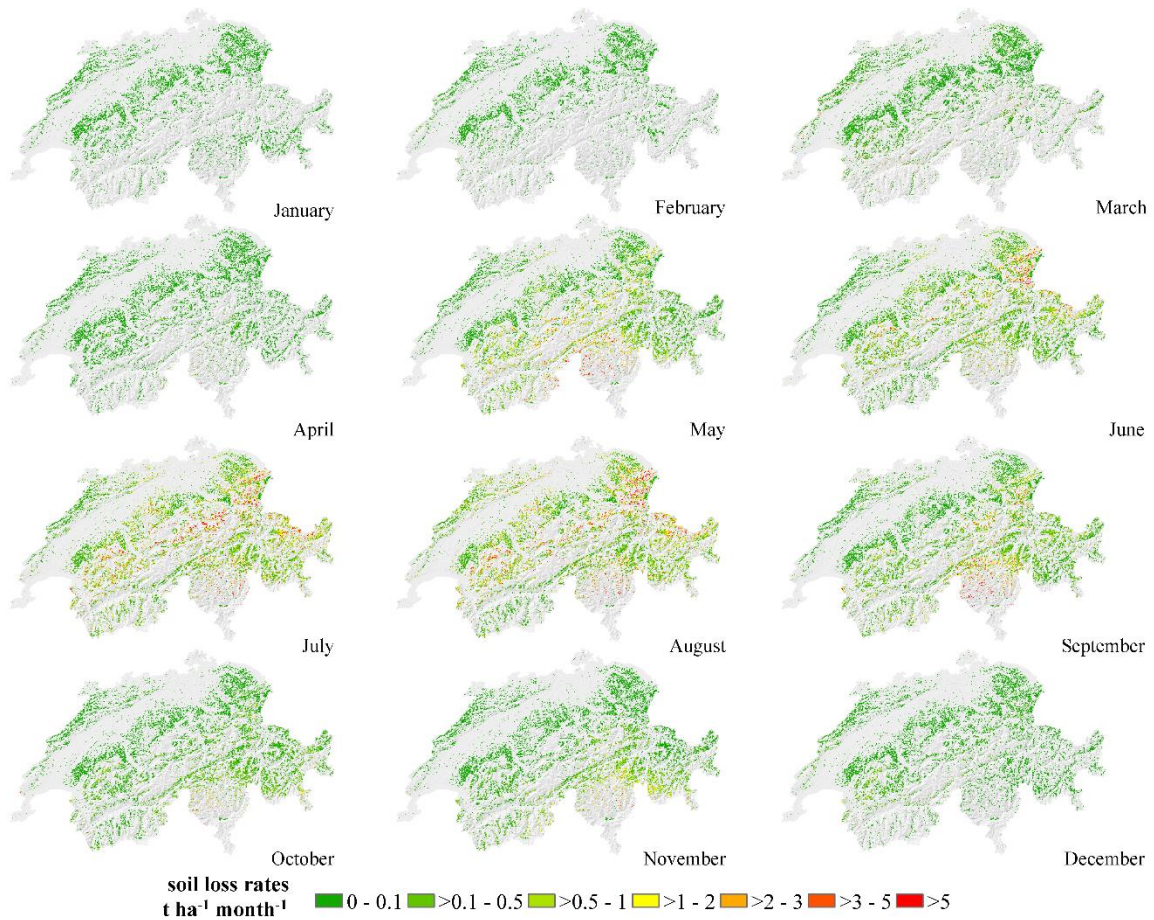
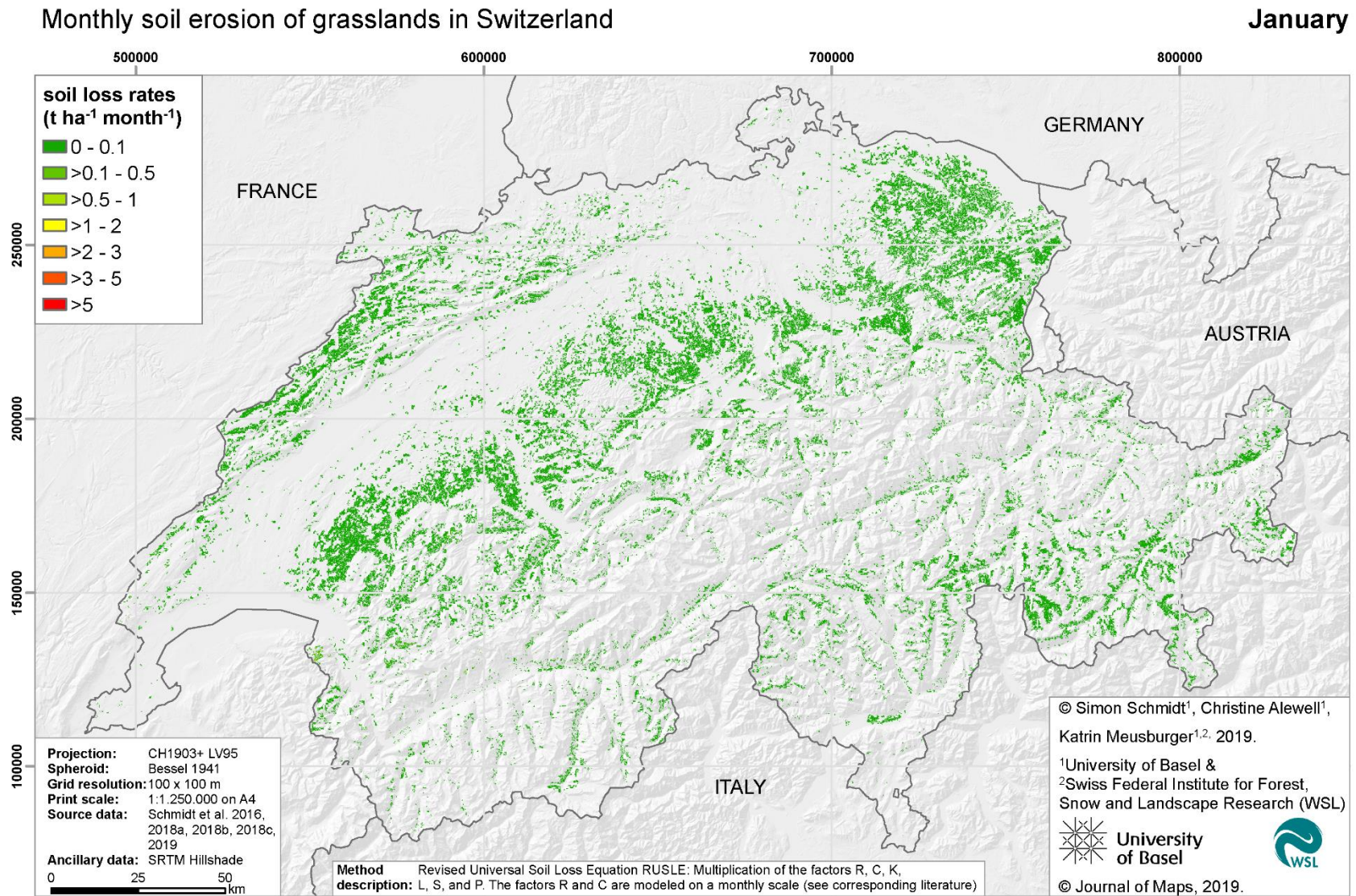
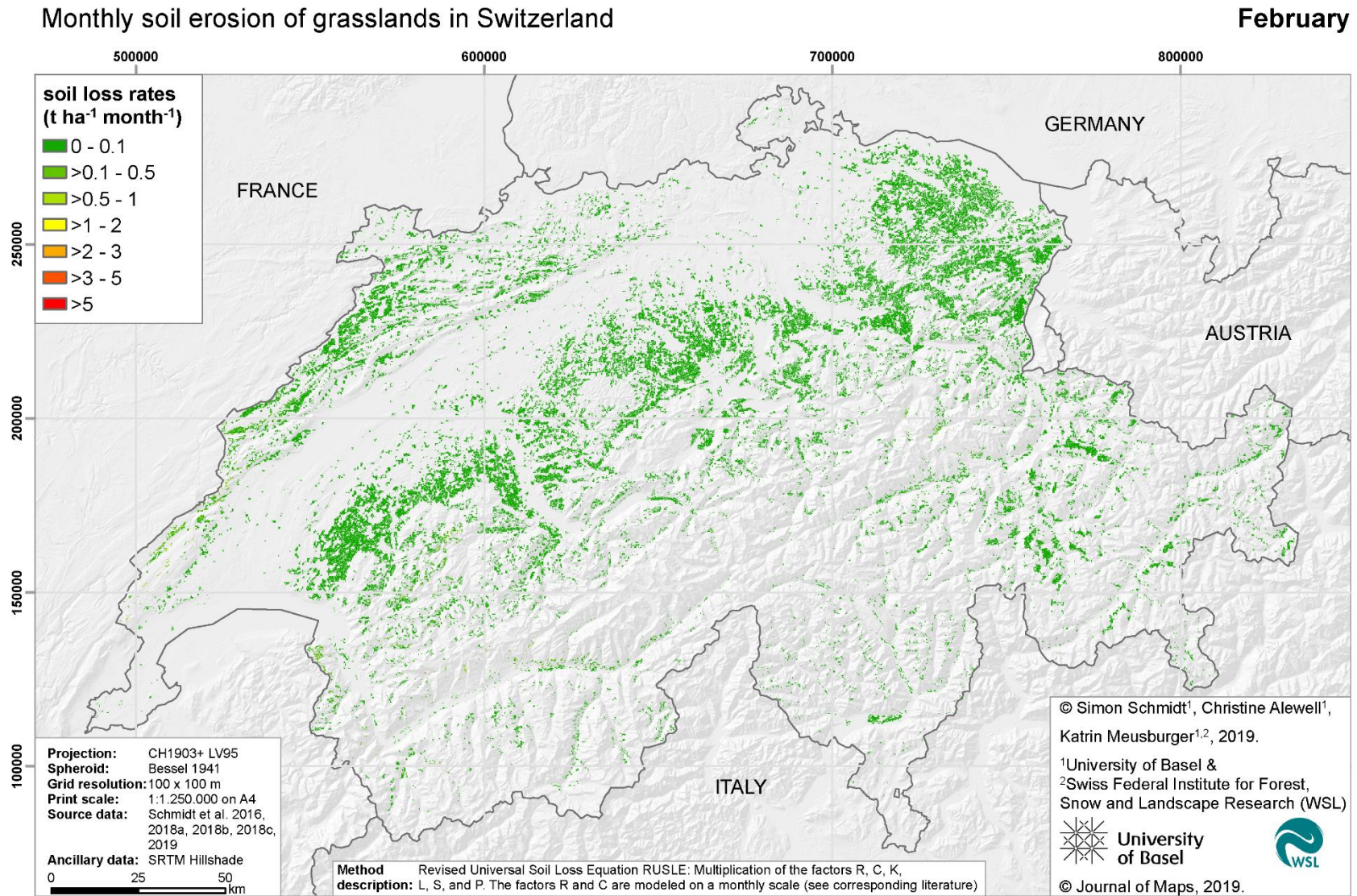
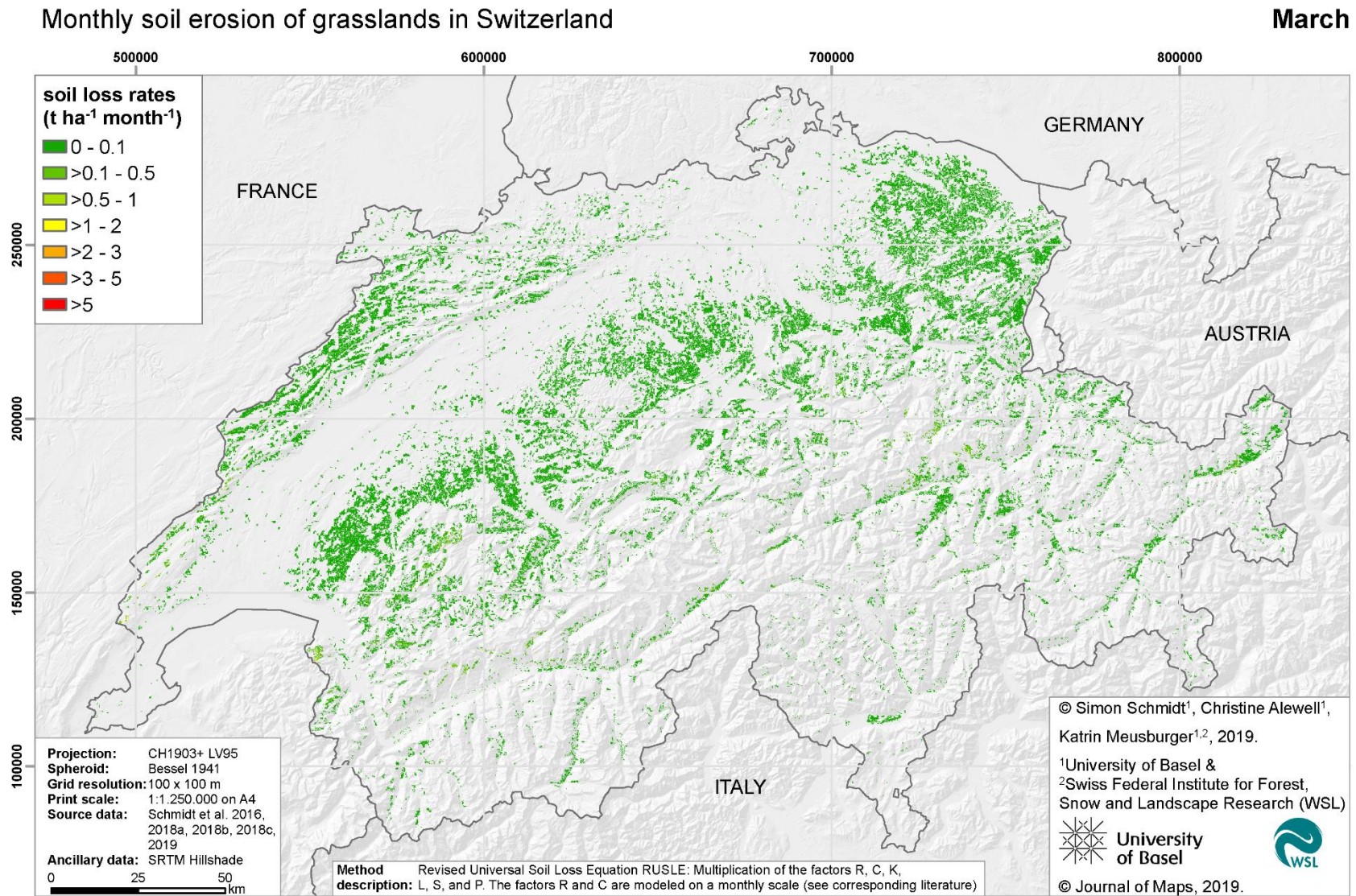


Fig. 7.3: Spatiotemporal patterns of monthly soil erosion risk at Swiss grassland. Due to data gaps caused by snow fall in winter, the predicted area is reduced in winter. The individual maps are displayed as a multiple mapset in the following pages

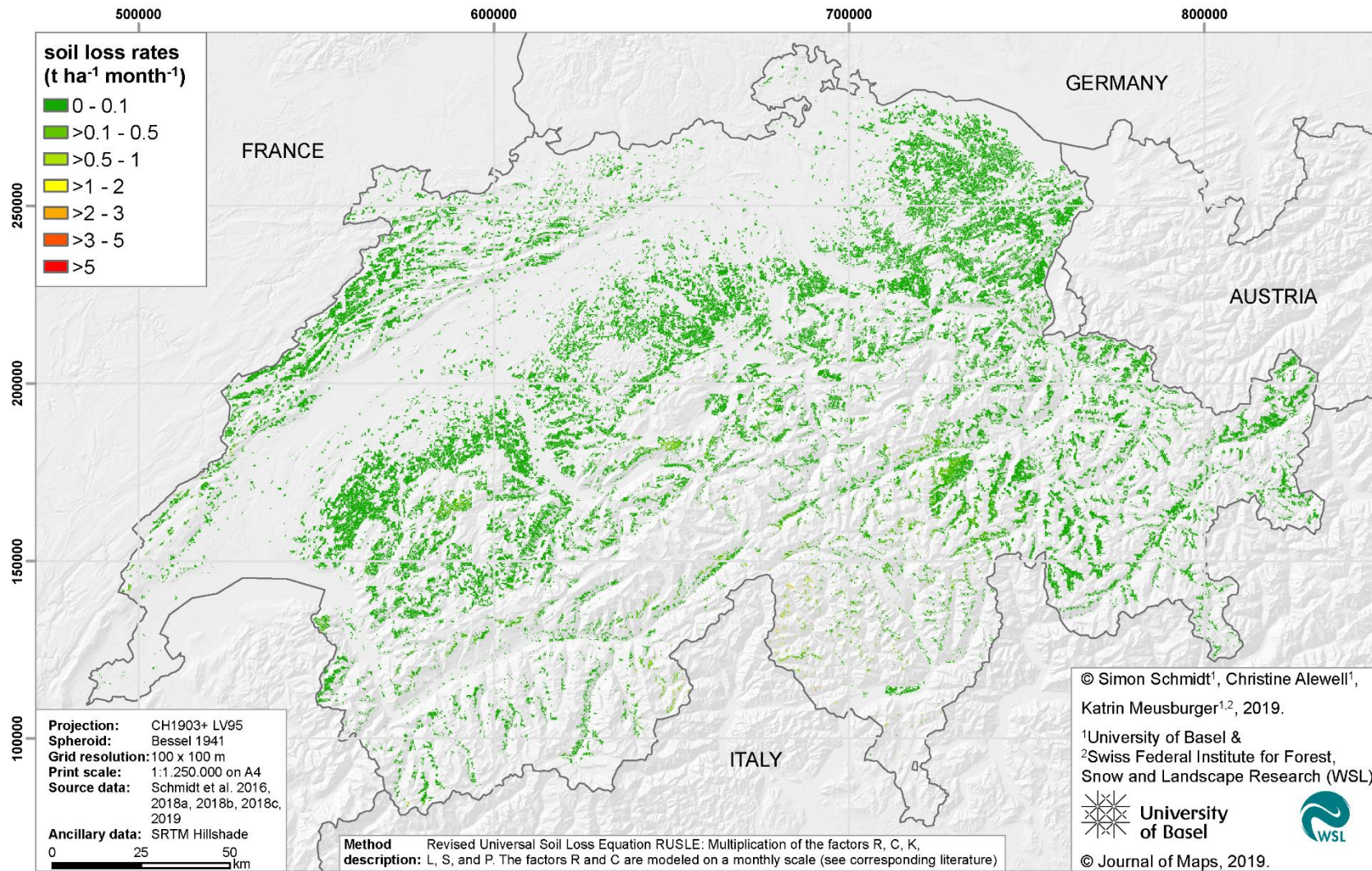


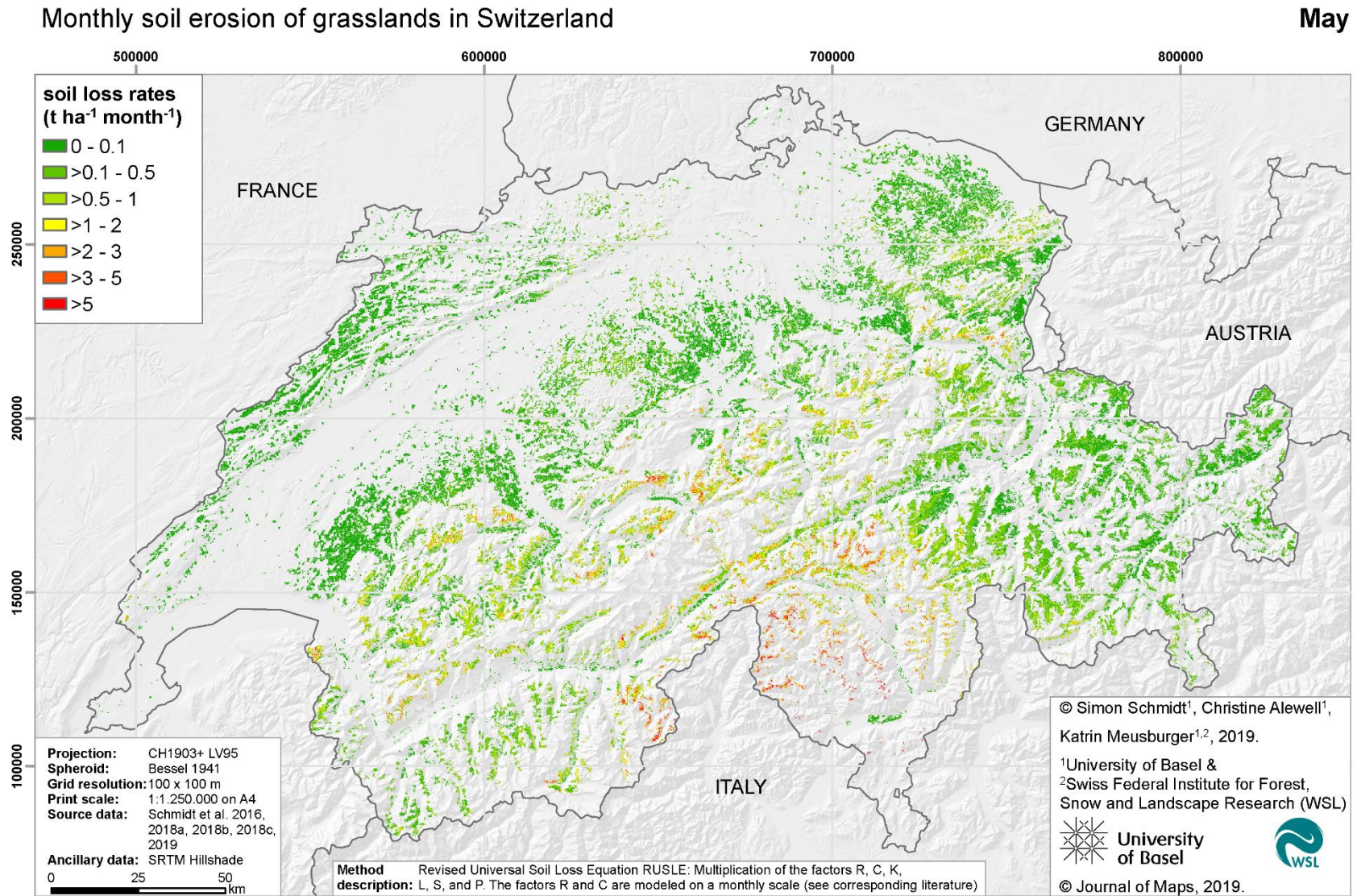


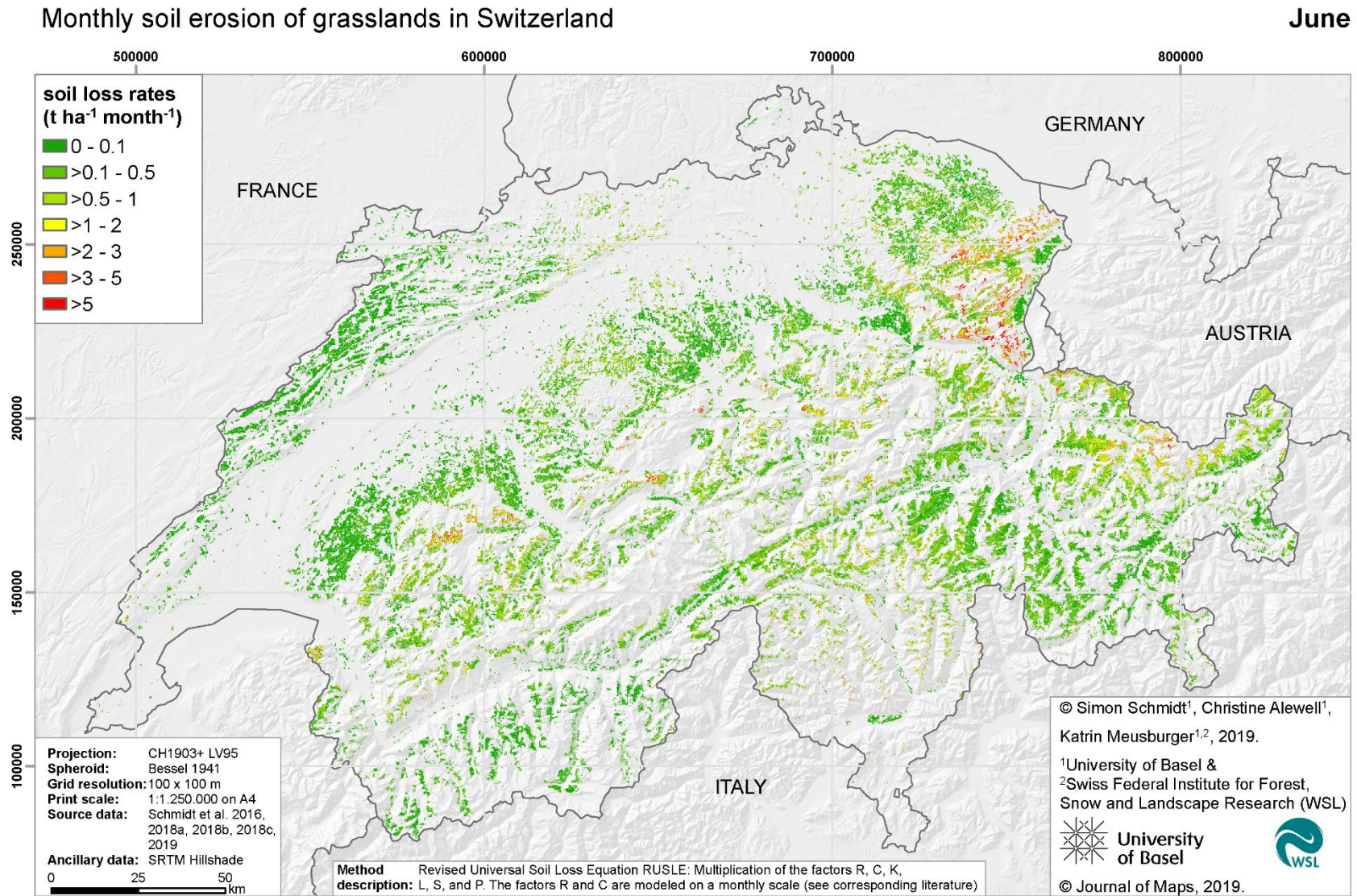


Monthly soil erosion of grasslands in Switzerland

April

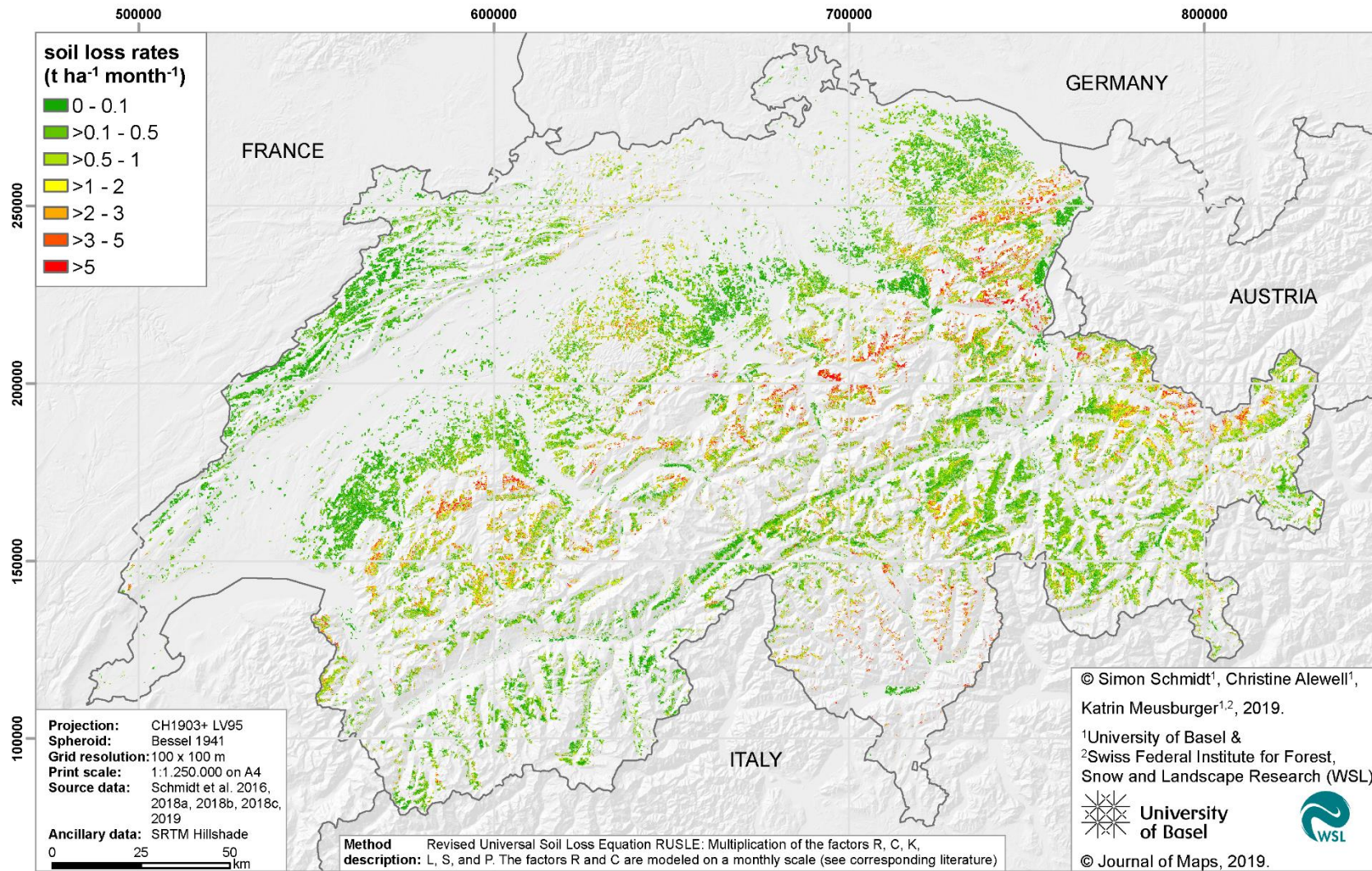


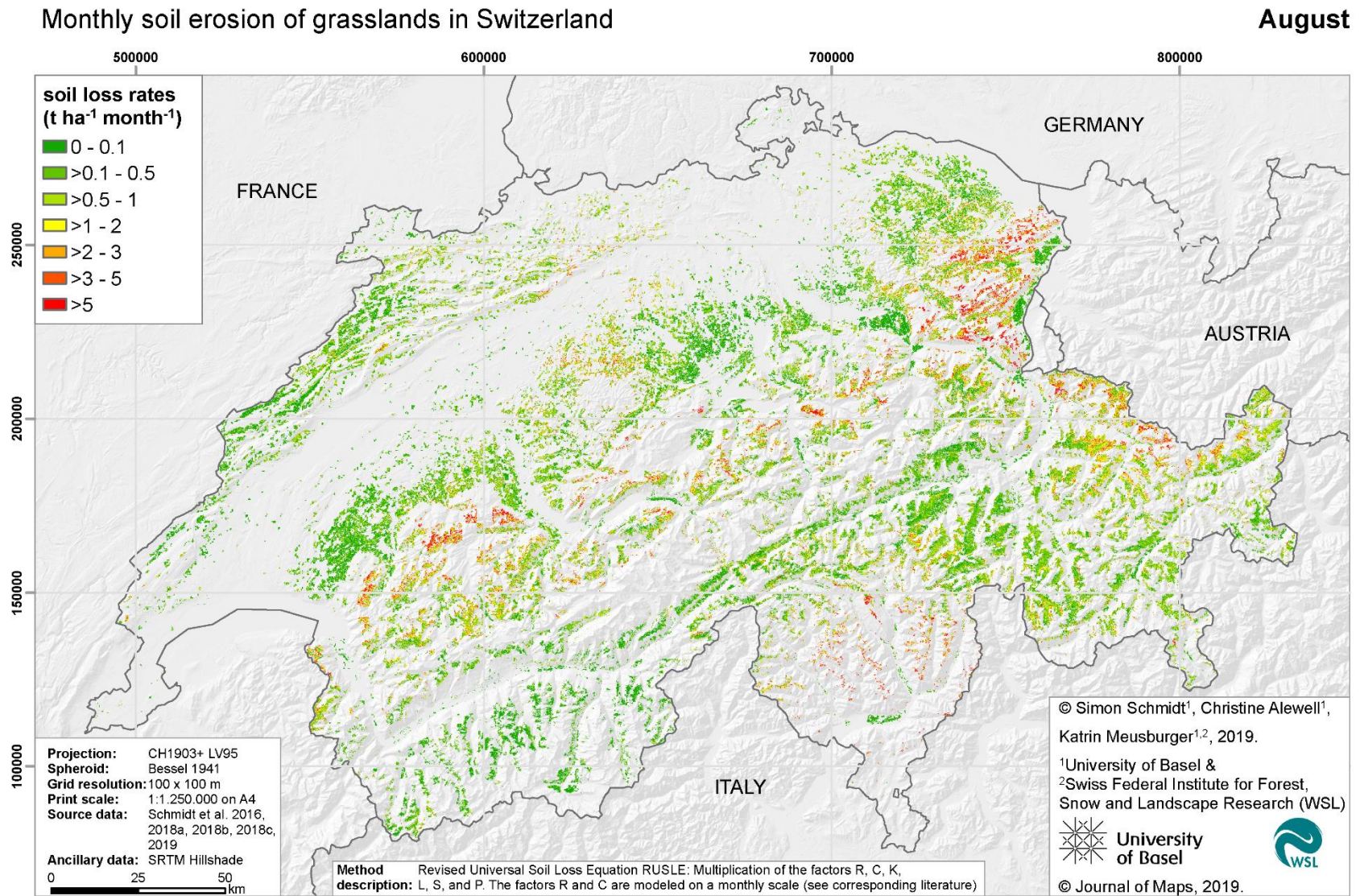


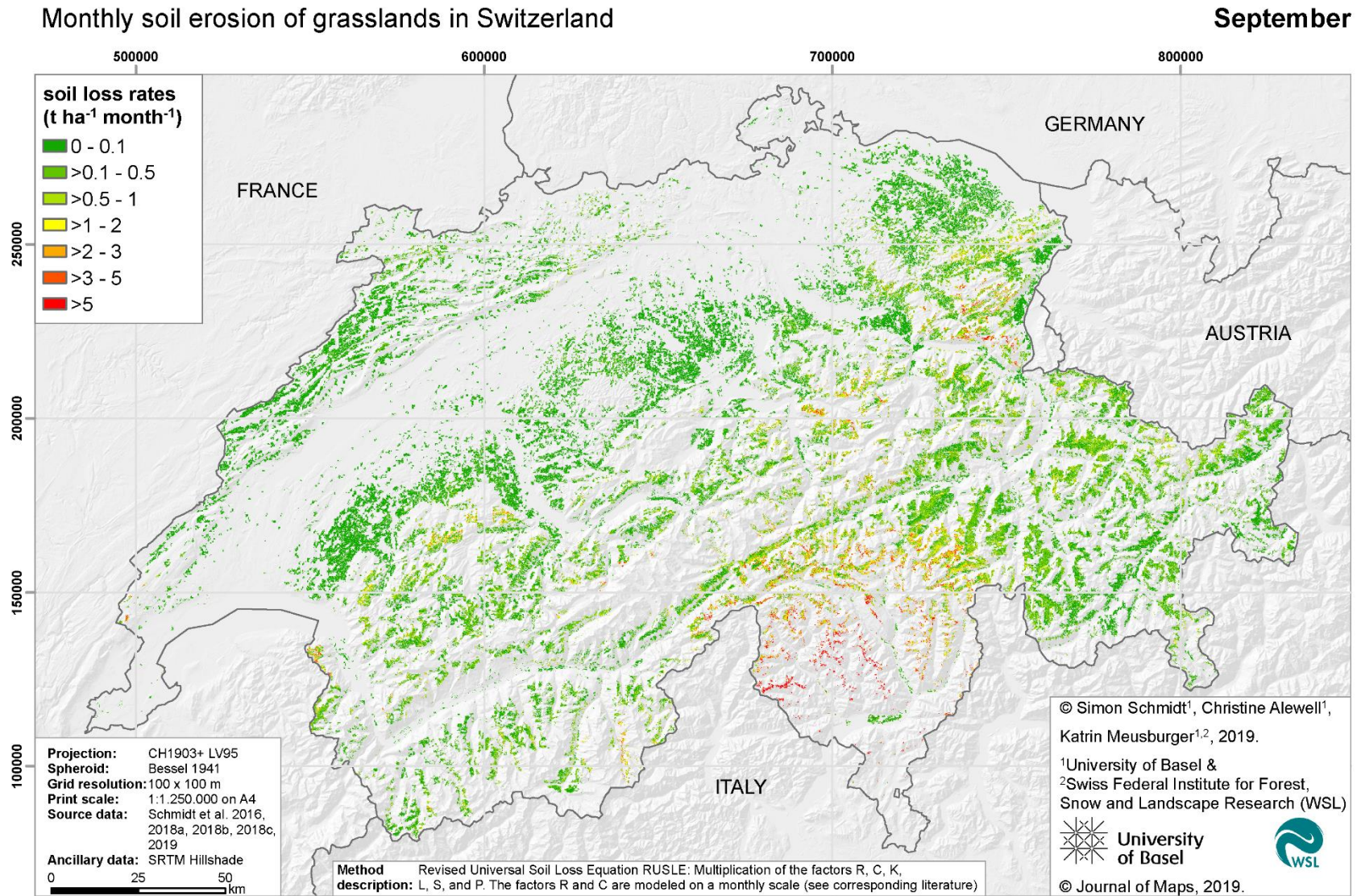


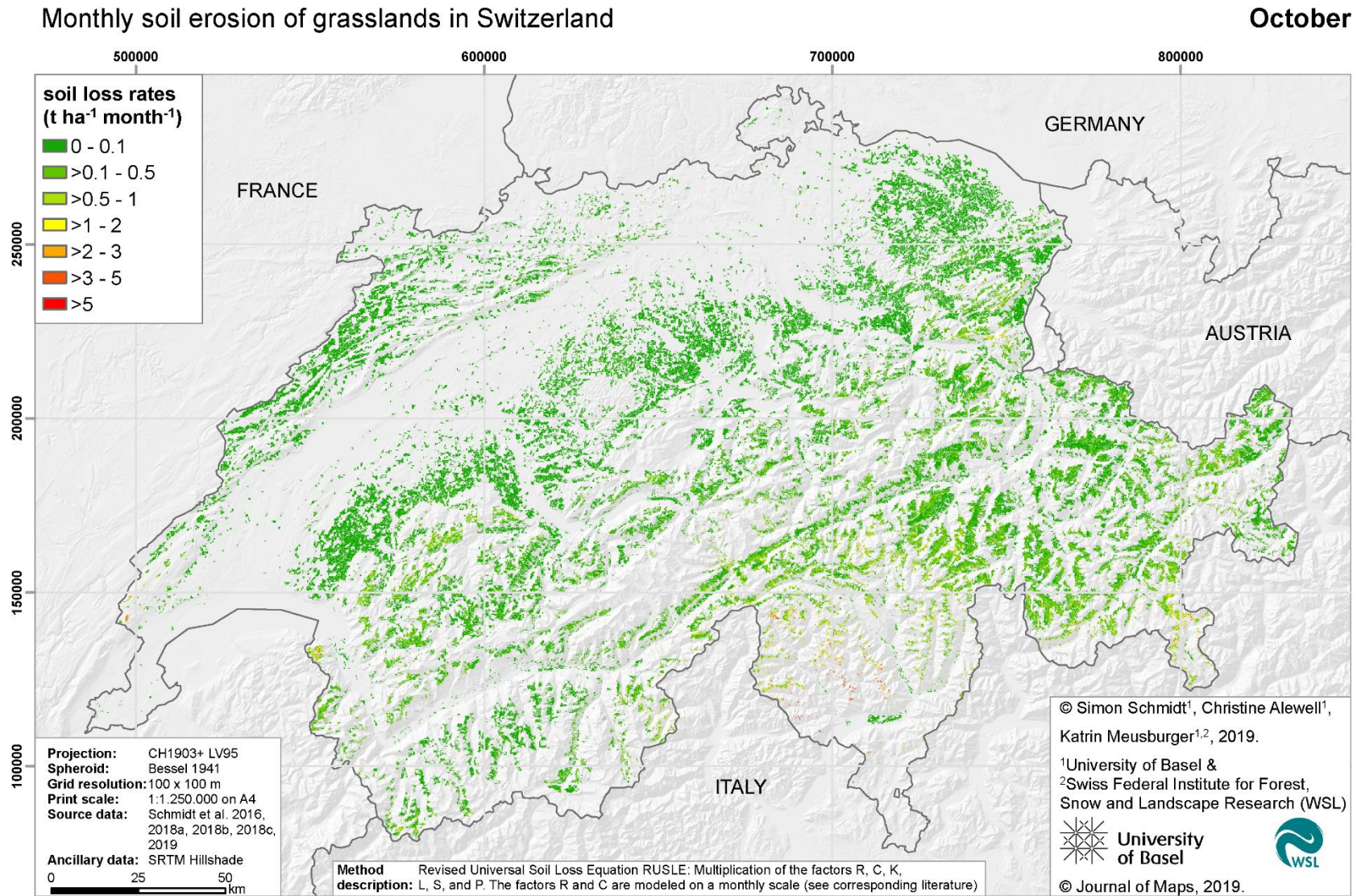
Monthly soil erosion of grasslands in Switzerland

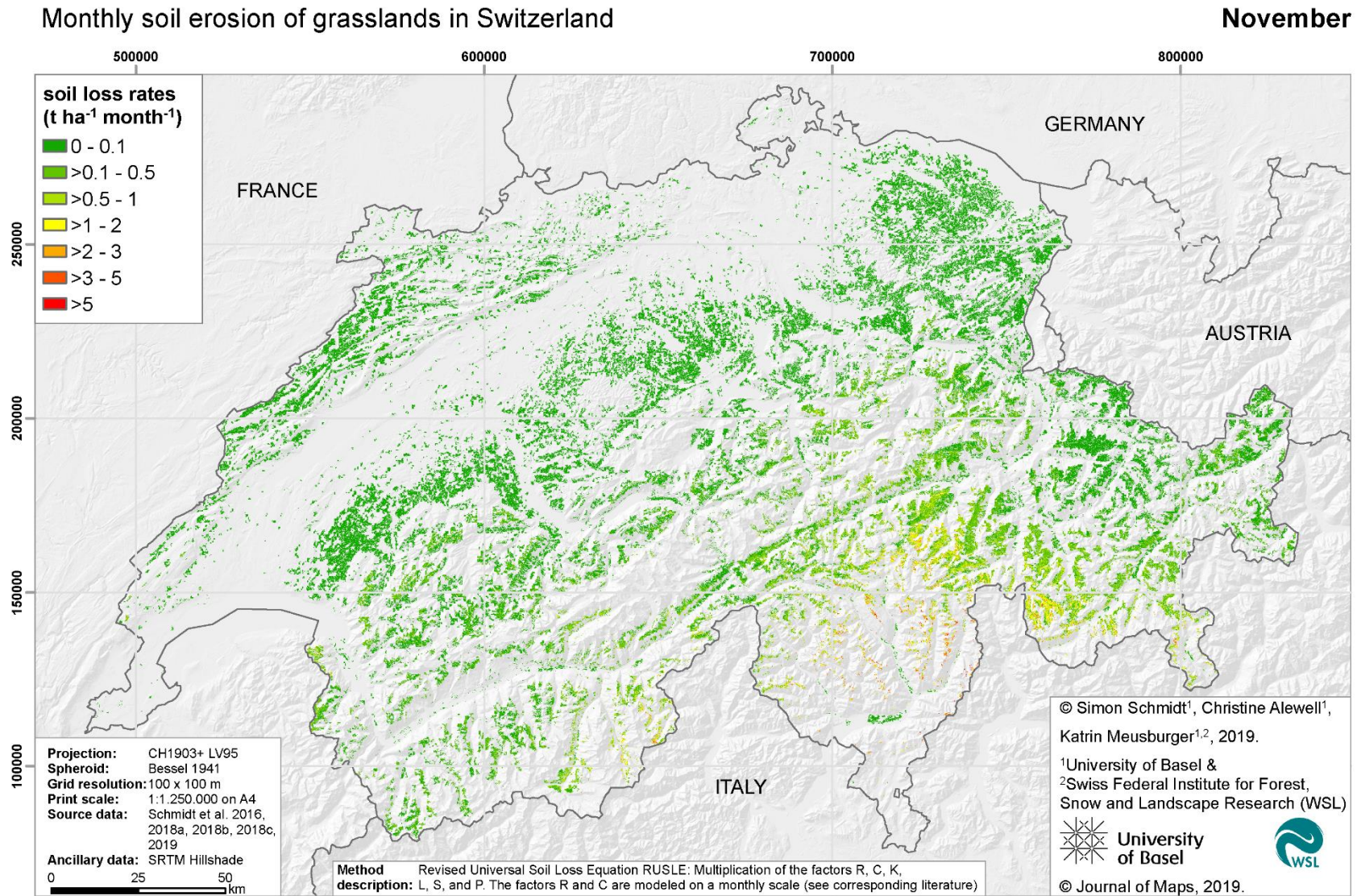
July

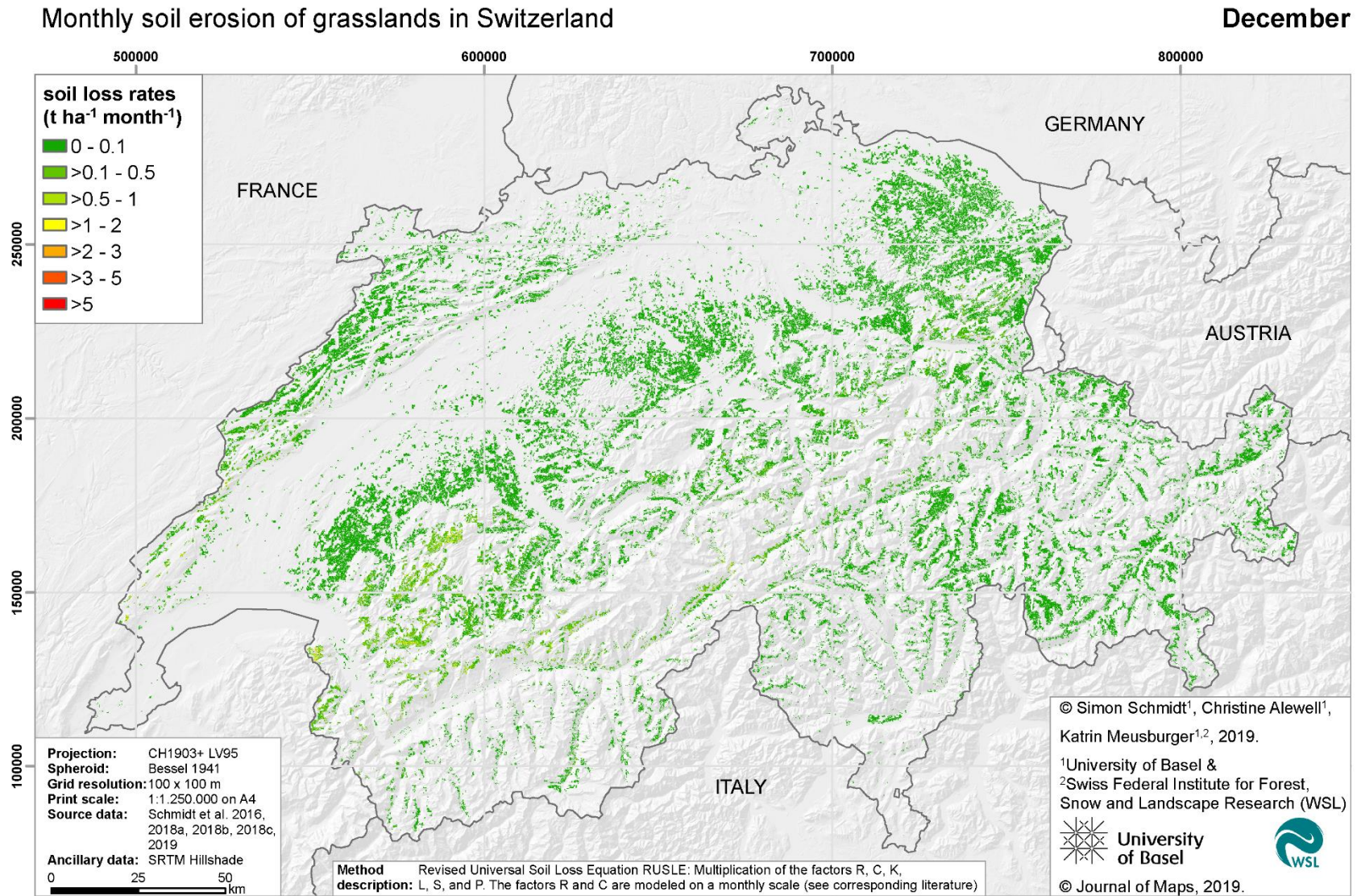












7.3.2. Comparison of dynamic and annual soil erosion rates

The benefits of a higher temporal resolution are obvious when estimated soil loss rates on a monthly temporal resolution are compared with soil loss rates on an annual resolution. The mean annual soil loss rate ($4.55 \text{ t ha}^{-1} \text{ yr}^{-1}$) would indicate hypothetical average monthly soil loss rates of $0.38 \text{ t ha}^{-1} \text{ yr}^{-1}$ (Fig. 7.4) which would be an overestimation of mean monthly soil loss in winter (by $0.18 \text{ t ha}^{-1} \text{ month}^{-1}$) and an underestimation in summer (by $0.64 \text{ t ha}^{-1} \text{ month}^{-1}$). Thus a higher temporal resolution results in better knowledge of risky time periods of soil erosion by water, with a significant peak of soil loss rates on Swiss grasslands in summer and nearly zero risk of soil erosion by water in winter.

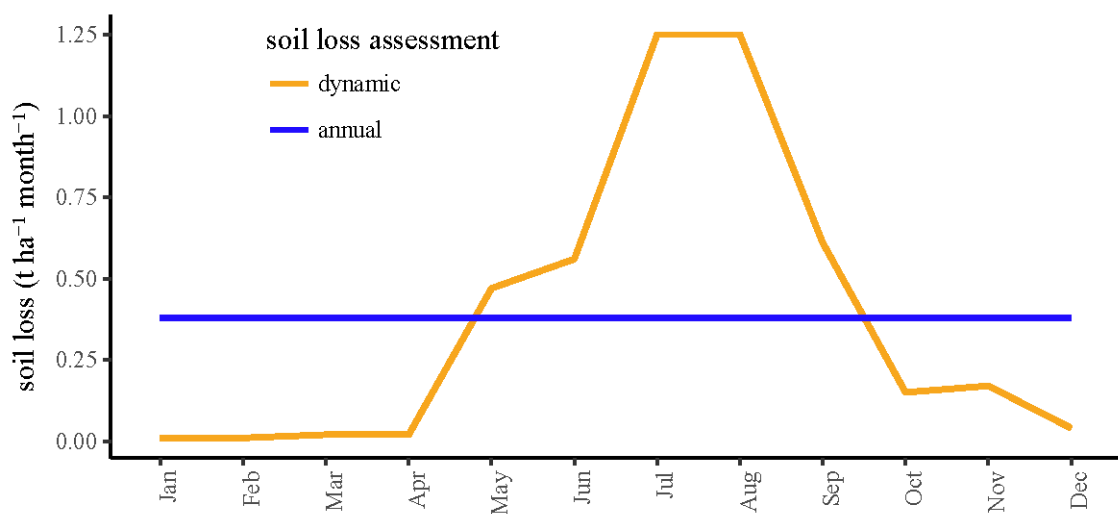


Fig. 7.4: Comparison of the distribution of monthly soil loss rates for Swiss grasslands (dynamic) and a mean annual soil loss rate (annual), divided by twelve to result in a pseudo-monthly resolution.

Overall, focusing on the monthly distribution of soil loss rates and rainfall erosivity (Fig. 7.5), the latter seems to be the most influential factor regarding the intra-annual dynamics of soil loss due to water erosion (Schmidt et al., 2016). However, the rainfall erosivity is considered in the model twice, as an individual factor (Schmidt et al., 2016) and as a weighting factor for the C-factor (Schmidt et al., 2018b). Furthermore, our simulation does not consider soil loss induced by snow related erosional processes. As measurements with sediment traps or radionuclides have demonstrated, overall sediment loss is most likely highest in late winter and spring (Ceaglio et al., 2012; Meusburger et al., 2014), when avalanches, snow melt and snow ablation are triggering soil erosion on damaged and vulnerable soil surfaces.

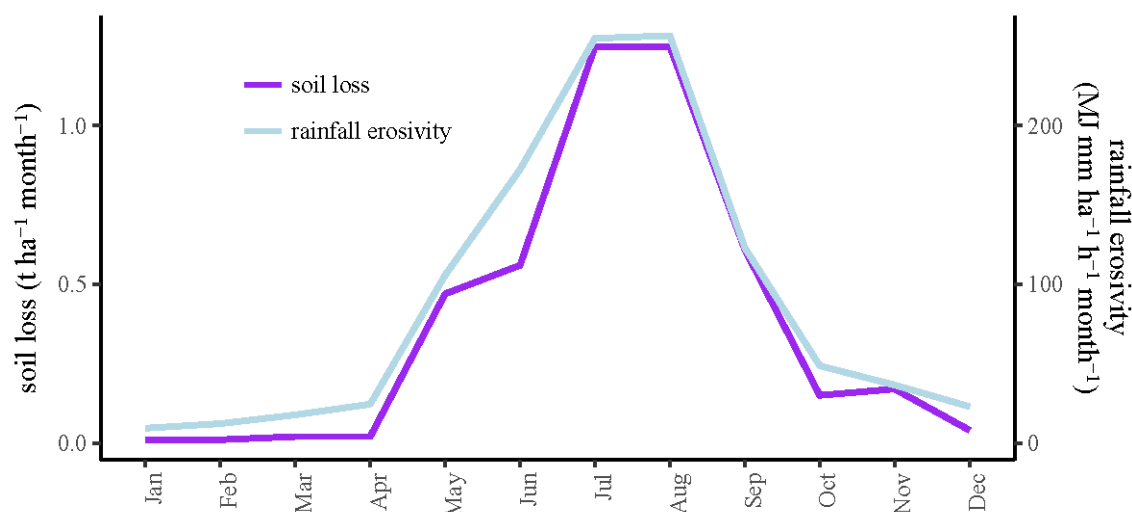


Fig. 7.5: Influence of the temporal pattern of the monthly rainfall erosivity for the temporal pattern of the soil loss rates on Swiss grasslands.

7.4.3. Soil loss rates and soil formation rates

The average annual soil loss of $4.55 \text{ t ha}^{-1} \text{ yr}^{-1}$ clearly exceeds the maximum tolerable soil loss of Switzerland ($2 \text{ t ha}^{-1} \text{ yr}^{-1}$; Schaub and Prasuhn, 1998) by a factor of 2. The average annual soil erosion rate of $4.55 \text{ t ha}^{-1} \text{ yr}^{-1}$ would hypothetically equal a total eroded soil mass of 5.26 Mt per year, related to the national grassland area of 1.155.980 ha.

Soil formation rates for alpine grasslands soils with siliceous lithology were estimated by Alewell et al. (2015a) as $0.54\text{-}1.13 \text{ t ha}^{-1} \text{ yr}^{-1}$ for old soils ($>10\text{-}18 \text{ kyr}$) and $1.19\text{-}2.48 \text{ t ha}^{-1} \text{ yr}^{-1}$ for young soils ($>1\text{-}10 \text{ kyr}$). In both cases the predicted average soil loss exceeds these rates. Only soil formation rates of very young soils ($\leq 1 \text{ kyr}$; $4.15\text{-}8.81 \text{ t ha}^{-1} \text{ yr}^{-1}$) can compensate the annual soil loss. In conclusion, the predicted soil loss rates for Swiss grasslands imply a non-reversible loss of the valuable soil resource.

7.4 Conclusions

The monthly soil erosion maps presented here form the first dynamic soil erosion approach on a national scale with a monthly temporal resolution. They enable the quantification of soil erosion risk, and provide information about the spatiotemporal patterns of soil loss due to water erosion on Swiss grasslands. These patterns show that summer is the season with highest soil erosion by water risk, which is 3/6/48 times higher than in autumn/spring/winter, respectively, leaving the soil surface damaged and vulnerable for potential snow and frost induced processes (snow gliding, ablation, melt, avalanches). In contrast, to a monthly temporal resolution, annual assessments tend to overestimate the soil erosion by water risk in winter and underestimate it in summer. The analysis and integration of each erosion factor reveals that the cover and management factors is highly sensitive and that the actual state of vegetation cover is crucial. Nonetheless, regarding the intra-annual pattern the higher fraction of green vegetation cover in summer is incapable to compensate the impact of high rainfall erosivity in summer. However,

the strong impact of rainfall erosivity within RUSLE, especially as a weighting factor for soil loss ratios, needs to be discussed in future studies.

The maps are suitable to quantify the actual soil erosion risk considering natural preconditions and land use. The mapping could be further developed to monitor the soil erosion risk by the use of real-time data (e.g. satellite and radar data, land use information, and topography data) as well as by mapping support and management practices via the P-factor.

Such monthly erosion risk maps are of high importance for policy, soil scientist, environmentalists, and agronomists because they serve as a knowledge base to answer the question about where and when soil damage might occur on Swiss grassland. RUSLE does not include snow induced processes, so the overall soil loss might not necessarily be greatest in the summer, but our modelling confirms that highest damage due to grazing (low C factor) and high rainfall erosivity leaves the soils damaged and vulnerable after the summer, leading to a high risk of snow induced processes. As each factor is developed individually, it uses key information from different disciplines and can be merged with other sources of information to enable more targeted interventions e.g. for soil and environmental protection, hazard mitigation, land use change, and agricultural management.

Based on the monthly maps, a controlled spatial and temporal soil erosion protection strategy, such as a change in stocking rates for specific hotspots and periods or the fencing of hotspots, is now feasible. The approach for grasslands with a particular focus on the Alpine conditions could serve as a prototype for erosion mapping on grassland in other grassland dominated regions and countries like Austria, Germany, Italia, Slovenia, or France and would help to protect the unique nature of these grasslands.

7.5 Software

The monthly maps of soil erosion by water for Swiss grasslands are a product of statistical, remote sensing, geoinformation and cartographic approaches which are described in detail in the corresponding literature of each erosion factor (Table 7.2).

The combination of the five factors of monthly soil erosion maps was realized in ESRI ArcGIS (v 10.3.1) likewise the layout of the map was designed in the same commercial software. R (v 3.4.3) and RStudio (v 1.1.423) were used for statistical analysis and interpretation of the erosion maps and underlying data.

7.6 Geolocation information

Country: Switzerland; scale: national scale; coordinates: Top-Left N 47.808463° E 5.955889° and Bottom-Right N 45.817967° E 10.492063°

Acknowledgement

This work was supported by the Swiss Federal Office for the Environment (FOEN) under Grant number N° N222-0350 and N° P182-1535. The authors would like to thank all data

providers (Swisstopo, MeteoSwiss, Swiss cantonal offices, Copernicus Global Land Services, European Space Agency ESA, National Aeronautics and Space Administration NASA) for making their data available for this research. The authors would like to thank the editor C. Pain and the reviewers M. Calapano, N. Scarle, G. Buttafuoco, and M. Conforti for their valuable comments and suggestions to improve the quality of the paper.

Data availability statement

Raw data were generated at Swisstopo, MeteoSwiss, Swiss cantonal offices, Copernicus Global Land Services, European Space Agency ESA, and National Aeronautics and Space Administration NASA. Derived data supporting the findings of this study are available from the corresponding author SS on request.

CHAPTER 8

Final remarks and outlook

A finer temporal resolution in soil erosion modeling enables not only a better process understanding of soil erosion risk but even more the possibility of an adopted land use management. Especially for remote areas, like most of the alpine grasslands, a modeling approach based on digital data is desirable. In this study, we developed a set of soil erosion risk maps based on geodata to predict the soil loss of Swiss grasslands on a monthly scale. These maps communicate information about when and where soils are endangered by erosion. We elaborated each of the USLE/RUSLE factor individually (except P) to understand the efficacies of each erosion risk factor.

In the following sub-chapter, I briefly address the innovations of the individual erosion factors and the dynamic soil erosion assessment of Swiss grasslands. The relevance of the here discussed results for soil protection, agriculture, and policy is presented with proposed mitigation strategies for a targeted, time-dependent erosion control. Subsequently, the advantages and limitations of the approach are presented with a recommendation for further improvements and follow-ups of the grassland mapping.

8.1 Innovations in the dynamic soil erosion risk mapping of Swiss grasslands

The modeling of the soil loss rates of grassland and the identification of spatio-temporal patterns of erosion risk is a major improvement for Swiss erosion studies. So far neither grassland areas nor temporal patterns have been considered in previous research. Following a dynamic approach with a monthly temporal resolution enables new insights into the processes and risk of sheet erosion in Switzerland's grassland areas.

The months with the highest predicted soil loss are July and August (average $1.25 \text{ t ha}^{-1} \text{ month}^{-1}$). However, high soil loss is not equally distributed in Switzerland. Spatial patterns reveal hotspots in the Alps (Appenzell Innerrhoden, Appenzell Ausserrhoden, and parts of the cantons St. Gallen, Nidwalden, Obwalden, Bern, and Fribourg). Winter is the season with the lowest risk of soil loss mainly due to the low rainfall erosivity. However, processes like snow gliding cannot be included in the present model and need to be considered separately (Ceaglio et al., 2012; Meusburger et al., 2014; Stanchi et al., 2014). The annual sum of soil loss on Swiss grasslands of all the predicted monthly soil losses is $4.55 \text{ t ha}^{-1} \text{ yr}^{-1}$. That soil erosion rate would hypothetically equal to a total eroded soil mass of 5.26 Mt per year, related to the national

grassland area of 1155980 ha. Compared to the European assessment ($2.46 \text{ t ha}^{-1} \text{ yr}^{-1}$; Panagos et al., 2015e), the soil loss of Swiss grasslands is more than twofold higher than the average of the EU countries (including arable, forest and semi-natural areas). However, it needs to be considered that no specific methodological adaptations (e.g. of the C- and LS-factor) for grassland nor the Alps have been applied for Europe. Instead, slopes with inclinations exceeding 50% were not part of that assessment. It is evident that the high proportion of grasslands located in steep alpine areas result in higher erosion rates as for the European average.

The predicted average soil loss of $4.55 \text{ t ha}^{-1} \text{ yr}^{-1}$ exceeds the soil formation rates of old soils ($>10\text{-}18 \text{ kyr}$; $0.54\text{-}1.13 \text{ t ha}^{-1} \text{ yr}^{-1}$) and young soils ($>1\text{-}10 \text{ kyr}$; $1.19\text{-}2.48 \text{ t ha}^{-1} \text{ yr}^{-1}$) by far. Only soil formation rates of very young soils ($\leq 1 \text{ kyr}$; $4.15\text{-}8.81 \text{ t ha}^{-1} \text{ yr}^{-1}$) can compensate the soil loss within a year (Alewell et al., 2015a). In conclusion, the predicted soil loss rates for Swiss grasslands, in general, imply a non-reversible loss of the valuable resource soil.

According to the results for Switzerland, soil loss is significant on grassland and the anthropogenic contribution due to the intensified land use has a meaningful impact to soil loss rates as the trends in cultivation area and animal numbers demonstrate (Troxler et al., 2004; Meusburger and Alewell, 2008). Following the steady increase of forest areas (Federal Statistical Office Switzerland, 2018b) and the observations over the last 50 years in Switzerland (see chapter 1.3), it is to expect that pressure on pastures will be further intensified. By the aspect of high demand of Swiss food products and a continuous increase in population (Federal Statistical Office Switzerland, 2018a), soil erosion on grassland could drastically become an environment and political issue of high concern as soon as the cultivation of suitable grassland is limited. Borrelli et al. (2018) also emphasize the consideration of soil erosion in semi-natural habitats as grasslands and forests which contribute to a large share of global soil loss.

By capturing the soil loss rates of Swiss grassland we developed a more realistic soil loss assessment for Switzerland. However, each erosion factor needed to be modified according to the specific conditions of Swiss grasslands.

Rainfall erosivity is by far the most crucial factor as it is considered twice in the USLE/RUSLE (as individual factor and in the C-factor). However, it should be considered, that there is no direct relationship of rainfall and soil loss as rainfall erosivity does only take into account extreme events exceeding specific thresholds of duration, energy, and rainfall volume. In Switzerland, the complex topography is one of the main driving forces for the spatial patterns of rainfall erosivity as a clear tendency among different regions is apparent (see Appendix A.3.2.). A combination of a spatial resolution of 100 m with a monthly temporal resolution like presented in this thesis is so far unique in Switzerland. In particular, the R-factor communicates relevant information not only of interest for soil erosion. The spatio-temporal knowledge of increased rainfall erosivity is also of high value for hazard control in the Alps as other processes are likewise depending on the energy and intensity of rainfall (e.g. landslides, flash floods, mudflows). A combination of the spatio-temporal R-factor patterns with maps like the Pan-European landslide susceptibility mapping (ELSUS; Wilde et al., 2018) enable more targeted interventions. Furthermore, agricultural management and landscape planning can be supported by considering the spatio-temporal dynamics of R-factors.

Likewise relevant for other disciplines are the results of the monthly cover and management factor on Swiss grasslands. The weighting of soil loss ratios with the R-factor overrules the protective character of soil cover by plants in summer, although results present the natural growth cycle of plants within a year with an apparent maximum in summer and a temporal shift

according to elevation gradient. The later procedure follows the original approach to estimate C-factors. However, often, the C-factor is determined based on a direct relationship of soil cover and cover and management factor without considering the influence of rainfall characteristics. Such a simplified approach ignoring the weighting of soil loss ratios with rainfall erosivity would in our case result in very low C-factors and low soil loss rates in summer due to the high fraction of vegetation cover. Ultimately, there is an essential need to address the suitability of our presented C-factor approach with more empirical studies.

Next to the information about rainfall erosivity and soil cover, the condition of the soil itself is an essential component of soil erosion assessment. The presented national soil erodibility map is based on a comprehensive dataset that is now available with the LUCAS topsoil samples. This map might replace the previous K-factor map which was based on a variety of different soil data polygons with high uncertainties in the Alpine zone. Now, the regionalized K-factors are directly comparable (same data, covariates, methods) with the K-factors of other European countries. Highest K-factors are modeled for the top mountain ranges and the Swiss midland (especially the mires of the Seeland). However, the average soil erodibility ($0.0327 \text{ t ha h ha}^{-1} \text{ MJ}^{-1} \text{ mm}^{-1}$) of Switzerland is low to medium.

More easily to obtain are informations about the topography (slope length and slope steepness) with digital elevation models and geoinformation techniques (e.g. slope determination, flow accumulation, raster calculator). A continuous LS-factor mapping is enabled with the high resolution (2 m) digital elevation model of Switzerland. As the behavior of the S-factor was unknown for slope gradients $> 50\%$ (which represent 4.7% of the Swiss area), a new approach had to be developed. The new S-factor fitted by a total of 12 empirical equations. Simultaneously, the maximal flow threshold of the L-factor was limited to 100 m. Different rainfall experiments in the Alps support that new LS-factor approach for Switzerland.

So far, the extent of the Swiss grassland areas was only estimated. With new spatial data, especially satellite data, and classification techniques, the detection of grassland is now possible. Even segregation of temporal and permanent grassland can be made based on the CCI Land Cover dataset. This information is of high interest as baseline data for many fields of research (e.g. nature conservation, biodiversity, ecology, geobotany, agronomy, alpine research, soil sciences). The new Swiss grassland map of 2015 forms the base for soil erosion modeling on Swiss grassland.

8.2 Mitigating soil erosion – Value of the Swiss erosion risk map for grasslands

The presented monthly maps and the quantification of soil erosion on Swiss grasslands are primarily intended to serve as a tool for stakeholders and policymakers. They form the base for decision making of political contents regarding soil protection, agricultural management, and environment. The subject of the present project is the provision of the information about the spatial location, temporal timing, and quantification of soil erosion by water on grasslands. A discussion about suitable mitigation strategies and their practicability might now be continued on a political level.

In principle, most of the mitigation strategies will be targeting the factors C and P as they are most adjustable by land use management (Durán Zuazo and Rodríguez Pleguezuelo, 2008; Maetens et al., 2012; Biddoccu et al., 2014; Eshel et al., 2015; Biddoccu et al., 2016). These factors can easily be altered by a change of farming strategies (McCool et al., 1995; Panagos et al., 2015e), especially changing the composition of vegetation, the land pressure, the livestock rates and composition, and the management.

Vegetation: A relatively closed vegetation cover is one of the best methods to control soil erosion as sediment yield and soil stability is directly related to vegetation cover (Francis and Thornes, 1990; Casermeiro et al., 2004; Schindler Wildhaber et al., 2012). Usually, the vegetation cover on grazed grassland is reduced by the grazing of animals, uprooting plants, and trampling (Schauer, 2000). Also, selective grazing of animals (e.g. cattle) leads to a decrease in plant biodiversity. High plant biodiversity protects the soil of grasslands against erosion (Merz et al., 2009; Martin et al., 2010). Thus, a reduction of grazing animals and mixed-species grazing (with different grazing preferences) would keep the vegetation cover and biodiversity high. The application of fertilizer is recommendable for the development of a stable, balanced, and site-appropriate vegetation cover with a dense sward and an increased soil structure and soil activity (Troxler, 2014). However, the application of fertilizer should be made with care and according to the conditions of the soil.

Pressure: The trampling of animals affects soils and plants likewise. Trampling causes soil compaction, reduced infiltration with less plant available water and as a consequence, increased surface runoff. Additionally, the high pressure on the soil reduces plant growth, humus availability and soil fertility. According to Scott and Robertson (2009), animal claws effectuate a pressure of 200-500 kPa on soils. The effects of trampling can be reduced by a change in grazing animal species and a reduction of livestock weight and stocking densities. Trampling is even intensified during wet weather conditions as soils are more prone to compaction. An extensification of pastures and reduction of stocking rate is a recommended mitigation action. The weight of harvest machines for hay farming has similar effects on the soil as livestock trampling. Reduced tire pressure and an adjusted tire type could be more soil conserving.

Livestock: Grazing animals differ by weight, grazing radius, and grazing preferences. Though, it is recommended to select the type of animal for specific pastures carefully. Cattle and sheep are different in weight, but sheep prefer to graze on highest elevation ranges with young grass what might expose these remote soils to overgrazing (Troxler, 2014). According to slope gradients, the livestock composition should be changed. In general, it is recommended to utilize grasslands on slopes with less than 40% inclination for heavy cows. Younger cows are preferable for gradients between 40% and 60%. All areas steeper than 40% should be used solely for sheep and goats (Troxler, 2014). A change in livestock species, stocking rates, and grazing area is a valuable measure for soil erosion control.

Management: Different pasture systems have various effects on soil erosion. Continuous grazing is the grazing system with the highest risk for soil erosion as livestock is kept in only one paddock all year long. As such, the overgrazing causes extreme pressure on soils and vegetation. Other systems are rotation grazing, with a systematical change of pastures, or strip grazing with a daily change of pastures. It is evident that such systems reduce the trampling and

let the pasture recover to be productive again. A control of success of a managing shift from continuous grazing to rotation grazing significantly reduces soil erosion rates (Bauer, 2013; Bauer et al., 2013). Mobile milking parlors and cattle watering tanks prevent long periodical walking distances of cows to central milking parlors and supply stations. That management change reduces trampling and the development of cattle trails (Troxler et al., 1992).

Information about the fraction of vegetation cover is already included in C-factor. However, to include land management practices in further erosion risk assessments, a parametrization of the management of meadows, different pasture systems, stocking density, grazing livestock weights and type need to be established. Reliable and area-wide data to develop such P-factors for the management of grasslands are currently not available in Switzerland. Measurements of grassland management practices on a unit plot scale would be the most promising empirical approach to assess the P-factor for Swiss grasslands. Other potential approaches could be the establishment of a geometry factor based on geodata and aerial photographs, to capture the shapes of pastures, the trampling paths of cattle, or the location of the milking parlor and cattle watering tanks in combination with extensive literature research. A project at the University of Basel already aims to automatically extract cattle trails from aerial photographs (see chapter 8.3). Contour farming, stone walls, and grass margins were used to parametrize the P-factor for the European Union's agricultural area (Panagos et al., 2015d). These information origins from the European Union's LUCAS observations.

Soil erodibility (K) and the slope length factor (L) can also be managed by human interventions. For example, farmers could improve the soil stability by an increased stone cover, better root penetration or shortened slope lengths by the creation of natural or artificial barriers. The positive effect of the surface stone cover is already included in the soil erosion risk assessment for Swiss grassland. However, such measures are poorly practicable and less effective as an alteration of the soil organic carbon content in interaction with an increased vegetation cover. Reversely, some of these soil protecting agricultural practices would result in a loss of profit and farmers take on the role of landscape conservationists. A change in subsidies from quantity to quality could compensate that agricultural transition. It is also possible to alter the rainfall erosivity (R). However that might be only possible on a larger temporal scale by climate change mitigation. As positive trends in rainfall erosivity are to be expected for Switzerland (Meusburger et al., 2012), a mitigation of the causes for climate change would have a positive future effect for soil erosion protection likewise. The investigation of long-term rainfall erosivity trends may play a key role in understanding the climate change related dynamics of the R-factor. Such a statistical trend analysis can be conducted with daily rainfall observations for selected stations in Switzerland that are dating back for more than a century (MeteoSwiss, 2018b).

8.3 Evaluation of the approach and future proceedings

It was shown that the existing datasets for Switzerland are suitable for erosions modeling and their resolution is sufficient for modeling soil erosion rates on a monthly scale as they can serve as the base data for the R-, K-, C-, and LS-factor and meet the recommended temporal

resolution (see chapter 1.6). However, as models are only approximations to the real conditions and processes, limitations and drawbacks are expectable.

Drawbacks of the model are the unconsidered erosion effects of snow processes. A potential solution might be the inclusion of a winter factor for RUSLE as already proposed by Stanchi et al. (2014). Furthermore, the approach does only capture sheet erosion. Features of rill erosion, gully erosion, and landslides in the landscape might be obtained by the underlying data (e.g. Swissimage, SwissAlti3D) but cannot be quantified. It should be considered that the proposed model predicts only the semi-actual erosion risk, like real-time land use and support practices data (P-factor), are missing. However, a rapid improvement of soil erosion models is to be expected for the future that will even allow real-time modeling and validation of soil loss. Regardless, the ultimate base for the underlying empirical relationships will be an extended network of field observations, measurements, and data with special emphasize on grassland management.

Subsequently, the utilized model can further be improved if the following changes, modifications, and adoption are made in the future:

(1) Upgraded datasets:

The necessary upgrade of the ERK2 for arable land demonstrates the rapid advances in geoinformation. The erosion risk map for grasslands also needs to be upgraded as soon as the used datasets are outdated. We used the most state-of-the-art data and technology for modeling to make the map valid for the next years. However, during the lifespan of the project, datasets were already upgraded, refined or replaced. For example, the Swiss orthophotos Swissimage FCIR and RGB are now replaced by a single product with four spectral bands (NIR, R, G, B; Swisstopo, 2017b) which would increase the mapping accuracy of the C-factor. Newly extended databases of Swiss soil samples (soil samples of 1600 sites within the framework of the Biodiversity Monitoring in Switzerland; Meuli et al., 2017) should be published soon. Additional sampling campaigns for LUCAS are currently undergoing and scheduled for 2021 (Orgiazzi et al., 2018). Based on that, time series, changes in soil properties and thus in the K-factor are expected to be observed. Further, the grassland map could be improved with land use data from detailed agriculture information systems (e.g. GELAN, LAWIS, ACORDA, AGRICOLA, WALLIS; Bundesamt für Landwirtschaft BLW, 2018) which will be published nationwide in the next years. New satellite products with a high repeating rate as Sentinel-2 (5 days) are a valuable source for identifying temporal patterns in the future. These data need to be included in a second version of the map.

(2) Ground truth data:

Ground truth data are of relevance for supporting and proofing the results. Therefore, future measurements of soil loss rates and mapping of signs of erosion are a key for evaluating the projections. In a pilot region of Switzerland, a program called “Air-rosion” introduced a digital alert that informs the erosion researcher about upcoming high intensified rainfall events and potential erosion (Noll, 2017). Based on that information, in-situ observation of soil erosion with direct measurements and recordings is possible. This project is combined with the acquirement of aerial photographs by unmanned aerial vehicles (UAVs) of the affected site. A project like this passes over from an erosion risk mapping to erosion risk monitoring. Such monitoring would be a significant validation database for the erosion maps.

Furthermore, the building of an extended ground database, especially with rainfall experiments at different locations, would be beneficial for improving, refining, and better validating the LS-factor for steep alpine environments.

(3) Linkage to other erosion projects:

The conception of the most recent research project of the environmental geoscience working group at the University Basel (“weObserve: Integrating Citizen Observers and High Throughput Sensing Devices for Big Data Collection, Integration, and Analysis”) is a crowdsourced data collection system of alpine soil erosion (Swiss National Science Foundation, 2017). That system, called COSA (“Citizens’ Observatory Smartphone App”), should help to build a detailed erosion database by volunteers (e.g. hikers, bikers) for a better understanding of the spatial patterns and temporal dynamics of soil erosion (Alewell et al., 2015b). That approach selectively monitors soil erosion but is yet not able to assess the grassland soil erosion risk on a national scale. Both projects would profit from each other as the erosion risk map could serve as a base map for orientation, and the COSA-project could contribute the ground truth data.

Furthermore, part of the weObserve-project is an object-based image analysis that should later be replaced by convolutional neural networks to identify and quantify soil erosion and signs of erosion automatically (e.g. cattle trails, degraded bare soil) in aerial photographs (Zweifel et al., 2018). Another approach to automatically detect soil erosion in the Alps from aerial photos is under development in the canton Uri (Batkitar, 2014; Geilhausen et al., 2017). Such routines help to analyze trends in soil erosion by time-series of aerial photos or better identify degraded bare soil.

Further research projects of the group in Basel are dealing with fallout radionuclides inventories, compound-specific stable isotopes, and biomarker that were used for quantifying erosion and deposition or tracing of eroded sediments. These projects may serve to calibrate the soil loss rates of the erosion risk map for grassland and to widen the knowledge about sediment dislocation after erosion.

Meusburger et al. (2010a) and Meusburger et al. (2010b) already discussed the difficulty of differentiating dry vegetation and (degraded) bare soil in aerial photographs and satellite images. We were facing a similar problem in chapter 4 with the spatial high resolution Swissimage orthophotos. There is an urgent need for solving that limitation in image classification for future improvements in erosion risk assessments on Swiss grasslands. Frequently, alpine erosion starts at edges of degraded bare soil surfaces. As soon as such surfaces are appropriately identified, initial spots of potential soil erosion can better be localized. The project mentioned above “weObserve” with its object-based image classification could be a first step in establishing a technique for segregation bare soil from dry vegetation cover. Hyperspectral remote sensing images such as recorded by the Hyperspectral Imager (Hyperion) on board of the Earth Observing-1 satellite (EO-1; Goetz, 2009) or the future Sentinel-10 mission run by the European Space Agency and PRISMA operated by the Italian Space Agency in combination with extended field spectroscopy in the Alps might be another feasible methodology to narrow the hotspots of soil erosion on Swiss grasslands.

The approach for grasslands with a particular focus on the Alpine conditions could serve as a prototype for erosion mapping on grassland in other mountainous countries like Austria,

Germany, Italia, Slovenia, or France. The establishment of a comprehensible Alpine-wide grassland erosion risk map is of crucial importance for the recommendation of action within the Alpine Convention. Such a proposal would help to protect the unique nature of the Alps, the soils, the economy, the agriculture, the traditions, and the humans.

Bibliography

- Adams, J.B., Sabol, D.E., Kapos, V., Filho, R.A., Roberts, D.A., Smith, M.O., & Gillespie, A.R. (1995). Classification of multispectral images based on fractions of endmembers. Application to land-cover change in the Brazilian Amazon. *Remote Sensing of Environment*, 52, 137–154. doi:10.1016/0034-4257(94)00098-8.
- Agnese, C., Bagarello, V., Corrao, C., D'Agostino, L., & D'Asaro, F. (2006). Influence of the rainfall measurement interval on the erosivity determinations in the Mediterranean area. *Journal of Hydrology*, 329, 39–48. doi:10.1016/j.jhydrol.2006.02.002.
- AGRIDEA (2007). Wie viel Erde geht verloren?
https://agridea.abacuscity.ch/abauserimage/Agridea_2_Free/1194_2_D.pdf?xet=1536638629317.
- Alewell, C., Egli, M., & Meusburger, K. (2015a). An attempt to estimate tolerable soil erosion rates by matching soil formation with denudation in Alpine grasslands. *Journal of Soils and Sediments*, 15, 1383–1399. doi:10.1007/s11368-014-0920-6.
- Alewell, C., & Imhof, A. (2008). Bodenerosion. Einfluss der Landnutzung und des Klimas am Beispiel des Urserentals in Uri. *Umweltperspektiven*, 1, 40–41.
- Alewell, C., Meusburger, K., Brodbeck, M., & Bänninger, D. (2008). Methods to describe and predict soil erosion in mountain regions. *Landscape and Urban Planning*, 88, 46–53. doi:10.1016/j.landurbplan.2008.08.007.
- Alewell, C., Meusburger, K., Juretzko, G., Mabit, L., & Ketterer, M.E. (2014). Suitability of ²³⁹⁺²⁴⁰Pu and ¹³⁷Cs as tracers for soil erosion assessment in mountain grasslands. *Chemosphere*, 103, 274–280. doi:10.1016/j.chemosphere.2013.12.016.
- Alewell, C., Meusburger, K., Kandl, D., Fetai, I., Roth, V., Rugolo, V., Schuldt, H., & Vetter, T. (2015b). COSA – AlpErosion: Monitoring the degradation of Alpine soils with COSA, a Citizens' Observatory Smartphone App. *BGS Bulletin*, 36, 19–22.
- Alewell, C., Schaub, M., & Conen, F. (2009). A method to detect soil carbon degradation during soil erosion. *Biogeosciences*, 6, 2541–2547. doi:10.5194/bg-6-2541-2009.
- Alexandridis, T.K., Sotiropoulou, A.M., Bilas, G., Karapetsas, N., & Silleos, N.G. (2015). The Effects of Seasonality in Estimating the C-Factor of Soil Erosion Studies. *Land Degradation & Development*, 26, 596–603. doi:10.1002/ldr.2223.
- André, J.E., & Anderson, H.W. (1961). Variation of soil erodibility with geology, geographic zone, elevation, and vegetation type in northern California wildlands. *Journal of Geophysical Research*, 66, 3351–3358. doi:10.1029/JZ066i010p03351.
- Angulo-Martínez, M., & Beguería, S. (2009). Estimating rainfall erosivity from daily precipitation records. A comparison among methods using data from the Ebro Basin (NE Spain). *Journal of Hydrology*, 379, 111–121. doi:10.1016/j.jhydrol.2009.09.051.
- Arata, L., Meusburger, K., Frenkel, E., A'Campo-Neuen, A., Iurian, A.-R., Ketterer, M.E., Mabit, L., & Alewell, C. (2016). Modelling Deposition and Erosion rates with RadioNuclides (MODERN) - Part 1. A new conversion model to derive soil redistribution rates from inventories of fallout radionuclides. *Journal of environmental radioactivity*, 162-163, 45–55. doi:10.1016/j.jenvrad.2016.05.008.
- Arino, O., & Ramoino, F. (2017). Land Cover CCI. Product User Guide Version 2.0. Louvain-la-Neuve.

- Arnhold, S., Lindner, S., Lee, B., Martin, E., Kettering, J., Nguyen, T.T., Koellner, T., Ok, Y.S., & Huwe, B. (2014). Conventional and organic farming. Soil erosion and conservation potential for row crop cultivation. *Geoderma*, 219-220, 89–105. doi:10.1016/j.geoderma.2013.12.023.
- Asis, A.M. de, & Omasa, K. (2007). Estimation of vegetation parameter for modeling soil erosion using linear Spectral Mixture Analysis of Landsat ETM data. *ISPRS Journal of Photogrammetry and Remote Sensing*, 62, 309–324. doi:10.1016/j.isprsjprs.2007.05.013.
- Asis, A.M. de, Omasa, K., Oki, K., & Shimizu, Y. (2008). Accuracy and applicability of linear spectral unmixing in delineating potential erosion areas in tropical watersheds. *International Journal of Remote Sensing*, 29, 4151–4171. doi:10.1080/01431160701874579.
- Auerswald, K. (1986). Eignung der Hangneigungsfaktoren verschiedener Erosionsmodelle unter bayerischen Anbauverhältnissen. *Zeitschrift für Kulturtechnik und Flurbereinigung*, 27, 218–224.
- Auerswald, K., Fiener, P., Martin, W., & Elhaus, D. (2014). Use and misuse of the K factor equation in soil erosion modeling. An alternative equation for determining USLE nomograph soil erodibility values. *CATENA*, 118, 220–225. doi:10.1016/j.catena.2014.01.008.
- Bachmann, M. (2007). *Automatisierte Ableitung von Bodenbedeckungsgraden durch MESMA-Entmischung*. Würzburg.
- Badura, M., Kuenzer, N., Sutor, G., Kals, R., & Schmid, S. (2018). *Quo vadis soil protection in the Alps? Assessment of the Alpine Convention Soil Conservation Protocol and preparation/implementation of an international conference*. Dessau-Roßlau.
- Bahravi, J.A., Elhag, M., Aldhebiani, A.Y., Galal, H.K., Hegazy, A.K., & Alghailani, E. (2016). Soil Erosion Estimation Using Remote Sensing Techniques in Wadi Yalamlam Basin, Saudi Arabia. *Advances in Materials Science and Engineering*, 2016, 1–8. doi:10.1155/2016/9585962.
- Ballabio, C., Borrelli, P., Spinoni, J., Meusburger, K., Michaelides, S., Beguería, S., Klik, A., Petan, S., Janeček, M., Olsen, P., Aalto, J., Lakatos, M., Rymaszewicz, A., Dumitrescu, A., Tadić, M.P., Diodato, N., Kostalova, J., Rousseva, S., Banasik, K., Alewell, C., & Panagos, P. (2017). Mapping monthly rainfall erosivity in Europe. *The Science of the total environment*, 579, 1298–1315. doi:10.1016/j.scitotenv.2016.11.123.
- Banasik, K., & Górski, D. (1993). Evaluation of Rainfall Erosivity for East Poland. *Proceedings of the Warsaw Symposium*.
- Banasik, K., Górski, D., & Mitchell, J.K. (2001). Rainfall Erosivity for East and Central Poland. *International Symposium on Soil Erosion Research for the 21st Century*, 279–282.
- Bänninger, D., Brodbeck, M., Hohwieler, N., Meusburger, K., & Alewell, C. (2006). Soil Degradation in the Swiss Alps. In Bierlin B., & J. Pasotti (Eds.), *Deserts and Desertification in High Altitude Areas* (pp. 6–8).
- Batkitar, D. (2014). *Machbarkeitsstudie: Auf Fernerkundung basierende Erfassungsmethode von Bodenerosion*. Wädenswil.
- Bätzing, W. (2015). *Die Alpen. Geschichte und Zukunft einer europäischen Kulturlandschaft*. München.
- Bauer, C. (2013). *Einfluss von Nutzungsumstellungen auf die Bodenerosion von schweizerischen Schafalpen*. Basel.
- Bauer, C., Meusburger, K., Alewell, C., Prasuhn, V., & Werder, C. (2013). Bodenerosion auf Schafalpen. *Forum Kleinwiederkäuer*, 4, 12–14.

- Begert, M., Schlegel, T., & Kirchhofer, W. (2005). Homogeneous temperature and precipitation series of Switzerland from 1864 to 2000. *International Journal of Climatology*, 25, 65–80. doi:10.1002/joc.1118.
- Biddoccu, M., Ferraris, S., Opsi, F., & Cavallo, E. (2016). Long-term monitoring of soil management effects on runoff and soil erosion in sloping vineyards in Alto Monferrato (North–West Italy). *Soil and Tillage Research*, 155, 176–189. doi:10.1016/j.still.2015.07.005.
- Biddoccu, M., Opsi, F., & Cavallo, E. (2014). Relationship between runoff and soil losses with rainfall characteristics and long-term soil management practices in a hilly vineyard (Piedmont, NW Italy). *Soil Science and Plant Nutrition*, 60, 92–99. doi:10.1080/00380768.2013.862488.
- Bilotta, G.S., Brazier, R.E., & Haygarth, P.M. (2007). The Impacts of Grazing Animals on the Quality of Soils, Vegetation, and Surface Waters in Intensively Managed Grasslands. *Advances in Agronomy*, 94, 237–280. doi:10.1016/S0065-2113(06)94006-1.
- Blair, S. (2013). "V" for Vegetation. The mission of Proba-V. *European Space Agency Bulletin*, 10–21.
- Blume, H.-P., Brümmer, G.W., Fleige, H., Horn, R., Kandeler, E., Kögel-Knabner, I., Kretschmar, R., Stahr, K., & Wilke, B.-M. (2016). *Scheffer/Schachtschabel Soil Science*. (1st ed.). Berlin, Heidelberg, s.l.: Springer Berlin Heidelberg.
- Boardman, J.W., & Kruse, F.A. (1994). Automated spectral analysis - a geological example using AVIRIS data, North Grapevine Mountains, Nevada. *10th Thematic Conference on Geologic Remote Sensing - Exploration, Environment, and Engineering, San Antonio, TX*, 407–418.
- Bochet, E., Poesen, J., & Rubio, J.L. (2006). Runoff and soil loss under individual plants of a semi-arid Mediterranean shrubland. Influence of plant morphology and rainfall intensity. *Earth Surface Processes and Landforms*, 31, 536–549. doi:10.1002/esp.1351.
- Bonilla, C., & Vidal, K. (2011). Rainfall erosivity in Central Chile. *Journal of Hydrology*, 410, 126–133. doi:10.1016/j.jhydrol.2011.09.022.
- Bontemps, S., Boettcher, M., Brockmann, C., Kirches, G., Lamarche, C., Radoux, J., Santoro, M., Vanbogaert, E., Wegmüller, U., Herold, M., Achard, F., Ramoino, F., Arino, O., & Defourny, P. (2015). Multi-year global land cover mapping at 300 m and characterization for climate modelling. Achievements of the Land Cover component of the ESA Climate Change Initiative. *ISPRS - International Archives of the Photogrammetry, Remote Sensing and Spatial Information Sciences*, XL-7/W3, 323–328. doi:10.5194/isprsarchives-XL-7-W3-323-2015.
- Borrelli, P., Diodato, N., & Panagos, P. (2016). Rainfall erosivity in Italy. A national scale spatio-temporal assessment. *International Journal of Digital Earth*, 1–16. doi:10.1080/17538947.2016.1148203.
- Borrelli, P., Panagos, P., Lugato, E., Alewell, C., Ballabio, C., Montanarella, L., & Robinson, D.A. (2018). Lateral carbon transfer from erosion in noncroplands matters. *Global change biology*, 24, 3283–3284. doi:10.1111/gcb.14125.
- Borrelli, P., Robinson, D.A., Fleischer, L.R., Lugato, E., Ballabio, C., Alewell, C., Meusburger, K., Modugno, S., Schütt, B., Ferro, V., Bagarello, V., van Oost, K., Montanarella, L., & Panagos, P. (2017). An assessment of the global impact of 21st century land use change on soil erosion. *Nature Communications*, 8, 2013. doi:10.1038/s41467-017-02142-7.

- Bosco, C., Rigo, D. de, Dewitte, O., Poesen, J., & Panagos, P. (2015). Modelling soil erosion at European scale. Towards harmonization and reproducibility. *Natural Hazards and Earth System Science*, *15*, 225–245. doi:10.5194/nhess-15-225-2015.
- Bosco, C., Rusco, E., Montanarella, L., & Panagos, P. (2009). Soil erosion in the Alpine area: risk assessment and climate change. *Studi Trentini di Scienze Naturali*, 119–125.
- Bötsch, M. (2004). Swiss agricultural policy and its focus on grassland. In A. Lüscher, B. Jeangros, W. Kessler, O. Huguenin, M. Lobsiger, M. Millar, & D. Suter (Eds.), *Land Use Systems in Grassland Dominated Regions* (pp. 5–11). Zürich.
- Brenning, A., Bangs, D., & Becker, M. (2018). Package 'RSAGA'. <https://cran.r-project.org/web/packages/RSAGA/RSAGA.pdf>.
- Brown, L. (1981). World population growth, soil erosion, and food security. *Science*, *214*, 995–1002. doi:10.1126/science.7302578.
- Brown, L., & Foster, G. (1987). Storm Erosivity Using Idealized Intensity Distributions. *Transactions of the ASAE*, *30*, 379–386. doi:10.13031/2013.31957.
- Bryan, R.B. (2000). Soil erodibility and processes of water erosion on hillslope. *Geomorphology*, *32*, 385–415. doi:10.1016/S0169-555X(99)00105-1.
- Bundesamt für Landwirtschaft BLW (2017). Landwirtschaftliche Zonen. Landwirtschaftliche Zonen.
- Bundesamt für Landwirtschaft BLW (2018). Kantonale Datenerhebung. <https://www.blw.admin.ch/blw/de/home/politik/datenmanagement/agate/kantonedatenerhebung.html>.
- Busetto, L., Colombo, R., Migliavacca, M., Cremonese, E., Meroni, M., Galvagno, M., Rossini, M., Siniscalco, C., Morra die Cella, U., & Pari, E. (2010). Remote sensing of larch phenological cycle and analysis of relationships with climate in the Alpine region. *Global change biology*, *104*, 88. doi:10.1111/j.1365-2486.2010.02189.x.
- Butt, M.J., Waqas, A., & Mahmood, R. (2010). The Combined Effect of Vegetation and Soil Erosion in the Water Resource Management. *Water Resources Research*, *24*, 3701–3714. doi:10.1007/s11269-010-9627-7.
- Camacho, F. (2016). *Quality Assessment Report LAI, FAPAR, FCover Collection 300m. Version 1*.
- Casermeiro, M.A., Molina, J.A., La Cruz Caravaca, M.T. de, Hernando Costa, J., Hernando Massanet, M.I., & Moreno, P.S. (2004). Influence of scrubs on runoff and sediment loss in soils of Mediterranean climate. *CATENA*, *57*, 91–107. doi:10.1016/S0341-8162(03)00160-7.
- Ceaglio, E., Meusburger, K., Freppaz, M., Zanini, E., & Alewell, C. (2012). Estimation of soil redistribution rates due to snow cover related processes in a mountainous area (Valle d'Aosta, NW Italy). *Hydrology and Earth System Sciences*, *16*, 517–528. doi:10.5194/hess-16-517-2012.
- Chang, K.-t., & Tsai, B.-w. (1991). The Effect of DEM Resolution on Slope and Aspect Mapping. *Cartography and Geographic Information Systems*, *18*, 69–77. doi:10.1559/152304091783805626.
- Chen, B., Huang, B., & Xu, B. (2015). Comparison of Spatiotemporal Fusion Models. A Review. *Remote Sensing*, *7*, 1798–1835. doi:10.3390/rs70201798.
- Chesworth, W. (Ed.) (2008). *Encyclopedia of Soil Science*. Dordrecht: Springer.
- Chisholm, M. (2008). *Analyse der Bodenerosion mit der AVErosionExtension für ArcView*. Bern.

- Colombo, C., Palumbo, G., Aucelli, P.P.C., Angelis, A.d., & Roskopf, C.M. (2010). Relationships between soil properties, erodibility and hillslope features in Central Apennines, Southern Italy. *Proceedings of the 19th World Congress of Soil Science, Brisbane, Australia, 1-6 August 2010.*, 117–120.
- Conrad, O., Bechtel, B., Bock, M., Dietrich, H., Fischer, E., Gerlitz, L., Wehberg, J., Wichmann, V., & Böhner, J. (2015). System for Automated Geoscientific Analyses (SAGA) v. 2.1.4. *Geoscientific Model Development*, 8, 1991–2007. doi:10.5194/gmd-8-1991-2015.
- Council of the European Union (2009). Council Regulation. *EC*.
- da Silva, A.M. (2004). Rainfall erosivity map for Brazil. *CATENA*, 57, 251–259. doi:10.1016/j.catena.2003.11.006.
- da Silva, A.M., Wiecheteck, M., & Zuercher, B.W. (2011). Spatial Assessment of Indices for Characterizing the Erosive Force of Rainfall in El Salvador Republic. *Environmental Engineering Science*, 28, 309–316. doi:10.1089/ees.2010.0296.
- da Silva, R.M., Santos, C.A.G., de Lima Silva, Valeriano Carneiro, & e Silva, L.P. (2013). Erosivity, surface runoff, and soil erosion estimation using GIS-coupled runoff–erosion model in the Mamuaba catchment, Brazil. *Environmental Monitoring and Assessment*, 185, 8977–8990. doi:10.1007/s10661-013-3228-x.
- Dabney, S.M., Yoder, D.C., Vieira, D., & Bingner, R.L. (2011). Enhancing RUSLE to include runoff-driven phenomena. *Hydrological Processes*, 25, 1373–1390. doi:10.1002/hyp.7897.
- Dabney, S.M., Yoder, D.C., & Vieira, D.A.N. (2012). The application of the Revised Universal Soil Loss Equation, Version 2, to evaluate the impacts of alternative climate change scenarios on runoff and sediment yield. *Journal of Soil and Water Conservation*, 67, 343–353. doi:10.2489/jswc.67.5.343.
- Davison, P., Hutchins, M.G., Anthony, S.G., Betson, M., Johnson, C., & Lord, E.I. (2005). The relationship between potentially erosive storm energy and daily rainfall quantity in England and Wales. *The Science of the total environment*, 344, 15–25. doi:10.1016/j.scitotenv.2005.02.002.
- de Carvalho, D.F., Durigon, V.L., Antunes, M.A.H., Almeida, W.S.d., & Oliveira, P.T.S.d. (2014). Predicting soil erosion using Rusle and NDVI time series from TM Landsat 5. *Pesquisa Agropecuária Brasileira*, 49, 215–224. doi:10.1590/S0100-204X2014000300008.
- de Jong, S.M. (1994). Derivation of vegetation variables from a Landsat TM image for modelling soil erosion. *Earth Surface Processes and Landforms*, 19. doi:10.1002/esp.3290190207.
- de Jong, S.M., Brouwer, L.C., & Riezebos, H.T. (1998). *Erosion hazard assessment in the La Peyne catchment, France. Working Paper EU DeMon-II Project*. Utrecht.
- de Jong, S.M., & Epema, G.F. (2010). Imaging Spectrometry for Surveying and Modelling Land Degradation. In F.D. van der Meer, & S.M. de Jong (Eds.), *Imaging spectrometry. Basic principles and prospective applications*. Dordrecht.
- Defila, C., & Clot, B. (2001). Phytophenological trends in Switzerland. *International Journal of Biometeorology*, 45, 203–207. doi:10.1007/s004840100101.
- Dennison, P.E., & Roberts, D.A. (2003). Endmember selection for multiple endmember spectral mixture analysis using endmember average RMSE. *Remote Sensing of Environment*, 87, 123–135. doi:10.1016/S0034-4257(03)00135-4.
- Desmet, P.J.J., & Govers, G. (1996). A GIS procedure for automatically calculating the USLE LS factor on topographically complex landscape units. *Journal of Soil and Water Conservation*, 51, 427–433.

- Didan, K., Munoz, A.B., Solano, R., & Huete, A. (2015). MOD13Q1 MODIS/Terra Vegetation Indices 16-Day L3 Global 250m SIN Grid V006. Arizona.
- Diek, S., Fornallaz, F., Schaepman, M., & Jong, R. de (2017). Barest Pixel Composite for Agricultural Areas Using Landsat Time Series. *Remote Sensing*, *9*, 1245. doi:10.3390/rs9121245.
- Diek, S., Schaepman, M., & Jong, R. de (2016). Creating Multi-Temporal Composites of Airborne Imaging Spectroscopy Data in Support of Digital Soil Mapping. *Remote Sensing*, *8*, 906. doi:10.3390/rs8110906.
- Diodato, N. (2005). Predicting RUSLE (Revised Universal Soil Loss Equation) Monthly Erosivity Index from Readily Available Rainfall Data in Mediterranean Area. *The Environmentalist*, *26*, 63–70. doi:10.1007/s10669-006-5359-x.
- Dotterweich, M. (2013). The history of human-induced soil erosion. Geomorphic legacies, early descriptions and research, and the development of soil conservation—A global synopsis. *Geomorphology*, *201*, 1–34. doi:10.1016/j.geomorph.2013.07.021.
- Durán Zuazo, V.H., & Rodríguez Pleguezuelo, C.R. (2008). Soil-erosion and runoff prevention by plant covers. A review. *Agronomy for Sustainable Development*, *28*, 65–86. doi:10.1051/agro:2007062.
- Efron, B., & Gong, G. (1983). A Leisurely Look at the Bootstrap, the Jackknife, and Cross-Validation. *The American Statistician*, *37*, 36–48. doi:10.1080/00031305.1983.10483087.
- Efron, B., & Tibshirani, R. (1997). Improvements on Cross-Validation. The .632+ Bootstrap Method. *Journal of the American Statistical Association*, *92*, 548. doi:10.2307/2965703.
- Efthimiou, N. (2016). Performance of the RUSLE in Mediterranean Mountainous Catchments. *Environmental Processes*, *3*, 1001–1019. doi:10.1007/s40710-016-0174-y.
- Ellenberg, H., Leuschner, C., & Dierschke, H. (2010). *Vegetation Mitteleuropas mit den Alpen. In ökologischer, dynamischer und historischer Sicht ; 203 Tabellen.* (6th ed.). Stuttgart.
- ESDAC (2018). Soil Erodibility (K- Factor) High Resolution dataset for Europe. <https://esdac.jrc.ec.europa.eu/content/soil-erodibility-k-factor-high-resolution-dataset-europe>.
- Eshel, G., Egozi, R., Goldwasser, Y., Kashti, Y., Fine, P., Hayut, E., Kazukro, H., Rubin, B., Dar, Z., Keisar, O., & DiSegni, D.M. (2015). Benefits of growing potatoes under cover crops in a Mediterranean climate. *Agriculture, Ecosystems & Environment*, *211*, 1–9. doi:10.1016/j.agee.2015.05.002.
- Estrada-Carmona, N., Harper, E.B., DeClerck, F., & Fremier, A.K. (2016). Quantifying model uncertainty to improve watershed-level ecosystem service quantification. A global sensitivity analysis of the RUSLE. *International Journal of Biodiversity Science, Ecosystem Services & Management*, *13*, 40–50. doi:10.1080/21513732.2016.1237383.
- Eurostat (2009). LUCAS 2009. Land Use / Cover Area Frame Survey. <http://ec.europa.eu/eurostat/documents/205002/208938/LUCAS+2009+Instructions/8ffdb9d8-b911-40b6-8f9a-8788bf696aa3>.
- Evrard, O., Persoons, E., Vandaele, K., & van Wesemael, B. (2007). Effectiveness of erosion mitigation measures to prevent muddy floods. A case study in the Belgian loam belt. *Agriculture, Ecosystems & Environment*, *118*, 149–158. doi:10.1016/j.agee.2006.02.019.
- FAO (2015). *Status of the world's soil resources. Main report.* Rome: FAO; ITPS.
- Farr, T.G., Rosen, P.A., Caro, E., Crippen, R., Duren, R., Hensley, S., Kobrick, M., Paller, M., Rodriguez, E., Roth, L., Seal, D., Shaffer, S., Shimada, J., Umland, J., Werner, M., Oskin,

- M., Burbank, D., & Alsdorf, D. (2007). The Shuttle Radar Topography Mission. *Reviews of Geophysics*, 45, 1485. doi:10.1029/2005RG000183.
- Federal Office for Agriculture (1997). Boundaries of agricultural zones in Switzerland. https://www.geocat.ch/geonetwork/srv/eng/md.viewer#/full_view/6e4544bc-55f4-4aef-b36a-e36fe376eaf8/tab/complete.
- Federal Office for Agriculture (2010). Erosion risk map of Switzerland, qualitative 2 (valley region and mountain zones I+II). https://www.geocat.ch/geonetwork/srv/eng/md.viewer#/full_view/c71cbdaf-d9db-42b6-a5d3-a24b6aa075a7/tab/complete.
- Federal Statistical Office Switzerland (2017). Statistischer Atlas der Schweiz. 15.11.2017. https://www.atlas.bfs.admin.ch/maps/13/de/12714_5875_5874_4801/20931.html.
- Federal Statistical Office Switzerland (2018a). Bilanz der ständigen Wohnbevölkerung nach institutionellen Gliederungen, Staatsangehörigkeit (Kategorie), Geschlecht und demographischen Komponenten. <https://www.bfs.admin.ch/bfs/en/home/statistics/catalogues-databases/data.assetdetail.6067441.html>.
- Federal Statistical Office Switzerland (2018b). Swiss Forestry statistics. <https://www.bfs.admin.ch/bfs/de/home/statistiken/kataloge-datenbanken/daten.assetdetail.5708654.html>.
- Felix, R., & Johannes, B. (1995). Bodenerosionsuntersuchungen auf Testparzellen im Kalkhochgebirge. *Mitteilungen der Österreichischen Geographischen Gesellschaft*, 137, 76–92.
- Figueiredo, T. de, & Poesen, J. (1998). Effects of surface rock fragment characteristics on interrill runoff and erosion of a silty loam soil. *Soil Tillage Research*, 46, 81–95. doi:10.1016/S0167-1987(98)80110-4.
- Filippa, G., Cremonese, E., Galvagno, M., Migliavacca, M., Di Morra Cella, U., Petey, M., & Siniscalco, C. (2015). Five years of phenological monitoring in a mountain grassland. Inter-annual patterns and evaluation of the sampling protocol. *International Journal of Biometeorology*, 59, 1927–1937. doi:10.1007/s00484-015-0999-5.
- Fontana, F., Rixen, C., Jonas, T., Aberegg, G., & Wunderle, S. (2008). Alpine Grassland Phenology as Seen in AVHRR, VEGETATION, and MODIS NDVI Time Series - a Comparison with In Situ Measurements. *Sensors*, 8, 2833–2853. doi:10.3390/s8042833.
- Foody, G.M. (2006). Sub-Pixel Methods in Remote Sensing. In S.M. de Jong, & F.D. van der Meer (Eds.), *Remote Sensing Image Analysis. Including the Spatial Domain*. Dordrecht.
- Foster, G.R. (1982). Modeling the erosion process. In C.T. Haan, H.P. Johnson, & D.L. Brakensiek (Eds.), *Hydrologic modeling of small watersheds* (pp. 297–382). St. Joseph.
- Foster, G.R., McCool, D.K., Renard, K.G., & Moldenhauer, W.C. (1981). Conversion of the universal soil loss equation to SI metric units. *Journal of Soil and Water Conservation*, 36, 355–359.
- Foster, G.R., Yoder, D.C., Weesies, G.A., McCool, D.K., McGregor, K.C., & Bingner, R.L. (2008). *Draft User's Guide, Revised Universal Soil Loss Equation Version 2 (RUSLE-2)*. Washington, DC.
- Francis, C.F., & Thornes, J.B. (1990). Runoff hydrographs from three Mediterranean vegetation cover types. In J.B. Thornes (Ed.), *Vegetation and erosion. Processes and environments* (pp. 363–384). Chichester: Wiley.

- Frankenberg, P., Geier, B., Proswitz, E., Schutz, J., & Seeling, S. (1995). Untersuchungen zu Bodenerosion und Massenbewegungen im Gunzesrieder Tal/Oberallgäu. *Austrian Journal of Forest Science*, *114*, 214–231.
- Frei, P., Kotlarski, S., Liniger, M.A., & Schär, C. (2017). Snowfall in the Alps. Evaluation and projections based on the EURO-CORDEX regional climate models. *The Cryosphere Discussions*, 1–38. doi:10.5194/tc-2017-7.
- Friedli, S. (2006). *Digitale Bodenerosionsgefährdungskarte Der Schweiz Im Hektarraster – Unter Besonderer Berücksichtigung des Ackerlandes*. Bern.
- Fuhrer, J., Beniston, M., Fischlin, A., Frei, C., Goyette, S., Jasper, K., & Pfister, C. (2006). Climate risks and their impact on agriculture and forests in Switzerland. In H. Wanner, M. Grosjean, R. Röthlisberger, & E. Xoplaki (Eds.), *Climate Variability, Predictability and Climate Risks* (pp. 79–102). Dordrecht.
- Gallo, K., Tarpley, D., Mitchell, K., Csiszar, I., Owen, T., & Reed, B. (2001). Monthly fractional green vegetation cover associated with land cover classes of the conterminous USA. *Geophysical Research Letters*, *28*, 2089–2092. doi:10.1029/2000GL011874.
- Ganasri, B.P., & Ramesh, H. (2016). Assessment of soil erosion by RUSLE model using remote sensing and GIS - A case study of Nethravathi Basin. *Geoscience Frontiers*, *7*, 953–961. doi:10.1016/j.gsf.2015.10.007.
- Gao, G.Y., Fu, B.J., Lü, Y.H., Liu, Y., Wang, S., & Zhou, J. (2012). Coupling the modified SCS-CN and RUSLE models to simulate hydrological effects of restoring vegetation in the Loess Plateau of China. *Hydrology and Earth System Sciences*, *16*, 2347–2364. doi:10.5194/hess-16-2347-2012.
- García-Ruiz, J.M., Beguería, S., Nadal-Romero, E., González-Hidalgo, J.C., Lana-Renault, N., & Sanjuán, Y. (2015). A meta-analysis of soil erosion rates across the world. *Geomorphology*, *239*, 160–173. doi:10.1016/j.geomorph.2015.03.008.
- Garonna, I., Jong, R. de, Wit, A.J.W. de, Mücher, C.A., Schmid, B., & Schaepman, M.E. (2014). Strong contribution of autumn phenology to changes in satellite-derived growing season length estimates across Europe (1982–2011). *Global change biology*, *20*, 3457–3470. doi:10.1111/gcb.12625.
- Geilhausen, M., Laube, P., & Matile, L. (2017). *Erosion im Alpenen Raum Eine ArcGIS® Toolbox zur Identifizierung bewirtschaftungsbedingter Erosionsschäden nach der Vollzugshilfe Umweltschutz in der Landwirtschaft*. Wädenswil.
- Gilabert, M. (2000). A Mixture Modeling Approach to Estimate Vegetation Parameters for Heterogeneous Canopies in Remote Sensing. *Remote Sensing of Environment*, *72*, 328–345. doi:10.1016/S0034-4257(99)00109-1.
- Gisler, S., Liniger, H.P., & Prasuhn, V. (2010). *Technisch-wissenschaftlicher Bericht zur Erosionsrisikokarte der landwirtschaftlichen Nutzfläche der Schweiz im 2x2-Meter-Raster (ERK2)*. Bern.
- Gisler, S., Liniger, H.-P., & Prasuhn, V. (2011). Erosionsrisikokarte im 2x2-Meter-Raster (ERK2). *Agrarforschung Schweiz*, *2*.
- Goetz, A.F.H. (2009). Three decades of hyperspectral remote sensing of the Earth. A personal view. *Remote Sensing of Environment*, *113*, S5–S16. doi:10.1016/j.rse.2007.12.014.
- Gonseth, Y., Wohlgemuth, T., Sansonnens, B., & Buttler, A. (2001). Die biogeographischen Regionen der Schweiz. Erläuterungen und Einteilungsstandard. *Umwelt Materialien*, *137*.
- González, C., Resano, J., Mozos, D., Plaza, A., & Valencia, D. (2010). FPGA Implementation of the Pixel Purity Index Algorithm for Remotely Sensed Hyperspectral Image Analysis.

- EURASIP Journal on Advances in Signal Processing*, 2010, 969806.
doi:10.1155/2010/969806.
- Gotway, C.A., & Stroup, W.W. (1997). A Generalized Linear Model Approach to Spatial Data Analysis and Prediction. *Journal of Agricultural, Biological, and Environmental Statistics*, 2, 157–178.
- Grauso, S., Verrubbi, V., Zini, A., Crovato, C., & Sciortino, M. (2015). *Soil Erosion Estimate in Southern Latium (Central Italy) Using RUSLE and Geostatistical Techniques*. Rome.
- Grazhdani, S., & Shumka, S. (2007). An approach to mapping soil erosion by water with application to Albania. *Desalination*, 213, 263–272. doi:10.1016/j.desal.2006.03.612.
- Green, A.A., Berman, M., Switzer, P., & Craig, M.D. (1988). A transformation for ordering multispectral data in terms of image quality with implications for noise removal. *IEEE Transactions on Geoscience and Remote Sensing*, 26, 65–74. doi:10.1109/36.3001.
- Gupta, B.C., & Guttman, I. (2013). *Statistics and probability with applications for engineers and scientists*. Hoboken, New Jersey: John Wiley & Sons Inc.
- Hanel, M., Máca, P., Bašta, P., Vlnas, R., & Pech, P. (2016). Rainfall erosivity factor in the Czech Republic and its Uncertainty. *Hydrology and Earth System Sciences Discussions*, 1–24. doi:10.5194/hess-2016-158.
- Harrell, F., Jr. (2015). *Regression Modeling Strategies. With Applications to Linear Models, Logistic and Ordinal Regression, and Survival Analysis*. Cham.
- Hartwig, N.L., & Ammon, H.U. (2002). Cover crops and living mulches. *Weed Science*, 50, 688–699. doi:10.1614/0043-1745(2002)050[0688:AIACCA]2.0.CO;2.
- Hawkins, R.H. (1985). Hydrology and the Universal Soil Loss Equation. Application to Rangelands. *US Department of the Interior, Technical Note 365*, 1–40.
- Heidari Mozaffar, M., Valadan Zoej, M.J., Sahebi, M.R., & Rezaei, Y. (2008). Vegetation endmember extraction in Hyperion Images. *The International Archives of the Photogrammetry, Remote Sensing and Spatial Information Sciences. Vol. XXXVII. Part B7, Beijing*, 409–412.
- Heinz, D.C., & Chein-I-Chang (2001). Fully constrained least squares linear spectral mixture analysis method for material quantification in hyperspectral imagery. *IEEE Transactions on Geoscience and Remote Sensing*, 39, 529–545. doi:10.1109/36.911111.
- Hengl, T. (2007). *A practical guide to geostatistical mapping of environmental variables*. Luxembourg: Publications Office.
- Hengl, T., Heuvelink, G., & Rossiter, D. (2007). About regression-kriging. From equations to case studies. *Computers & Geosciences*, 33, 1301–1315. doi:10.1016/j.cageo.2007.05.001.
- Hengl, T., Heuvelink, G., & Stein, A. (2004). A generic framework for spatial prediction of soil variables based on regression-kriging. *Geoderma*, 120, 75–93. doi:10.1016/j.geoderma.2003.08.018.
- Hensel, H., & Bork, H.-R. (1988). Computer aided Construction of Soil Erosion and Deposition Maps. *Geologisches Jahrbuch Reihe A*, 357–371.
- Hill, J., Mégier, J., & Mehl, W. (1995). Land degradation, soil erosion and desertification monitoring in Mediterranean ecosystems. *Remote Sensing Reviews*, 12, 107–130. doi:10.1080/02757259509532278.
- Hollinger, S.E., Angel, J.R., & Palecki, M.A. (2002). *Spatial Distribution, Variation, and Trends in Storm Precipitation Characteristics Associated with Soil Erosion in the United States*.

- Hotz, M.-C., & Weibel, F. (Eds.) (2005). *Arealstatistik Schweiz. Zahlen, Fakten, Analysen*. Neuchâtel.
- Hudson, B.D. (1992). The Soil Survey as Paradigm-based Science. *Soil Science Society of America Journal*, *56*, 836. doi:10.2136/sssaj1992.03615995005600030027x.
- Hurni, H. (1978). Bestimmung der Erosivität von Hagelereignissen. Empirische Bestimmung der Erosivität von Hagelereignissen. *Unpublished manuscript*.
- Iaich, H., Moussadek, R., Baghdad, B., Mrabet, R., Douaik, A., Abdelkrim, D., & Bouabdli, A. (2016). Soil erodibility mapping using three approaches in the Tangiers province –Northern Morocco. *International Soil and Water Conservation Research*, *4*, 159–167. doi:10.1016/j.iswcr.2016.07.001.
- Inoubli, N., Raclot, D., Mekki, I., Moussa, R., & Le Bissonnais, Y. (2017). A Spatiotemporal Multiscale Analysis of Runoff and Erosion in a Mediterranean Marly Catchment. *Vadose Zone Journal*, *16*, 0. doi:10.2136/vzj2017.06.0124.
- Inoue, T., Nagai, S., Kobayashi, H., & Koizumi, H. (2015). Utilization of ground-based digital photography for the evaluation of seasonal changes in the aboveground green biomass and foliage phenology in a grassland ecosystem. *Ecological Informatics*, *25*, 1–9. doi:10.1016/j.ecoinf.2014.09.013.
- Isotta, F., Frei, C., Weigluni, V., Perčec T., M., Lassègues, P., Rudolf, B., Pavan, V., Cacciamani, C., Antolini, G., Ratto, S., Munari, M., Micheletti, S., Bonati, V., Lussana, C., Ronchi, C., Panettieri, E., Marigo, G., & Vertačnik, G. (2014). The climate of daily precipitation in the Alps. Development and analysis of a high-resolution grid dataset from pan-Alpine rain-gauge data. *International Journal of Climatology*, *34*, 1657–1675. doi:10.1002/joc.3794.
- James, G., & Witten, D. (2015). *An introduction to statistical learning. With applications in R*. (6th ed.). New York, NY: Springer.
- Jeanros, B., & Thomet, B. (2004). Multi-functionality of grassland systems in Switzerland. In A. Lüscher, B. Jeanros, W. Kessler, O. Huguenin, M. Lobsiger, M. Millar, & D. Suter (Eds.), *Land Use Systems in Grassland Dominated Regions*. Zürich.
- Jenny, H. (1941). *Factors of Soil Formation: A System of Quantitative Pedology*. New York: McGraw-Hill Book Company Inc.
- Jing, Z., Xu-dong, Z., Jin-xing, Z., Xiao-ling, Z., & Zhong-jian, W. (2009). Calculation and Characterization of Rainfall Erosivity in Small Watersheds of Hilly Region in Northwest Hunan (in chinese). *Journal of Ecology and Rural Environment*, *25*, 32–36.
- Jonas, T., Rixen, C., Sturm, M., & Stoeckli, V. (2008). How alpine plant growth is linked to snow cover and climate variability. *Journal of Geophysical Research*, *113*, 377. doi:10.1029/2007JG000680.
- Jury, W.A., & Horton, R. (2004). *Soil physics*. Hoboken, NJ.
- Karaburun, A. (2010). Estimation of C factor for soil erosion modeling using NDVI in Buyukcekmece watershed. *Ozean Journal of Applied Sciences*, *3*, 77–85.
- Karydas, C.G., & Panagos, P. (2016). Modelling monthly soil losses and sediment yields in Cyprus. *International Journal of Digital Earth*, *9*, 766–787. doi:10.1080/17538947.2016.1156776.
- Karydas, C.G., & Panagos, P. (2017). The G2 erosion model. An algorithm for month-time step assessments. *Environmental research*, *161*, 256–267. doi:10.1016/j.envres.2017.11.010.

- Kerdiles, H., & Grondona, M.O. (1995). NOAA-AVHRR NDVI decomposition and subpixel classification using linear mixing in the Argentinean Pampa. *International Journal of Remote Sensing*, *16*, 1303–1325. doi:10.1080/01431169508954478.
- Keshava, N., & Mustard, J.F. (2002). Spectral unmixing. *IEEE Signal Processing Magazine*, *19*, 44–57. doi:10.1109/79.974727.
- Kilinc, A.W., & Richardson, E.V. (1973). Mechanics of soil erosion from overland flow generated by simulated rainfall. *Colorado State University*.
- King, D., Daroussin, J., & Tavernier, R. (1994). Development of a soil geographic database from the Soil Map of the European Communities. *CATENA*, *21*, 37–56. doi:10.1016/0341-8162(94)90030-2.
- Kinnell, P.I.A. (2010). Event soil loss, runoff and the Universal Soil Loss Equation family of models. A review. *Journal of Hydrology*, *385*, 384–397. doi:10.1016/j.jhydrol.2010.01.024.
- Klik, A., Haas, K., Dvorackova, A., & Fuller, I.C. (2015). Spatial and temporal distribution of rainfall erosivity in New Zealand. *Soil Research*, *53*, 815–825. doi:10.1071/SR14363.
- Konz, N., Baenninger, D., Konz, M., Nearing, M., & Alewell, C. (2010). Process identification of soil erosion in steep mountain regions. *Hydrology and Earth System Sciences*, *14*, 675–686. doi:10.5194/hess-14-675-2010.
- Konz, N., Prasuhn, V., & Alewell, C. (2012). On the measurement of alpine soil erosion. *CATENA*, *91*, 63–71. doi:10.1016/j.catena.2011.09.010.
- Konz Hohwieler, N. (2010). *Quantification of soil erosion in the Alps - Measurement and Modeling*. Basel.
- Köppen, W. (1936). *Das geographische System der Klimate*. Berlin.
- Kuhlman, T., Reinhard, S., & Gaaff, A. (2010). Estimating the costs and benefits of soil conservation in Europe. *Land Use Policy*, *27*, 22–32. doi:10.1016/j.landusepol.2008.08.002.
- Kuhn, M., & Johnson, K. (2013). *Applied Predictive Modeling*. New York, NY: Springer New York.
- Kulikov, M., Schickhoff, U., & Borchardt, P. (2016). Spatial and seasonal dynamics of soil loss ratio in mountain rangelands of south-western Kyrgyzstan. *Journal of Mountain Science*, *13*, 316–329. doi:10.1007/s11629-014-3393-6.
- Kulikov, M., Schickhoff, U., Gröngröft, A., & Borchardt, P. (2017). Modelling Soil Erodibility in Mountain Rangelands of South-Western Kyrgyzstan. *Pedosphere*. doi:10.1016/S1002-0160(17)60402-8.
- Kutner, M.H., Nachtsheim, C., Neter, J., & Li, W. (2005). *Applied linear statistical models*. (5th ed.). Boston.
- Lacey, J.P., Chartin, C., Evrard, O., Onda, Y., Garcia-Sanchez, L., & Cerdan, O. (2015). Rainfall erosivity in subtropical catchments and implications for erosion and particle-bound contaminant transfer. A case-study of the Fukushima region. *Hydrology and Earth System Sciences Discussions*, *12*, 7225–7266. doi:10.5194/hessd-12-7225-2015.
- Lai, C., Xiaohong, C., Zhaoli, W., Xushu, W., Shiwei, Z., Xiaoqing, W., & Wenkui, B. (2016). Spatio-temporal variation in rainfall erosivity during 1960–2012 in the Pearl River Basin, China. *CATENA*, *137*, 382–391. doi:10.1016/j.catena.2015.10.008.
- Lal, R. (2001). Soil degradation by erosion. *Land Degradation & Development*, *12*, 519–539. doi:10.1002/ldr.472.
- Ledermann, T. (2012). *Multiple Implications of Soil Erosion and Conservation on Arable Farm Land in the Swiss Midlands*. Bern.

- Ledermann, T., Herweg, K., Liniger, H.P., Schneider, F., Hurni, H., & Prasuhn, V. (2010). Applying erosion damage mapping to assess and quantify off-site effects of soil erosion in Switzerland. *Land Degradation & Development*, *21*, 353–366. doi:10.1002/ldr.1008.
- Lee, J.S., & Won, J.Y. (2012). Suggestion of Cover-Management Factor Equation for Mountain Area in RUSLE. *Journal of korean society of hazard mitigation*. 10.9798/KOSHAM.2012.12.2.079.
- Lee, J.S., & Won, J.Y. (2013). Analysis of the Characteristic of Monthly Rainfall Erosivity in Korea with Derivation of Rainfall Energy Equation (in korean). *Journal of korean society of hazard mitigation*, *13*, 177–184. doi:10.9798/KOSHAM.2013.13.3.177.
- Leek, R., & Olsen, P. (2000). Modelling climatic erosivity as a factor for soil erosion in Denmark. Changes and temporal trends. *Soil Use and Management*, *16*, 61–65. doi:10.1111/j.1475-2743.2000.tb00175.x.
- Leilei, L., Jianrong, F., & Yang, C. (2014). The relationship analysis of vegetation cover, rainfall and land surface temperature based on remote sensing in Tibet, China. *IOP Conference Series: Earth and Environmental Science*, *17*, 12034. doi:10.1088/1755-1315/17/1/012034.
- Leitinger, G., Tasser, E., Newesely, C., Obojes, N., & Tappeiner, U. (2010). Seasonal dynamics of surface runoff in mountain grassland ecosystems differing in land use. *Journal of Hydrology*, *385*, 95–104. doi:10.1016/j.jhydrol.2010.02.006.
- Liu, B.Y., Nearing, M.A., & Risse, L.M. (1994). Slope gradient effects on soil loss for steep slopes. *Transactions of the ASAE*, *37*, 1835–1840.
- Liu, B.Y., Nearing, M.A., Shi, P.J., & Jia, Z.W. (2000). Slope Length Effects on Soil Loss for Steep Slopes. *Soil Science Society of America Journal*, *64*, 1759. doi:10.2136/sssaj2000.6451759x.
- López-Vicente, M., Navas, A., & Machín, J. (2008). Identifying erosive periods by using RUSLE factors in mountain fields of the Central Spanish Pyrenees. *Hydrology and Earth System Sciences*, *12*, 523–535. doi:10.5194/hess-12-523-2008.
- Lu, D., Li, G., Valladares, G.S., & Batistella, M. (2004). Mapping soil erosion risk in Rondônia, Brazilian Amazonia. Using RUSLE, remote sensing and GIS. *Land Degradation & Development*, *15*, 499–512. doi:10.1002/ldr.634.
- Lugato, E., Panagos, P., Bampa, F., Jones, A., & Montanarella, L. (2014). A new baseline of organic carbon stock in European agricultural soils using a modelling approach. *Global change biology*, *20*, 313–326. doi:10.1111/gcb.12292.
- Ma, J.W., Xue, Y., Ma, C.F., & Wang, Z.G. (2003). A data fusion approach for soil erosion monitoring in the Upper Yangtze River Basin of China based on Universal Soil Loss Equation (USLE) model. *International Journal of Remote Sensing*, *24*, 4777–4789. doi:10.1080/0143116021000056028.
- Ma, X., He, Y., Xu, J., van Noordwijk, M., & Lu, X. (2014). Spatial and temporal variation in rainfall erosivity in a Himalayan watershed. *CATENA*, *121*, 248–259. doi:10.1016/j.catena.2014.05.017.
- Maetens, W., Vanmaercke, M., Poesen, J., Jankauskas, B., Jankauskiene, G., & Ionita, I. (2012). Effects of land use on annual runoff and soil loss in Europe and the Mediterranean. *Progress in Physical Geography*, *36*, 599–653. doi:10.1177/0309133312451303.
- Malone, B.P., Minasny, B., & McBratney, A.B. (2017). *Using R for digital soil mapping*. Cham: Springer.

- Mancino, G., Nolè, A., Salvati, L., & Ferrara, A. (2016). In-between forest expansion and cropland decline. A revised USLE model for soil erosion risk under land-use change in a Mediterranean region. *Ecological Indicators*, *71*, 544–550. doi:10.1016/j.ecolind.2016.07.040.
- Mannaerts, C.M., & Gabriels, D. (2000). Rainfall erosivity in Cape Verde. *Soil and Tillage Research*, *55*, 207–212. doi:10.1016/S0167-1987(00)00104-5.
- Martin, C., Pohl, M., Alewell, C., Körner, C., & Rixen, C. (2010). Interrill erosion at disturbed alpine sites. Effects of plant functional diversity and vegetation cover. *Basic and Applied Ecology*, *11*, 619–626. doi:10.1016/j.baae.2010.04.006.
- Marxer, P. (2003). *Oberflächenabfluß und Bodenerosion auf Brandflächen des Kastanienwaldgürtels der Südschweiz mit einer Anleitung zur Bewertung der post-fire Erosionsanfälligkeit (BA EroKaBr)*. Basel: Wepf in Komm.
- Mather, P.M., & Koch, M. (2011). *Computer processing of remotely-sensed images. An introduction*. (4th ed.). Hoboken, N.J., Chichester.
- Mayer, R., Kaufmann, R., Vorhauser, K., & Erschbamer, B. (2009). Effects of grazing exclusion on species composition in high-altitude grasslands of the Central Alps. *Basic and Applied Ecology*, *10*, 447–455. doi:10.1016/j.baae.2008.10.004.
- McBratney, A.B., Mendonça Santos, M.L., & Minasny, B. (2003). On digital soil mapping. *Geoderma*, *117*, 3–52. doi:10.1016/S0016-7061(03)00223-4.
- McBratney, A.B., Odeh, I.O.A., Bishop, T.F.A., Dunbar, M.S., & Shatar, T.M. (2000). An overview of pedometric techniques for use in soil survey. *Geoderma*, *97*, 293–327. doi:10.1016/S0016-7061(00)00043-4.
- McCool, D.K., Brown, L.C., Foster, G.R., Mutchler, C.K., & Meyer, L.D. (1987). Revised Slope Steepness Factor for the Universal Soil Loss Equation. *Transactions of the ASAE*, *30*, 1387–1396. doi:10.13031/2013.30576.
- McCool, D.K., Foster, G., & Weesies, G. (1997). Slope Length and Steepness Factor (LS). Chapter 4. In K.G. Renard, G.R. Foster, G.A. Weesies, D.K. McCool, & D.C. Yoder (Eds.), *Predicting soil erosion by water: a guide to conservation planning with the Revised Universal Soil Loss Equation (RUSLE)* (pp. 101–142). Washington D.C.: USDA.
- McCool, D.K., Foster, G.R., Renard, K.G., Yoder, D.C., & Weesies, G.A. (1995). The revised universal soil loss equation. *Interagency Workshop on Technologies to Address Soil Erosion on Department of Defense Lands, San Antonio, TX*.
- Merz, A., Alewell, C., Hiltbrunner, E., & Bärnninger, D. (2009). Plant-compositional effects on surface runoff and sediment yield in subalpine grassland. *Journal of Plant Nutrition and Soil Science*, *172*, 777–788. doi:10.1002/jpln.200800231.
- Meshesha, D., Tsunekawa, A., Tsubo, M., Haregeweyn, N., & Adgo, E. (2015). Evaluating spatial and temporal variations of rainfall erosivity, case of Central Rift Valley of Ethiopia. *Theoretical and Applied Climatology*, *119*, 515–522. doi:10.1007/s00704-014-1130-2.
- MeteoSwiss (2013). Documentation of MeteoSwiss Grid-Data Products. Monthly and Yearly Precipitation: RhiresM and RhiresY. Zürich.
- MeteoSwiss (2018a). Automatic monitoring network. <https://www.meteoswiss.admin.ch/home/measurement-and-forecasting-systems/land-based-stations/automatisches-messnetz.html>.
- MeteoSwiss (2018b). Bodenstationsdaten. <http://www.meteoschweiz.admin.ch/home/service-und-publikationen/produkte.subpage.html/de/data/products/2014/bodenstationsdaten.html>.

- MeteoSwiss (2018c). Normals 1981-2010: Precipitation total.
http://www.meteoswiss.admin.ch/product/input/climate-data/normwerte-pro-messgroesse/np8110/nvrep_np8110_rre150m0_e.pdf.
- Meuli, R.G., Wächter, D., Schwab, P., & Zimmermann, R. (2017). Connecting biodiversity monitoring and soil inventory - A Swiss case study. *Tagungsband BGS Jahrestagung Bern*, 20.
- Meusburger, K. (2010). *Soil Erosion in the Alps - Causes and Risk Assessment*. Basel.
- Meusburger, K., & Alewell, C. (2008). Impacts of anthropogenic and environmental factors on the occurrence of shallow landslides in an alpine catchment (Urseren Valley, Switzerland). *Natural Hazards and Earth System Science*, 8, 509–520. doi:10.5194/nhess-8-509-2008.
- Meusburger, K., & Alewell, C. (Eds.) (2014). *Soil Erosion in the Alps. Experience gained from case studies (2006–2013)*. Bern.
- Meusburger, K., Bänninger, D., & Alewell, C. (2010a). Estimating vegetation parameter for soil erosion assessment in an alpine catchment by means of QuickBird imagery. *International Journal of Applied Earth Observation and Geoinformation*, 12, 201–207. doi:10.1016/j.jag.2010.02.009.
- Meusburger, K., Konz, N., Schaub, M., & Alewell, C. (2010b). Soil erosion modelled with USLE and PESERA using QuickBird derived vegetation parameters in an alpine catchment. *International Journal of Applied Earth Observation and Geoinformation*, 12, 208–215. doi:10.1016/j.jag.2010.02.004.
- Meusburger, K., Leitinger, G., Mabit, L., Mueller, M.H., Walter, A., & Alewell, C. (2014). Soil erosion by snow gliding – a first quantification attempt in a subalpine area in Switzerland. *Hydrology and Earth System Sciences*, 18, 3763–3775. doi:10.5194/hess-18-3763-2014.
- Meusburger, K., Steel, A., Panagos, P., Montanarella, L., & Alewell, C. (2012). Spatial and temporal variability of rainfall erosivity factor for Switzerland. *Hydrology and Earth System Sciences*, 16, 167–177. doi:10.5194/hess-16-167-2012.
- Mikoš, M., Jošt, D., & Petkovšek, G. (2006). Rainfall and runoff erosivity in the alpine climate of north Slovenia. A comparison of different estimation methods. *Hydrological Sciences Journal*, 51, 115–126. doi:10.1623/hysj.51.1.115.
- Möller, M., Gerstmann, H., Gao, F., Dahms, T.C., & Förster, M. (2017). Coupling of phenological information and simulated vegetation index time series. Limitations and potentials for the assessment and monitoring of soil erosion risk. *CATENA*, 150, 192–205. doi:10.1016/j.catena.2016.11.016.
- Montandon, L.M., & Small, E.E. (2008). The impact of soil reflectance on the quantification of the green vegetation fraction from NDVI. *Remote Sensing of Environment*, 112, 1835–1845. doi:10.1016/j.rse.2007.09.007.
- Morgan, R.P.C. (2006). *Soil erosion and conservation*. (3rd ed.). Malden, Mass.: Blackwell.
- Mosimann, T., Crole-Rees, A., Maillard, A., Neyroud, J.-A., Thöni, M., Musy, A., & Rohr, W. (1990). *Bodenerosion im Schweizerischen Mittelland. Ausmass und Gegenmassnahmen*. Liebfeld-Bern.
- Mosimann, T., Maillard, A., Musy, A., Neyroud, J.-A., Rüttimann, M., & Weisskopf, P. (1991). *Erosionsbekämpfung in Ackerbaugebieten. Ein Leitfaden für die Bodenerhaltung*.
- Mosimann, T., & Rüttimann, M. (2000). *Bodenerosion selber abschätzen. Ein Schlüssel für Betriebsleiter und Berater*.
https://www.umwelt.sg.ch/home/Themen/Boden/Publikationen_und_weitere_Informationen

- /_jcr_content/Par/downloadlist_2/DownloadListPar/download_1.ocFile/Bodenerosion%20selber%20absch%C3%A4tzen.pdf.
- Musgrave, G.W. (1947). The quantitative evaluation of factors in water erosion - a first approximation. *Journal of Soil and Water Conservation*, 133–138.
- Nascimento, J.M.P., & Dias, J.M.B. (2005). Vertex component analysis. A fast algorithm to unmix hyperspectral data. *IEEE Transactions on Geoscience and Remote Sensing*, 43, 898–910. doi:10.1109/TGRS.2005.844293.
- Nearing, M.A. (1997). A Single, Continuous Function for Slope Steepness Influence on Soil Loss. *Soil Science Society of America Journal*, 61, 917. doi:10.2136/sssaj1997.03615995006100030029x.
- Nearing, M.A., Jetten, V., Baffaut, C., Cerdan, O., Couturier, A., Hernandez, M., Le Bissonnais, Y., Nichols, M.H., Nunes, J.P., Renschler, C.S., Souchère, V., & van Oost, K. (2005). Modeling response of soil erosion and runoff to changes in precipitation and cover. *CATENA*, 61, 131–154. doi:10.1016/j.catena.2005.03.007.
- Nigel, R., & Rughooputh, S. (2010). Mapping of monthly soil erosion risk of mainland Mauritius and its aggregation with delineated basins. *Geomorphology*, 114, 101–114. doi:10.1016/j.geomorph.2009.06.013.
- Nisi, L., Martius, O., Hering, A., Kunz, M., & Germann, U. (2016). Spatial and temporal distribution of hailstorms in the Alpine region. A long-term, high resolution, radar-based analysis. *Quarterly Journal of the Royal Meteorological Society*. doi:10.1002/qj.2771.
- Nogler, S. (2012). *Erosivität der Niederschläge im schweizerischen Mittelland*. Bern.
- Noll, D. (2017). *Projet Air-rosion. Projet pilote visant à observer l'érosion dans les grandes cultures à l'aide d'images aériennes à haute résolution prises par drone afin de prendre des mesures de prévention*.
- Nunes, A.N., Lourenço, L., Vieira, A., & Bento-Gonçalves, A. (2016). Precipitation and Erosivity in Southern Portugal. Seasonal Variability and Trends (1950-2008). *Land Degradation & Development*, 27, 211–222. doi:10.1002/ldr.2265.
- Nussbaum, M., Papritz, A., Baltensweiler, A., & Walthert, L. (2014). Estimating soil organic carbon stocks of Swiss forest soils by robust external-drift kriging. *Geoscientific Model Development*, 7, 1197–1210. doi:10.5194/gmd-7-1197-2014.
- Nussbaum, M., Spiess, K., Baltensweiler, A., Grob, U., Keller, A., Greiner, L., Schaepman, M.E., & Papritz, A. (2018). Evaluation of digital soil mapping approaches with large sets of environmental covariates. *SOIL*, 4, 1–22. doi:10.5194/soil-4-1-2018.
- Nussbaum, M., Walthert, L., Fraefel, M., Greiner, L., & Papritz, A. (2017). Mapping of soil properties at high resolution in Switzerland using boosted geosadditive models. *SOIL*, 3, 191–210. doi:10.5194/soil-3-191-2017.
- Odeh, I.O.A., McBratney, A.B., & Chittleborough, D.J. (1995). Further results on prediction of soil properties from terrain attributes. Heterotopic cokriging and regression-kriging. *Geoderma*, 67, 215–226. doi:10.1016/0016-7061(95)00007-B.
- Orgiazzi, A., Ballabio, C., Panagos, P., Jones, A., & Fernández-Ugalde, O. (2018). LUCAS Soil, the largest expandable soil dataset for Europe. A review. *European Journal of Soil Science*, 69, 140–153. doi:10.1111/ejss.12499.
- Orlandini, S., Moretti, G., Corticelli, M.A., Santangelo, P.E., Capra, A., Rivola, R., & Albertson, J.D. (2012). Evaluation of flow direction methods against field observations of overland flow dispersion. *Water Resources Research*, 48, 412. doi:10.1029/2012WR012067.

- Ostovari, Y., Ghorbani-Dashtaki, S., Bahrami, H.-A., Naderi, M., & Dematte, J.A.M. (2017). Soil loss estimation using RUSLE model, GIS and remote sensing techniques. A case study from the Dembecha Watershed, Northwestern Ethiopia. *Geoderma Reg.*, *11*, 28–36. doi:10.1016/j.geodrs.2017.06.003.
- Ozcan, A.U., Erpul, G., Basaran, M., & Erdogan, H.E. (2008). Use of USLE/GIS technology integrated with geostatistics to assess soil erosion risk in different land uses of Indagi Mountain Pass—Çankırı, Turkey. *Environmental Geology*, *53*, 1731–1741. doi:10.1007/s00254-007-0779-6.
- Özşahin, E. (2014). An assessment of monthly rainfall erosivity model for Amik Plain (Hatay, S TURKEY). *Photon*, 177–193.
- Pal, S.K., Majumdar, T.J., Bhattacharya, A.K., & Bhattacharyya, R. (2011). Utilization of Landsat ETM+ data for mineral-occurrences mapping over Dalma and Dhanjori, Jharkhand, India. An Advanced Spectral Analysis approach. *International Journal of Remote Sensing*, *32*, 4023–4040. doi:10.1080/01431161.2010.484430.
- Panagos, P., Ballabio, C., Borrelli, P., & Meusburger, K. (2016b). Spatio-temporal analysis of rainfall erosivity and erosivity density in Greece. *CATENA*, *137*, 161–172. doi:10.1016/j.catena.2015.09.015.
- Panagos, P., Ballabio, C., Borrelli, P., Meusburger, K., Klik, A., Rousseva, S., Tadić, M., Michaelides, S., Hrabalíková, M., Olsen, P., Aalto, J., Lakatos, M., Rymaszewicz, A., Dumitrescu, A., Beguería, S., & Alewell, C. (2015a). Rainfall erosivity in Europe. *The Science of the total environment*, *511*, 801–814. doi:10.1016/j.scitotenv.2015.01.008.
- Panagos, P., Ballabio, C., Yigini, Y., & Dunbar, M.B. (2013). Estimating the soil organic carbon content for European NUTS2 regions based on LUCAS data collection. *The Science of the total environment*, *442*, 235–246. doi:10.1016/j.scitotenv.2012.10.017.
- Panagos, P., Borrelli, P., & Meusburger, K. (2015b). A New European Slope Length and Steepness Factor (LS-Factor) for Modeling Soil Erosion by Water. *Geosciences*, *5*, 117–126. doi:10.3390/geosciences5020117.
- Panagos, P., Borrelli, P., Meusburger, K., Alewell, C., Lugato, E., & Montanarella, L. (2015c). Estimating the soil erosion cover-management factor at the European scale. *Land Use Policy*, *48*, 38–50. doi:10.1016/j.landusepol.2015.05.021.
- Panagos, P., Borrelli, P., Meusburger, K., van der Zanden, E.H., Poesen, J., & Alewell, C. (2015d). Modelling the effect of support practices (P-factor) on the reduction of soil erosion by water at European scale. *Environmental Science & Policy*, *51*, 23–34. doi:10.1016/j.envsci.2015.03.012.
- Panagos, P., Borrelli, P., Poesen, J., Ballabio, C., Lugato, E., Meusburger, K., Montanarella, L., & Alewell, C. (2015e). The new assessment of soil loss by water erosion in Europe. *Environmental Science & Policy*, *54*, 438–447. doi:10.1016/j.envsci.2015.08.012.
- Panagos, P., Borrelli, P., Spinoni, J., Ballabio, C., Meusburger, K., Beguería, S., Klik, A., Michaelides, S., Petan, S., Hrabalíková, M., Olsen, P., Aalto, J., Lakatos, M., Rymaszewicz, A., Dumitrescu, A., Perčec Tadić, M., Diodato, N., Kostalova, J., Rousseva, S., Banasik, K., & Alewell, C. (2016a). Monthly Rainfall Erosivity. Conversion Factors for Different Time Resolutions and Regional Assessments. *Water*, *8*, 119. doi:10.3390/w8040119.
- Panagos, P., Christos, K., Cristiano, B., & Ioannis, G. (2014a). Seasonal monitoring of soil erosion at regional scale. An application of the G2 model in Crete focusing on agricultural land uses. *International Journal of Applied Earth Observation and Geoinformation*, *27*, 147–155. doi:10.1016/j.jag.2013.09.012.

- Panagos, P., Imeson, A., Meusburger, K., Borrelli, P., Poesen, J., & Alewell, C. (2016c). Soil Conservation in Europe. Wish or Reality? *Land Degradation & Development*, 27, 1547–1551. doi:10.1002/ldr.2538.
- Panagos, P., Karydas, C., Borrelli, P., Ballabio, C., & Meusburger, K. (2014b). Advances in soil erosion modelling through remote sensing data availability at European scale. *Second International Conference on Remote Sensing and Geoinformation of the Environment 12th August 2014*, 92290I. doi:10.1117/12.2066383.
- Panagos, P., Karydas, C.G., Gitas, I.Z., & Montanarella, L. (2012a). Monthly soil erosion monitoring based on remotely sensed biophysical parameters. A case study in Strymonas river basin towards a functional pan-European service. *International Journal of Digital Earth*, 5, 461–487. doi:10.1080/17538947.2011.587897.
- Panagos, P., Meusburger, K., Alewell, C., & Montanarella, L. (2012b). Soil erodibility estimation using LUCAS point survey data of Europe. *Environ. Modelling & Software*, 30, 143–145. doi:10.1016/j.envsoft.2011.11.002.
- Panagos, P., Meusburger, K., Ballabio, C., Borrelli, P., & Alewell, C. (2014c). Soil erodibility in Europe: a high-resolution dataset based on LUCAS. *The Science of the total environment*, 479-480, 189–200. doi:10.1016/j.scitotenv.2014.02.010.
- Panagos, P., Standardi, G., Borrelli, P., Lugato, E., Montanarella, L., & Bosello, F. (2018). Cost of agricultural productivity loss due to soil erosion in the European Union. From direct cost evaluation approaches to the use of macroeconomic models. *Land Degradation & Development*, 1219, 134. doi:10.1002/ldr.2879.
- Panagos, P., van Liedekerke, M., Jones, A., & Montanarella, L. (2012c). European Soil Data Centre. Response to European policy support and public data requirements. *Land Use Policy*, 29, 329–338. doi:10.1016/j.landusepol.2011.07.003.
- Paringit, E.C., & Nadaoka, K. (2003). Sediment yield modelling for small agricultural catchments. Land-cover parameterization based on remote sensing data analysis. *Hydrological Processes*, 17, 1845–1866. doi:10.1002/hyp.1222.
- Perroud, M., & Bader, S. (2013). Klimaänderung in der Schweiz. Indikatoren zu Ursachen, Auswirkungen, Massnahmen. *Umwelt-Zustand*.
- Petkovšek, G., & Mikoš, M. (2004). Estimating the R factor from daily rainfall data in the sub-Mediterranean climate of southwest Slovenia / Estimation du facteur R à partir de données journalières de pluie dans le climat sub-méditerranéen du Sud-Ouest de la Slovénie. *Hydrological Sciences Journal*, 49. doi:10.1623/hysj.49.5.869.55134.
- Phillips, D.L., Newsome, S.D., & Gregg, J.W. (2005). Combining sources in stable isotope mixing models. Alternative methods. *Oecologia*, 144, 520–527. doi:10.1007/s00442-004-1816-8.
- Pimentel, D. (2000). Soil Erosion and the Threat to Food Security and the Environment. *Ecosystem Health*, 6, 221–226. doi:10.1046/j.1526-0992.2000.006004221.x.
- Pimentel, D., Harvey, C., Resosudarmo, P., Sinclair, K., Kurz, D., McNair, M., Crist, S., Shpritz, L., Fitton, L., Saffouri, R., & Blair, R. (1995). Environmental and economic costs of soil erosion and conservation benefits. *Science*, 267, 1117–1123. doi:10.1126/science.267.5201.1117.
- Piñeiro, G., Paruelo, J.M., Oesterheld, M., & Jobbágy, E.G. (2010). Pathways of Grazing Effects on Soil Organic Carbon and Nitrogen. *Rangeland Ecology & Management*, 63, 109–119. doi:10.2111/08-255.1.

- Poesen, J.W., Torri, D., & Bunte, K. (1994). Effects of rock fragments on soil erosion by water at different spatial scales. A review. *CATENA*, 23, 141–166. doi:10.1016/0341-8162(94)90058-2.
- Pohl, M., Alig, D., Körner, C., & Rixen, C. (2009). Higher plant diversity enhances soil stability in disturbed alpine ecosystems. *Plant and Soil*, 324, 91–102. doi:10.1007/s11104-009-9906-3.
- Porto, P. (2016). Exploring the effect of different time resolutions to calculate the rainfall erosivity factor R in Calabria, southern Italy. *Hydrological Processes*, 30, 1551–1562. doi:10.1002/hyp.10737.
- Prasuhn, V. (2010). Bodenerosion - ein vielseitiges Forschungsfeld. *Geosciences Actuel*, 25–29.
- Prasuhn, V. (2011). Soil erosion in the Swiss midlands. Results of a 10-year field survey. *Geomorphology*, 126, 32–41. doi:10.1016/j.geomorph.2010.10.023.
- Prasuhn, V. (2012). On-farm effects of tillage and crops on soil erosion measured over 10 years in Switzerland. *Soil and Tillage Research*, 120, 137–146. doi:10.1016/j.still.2012.01.002.
- Prasuhn, V. (2017). Langzeitmonitoring von Bodenerosion in der Schweiz – Ergebnisse von 20 Jahren Erosionsschadenkartierungen. *Jahrestagung der DBG "Horizonte des Bodens" 2.-7. September*.
- Prasuhn, V., Liniger, H., Gisler, S., Herweg, K., Candinas, A., & Clément, J.-P. (2013). A high-resolution soil erosion risk map of Switzerland as strategic policy support system. *Land Use Policy*, 32, 281–291. doi:10.1016/j.landusepol.2012.11.006.
- Prasuhn, V., Liniger, H.P., Hurni, H., & Friedli, S. (2010). Abschätzung des Bodenfaktors für die Übersichtskarte der Bodenerosionsgefährdung der Schweiz. *BGS Bulletin*, 30, 31–36.
- Prus, T., Kralj, T., Vrščaj, B., Ruprecht, J., Šporar, M., Suhadolc, M., Mihelič, R., & Stepančič, D. (2015). *Tla Slovenije s pedološko karto v merilu 1:250000. Soils of Slovenia with soil map 1:250000*. Luxembourg: Evropska komisija, Skupni raziskovalni center (JRC); = European Commission Joint Research Centre (JRC); Publications Office of the European Union.
- Puigdefábregas, J. (2005). The role of vegetation patterns in structuring runoff and sediment fluxes in drylands. *Earth Surface Processes and Landforms*, 30, 133–147. doi:10.1002/esp.1181.
- Punge, H.J., & Kunz, M. (2016). Hail observations and hailstorm characteristics in Europe. A review. *Atmospheric Research*, 176-177, 159–184. doi:10.1016/j.atmosres.2016.02.012.
- Quinlan, J.R. (1992). Learning with continuous classes. *Proceedings of the 5th Australian Joint Conference on Artificial Intelligence (AI '92), Hobart 16-18 November 1992*, 343–348.
- Quinlan, J.R. (1993). Combining instance-based and model-based learning. *Proceedings of the Tenth International Conference on International Conference on Machine Learning (ICML '93), Amherst 27-29 July 1993*, 236–243.
- Rajczak, J., Pall, P., & Schär, C. (2013). Projections of extreme precipitation events in regional climate simulations for Europe and the Alpine Region. *Journal of Geophysical Research: Atmospheres*, 118, 3610–3626. doi:10.1002/jgrd.50297.
- Rajczak, J., & Schär, C. (2017). Projections of Future Precipitation Extremes Over Europe. A Multimodel Assessment of Climate Simulations. *Journal of Geophysical Research: Atmospheres*, 122, 10773–10800. doi:10.1002/2017JD027176.
- Ramli, M.F., Yusoff, M.K., Mustapha, S., & Hiang, T.S. (2006). The effect of digital elevation model scale factor on soil erosion studies. Case study in Cameron Highlands, Malaysia. *Journal of Environmental Hydrology*, 14, 1–9.

- Rammig, A., Jonas, T., Zimmermann, N.E., & Rixen, C. (2010). Changes in alpine plant growth under future climate conditions. *Biogeosciences*, 7, 2013–2024. doi:10.5194/bg-7-2013-2010.
- Rehbein, K., Grob, U., Klausner, L., Franzen, J., & Keller, A. (2017). *Bodendatensatz Schweiz. Dokumentation Version 2 (Mai 2017)*. Zürich.
- Renard, K., Foster, G., Weesies, G., & Porter, J. (1991). RUSLE. Revised universal soil loss equation. *Journal of Soil and Water Conservation*, 46.
- Renard, K.G., & Ferreira, V.A. (1993). RUSLE Model Description and Database Sensitivity. *Journal of Environmental Quality*, 22, 458. doi:10.2134/jeq1993.00472425002200030009x.
- Renard, K.G., Foster, G., Weesies, G., McCool, D.K., & Yoder, D.C. (1997). *Prediction Soil Erosion by Water: A Guide to Conservation Planning with the Revised Universal Soil Loss Equation (RUSLE)*.
- Renard, K.G., & Freimund, J.R. (1994). Using monthly precipitation data to estimate the R-factor in the revised USLE. *Journal of Hydrology*, 157, 287–306. doi:10.1016/0022-1694(94)90110-4.
- Renard, K.G., Yoder, D.C., Lightle, D.T., & Dabney, S.M. (2010). Universal Soil Loss Equation and Revised Universal Soil Loss Equation. In R.P.C. Morgan, & M.A. Nearing (Eds.), *Handbook of Erosion Modelling* (pp. 136–167). Chichester, UK: John Wiley & Sons, Ltd.
- Renschler, C.S., Mannaerts, C., & Dieckrüger, B. (1999). Evaluating spatial and temporal variability in soil erosion risk—rainfall erosivity and soil loss ratios in Andalusia, Spain. *CATENA*, 34, 209–225. doi:10.1016/S0341-8162(98)00117-9.
- Risse, L.M., Nearing, M.A., Laflen, J.M., & Nicks, A.D. (1993). Error Assessment in the Universal Soil Loss Equation. *Soil Science Society of America Journal*, 57, 825. doi:10.2136/sssaj1993.03615995005700030032x.
- Roberts, D.A., Batista, G.T., Pereira, J., Waller, E.K., & Nelson, B.W. (1999). Change Identification Using Multitemporal Spectral Mixture Analysis: Applications in Eastern Amazonia. In C.D. Elvidge, & R.S. Lunetta (Eds.), *Remote sensing change detection. Environmental monitoring methods and applications* (pp. 137–161). Chelsea, Mich.
- Roberts, D.A., Smith, M.O., & Adams, J.B. (1993). Green vegetation, nonphotosynthetic vegetation, and soils in AVIRIS data. *Remote Sensing of Environment*, 44, 255–269. doi:10.1016/0034-4257(93)90020-X.
- Rogge, D.M., Rivard, B., Zhang, J., Sanchez, A., Harris, J., & Feng, J. (2007). Integration of spatial–spectral information for the improved extraction of endmembers. *Remote Sensing of Environment*, 110, 287–303. doi:10.1016/j.rse.2007.02.019.
- Römkens, M.J.M., Young, R.A., Poesen, J.W.A., McCool, D.K., El-Swaify, S.A., & Bradford, J.M. (1997). Soil erodibility factor (K). In K.G. Renard, G.R. Foster, G.A. Weesies, D.K. McCool, & D.C. Yoder (Eds.), *Predicting soil erosion by water: a guide to conservation planning with the Revised Universal Soil Loss Equation (RUSLE)* (pp. 65–99). Washington D.C.: USDA.
- RSI Research Systems, I. (2004). *ENVI User's Guide*.
- Sadeghi, S.H., & Tavangar, S. (2015). Development of stationnal models for estimation of rainfall erosivity factor in different timescales. *Natural Hazards*, 77, 429–443. doi:10.1007/s11069-015-1608-y.
- Sadeghi, S.H.R., & Hazbavi, Z. (2015). Trend analysis of the rainfall erosivity index at different time scales in Iran. *Natural Hazards*, 77, 383–404. doi:10.1007/s11069-015-1607-z.

- Sadeghi, S.H.R., Moatamednia, M., & Behzadfar, M. (2011). Spatial and Temporal Variations in the Rainfall Erosivity Factor in Iran. *Journal of Agricultural Science and Technology*, 451–464.
- Sanchez-Moreno, J.F., Mannaerts, C.M., & Jetten, V. (2014). Rainfall erosivity mapping for Santiago Island, Cape Verde. *Geoderma*, 217-218, 74–82.
doi:10.1016/j.geoderma.2013.10.026.
- Schaub, D., & Prasuhn, V. (1998). A map on soil erosion on arable land as a planning tool for sustainable land use in Switzerland. In H.-P. Blume (Ed.), *Towards sustainable land use. Furthering cooperation between people and institutions* (pp. 161–168). Reiskirchen: Catena Verl.
- Schäuble, H. (1999). *Erosionsprognosen mit GIS und EDV - Ein Vergleich verschiedener Bewertungskonzepte am Beispiel einer Gäulandschaft* -. Tübingen.
- Schauer, T. (2000). Der Einfluß der Schafbeweidung auf das Abfluß- und Abtragsgeschehen. *Interpraevent*, 65–74.
- Schindler Wildhaber, Y., Bänninger, D., Burri, K., & Alewell, C. (2012). Evaluation and application of a portable rainfall simulator on subalpine grassland. *CATENA*, 91, 56–62.
doi:10.1016/j.catena.2011.03.004.
- Schmidli, J., & Frei, C. (2005). Trends of heavy precipitation and wet and dry spells in Switzerland during the 20th century. *International Journal of Climatology*, 25, 753–771.
doi:10.1002/joc.1179.
- Schmidli, J., Schmutz, C., Frei, C., Wanner, H., & Schär, C. (2002). Mesoscale precipitation variability in the region of the European Alps during the 20th century. *International Journal of Climatology*, 22, 1049–1074. doi:10.1002/joc.769.
- Schmidt, S., Alewell, C., & Meusburger, K. (2018a). Change of permanent grasslands extent (1996-2015) and national grassland dataset of Switzerland. *Data in Brief*, 1992–1998.
doi:10.1016/j.dib.2018.09.039.
- Schmidt, S., Alewell, C., & Meusburger, K. (2018b). Mapping spatio-temporal dynamics of the cover and management factor (C-factor) for grasslands in Switzerland. *Remote Sensing of Environment*, 211, 89–104. doi:10.1016/j.rse.2018.04.008.
- Schmidt, S., Alewell, C., Panagos, P., & Meusburger, K. (2016). Regionalization of monthly rainfall erosivity patterns in Switzerland. *Hydrology and Earth System Sciences*, 20, 4359–4373. doi:10.5194/hess-20-4359-2016.
- Schmidt, S., Ballabio, C., Alewell, C., Panagos, P., & Meusburger, K. (2018c). Filling the European blank spot-Swiss soil erodibility assessment with topsoil samples. *Journal of Plant Nutrition and Soil Science*, 66, 3351. doi:10.1002/jpln.201800128.
- Schmidt, S., Tresch, S., & Meusburger, K. (2019). Modification of the RUSLE slope length and steepness factor (LS-factor) based on rainfall experiments at steep alpine grasslands. *MethodsX*, 6, 219–229. doi:10.1016/j.mex.2019.01.004.
- Schwarb, M., Daly, C., Frei, C., & Schär, C. (2001). Mean Seasonal Precipitation throughout the European Alps 1971-1990. In R. Wingartner (Ed.), *Hydrological Atlas of Switzerland*. Bern.
- Schwertmann, U., Vogl, W., & Kainz, M. (1987). *Bodenerosion durch Wasser. Vorhersage des Abtrags und Bewertung von Gegenmaßnahmen*. Stuttgart.
- Scott, J.T., & Robertson, D.A. (2009). Environmental effects of sheep farming. In R.W. McDowell (Ed.), *Environmental impacts of pasture-based farming* (pp. 144–186). Cambridge, MA: CABI.

- Shamshad, A., Azhari, M.N., Isa, M.H., Hussin, W.M.A.W., & Parida, B.P. (2008). Development of an appropriate procedure for estimation of RUSLE EI30 index and preparation of erosivity maps for Pulau Penang in Peninsular Malaysia. *CATENA*, 72, 423–432. doi:10.1016/j.catena.2007.08.002.
- Shirazi, M.A., & Boersma, L. (1984). A Unifying Quantitative Analysis of Soil Texture I. *Soil Science Society of America Journal*, 48, 142. doi:10.2136/sssaj1984.03615995004800010026x.
- Sideris, I., Gabella, M., & Germann, U. (2014). The CombiPrecip experience: development and operation of a real-time radar-rain gauge combination scheme in Switzerland. In 2014 International Weather Radar and Hydrology Symposium (Ed.).
- Smets, B., Jacobs, T., & Verger, A. (2017). Product User Manual. Leaf Area Index (LAI), Fraction of Photosynthetically Active Radiation (FAPAR), Fraction of Vegetation Cover (FCover), Collection 300m, Version 1. VITO.
- Smit, H.J., Metzger, M.J., & Ewert, F. (2008). Spatial distribution of grassland productivity and land use in Europe. *Agricultural Systems*, 98, 208–219. doi:10.1016/j.agry.2008.07.004.
- Smith, D.D. (1958). Factors affecting rainfall erosion and their evaluation. *International Association of Scientific Hydrology Publication*, 43, 97–107.
- Smith, D.D., & Whitt, D. (1948). Estimating soil losses from field areas. *Agricultural Engineering*, 29, 394–396.
- Smith, M.O., Johnson, P.E., & Adams, J.B. (1985). Quantitative determination of mineral types and abundances from reflectance spectra using principal components analysis. *Journal of Geophysical Research*, 90, C797. doi:10.1029/JB090iS02p0C797.
- Smith, M.O., Ustin, S.L., Adams, J.B., & Gillespie, A.R. (1990). Vegetation in deserts. I. A regional measure of abundance from multispectral images. *Remote Sensing of Environment*, 31, 1–26. doi:10.1016/0034-4257(90)90074-V.
- Spreafico, M., & Weingartner, R. (2005). Hydrologie der Schweiz. Ausgewählte Aspekte und Resultate. *Berichte des BWG, Serie Wasser*.
- Stanchi, S., Freppaz, M., Ceaglio, E., Maggioni, M., Meusburger, K., Alewell, C., & Zanini, E. (2014). Soil erosion in an avalanche release site (Valle d'Aosta, Italy): towards a winter factor for RUSLE in the Alps. *Natural Hazards and Earth System Science*, 14, 1761–1771. doi:10.5194/nhess-14-1761-2014.
- Steyerberg, E. (2009). *Clinical Prediction Models. A Practical Approach to Development, Validation, and Updating*. New York, NY.
- Strunk, H. (2003). Soil degradation and overland flow as causes of gully erosion on mountain pastures and in forests. *CATENA*, 50, 185–198. doi:10.1016/S0341-8162(02)00140-6.
- Studer, S., Appenzeller, C., & Defila, C. (2005). Inter-Annual Variability and Decadal Trends in Alpine Spring Phenology. A Multivariate Analysis Approach. *Climatic Change*, 73, 395–414. doi:10.1007/s10584-005-6886-z.
- Sun, W., Shao, Q., & Liu, J. (2013). Soil erosion and its response to the changes of precipitation and vegetation cover on the Loess Plateau. *Journal of Geographical Sciences*, 23, 1091–1106. doi:10.1007/s11442-013-1065-z.
- Sutter, R. (2007). *Erosion im Alpgebiet. Schlussbericht*. Appenzell.
- Sutter, R., & Keller, L. (2009). *Bodenerosion im Sömmerungsgebiet. Erkennen - vermeiden - beheben*. Lindau.
- Suttie, J.M., & Reynolds, S.G. (Eds.) (2005). *Grasslands of the world*. Rome.
- Swiss Federal Council (1998c). *Gewässerschutzverordnung. GSchV*.

- Swiss Federal Council (1998b). Verordnung über die Direktzahlverpflichtungen an die Landwirtschaft. *DZV*.
- Swiss Federal Council (1998d). Verordnung über Sömmerungsbeiträge. *SöBV*.
- Swiss Federal Council (1998a). Verordnung über Belastungen des Bodens. *VBBö*.
- Swiss National Science Foundation (2017). weObserve: Integrating Citizen Observers and High Throughput Sensing Devices for Big Data Collection, Integration, and Analysis. <http://p3.snf.ch/Project-167333>.
- Swisstopo (2017b). Swisstopo RS. 21.12.2017. https://shop.swisstopo.admin.ch/de/products/images/ortho_images/SWISSIMAGE_RS.
- Swisstopo (2017a). swissTLM3D. Wabern. <https://shop.swisstopo.admin.ch/en/products/landscape/tlm3D>.
- Swisstopo (2007). Vector25. Das digitale Landschaftsmodell der Schweiz. Wabern.
- Swisstopo (2010). SWISSIMAGE. Das digitale Farbornthophotomosaik der Schweiz. Wabern.
- Swisstopo (2018a). swissAlti3D. Das hoch aufgelöste Terrainmodell der Schweiz. https://www.swisstopo.admin.ch/content/swisstopo-internet/de/home/products/height/alti3d/_jcr_content/contentPar/tabs/items/dokumente/tabPar/downloadlist/downloadItems/846_1464690554132.download/swissALTI3D_detaillierte%20Produktinfo_201802_DE.pdf.
- Swisstopo (2018b). *swissBOUNDARIES3D. Grenzen schweizweit in 3D*. Wabern.
- Terranova, O.G., & Gariano, S.L. (2015). Regional investigation on seasonality of erosivity in the Mediterranean environment. *Environmental Earth Sciences*, 73, 311–324. doi:10.1007/s12665-014-3426-z.
- Theseira, M.A., Thomas, G., Taylor, J.C., Gemell, F., & Varjo, J. (2003). Sensitivity of mixture modelling to end-member selection. *International Journal of Remote Sensing*, 24, 1559–1575. doi:10.1080/01431160210146631.
- Torriani, D.S., Calanca, P., Schmid, S., Beniston, M., & Fuhrer, J. (2007). Potential effects of changes in mean climate and climate variability on the yield of winter and spring crops in Switzerland. *Climate Research*, 34, 59–69. doi:10.3354/cr034059.
- Tóth, G., Jones, A., & Montanarella, L. (2013). The LUCAS topsoil database and derived information on the regional variability of cropland topsoil properties in the European Union. *Environmental Monitoring and Assessment*, 185, 7409–7425. doi:10.1007/s10661-013-3109-3.
- Tresch, S. (2014). Influence of the slope steepness on soil erosion modelling measured with rainfall simulations in the Urseren Valley. *Master thesis, Basel*. doi:10.13140/RG.2.2.15260.54409.
- Troxler, J. (2014). Mitigation of soil erosion by careful land-use management. In K. Meusburger, & C. Alewell (Eds.), *Soil Erosion in the Alps. Experience gained from case studies (2006–2013)* (85–91). Bern.
- Troxler, J., Chatelain, C., & Schwery, M. (2004). Technical and economical evaluation of grazing systems for high altitude sheep pastures in Switzerland. In A. Lüscher, B. Jeangros, W. Kessler, O. Huguenin, M. Lobsiger, M. Millar, & D. Suter (Eds.), *Land Use Systems in Grassland Dominated Regions* (pp. 590–592). Zürich.
- Troxler, J., Jans, F., Wettstein, J.-B., Monteleone, P., & Gmür, P. (1992). Mobile Melkanlagen auf der Weide: Praktische Aspekte. *Landwirtschaft Schweiz*, 5, 337–334.
- USDA (1951). *Soil Survey Manual*. Washington D.C.

- USDA (1983). National Soil Survey Handbook (NSSH).
https://www.nrcs.usda.gov/wps/portal/nrcs/detail/national/soils/?cid=nrcs142p2_054242.
- van Delden, A. (2001). The synoptic setting of thunderstorms in western Europe. *Atmospheric Research*, 56, 89–110. doi:10.1016/S0169-8095(00)00092-2.
- van der Knijff, J.M., Jones, R.J.A., & Montanarella, L. (2000). *Soil Erosion Risk Assessment in Italy*. Ispra.
- van der Meer, F.D. (2002). Image classification through spectral unmixing. In A. Stein, F.D. van der Meer, & B. Gorte (Eds.), *Spatial Statistics for Remote Sensing*. Dordrecht: Kluwer Academic Publishers.
- van der Meer, F.D., & de Jong, S.M. (2000). Improving the results of spectral unmixing of Landsat Thematic Mapper imagery by enhancing the orthogonality of end-members. *International Journal of Remote Sensing*, 21, 2781–2797. doi:10.1080/01431160050121249.
- van der Meer, F.D., & Jong, S.M. de (Eds.) (2010). *Imaging spectrometry. Basic principles and prospective applications*. Dordrecht.
- van Rast, E., Vanmechelen, L., Thomasson, A.-J., Daroussin, J., Hollis, J.M., Jones, R.J.A., Jagne, M., & King, D. (1995). Elaboration of an extended knowledge database to interpret the 1:1,000,000 EU Soil Map for environmental purposes. In King, D., Jones, R.J.A. Thomasson, A.J. (Ed.), *European land information systems for agro-environmental monitoring. EUR 16232 EN* (pp. 71–84). Luxembourg.
- Vannoppen, W., Vanmaercke, M., Baets, S. de, & Poesen, J. (2015). A review of the mechanical effects of plant roots on concentrated flow erosion rates. *Earth-Science Reviews*, 150, 666–678. doi:10.1016/j.earscirev.2015.08.011.
- Vatandaşlar, C., & Yavuz, M. (2017). Modeling cover management factor of RUSLE using very high-resolution satellite imagery in a semiarid watershed. *Environmental Earth Sciences*, 76, 267. doi:10.1007/s12665-017-6388-0.
- Verheijen, F.G.A., Jones, R.J.A., Rickson, R.J., & Smith, C.J. (2009). Tolerable versus actual soil erosion rates in Europe. *Earth-Science Reviews*, 94, 23–38. doi:10.1016/j.earscirev.2009.02.003.
- Vrieling, A. (2006). Satellite remote sensing for water erosion assessment. A review. *CATENA*, 65, 2–18. doi:10.1016/j.catena.2005.10.005.
- Vrieling, A., de Jong, S.M., Sterk, G., & Rodrigues, S.C. (2008). Timing of erosion and satellite data. A multi-resolution approach to soil erosion risk mapping. *International Journal of Applied Earth Observation and Geoinformation*, 10, 267–281. doi:10.1016/j.jag.2007.10.009.
- Vrieling, A., Hoedjes, J.C.B., & van der Velde, M. (2014). Towards large-scale monitoring of soil erosion in Africa. Accounting for the dynamics of rainfall erosivity. *Global and Planetary Change*, 115, 33–43. doi:10.1016/j.gloplacha.2014.01.009.
- Wall, G.J., Dickinson, W.T., Rudra, R.P., & Coote, D.R. (1988). Seasonal soil erodibility variation in southwestern Ontario. *Canadian Journal of Soil Science*, 68, 417–424. doi:10.4141/cjss88-038.
- Wang, B., Yang, Q., & Liu, Z. (2009). Effect of conversion of farmland to forest or grassland on soil erosion intensity changes in Yanhe River Basin, Loess Plateau of China. *Frontiers of Forestry in China*, 4, 68–74. doi:10.1007/s11461-009-0015-5.

- Wang, B., Zheng, F., & Guan, Y. (2016a). Improved USLE- K factor prediction. A case study on water erosion areas in China. *International Soil and Water Conservation Research*, 4, 168–176. doi:10.1016/j.iswcr.2016.08.003.
- Wang, B., Zheng, F., Römkens, M.J.M., & Darboux, F. (2013a). Soil erodibility for water erosion. A perspective and Chinese experiences. *Geomorphology*, 187, 1–10. doi:10.1016/j.geomorph.2013.01.018.
- Wang, G., Fang, Q., Teng, Y., & Yu, J. (2016b). Determination of the factors governing soil erodibility using hyperspectral visible and near-infrared reflectance spectroscopy. *International Journal of Applied Earth Observation*, 53, 48–63. doi:10.1016/j.jag.2016.08.006.
- Wang, G., Gertner, G., Liu, X., & Anderson, A. (2001). Uncertainty assessment of soil erodibility factor for revised universal soil loss equation. *CATENA*, 46, 1–14. doi:10.1016/S0341-8162(01)00158-8.
- Wang, G., Wentz, S., Gertner, G.Z., & Anderson, A. (2002). Improvement in mapping vegetation cover factor for the universal soil loss equation by geostatistical methods with Landsat Thematic Mapper images. *International Journal of Remote Sensing*, 23, 3649–3667. doi:10.1080/01431160110114538.
- Wang, L.L., Yang, E., Huang, J., & Jiao, P. (2013b). Spatial and Temporal Characteristics of Rainfall Erosivity of Shanghai in Recent Ten Years. *Applied Mechanics and Materials*, 295-298, 2084–2089. doi:10.4028/www.scientific.net/AMM.295-298.2084.
- WBGU (1994). *Welt im Wandel: Die Gefährdung der Böden. Jahresgutachten 1994*. Bonn: Economica Verl.
- Weiss, M., Baret, F., Myneni, R.B., Pragnère, A., & Knyazikhin, Y. (2000). Investigation of a model inversion technique to estimate canopy biophysical variables from spectral and directional reflectance data. *Agronomie*, 20, 3–22. doi:10.1051/agro:2000105.
- Weisshaidinger, R., & Leser, H. (2006). Switzerland. In J. Boardman, & J. Poesen (Eds.), *Soil erosion in Europe*. Hoboken, NJ: Wiley-Interscience.
- Wellinger, R., Buser, H.-P., Krauss, J., & Theiler, R. (2006). Karotten: Anbau, Erntezeitpunkt und Lagerung. *Agrarforschung Schweiz*, 13, 412–417.
- Widmann, M., & Schär, C. (1997). A principal component and long-term trend analysis of daily precipitation in Switzerland. *International Journal of Climatology*, 17, 1333–1356. doi:10.1002/(SICI)1097-0088(199710)17:12<1333::AID-JOC108>3.0.CO;2-Q.
- Wiegand, T., Wiegand, K., & Pütz, S. (2008). Grassland Models. In *Encyclopedia of Ecology* (pp. 1754–1765). Amsterdam.
- Wilde, M., Günther, A., Reichenbach, P., Malet, J.-P., & Hervás, J. (2018). Pan-European landslide susceptibility mapping. ELSUS Version 2. *Journal of Maps*, 14, 97–104. doi:10.1080/17445647.2018.1432511.
- Wilkes, G., & Sawada, M. (2005). Geostatistically Derived Great Lakes USLE Monthly Rainfall Erosivity Factors. *Journal of Great Lakes Research*, 31, 155–165. doi:10.1016/S0380-1330(05)70247-1.
- Willen, D.W. (1965). Surface Soil Textural and Potential Erodibility Characteristics of Some Southern Sierra Nevada Forest Sites1. *Soil Science Society of America Journal*, 29, 213. doi:10.2136/sssaj1965.03615995002900020029x.
- Winchell, M.F., Jackson, S.H., Wadley, A.M., & Srinivasan, R. (2008). Extension and validation of a geographic information system-based method for calculating the Revised Universal Soil Loss Equation length-slope factor for erosion risk assessments in large

- watersheds. *Journal of Soil and Water Conservation*, 63, 105–111.
doi:10.2489/jswc.63.3.105.
- Wischmeier, W.H. (1971). A soil erodibility nomograph for farmland and construction sites. *Journal of Soil and Water Conservation*, 26, 189–193.
- Wischmeier, W.H., Johnson, C.B., & Cross, B.V. (1971). Soil erodibility nomograph for farmland and construction sites. *Journal of Soil and Water Conservation*, 26, 189–193.
- Wischmeier, W.H., & Mannering, J.V. (1969). Relation of soil properties to its erodibility. *Soil Sci. Soc. Amer. Proc.*, 33, 131–137.
- Wischmeier, W.H., & Smith, D.D. (1965). *Predicting Rainfall-Erosion Losses from Cropland East of the Rocky Mountains*. Washington.
- Wischmeier, W.H., & Smith, D.D. (1978). *Predicting rainfall erosion losses*. Washington: U.S. Gov. Print. Off.
- Yang, D., Kanae, S., Oki, T., Koike, T., & Musiak, K. (2003). Global potential soil erosion with reference to land use and climate changes. *Hydrological Processes*, 17, 2913–2928.
doi:10.1002/hyp.1441.
- Yang, X. (2014). Deriving RUSLE cover factor from time-series fractional vegetation cover for hillslope erosion modelling in New South Wales. *Soil Research*, 52, 253.
doi:10.1071/SR13297.
- Yang, X., & Yu, B. (2015). Modelling and mapping rainfall erosivity in New South Wales, Australia. *Soil Research*. doi:10.1071/SR14188.
- Yang, X., Yu, B., & Zhu, Q. (2015). Climate change impacts on rainfall erosivity and hillslope erosion in NSW. *21st International congress on Modelling and Simulation, Gold Coast, Australia*.
- Yimer, F., Ledin, S., & Abdelkadir, A. (2006). Soil property variations in relation to topographic aspect and vegetation community in the south-eastern highlands of Ethiopia. *Forest Ecology and Management*, 232, 90–99. doi:10.1016/j.foreco.2006.05.055.
- Yong-Zhong, S., Yu-Lin, L., Jian-Yuan, C., & Wen-Zhi, Z. (2005). Influences of continuous grazing and livestock exclusion on soil properties in a degraded sandy grassland, Inner Mongolia, northern China. *CATENA*, 59, 267–278. doi:10.1016/j.catena.2004.09.001.
- Zhang, W., & Li, H. (2015). RUSLE and GIS-based assessment of soil erosion in the mountain areas of Beijing, China. *International Conference on Advances in Energy and Environment Science ICAEES*.
- Zhang, W., Zhang, Z., Liu, F., Qiao, F., & Hu, S. (2011). Estimation of the USLE cover and management factor C using satellite remote sensing: A review. *19th International Conference on Geoinformatics 24.06.2011 - 26.06.2011, Shanghai*.
- Zhang, Y., Liu, B.-Y., Zhang, Q.-C., & Xie, Y. (2003). Effect of different vegetation types on soil erosion by water. *Acta Botanica Sinica*, 45, 1204–1209.
- Zhao, Q., Liu, Q., Ma, L., Ding, S., Xu, S., W., C., & Liu, P. (2015). Spatiotemporal variations in rainfall erosivity during the period of 1960–2011 in Guangdong Province, southern China. *Theoretical and Applied Climatology*. doi:10.1007/s00704-015-1694-5.
- Zhou, P., Luukkanen, O., Tokola, T., & Nieminen, J. (2008). Effect of vegetation cover on soil erosion in a mountainous watershed. *CATENA*, 75, 319–325.
doi:10.1016/j.catena.2008.07.010.
- Zhu, Q., Chen, X., Fan, Q., Jin, H., & Li, J. (2011). A new procedure to estimate the rainfall erosivity factor based on Tropical Rainfall Measuring Mission (TRMM) data. *Science China Technological Sciences*, 54, 2437–2445. doi:10.1007/s11431-011-4468-z.

- Zhu, Q., Yang, X., & Yu, Q. (2016). Assess the topographic resolution impact on soil loss. In *2016 IEEE International Geoscience and Remote Sensing Symposium (IGARSS)* (pp. 6055–6058): IEEE.
- Zingg, A. (1940). Degree and length of land slope as it affects soil loss in run-off. *Agricultural Engineering*, 59–64.
- Zweifel, L., Meusbürger, K., & Alewell, C. (2018). Spatio-temporal analysis of soil degradation in Swiss alpine grasslands based on Object-Based Image Analysis. *Geophysical Research Abstracts*, EGU2018-7162.
- Zwingli, H. (2017). Statistik zur Heumahd. Email. St. Gallen.

APPENDIX

Saisonale und räumliche Variabilität der Niederschlagserosivität in der Schweiz

This chapter is published in BGS Bulletin:

Simon Schmidt¹, Christine Alewell¹, Panos Panagos², and Katrin Meusburger^{1,2}: Saisonale und räumliche Variabilität der Niederschlagserosivität in der Schweiz, BGS Bulletin, 38, 37-46, 2017.

¹Environmental Geosciences, University Basel, Bernoullistrasse 30, CH-4056 Basel, Switzerland

²European Commission, Joint Research Centre, Institute for Environment and Sustainability, Via E. Fermi 2749, I-21027 Ispra, Italy

Abstract

One major controlling factor of water erosion is rainfall erosivity, which is quantified as the product of total storm energy of an erosive rainfall event and a maximum 30 min intensity. Rainfall erosivity is expressed as the R-factor in erosion models like the Universal Soil Loss Equation (USLE) and its revised version (RUSLE). R-factors were modelled on a monthly scale to catch simultaneously the highly spatial as well as temporal variability. The observations of a network with 87 precipitation gauging stations with a 10 min temporal resolution and a mean observation length of 19.5 years were used to calculate long-term monthly mean R-factors. Stepwise generalized linear regression (GLM) and leave-one-out cross-validation (LOOCV) select high resolution covariates which explain the spatial and the temporal patterns of R-factors within a month. The predicted R-factors of the regression equation and the corresponding residues are combined to 12 R-factor maps. The residues itself are interpolated by ordinary-kriging (regression-kriging). As spatial covariates, a variety of precipitation indicator data has been used such as snow depths, radar and ground observations of precipitation (CombiPrecip), daily alpine precipitation (EURO4M-APGD), and monthly precipitation sums (RhiresM). Elevation and slope are derived from a digital elevation model (SwissAlti3D) as explanatory variables. The comparison of the 12 monthly rainfall erosivity maps showed highest rainfall erosivity in summer (June, July, and August). In particular, the southern Alps (Canton Ticino), the alpine area of the northern Alps and parts of the Valley region are affected by high R-factors during that period. The 4 months from June to September have a share of 62% of the total annual R-Factor of Switzerland. The identification of regions and time slots with increased erosivity enables the introduction of selective erosion control and a better knowledge about dynamics of erosion processes within a year.

Zusammenfassung

Eine der treibenden Kräfte der Wassererosion ist die Niederschlagserosivität, die als Produkt der Energie eines erosiven Niederschlagsereignisses und der maximalen Niederschlagsintensität innerhalb 30 Minuten quantifiziert wird. In Erosionsmodellen wie der Universal Soil Loss Equation (USLE) und der revidierten Version (RUSLE) geht die Erosivität als R-Faktor ein. Um zeitgleich die stark ausgeprägte räumliche aber auch saisonale Variabilität zu erfassen, wurde der R-Faktor auf monatlicher Skala modelliert. Langjährige monatliche R-Faktoren basieren auf Messdaten von 87 Schweizer Niederschlagsmessstationen mit einer Auflösung von 10 Minuten über einen mittleren Messzeitraum von 19.5 Jahre. Ein stufenweises lineares Regressionsmodell (stepwise GLM) und eine leave-one-out cross-validation (LOOCV) selektieren hochaufgelöste Kovariaten, die die raumzeitlichen Muster der R-Faktoren erklären. Die über die entsprechenden Regressionsgleichungen vorhergesagten monatlichen R-Faktoren sind mit den dazugehörigen Residuen zu 12 R-Faktor-Karten kombiniert. Die Residuen selbst sind über ordinary kriging interpoliert (Regression-Kriging). Als räumliche Kovariaten gehen verschiedene Niederschlagsgrößen wie Schneehöhen, Radar- und Bodenbeobachtungen des Niederschlags (CombiPrecip), tägliche alpine Niederschläge (EURO4M-APGD) und monatliche Niederschlagssummen (RhiresM) ein. Aus einem digitalen Höhenmodell (SwissAlti3D) sind Geländehöhe und Hangneigung als erklärende Variablen abgeleitet. Die Gegenüberstellung der 12 monatlichen R-Faktor-Karten zeigt, dass die Sommermonate (Juni, Juli, und August) von höchster Erosivität geprägt sind. Insbesondere die Südalpen (Kanton Tessin), die Bergzonen der Nordalpen und Teile der Talzone weisen in diesem Zeitraum hohe R-Faktoren auf. Zwischen Juni und September wird ein Anteil von 62% an der Jahresniederschlagserosivität der Schweiz registriert. Die Identifikation von Regionen und Zeiträumen erhöhter Erosivität ermöglicht einen zielgerichteten Erosionsschutz und ein besseres Verständnis der Dynamiken von Erosionsprozessen innerhalb eines Jahres.

Keywords: rainfall erosivity, R-factor, Erosivität, dynamic erosion modelling, C-factor

A.1. Einleitung

In der Schweiz wird seit vielen Jahren Bodenerosionsforschung betrieben. Zahlreiche Forschungsarbeiten haben den Bodenabtrag durch Wasser auf Schweizer Böden gemessen (Konz et al., 2012; Alewell et al., 2014), kartiert (Mosimann et al., 1990; Prasuhn, 2011; 2012) und modelliert (Gisler et al., 2011; Prasuhn et al., 2013). Seit den 50er Jahren kann eine Zunahme der Erosionsgefährdung sowohl für die landwirtschaftliche Nutzfläche (Weisshaidinger and Leser, 2006) als auch für die alpinen Grünlandflächen (Meusburger and Alewell, 2008) nachgewiesen werden. Nach Mosimann et al. (1991) sind circa 20% des Schweizer Kulturlands durch Wassererosion gefährdet. Die damit verbundenen jährlichen finanziellen Aufwendungen belaufen sich auf schätzungsweise 53 Millionen Schweizer Franken (Ledermann, 2012). Unter dem Aspekt zukünftiger Klimaszenarien mit einer zu erwartenden Zunahme der Niederschlagshäufigkeit und -intensität werden die Gefährdung der Böden durch Wassererosion und die damit verbundenen Kosten weiter ansteigen (Fuhrer et al., 2006). Ein Trend erhöhter Niederschlagserosivität ist bereits heute in den Monaten zwischen Mai und Oktober ersichtlich (Meusburger et al., 2012). Niederschlag kann generell als die treibende Kraft im Erosionsprozess gesehen werden da er über die Prozesse der raschen Befeuchtung sowie der Planschwirkung der Tropfen direkten Einfluss auf die Mobilisierung von Bodenmaterial hat, aber gleichzeitig auch Transportmedium des Materials ist. In den empirischen Erosionsmodellen Universal Soil Loss Equation (USLE) und Revised Universal Soil Loss Equation (RUSLE) (Renard et al., 1997; Foster et al., 2008; Foster et al., 2008) fliesst die Wirkung des Niederschlags auf Böden in Form der Niederschlagserosivität als R-Faktor ein. Die weiteren Erosionsfaktoren der USLE und RUSLE sind Bodenbedeckung C, Bodenerodierbarkeit K, Hanglänge und Hangneigung LS, und Schutzmassnahmen P. Der langjährige Bodenabtrag durch Wasser kann über die Multiplikation dieser 5 Faktoren errechnet werden (Schwertmann et al., 1987). Neben der unmittelbaren Quantifizierung des Bodenabtrags können aus den individuellen Faktoren wichtige Aussagen abgeleitet werden.

Aufgrund der hohen klimatischen Kontraste in der Schweiz, die im Wesentlichen durch die Topographie bedingt sind, resultiert eine räumliche und zeitliche Variabilität des Wetters. Diese Variabilität hat zur Folge, dass bestimmte räumliche aber auch zeitliche Muster in der Verteilung der Niederschlagserosivität entstehen. Meusburger et al. (2012) wies auf die starke Saisonalität und räumliche Variation hin, allerdings wurden diese Muster der R-Faktoren für die Schweiz nicht kartographisch erfasst. Der R-Faktor für die Schweiz wurde bisher entweder als langjähriger Faktor (Friedli, 2006; Gisler et al., 2011; Meusburger et al., 2012; Prasuhn et al., 2013) oder als saisonale Mittelwerte auf Landesebene (Panagos et al., 2015a) berechnet. Hochaufgelöste Datensätze von MeteoSchweiz (z.B. CombiPrecip) und Swisstopo (z.B. SwissAlti3D) ermöglichen inzwischen die Berechnung der Niederschlagserosivität auf monatlicher Ebene. Durch die Kartierung monatlicher R-Faktoren kann eine Identifikation von zeitlichen Fenstern und Regionen hoher R-Faktoren zusammen mit raum-zeitlicher Vegetationsdynamiken (niedrige oder instabile Vegetationsbedeckungen) als Entscheidungshilfe im Boden- und Naturschutz dienen, um Bodenerosion, Hochwasser und Naturkatastrophen zielgerichtet vermeiden und bekämpfen zu können.

Um ein verbreitetes Verständnis über die Dynamiken des R-Faktors zu erlangen, werden in dieser Arbeit die raum-zeitlichen Muster der Niederschlagserosivität in der Schweiz untersucht, indem (i) monatliche R-Faktor-Karten auf Basis eines Regression-Kriging-Ansatzes mit hochaufgelösten Kovariaten erstellt und (ii) die raum-zeitlichen Variationen der Niederschlagserosivität in der Schweiz analysiert werden.

Die vorliegende Studie ist als Erweiterung der Berechnung langjähriger R-Faktoren der Schweiz durch Meusburger et al. (2012) zu sehen. Eine ausführlichere Beschreibung der vorliegenden Forschung ist in Schmidt et al. (2016) veröffentlicht.

A.2. Material und Methoden

A.2.1. Berechnung der Niederschlagserosivität (R-Faktor)

Die Niederschlagserosivität wird im Erosionsmodell RUSLE als R-Faktor ausgedrückt und durch das Produkt der gesamten Energie eines erosiven Niederschlagsereignisses und seiner maximalen Intensität innerhalb 30 Minuten quantifiziert (Brown and Foster, 1987; Wischmeier and Smith, 1978). Die Festlegung des Grenzwertes eines erosiven Niederschlagsereignisses folgt der Definition von Renard et al. (1997) unter Modifikation durch Meusburger et al. (2012).

Die Niederschlagsenergie (e_r , MJ ha⁻¹ mm⁻¹) eines jeden Zeitintervalls wird durch die Niederschlagsintensität (i_r , mm h⁻¹) während dieser Zeitspanne ausgedrückt und wie folgt berechnet:

$$e_r = 0.29[1 - 0.72 \exp(-0.05i_r)] \quad (\text{A.1})$$

Die Ereignisniederschlagserosivität (EI_{30}) ergibt sich aus dem Produkt der Niederschlagsenergie (e_r) eines erosiven Ereignisses und seiner maximalen Niederschlagsmenge (v_r , mm) während einer Zeiteinheit r unter Berücksichtigung der maximalen Niederschlagsintensität innerhalb 30 Minuten (I_{30} , mm h⁻¹).

$$EI_{30} = (\sum_{r=1}^k e_r v_r) I_{30} \quad (\text{A.2})$$

Die monatliche Niederschlagserosivität (R_{mo} , MJ mm ha⁻¹ h⁻¹ month⁻¹) ist der Mittelwert der aufsummierten Ereignisniederschlagserosivität (EI_{30}) über den Zeitraum eines Monats:

$$R_{mo} = \frac{1}{n} \sum_{j=1}^n \sum_{k=1}^{m_j} (EI_{30})_k \quad (\text{A.3})$$

Wobei n der Anzahl an Jahren mit der Anzahl der erosiven Ereignisse (m_j) innerhalb eines bestimmten Monats j entspricht. k ist der Index eines Einzelereignisses mit seiner entsprechenden Ereignisniederschlagserosivität.

Schnee, Schneeschmelze und Niederschlag auf gefrorenem Boden (Temperaturgrenzwert von 0°C) werden nicht im R-Faktor berücksichtigt (Renard et al., 1997).

A.2.2. Niederschlagsmessnetz

Die monatlichen R-Faktoren wurden aus Niederschlagsmessungen von 87 automatischen Messstationen mit Messintervallen von 10 Minuten abgeleitet. Mit einer mittleren Messperiode von 19.5 Jahren pro Station wird das vorgeschlagene Minimum der Beobachtungszeit (15 Jahre) zur Berechnung des R-Faktors erfüllt (Foster et al., 2008). Die Stationen decken alle landwirtschaftliche Zonen der Schweiz ab (Fig. A.1). Um den Einfluss des Schnees auszuschliessen sind ausserdem Temperaturen in stündlicher Auflösung für 71 Stationen erfasst oder von der nächstgelegenen Stationen abgeleitet (16 Stationen, Distanz <20 km).

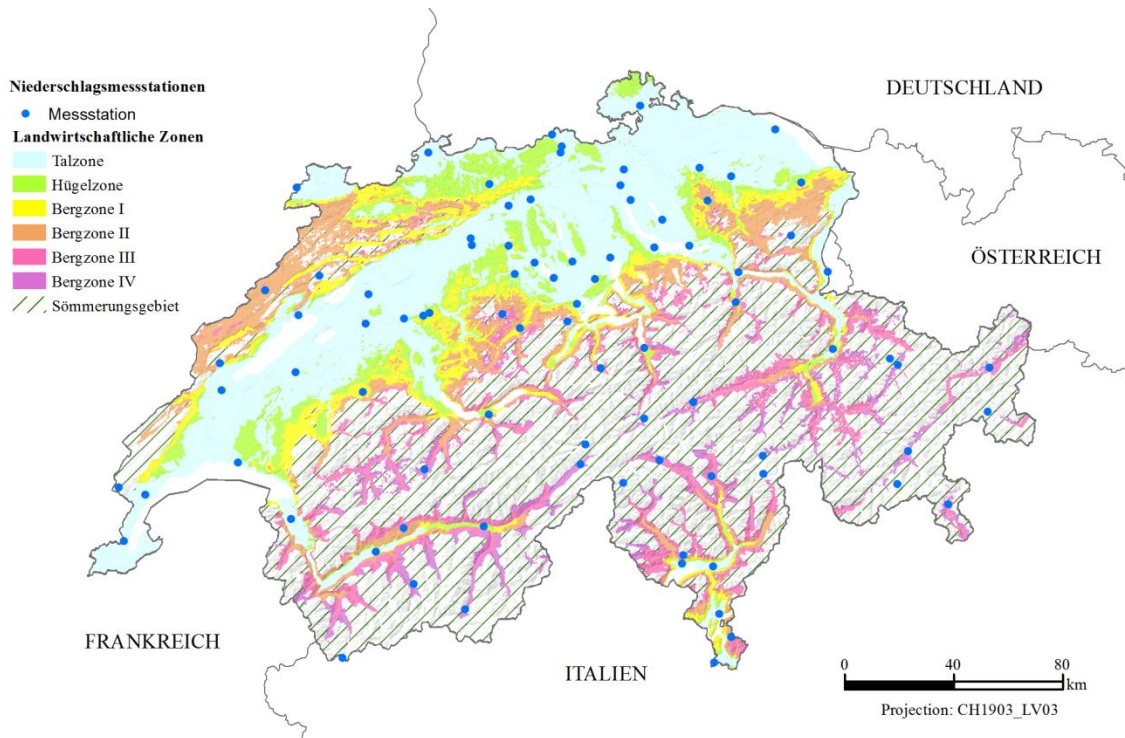


Fig. A.1: Landwirtschaftliche Zonen (Bundesamt für Landwirtschaft BLW, 2017) und Standorte der 87 Messstationen.

A.2.3. Datensätze und Kovariaten

In einem Land mit abgelegenen Hochgebirgsregionen wie der Schweiz ist für die Regionalisierung der punktuell an den Messstationen erfassten R-Faktoren eine Vielzahl an erosionsbeeinflussenden Kovariaten notwendig. Hauptsächlich wird die Niederschlagserosivität durch Niederschlagsparameter und Relief gesteuert (Meusburger et al., 2012; Panagos et al., 2015a; 2016a).

Daher gehen in die Berechnung als Annäherung an den Schnee als steuernde Grösse stündliche Schneehöhen (an 58 Stationen, stündliche zeitl. Auflösung, Zeitraum 1988-2010, MeteoSwiss) ein. Diese wurden als langjährige mittlere monatliche Schneehöhen zusammengefasst und interpoliert (IDW). Niederschlagsparameter werden durch stündliche CombiPrecip-Daten (geostatistische Kombination von Punktmessungen an 150 Stationen und drei C-Band Radar-Beobachtungen, 1 km räuml. Auflösung, Zeitraum 2005-2015, Sideris et al., 2014) ausgedrückt, die zu vieljährigen monatlichen Mittelwerten aggregiert sind. Darüber hinaus stammen langjährige mittlere Tagesniederschlagssummen auf Monatebene vom Datensatz EURO4M-APGD (5 km räuml. Auflösung, Zeitraum 1971-2008, Isotta et al., 2014). Langjährige mittlere monatliche Niederschlagssummen sind aus RhiresM (1 km räuml. Auflösung, Zeitraum 1961-2015, MeteoSwiss, 2013) gemittelt. Reliefgrössen wie Geländehöhe und Hangneigung sind aus dem digitalen Höhenmodell SwissAlti3D (Swisstopo) mit einer Auflösung von 2 m extrahiert. Mit den hochaufgelösten Datensätzen liegt eine Informationsgrundlage vor, die in dieser Detaildichte bisher nicht in Europäische (Panagos et al., 2015a; 2016a) oder Schweizer (Meusburger et al., 2012) R-Faktor-Modellierungen Eingang gefunden hat.

A.2.4. Regionalisierung der monatlichen R-Faktoren für die Schweiz

Modellierungen zeigen, dass eine Kombination aus einem Regressionsmodell und einer Kriging-Interpolation der Residuen (Regression-Kriging) gut geeignet ist, um Niederschlagserosivität zu modellieren (Hanel et al., 2016; Meusburger et al., 2012; Angulo-Martínez and Beguería, 2009). Für

die Regionalisierung der monatlichen R-Faktoren an den 87 Stationen der Schweiz wird daher ein Regression-Kriging-Ansatz verfolgt (Hengl et al., 2004; 2007). Über ein allgemeines lineares Modell (generalized linear model, GLM; Gotway and Stroup, 1997) wird eine Regression zwischen den an den 87 Standorten berechneten monatlichen R-Faktoren (R_{mo}) und den hochaufgelösten Kovariaten durchgeführt. Das GLM stellt eine Beziehung zwischen R-Faktoren (Zielvariable) und Kovariaten her um die Niederschlagserosivität mit der bestmöglichen Auflösung der Kovariaten abzuschätzen (Odeh et al., 1995; McBratney et al., 2000). Im zweiten Schritt des Regression-Kriging werden die Residuen des GLM über ordinary kriging interpoliert (McBratney et al., 2000; Hengl et al., 2004) und die vorausberechneten R-Faktoren des GLM mit den entsprechenden Residuenkarten aufsummiert. Durch diese Kombination kann der Standardfehler der R-Faktor-Karte berücksichtigt werden. Für jeden Monat wird das Regression-Kriging wiederholt um 12 individuell errechnete R-Faktor-Karten zu erhalten.

Zusätzlich wird eine leave-one-out cross-validation (LOOCV) zur weiteren Qualitätskontrolle hinzugefügt (Efron and Tibshirani, 1997). Für jedes der 12 GLM werden über eine automatisierte stufenweise Auswahl (stepwise feature selection) signifikante Kovariaten (α -to-enter 0.1; Kutner et al., 2005) gewählt. In der Berechnung bleiben Ausreisser (Bonferroni-adjusted outlier test) und Beobachtungen mit hohem Einfluss (Cook's distance) unberücksichtigt. Die Anpassungsgüte des Modells (goodness-of-fit) wird über das Bestimmtheitsmass (R^2), den mittleren quadratischen Fehler (RMSE), und die Devianz beschrieben. In der Fehlerdiagnose des Regressionsmodells wird die Normalverteilung, die Homoskedastizität, der variance inflation factor (vif), und die Autokorrelation bewertet. Die Regionalisierung der R_{mo} sind mit dem R-package „caret“ (v6.0-68) und in ESRI ArcGIS (v10.2.2.) umgesetzt.

A.2.5. Summenkurven der täglichen R-Faktoren

Die R-Faktoren eines jeden Tages im Jahr sind über den Messzeitraum (durchschnittlich 19.5 Jahre) je Station gemittelt und zu jährlichen R-Faktor-Summenkurven kumuliert. Tagessummen von Stationen innerhalb einer landwirtschaftlichen Zone werden zu mittleren Werten zusammengefasst. Die landwirtschaftlichen Zonen repräsentieren vor allem Einheiten ähnlicher Landnutzung, Relief, und Hangneigungsklasse. Als Ergänzung können Schmidt et al. (2016) Summenkurven für die biogeographischen Regionen der Schweiz entnommen werden.

A.3. Ergebnisse und Diskussion

A.3.1. Monatliche R-Faktor-Karten der Schweiz

Alle Kovariaten sind mindestens für einen Monat im stepwise GLM signifikant ($p < 0.1$) und können die R_{mo} erklären. Die Berechnungen eines jeden Monats basieren auf einer automatisierten Auswahl an Kovariaten entsprechend des Akaike information criterion (AIC). Table 1 zeigt die Auswahl der Kovariaten in den entsprechenden Regressionsgleichungen sowie R^2 und RMSE nach Monat. Pro Monat wurden ein bis drei Ausreiser ausgeschlossen.

Zur Vergleichbarkeit der raum-zeitlichen Muster sind die Farbskalen der monatlichen R-Faktor-Karten (Fig. A.2) einheitlich zwischen 0 und 200 MJ mm ha⁻¹ h⁻¹ month⁻¹ gestreckt, obgleich die absoluten Werte im Sommer weitaus höher liegen (Table 2).

Table A.1: Regressionsgleichungen der 12 Monate und entsprechende Bestimmtheitsmasse R^2 , mittlere quadratische Fehler RMSE und ausgeschlossene Ausreisserstationen

Monat	Regressionsgleichung	R^2	RMSE (MJ mm ha ⁻¹ h ⁻¹ month ⁻¹)	ausgeschlossene Ausreisser
Januar	$R_{Jan} = 2.101 - 4.150 \cdot \text{CombiPrecip}_{Jan} - 0.006 \cdot \text{Schneehöhe}_{Jan} + 0.017 \cdot \text{Rhires}_{Jan} - 0.001 \cdot \text{Geländehöhe}$	0.52	6.98	Method
Februar	$R_{Feb} = 2.702 - 13.812 \cdot \text{CombiPrecip}_{Feb} - 0.007 \cdot \text{Schneehöhe}_{Feb} + 0.019 \cdot \text{Rhires}_{Feb} + 0.211 \cdot \text{EURO4M-APGD}_{Feb} - 0.001 \cdot \text{Geländehöhe}$	0.53	12.96	Monte Generoso, Napf, Säntis
März	$R_{Mar} = 2.534 - 7.735 \cdot \text{CombiPrecip}_{Mar} - 0.006 \cdot \text{Schneehöhe}_{Mar} + 0.018 \cdot \text{Rhires}_{Mar} + 0.170 \cdot \text{EURO4M-APGD}_{Mar} - 0.001 \cdot \text{Geländehöhe}$	0.49	13.10	C. du G. St-Bernard, Säntis
April	$R_{Apr} = 2.330 - 3.319 \cdot \text{CombiPrecip}_{Apr} - 0.008 \cdot \text{Schneehöhe}_{Apr} + 0.023 \cdot \text{Rhires}_{Apr} - 0.001 \cdot \text{Geländehöhe} - 0.019 \cdot \text{Hangneigung}$	0.65	21.01	C. du G. St-Bernard, Säntis, Weissfluhjoch
Mai	$R_{May} = 2.965 + 2.072 \cdot \text{CombiPrecip}_{Mai} - 0.002 \cdot \text{Schneehöhe}_{Mai} + 0.015 \cdot \text{Rhires}_{Mai} - 0.001 \cdot \text{Geländehöhe}$	0.60	73.39	Davos, C. du G. St-Bernard,
Juni	$R_{Jun} = 3.890 + 0.014 \cdot \text{Rhires}_{Jun} - 0.001 \cdot \text{Geländehöhe}$	0.58	126.03	C. du G. St-Bernard
Juli	$R_{Jul} = 3.926 + 5.710 \cdot \text{CombiPrecip}_{Jul} + 0.251 \cdot \text{EURO4M-APGD}_{Jul} - 0.001 \cdot \text{Geländehöhe}$	0.66	138.77	Monte Generoso, C. du G. St-Bernard, Stabio
August	$R_{Aug} = 3.627 + 0.010 \cdot \text{Rhires}_{Aug} + 0.194 \cdot \text{EURO4M-APGD}_{Aug} - 0.001 \cdot \text{Geländehöhe}$	0.47	330.16	C. du G. St-Bernard, Stabio
September	$R_{Sep} = 2.760 + 2.243 \cdot \text{CombiPrecip}_{Sep} + 0.539 \cdot \text{EURO4M-APGD}_{Sep} - 0.001 \cdot \text{Geländehöhe}$	0.64	81.91	C. du G. St-Bernard, Stabio
Oktober	$R_{Oct} = 2.753 + 0.0161 \cdot \text{Rhires}_{Okt} - 0.001 \cdot \text{Geländehöhe}$	0.62	81.60	Piz Corvatsch, C. du G. St-Bernard, Stabio
November	$R_{Nov} = 2.665 + 3.787 \cdot \text{CombiPrecip}_{Nov} - 0.034 \cdot \text{Schneehöhe}_{Nov} + 0.166 \cdot \text{EURO4M-APGD}_{Nov}$	0.10	55.72	Piz Corvatsch, C. du G. St-Bernard, Saetis
Dezember	$R_{Dec} = 2.437 + 0.013 \cdot \text{Rhires}_{Dez} - 0.001 \cdot \text{Geländehöhe}$	0.26	177.65	C. du G. St-Bernard

CombiPrecip = Kombination von Bodenstations- und Radarmessungen des Niederschlags

Rhires = monatliche Niederschlagssummen

EURO4M-APGD = alpine Tagesniederschlagssummen

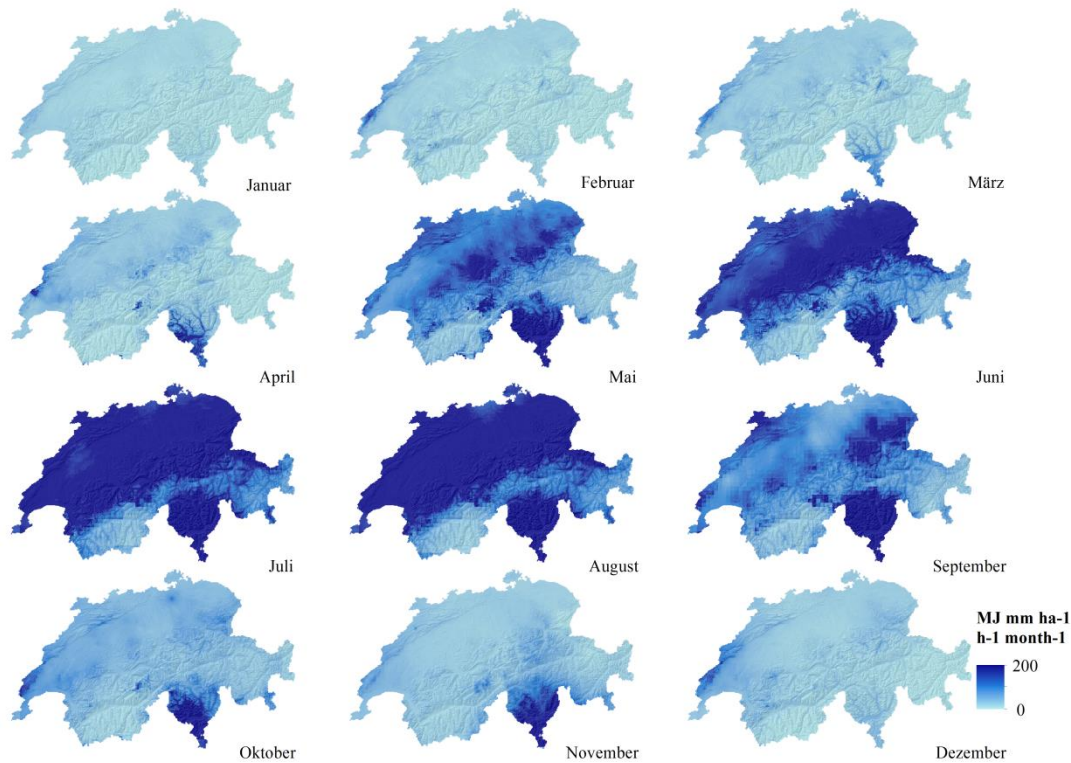


Fig. A.2: Monatliche R-Faktor-Karten der Schweiz (einheitliche Farbstreckung von 0 bis 200 MJ mm ha⁻¹ h⁻¹ month⁻¹) berechnet über Regression-Kriging

Table A.2: Monatliche nationale R-Faktoren (R_{mo}) in MJ mm ha⁻¹ h⁻¹ month⁻¹

Monat	Minimum	Maximum	Mittelwert
Januar	0.2	71.3	10.5
Februar	0.0	247.3	13.5
März	0.0	179.0	20.1
April	0.2	1014.4	28.8
Mai	8.3	1717.8	120.2
Juni	3.6	1262.1	174.8
Juli	12.6	1481.1	255.4
August	8.3	1994.9	263.5
September	6.8	6107.9	147.7
Oktober	5.7	977.0	57.0
November	4.9	357.1	41.6
Dezember	1.3	234.4	24.9

Die zeitlichen Muster der Regionalisierung der modellierten R_{mo} zeigen eine hohe jahreszeitliche Dynamik mit niedrigsten nationalen Mittelwerten im Januar (10.5 MJ mm ha⁻¹ h⁻¹ month⁻¹) und höchsten Werten im August (263.5 MJ mm ha⁻¹ h⁻¹ month⁻¹). Wie die Übereinstimmung der R-Faktor-Karten im Sommer mit der Karte der extremen 100jährigen Punktniederschläge (Spreafico and Weingartner, 2005) zeigt, sind hohe sommerliche R_{mo} mit Extremniederschlägen der Schweiz kongruent. Diese R-Faktoren resultieren auch aus den Gewitterzyklen in der Schweiz, die am Ende des Frühlings (Mai) einsetzen und bis zum Herbstbeginn (September) anhalten (van Delden, 2001; Perroud and Bader, 2013; Nisi et al., 2016; Punge and Kunz, 2016). Ab September zeigt sich national eine Abnahme der Erosivität.

Räumliche Muster erhöhter Erosivität im Frühling sind in den Bergzonen I und II sowie der Sömmerungsgebiete im Bereich des Jura, in den Bergzonen der westlichen und östlichen Teilen der Nordalpen sowie in den südlichen landwirtschaftlichen Zonen des Kantons Tessins zu beobachten.

Hohe winterliche R_{mo} kommen durch orographische Niederschläge zustande, die aus Tiefdruckgebieten Nordeuropas und nordwestlicher Fronten entstehen. In den Frühlingsmonaten ist eine Zunahme der Erosivität im Tessin beobachtbar. Das leicht verfrühte Einsetzen der Gewitterperiode an der Südflanke der Alpen bewirkt hier intensivere Regenfälle und damit höhere R_{mo} . Im Sommer sind insbesondere die Südalpen, Bergzonen der Nordalpen und Teile der Talzone von hoher Erosivität geprägt. Sommergewitter haben vor allem im alpinen Bereich hohen Einfluss auf erosive Ereignisse. An der Südflanke der Alpen kommt hinzu, dass orographische Regenfälle, verursacht durch das Aufsteigen warmer feuchter Luftmassen aus dem Mittelmeerraum zu intensivem Abregnen führen (Schwarb et al., 2001 Perroud and Bader, 2013). Im Herbst deutet sich besonders in der Nordschweiz ein schneller Rückgang der Erosivität an. Ganzjährig weisen die Tal-, Bergzonen, und Sömmerungsgebiete der Kantone Wallis und Graubünden die niedrigsten R-Faktoren auf, was durch die geringere Konvektion und damit schwächere Niederschlagserosivität begründet ist.

A.3.2. Summenkurven der täglichen Erosivität

Fig. A.3 präsentiert die kumulierten Summenkurven der täglichen R-Faktoren gemittelt nach landwirtschaftlichen Zonen und auf Landesebene. Die grösste Steigung der Kurve für die Schweiz liegt innerhalb des Zeitfensters von Anfang Juni bis Ende September mit einem Anteil von 62% an der Jahressumme der Niederschlagserosivität.

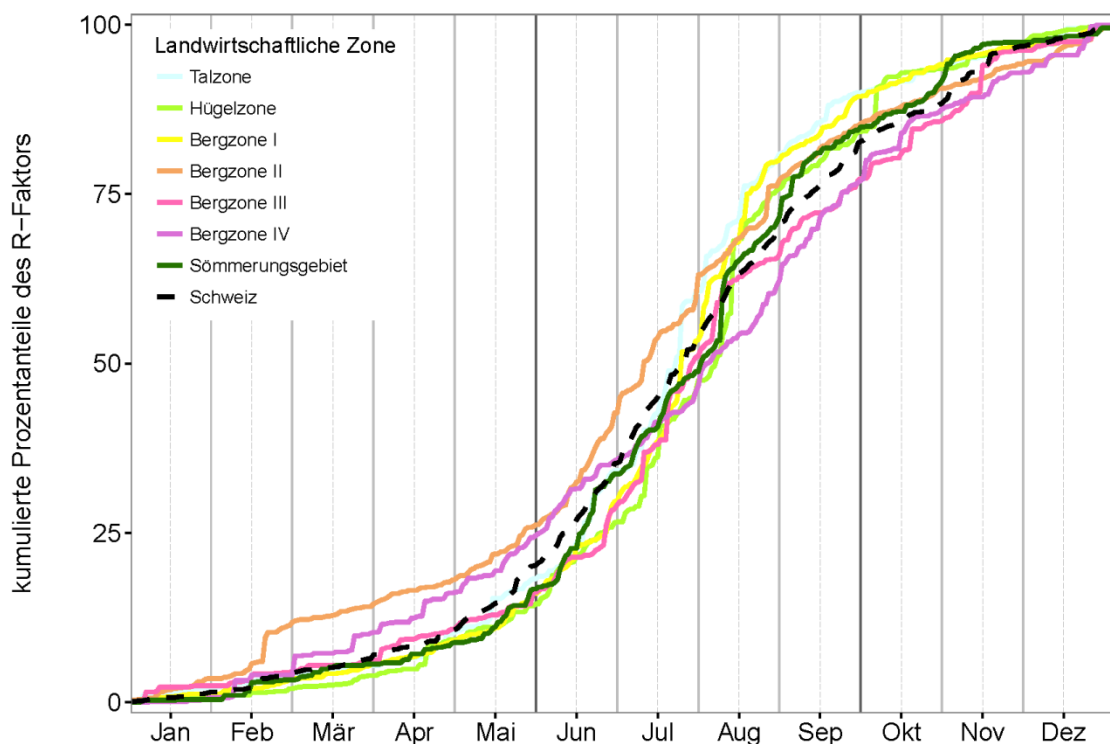


Fig. A.3: Summenkurve der täglichen R-Faktoren für die landwirtschaftlichen Zonen der Schweiz

Generell beschreiben die Kurven aller Zonen einen ähnlichen Trend mit höchsten Anteilen (Steigungen) im Jahresabschnitt Juni-September. Die Zonen Bergzone I (72.8%) und Talzone (71.7%) haben in dieser Periode jeweils über zwei Drittel Anteil an der Jahressumme der Erosivität. Dieser hohe Anteil der Niederschlagserosivität innerhalb relativ kurzer Zeit (4 Monate) kann grossen Einfluss auf die Gefährdung des Bodens durch Wassererosion haben, da er vor allem in diesen landwirtschaftlich geprägten Zonen auf niedrige (nach Ernte von Getreide, Karotten, etc.) und instabile Vegetationsbedeckung (nach Spätsaat) trifft (Hartwig and Ammon, 2002; Wellinger et al., 2006; Torriani et al., 2007; Prasuhn, 2011). Zudem können die hohen Erosivitätsraten auch bei

Vorerntefeldfrüchten (z.B. Getreide, Mais) zu einer Beschädigung durch Umknicken der Halme führen. Böden sind an den Rändern des Zeitfensters (Mai und September) oftmals bereits wassergesättigt und damit stärker erodierbar.

Die Summenkurven einzelner Stationen (Basel, Bern, Glarus, Lugano, Visp) verschiedener Schweizer Landesteile sind in Fig. A.4 gegenübergestellt.

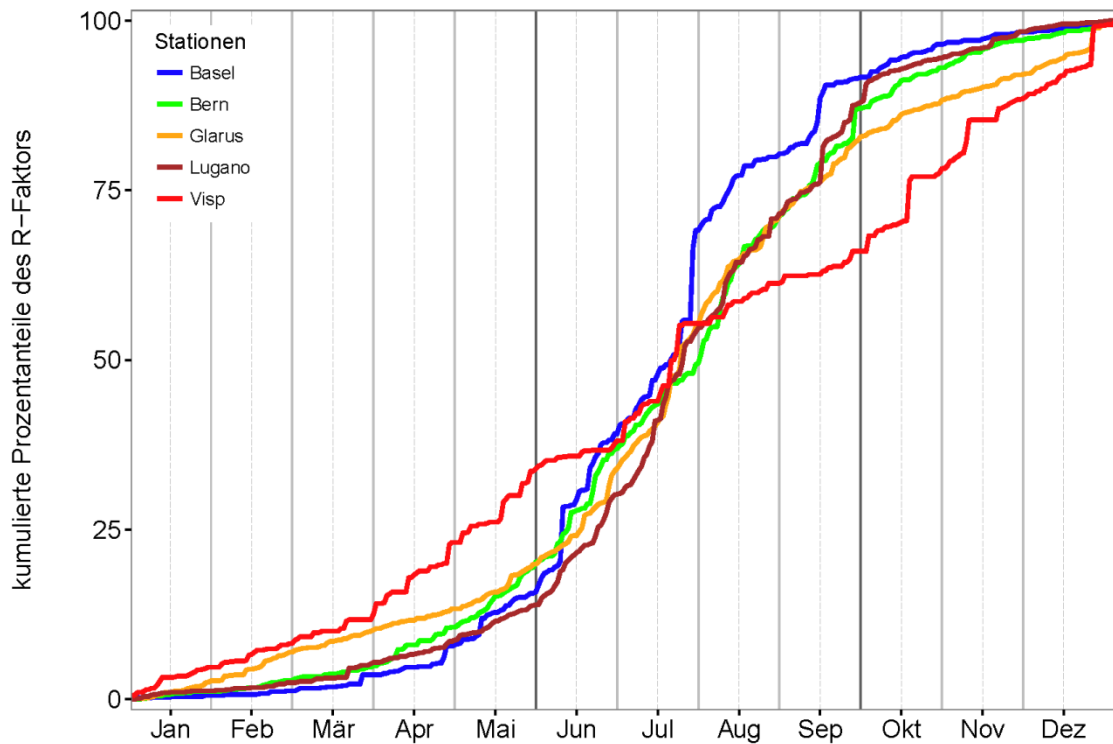


Fig. A.4: Summenkurve der täglichen R-Faktoren für ausgewählte Stationen der Schweiz

Die Stationen Basel und Lugano haben zwischen Juni und September die höchste Steigung mit 74.0 resp. 76.1 Prozentanteilen. In Visp im Wallis zeigt sich entsprechend der ganzjährig gleichmässigen Erosivität (vgl. Fig. A.2), dass die Niederschlagserosivität relativ gleichförmig über das Jahr verteilt ist. Mosimann et al. (1990) berechnet für die Messstation Bern einen Anteil von 80% für die 6-Monats-Periode von April bis September. Dieser Anteil an der Jahressumme kann mit der aktuellen Messreihe (1988-2010) von Bern bestätigt werden (82.9%, Fig. A.4).

Zur Berechnung des relativen Bodenabtrags als Komponente des RUSLE C-Faktors (Wischmeier and Smith, 1978; Renard et al., 1997) sind kumulierte R-Faktoren für bestimmte Jahresabschnitte der Entwicklungszustände von Kulturen erforderlich. Die Summenkurven ermöglichen, Anteile des R-Faktors am Jahres-R-Faktor mit täglicher Auflösung zu bestimmen. Über die Berechnung des C-Faktors hinaus können mittels der anteiligen R-Faktoren jahreszeitliche Zeitfenster identifiziert werden, in welchen die Kurve eine verhältnismässig hohe Steigung und damit der R-Faktor in dieser Periode einen hohen Einfluss besitzt. Die Kombination der Erosivitätsanteile und monatlichen R-Faktor-Karten mit zeitlich variablen C-Faktoren ermöglicht eine hochaufgelöste Abschätzung zeitlicher aber auch räumlicher Erosionsmuster für die Schweiz, in denen eine hohe Erosivität auf geringe oder instabile Vegetationsbedeckung trifft.

A.4. Schlussfolgerungen

Die präsentierte Modellierung visualisiert zeitgleich die räumliche und zeitliche Variation der Niederschlagserosivität in der Schweiz. Die raum-zeitliche Kartierung der monatlichen R-Faktoren ermöglicht die Identifikation von Regionen, in denen ganzjährig eine nur geringe Erosivität zu erwarten ist (Wallis, Graubünden), aber auch jener Regionen wie etwa der Talzone, die nur in bestimmten Monaten durch erhöhte R-Faktoren gefährdet ist.

Intensive Regenfälle sind im August für die höchste Erosivität (mittlerer monatlicher R-Faktor für die Schweiz $263.5 \text{ MJ mm ha}^{-1} \text{ h}^{-1} \text{ month}^{-1}$) verantwortlich. Räumliche Muster der Erosivität im Sommer weiten sich vornehmlich auf die Südalpen (Kanton Tessin), die Bergzonen der Nordalpen und Teile der Talzone aus. Ein Grossteil der jährlichen R-Faktor-Summe (62%) beschränkt sich in der Schweiz auf die Zeitspanne zwischen Juni und September.

Das Verständnis der Dynamiken des R-Faktors in der Schweiz ermöglicht das zielgerichtete und zeitlich dynamische Management von Landwirtschaft, Trockenperioden und die Kontrolle von Naturkatastrophen (z.B. Hochwasserschutz, Hangrutschgefährdung). Massgeblich sind die Ergebnisse jedoch für den Bodenschutz von grosser Relevanz. Landwirte können zielgerichtet Erosionsschutzmassnahmen einführen oder Fruchtfolgen verändern. Durch dieses Eingreifen wird der Einfluss des Regens auf die Böden und Vegetation minimiert und gleichzeitig die Bodenstabilität und -bedeckung in gefährdeten Zeiträumen erhöht. Selektiver Erosionsschutz kann damit nicht nur Bodenschutz optimieren, sondern auch die direkten Kosten der Erosion vermindern, da die finanziellen Aufwendungen der Einführung von Schutzmassnahmen auf ein notwendiges Minimum reduziert werden.

Danksagung

Die Forschungsarbeit wurde vom Bundesamt für Umwelt (BAFU) (Projektnummer N222-0350) finanziert. Ausserdem bedanken sich die Autoren bei MeteoSchweiz, Swisstopo und den Kantonen Luzern, Bern und St. Gallen für die zur Verfügung gestellten Daten.

Supporting Information to Chapter 3

Table S3.1. Monthly erosivity density (ED_{mo87} ; $MJ\ ha^{-1}\ h^{-1}$) at the 87 stations calculated by R_{mo87}/P_{mo87} .

#	acronym	station	y-coordinate (CH1903)	x-coordinate (CH1903)	January	February	March	April	May	June	July	August	September	October	November	December
1	ABO	Adelboden	609400	148975	0.31	0.32	1.38	2.00	1.00	0.24	0.29	1.99	1.99	0.10	0.65	0.30
2	AIG	Aigle	560400	130713	0.90	0.72	0.64	2.56	1.57	0.34	0.96	4.08	4.08	0.27	1.01	0.79
3	ALT	Altdorf	690174	193558	0.56	0.51	0.52	2.83	0.28	0.18	1.44	3.07	3.07	0.55	0.52	0.26
4	BAS	Basel/Binningen	610911	265600	0.47	4.07	0.74	1.66	0.29	0.18	7.06	4.18	4.18	0.71	0.54	0.53
5	BER	Bern/Zollikofen	601929	204409	2.23	3.57	0.98	0.82	2.18	0.36	5.93	1.23	1.23	0.91	0.45	0.46
6	BEZ	Beznau	659808	267693	2.99	2.81	1.03	0.51	0.30	0.47	12.87	0.80	0.80	1.09	0.21	0.33
7	BUF	Buffalora	816494	170225	9.77	*	4.33	0.66	0.31	1.79	8.96	0.29	0.29	0.76	0.35	0.74
8	BUS	Buchs/Aarau	648389	248365	4.27	2.53	3.21	0.40	0.23	1.75	8.00	0.42	0.42	0.53	0.38	0.61
9	CDF	La Chaux-de-Fonds	550923	214893	0.73	0.88	2.65	0.46	0.37	2.85	1.86	0.16	0.16	0.44	0.24	0.35
10	CGI	Nyon/Changins	506880	139573	0.45	0.80	7.69	0.75	1.66	3.45	1.91	0.27	0.27	0.22	0.34	1.76
11	CHA	Chasseral	570842	220154	0.31	0.28	3.41	0.77	1.99	0.86	0.51	0.31	0.31	0.47	0.34	2.58
12	CHU	Chur	759471	193157	0.86	0.70	1.57	1.70	3.40	0.97	0.07	0.34	0.34	1.79	3.47	8.04
13	CHZ	Cham	677825	226880	0.95	1.26	2.71	3.57	1.75	0.30	0.20	0.76	0.76	0.82	4.43	12.63

14	CIM	Cimetta	704433	117452	0.67	2.07	0.74	3.25	0.50	0.19	0.18	1.14	1.14	0.59	1.93	2.88
15	COM	Acquarossa/ Comprovasco	714998	146440	0.45	0.99	0.56	2.57	0.36	0.10	0.45	1.35	1.35	1.61	1.93	1.02
16	COV	Piz Corvatsch	783146	143519	*	*	*	*	0.34	0.23	1.51	2.69	2.69	3.74	*	*
17	DAV	Davos	783514	187457	0.55	0.70	0.59	1.81	0.38	0.21	2.88	0.98	0.98	6.56	1.13	0.97
18	DIS	Disentis/Sedrun	708188	173789	1.23	2.82	1.15	1.17	0.23	0.43	4.69	0.50	0.50	5.22	0.61	0.78
19	DOL	La Dôle	497061	142362	0.81	1.38	0.50	0.37	0.18	0.91	2.68	0.22	0.22	1.73	0.22	0.17
20	ENG	Engelberg	674156	186097	3.73	3.77	0.15	0.38	0.20	1.14	0.73	0.18	0.18	1.84	0.30	0.21
21	EVO	Evolène / Villa	605415	106740	4.02	10.41	0.58	1.49	0.50	4.59	0.56	0.62	0.62	4.87	0.34	0.69
22	FAH	Fahy	562458	252676	1.69	2.27	0.13	0.06	0.39	2.76	0.38	0.39	0.39	0.73	1.57	0.51
23	FRE	Bullet / La Fraz	534221	188081	0.42	0.64	0.62	1.39	1.41	0.39	0.29	1.14	1.14	0.33	0.27	1.05
24	GEN	Monte Generoso	722250	87300	0.65	1.64	0.29	1.05	1.38	4.07	0.30	1.65	1.65	0.57	0.33	4.07
25	GLA	Glarus	723752	210567	0.41	0.69	0.11	5.60	1.26	0.19	0.29	2.24	2.24	1.31	1.64	3.76
26	GOE	Goesgen	640417	245937	0.28	0.46	0.74	5.11	1.72	0.20	0.95	7.68	7.68	3.09	3.76	5.79
27	GRH	Grimsel Hospiz	668583	158215	0.13	0.16	0.89	5.18	0.52	0.09	1.93	7.45	7.45	4.90	2.27	1.09
28	GSB	Col du Grand St- Bernard	579200	79720	0.21	0.14	0.65	3.54	0.22	0.10	5.17	9.04	9.04	3.80	1.80	0.21
29	GUE	Guetsch ob Andermatt	690140	167590	0.24	0.26	1.77	9.57	0.27	0.19	6.42	9.65	9.65	10.00	1.35	0.36
30	GUT	Guettingen	738419	273960	1.76	1.18	1.12	4.68	0.22	0.31	7.52	5.04	5.04	10.80	0.81	0.48
31	GVE	Genève-Cointrin	498903	122624	1.76	3.31	0.63	4.77	0.23	1.95	14.23	3.21	3.21	12.09	0.40	1.24
32	HIR	Hinterrhein	733900	153980	14.95	5.78	0.54	0.22	0.40	2.04	6.38	0.32	0.32	1.89	0.13	0.70
33	HOD	Hochtorf	663850	225520	3.29	2.57	0.32	0.22	0.98	2.17	2.80	0.16	0.16	3.02	0.34	2.83
34	HOE	Hörnli	713515	247755	2.09	1.25	0.14	0.35	1.51	2.27	2.38	0.08	0.08	0.82	0.16	2.43
35	INT	Interlaken	633019	169093	0.82	1.23	0.27	0.53	1.85	0.83	0.55	0.35	0.35	0.11	0.43	2.46

36	JON	Jona	706760	231280	0.86	0.72	0.34	0.28	2.16	0.36	24.96	0.22	0.22	0.23	0.57	0.75
37	KAP	Kappelen	588926	213323	0.58	0.53	0.48	1.08	5.18	0.24	1.25	0.51	0.51	1.43	3.96	0.40
38	KLO	Zuerich/Kloten	682706	259337	0.39	0.51	1.62	3.04	3.31	0.17	0.47	1.78	1.78	0.17	5.34	0.22
39	KRD	Krauchtal Dietersweg	611299	206530	0.18	1.80	1.07	5.52	1.59	0.23	1.31	1.61	1.61	0.20	3.96	0.44
40	KRL	Krauchtal Lindenberg	609041	205426	0.74	0.76	1.47	3.09	2.06	0.18	0.95	1.65	1.65	0.74	2.93	0.27
41	LAT	Langenthal	626820	231515	0.97	1.04	1.64	1.67	0.57	0.35	1.53	0.74	0.74	1.69	0.92	0.65
42	LAU	Langnau	640360	231200	2.43	2.52	1.25	0.69	0.20	0.57	2.55	0.43	0.43	1.00	0.84	0.49
43	LEI	Leibstadt	656378	272111	2.14	1.12	0.80	0.71	0.15	1.95	3.33	0.33	0.33	0.63	0.33	1.10
44	LUG	Lugano	717873	95884	3.92	3.01	1.33	0.40	0.20	1.26	0.35	0.17	0.17	0.46	0.11	3.72
45	LUZ	Luzern	665540	209848	3.22	4.60	0.40	0.27	0.33	2.38	0.57	0.08	0.08	0.79	0.58	2.69
46	MAG	Magadino/ Cadenazzo	715475	113162	2.13	1.85	0.62	0.13	0.96	2.06	1.39	0.13	0.13	0.14	0.17	3.42
47	MAH	Method	534870	178070	0.17	0.82	1.38	0.85	5.63	2.16	40.98	0.99	0.99	0.10	0.52	0.68
48	MTO	Moechaltofen	696925	240800	0.37	0.83	0.70	0.58	2.24	0.46	0.18	0.77	0.77	0.11	0.52	0.90
49	MUB	Mueleberg	587788	202478	0.33	0.72	0.83	1.14	2.00	0.35	0.17	1.87	1.87	0.22	2.88	0.46
50	MVE	Montana	601706	127482	0.23	0.15	3.22	2.72	1.04	0.23	0.51	3.86	3.86	0.71	3.22	0.34
51	NAP	Napf	638132	206078	0.21	0.29	1.78	1.84	0.22	0.20	0.31	2.05	2.05	1.59	2.92	0.20
52	NEU	Neuchâtel	563150	205600	0.47	0.38	4.67	2.57	0.41	0.19	1.40	0.73	0.73	3.73	5.57	0.13
53	OTL	Locarno/Monti	704160	114350	1.03	0.46	3.65	0.40	0.08	0.17	1.09	0.14	0.14	1.98	0.62	0.36
54	PAY	Payerne	562127	184612	3.40	0.85	4.35	0.67	0.94	0.47	2.27	0.16	0.16	2.28	1.15	0.52
55	PIL	Pilatus	661910	203410	1.24	*	0.78	0.12	0.25	0.50	1.38	0.36	0.36	1.03	0.23	0.80
56	PIO	Piotta	695888	152261	3.48	1.59	1.18	0.28	0.38	1.46	1.28	0.31	0.31	0.21	0.28	3.06
57	PLF	Plaffeien	586808	177400	5.09	2.76	1.23	0.12	0.88	1.44	0.44	0.27	0.27	0.20	0.56	6.57

58	PSI	PSI Wuerenlingen	659540	265600	2.41	1.73	0.18	1.31	1.26	2.87	0.31	0.64	0.64	0.16	0.54	2.02
59	PUY	Pully	540811	151514	0.96	1.98	0.43	0.38	2.51	0.89	0.27	0.86	0.86	0.23	0.72	0.72
60	REH	Zuerich/Affoltern	681428	253545	0.96	0.58	0.41	0.29	3.79	0.80	0.18	1.67	1.67	0.30	0.96	0.79
61	ROB	Poschiavo/Robbia	801850	136180	0.48	1.87	0.76	1.34	3.79	0.18	0.14	2.30	2.30	0.28	0.75	0.29
62	ROE	Robiì	682587	144091	0.17	*	0.85	0.28	1.16	0.09	0.15	2.32	2.32	0.13	0.26	0.11
63	ROO	Root	672060	218910	0.83	0.40	2.60	0.92	0.37	0.30	0.24	1.26	1.26	1.09	1.61	0.51
64	RUE	Ruenenberg	633246	253845	0.84	3.22	6.02	1.50	0.21	0.19	0.72	3.65	3.65	3.44	5.43	0.47
65	SAE	Saentis	744200	234920	*	*	0.85	0.35	0.21	0.17	0.77	0.39	0.39	1.12	0.45	0.13
66	SAM	Samedan	787210	155700	1.25	0.49	4.79	1.84	0.37	0.47	2.58	1.77	1.77	1.94	0.77	1.05
67	SBE	S. Bernardino	734112	147296	0.76	0.31	0.58	0.21	0.18	0.81	0.97	0.19	0.19	0.38	0.53	1.15
68	SBO	Stabio	716034	77964	2.53	0.52	0.63	0.28	0.18	1.54	0.87	0.20	0.20	0.28	0.42	2.43
69	SCU	Scuol	817135	186393	6.18	3.08	1.00	0.18	0.59	5.00	0.62	0.28	0.28	0.41	0.14	6.14
70	SEM	Sempach	656880	219360	1.79	5.53	0.11	0.75	1.08	2.51	0.21	0.22	0.22	0.31	0.26	6.83
71	SHA	Schaffhausen	688698	282796	1.01	4.01	0.32	1.13	2.54	0.62	0.41	0.51	0.51	0.35	0.19	2.28
72	SHE	Schoefheim	644500	200940	0.56	2.67	0.14	1.31	1.93	0.45	0.14	1.17	1.17	0.23	0.19	1.00
73	SIO	Sion	591630	118575	0.96	3.58	0.46	2.67	4.33	0.47	0.68	5.33	5.33	1.73	0.72	0.50
74	SMA	Zuerich/Fluntern	685117	248061	0.64	0.64	0.60	1.70	0.97	0.25	0.27	2.77	2.77	0.60	2.22	0.46
75	STG	St. Gallen	747861	254586	0.18	2.91	0.54	2.97	0.33	0.25	0.14	2.61	2.61	2.24	2.87	0.06
76	SUR	Sursee	649930	225040	0.18	0.24	1.17	2.27	0.35	0.34	0.36	1.22	1.22	4.36	2.95	3.71
77	TAE	Aadorf/Toenikon	710514	259821	0.27	0.11	0.60	1.52	0.39	0.28	0.48	0.75	0.75	8.88	1.35	0.22
78	ULR	Ulrichen	666740	150760	0.69	0.06	1.84	1.40	0.12	0.33	0.80	0.38	0.38	4.17	0.23	0.75
79	VAD	Vaduz	757718	221696	1.16	1.88	0.51	2.38	0.13	0.74	0.47	0.30	0.30	1.67	0.39	1.19

80	VIS	Visp	631149	128020	2.21	3.39	1.01	3.26	0.66	1.61	1.14	0.75	0.75	0.85	0.27	0.74
81	WAE	Waedenswil	693849	230708	1.15	8.03	0.20	0.05	0.33	1.35	0.17	0.15	0.15	0.55	0.21	0.43
82	WEE	Weesen	724969	221377	0.98	13.71	0.18	0.69	1.11	0.67	0.15	0.21	0.21	0.36	0.18	0.52
83	WFJ	Weissfluhjoch	780615	189635	*	*	*	0.58	3.81	0.46	0.25	0.18	0.18	0.22	0.26	*
84	WIL	Will	722100	256700	0.85	9.50	0.19	0.30	3.69	0.44	0.16	0.67	0.67	0.63	0.60	0.41
85	WSA	Wilisau	642650	220780	1.17	15.09	0.25	0.89	3.16	0.35	0.75	1.14	1.14	0.41	0.79	0.51
86	WYN	Wynau	626400	233850	0.32	9.33	0.56	1.19	1.98	0.42	0.31	1.67	1.67	0.19	0.31	0.77
87	ZER	Zermatt	624350	97566	0.84	9.64	4.80	3.14	0.80	0.37	1.02	1.52	1.52	1.11	1.78	0.85

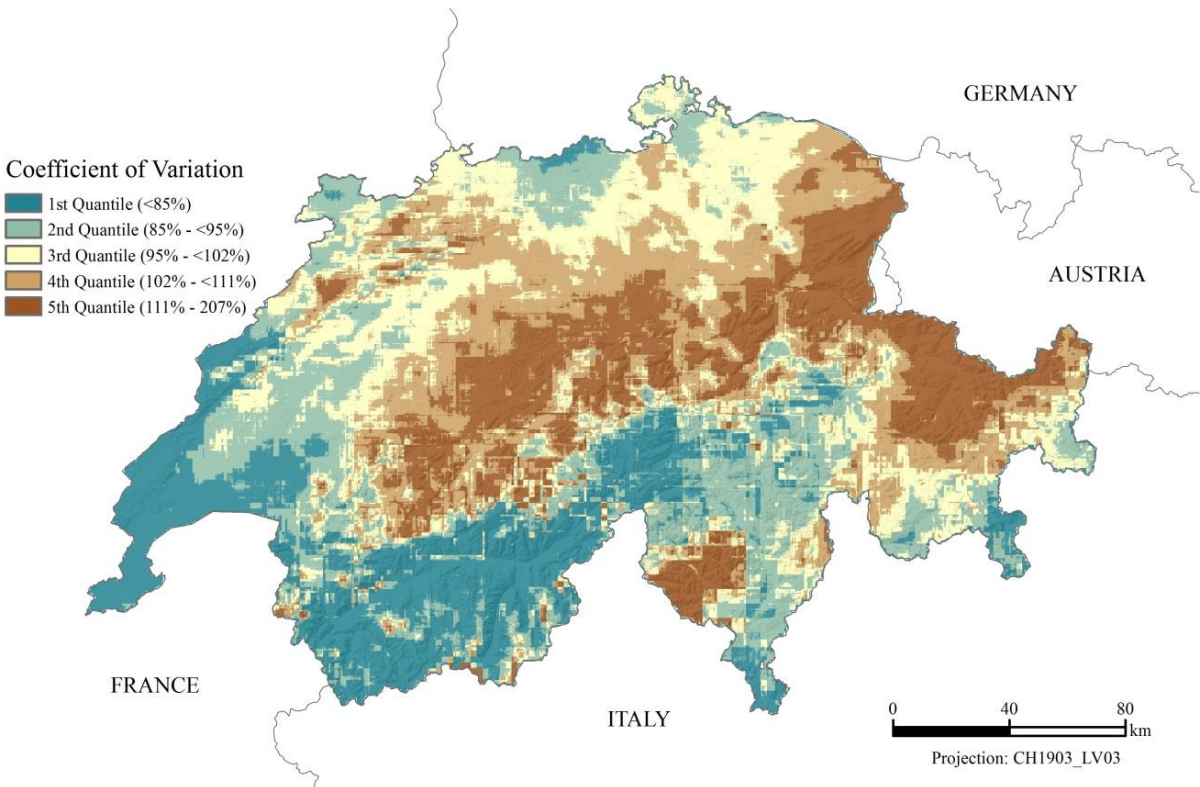


Fig. S3.1. Coefficient of Variation map for Switzerland showing the variability of monthly rainfall erosivity among a year.

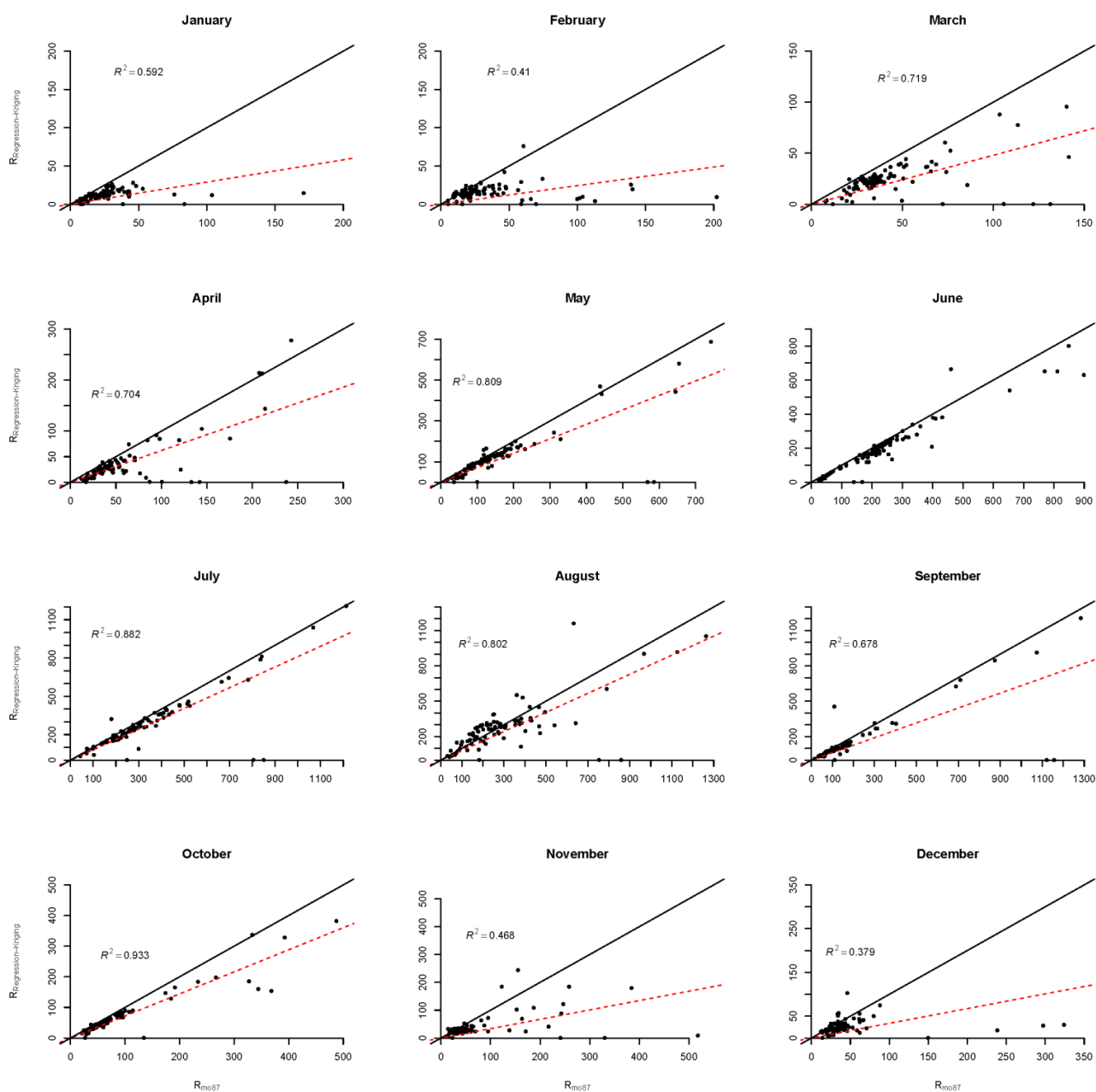


Fig. S3.2. Relationships of the R-factors ($\text{MJ mm ha}^{-1} \text{h}^{-1} \text{month}^{-1}$) at the 87 stations (extracted from the 10-minutes data; R_{87}) and the interpolated R-factors at the 87 stations (extracted after the interpolation with Regression-Kriging; $R_{Regression-Kriging}$). The black line represents the 1:1 line, the red dashed line represents the linear regression line.

Supporting Information to Chapter 4

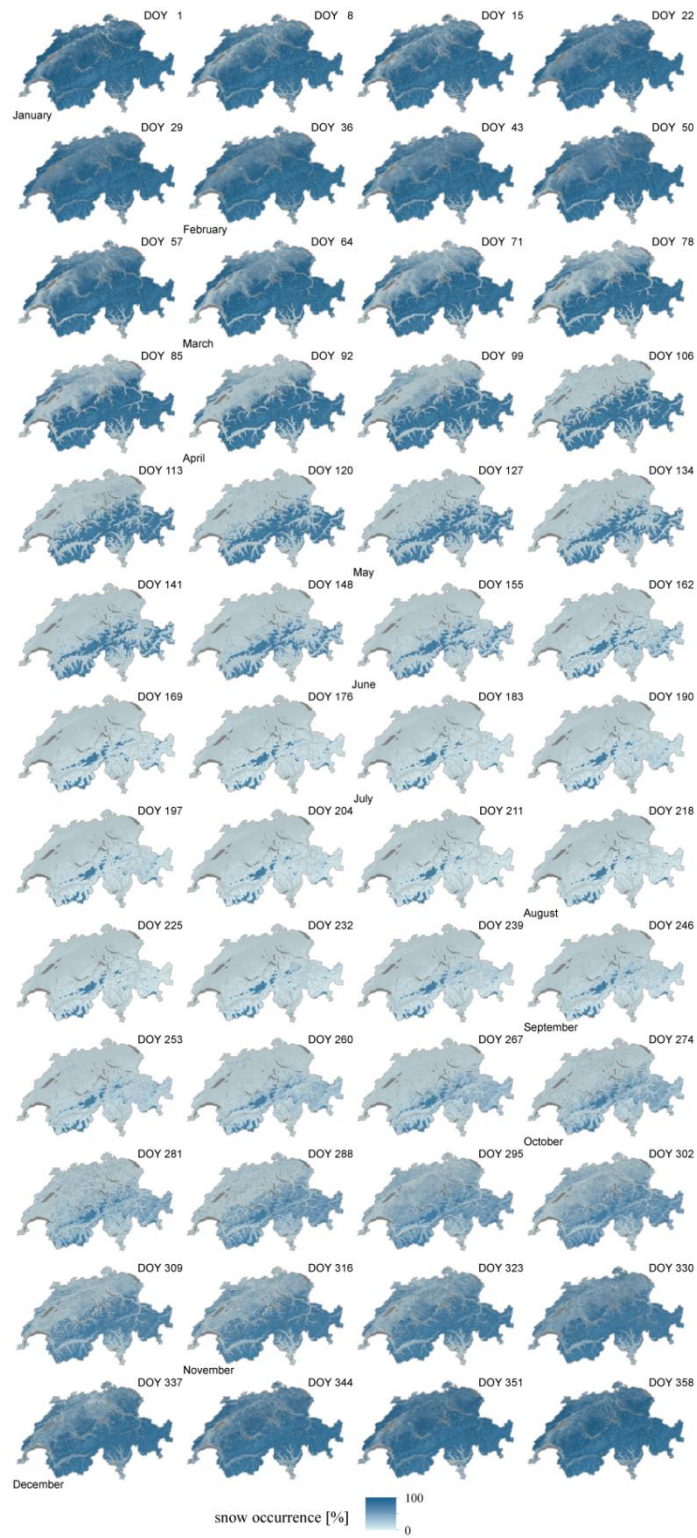


Fig. S4.1: Dynamic long-term snow occurrence for Switzerland (2000 to 2012) derived from the CCI Land Cover (ESA) (spat. res. 500 m)

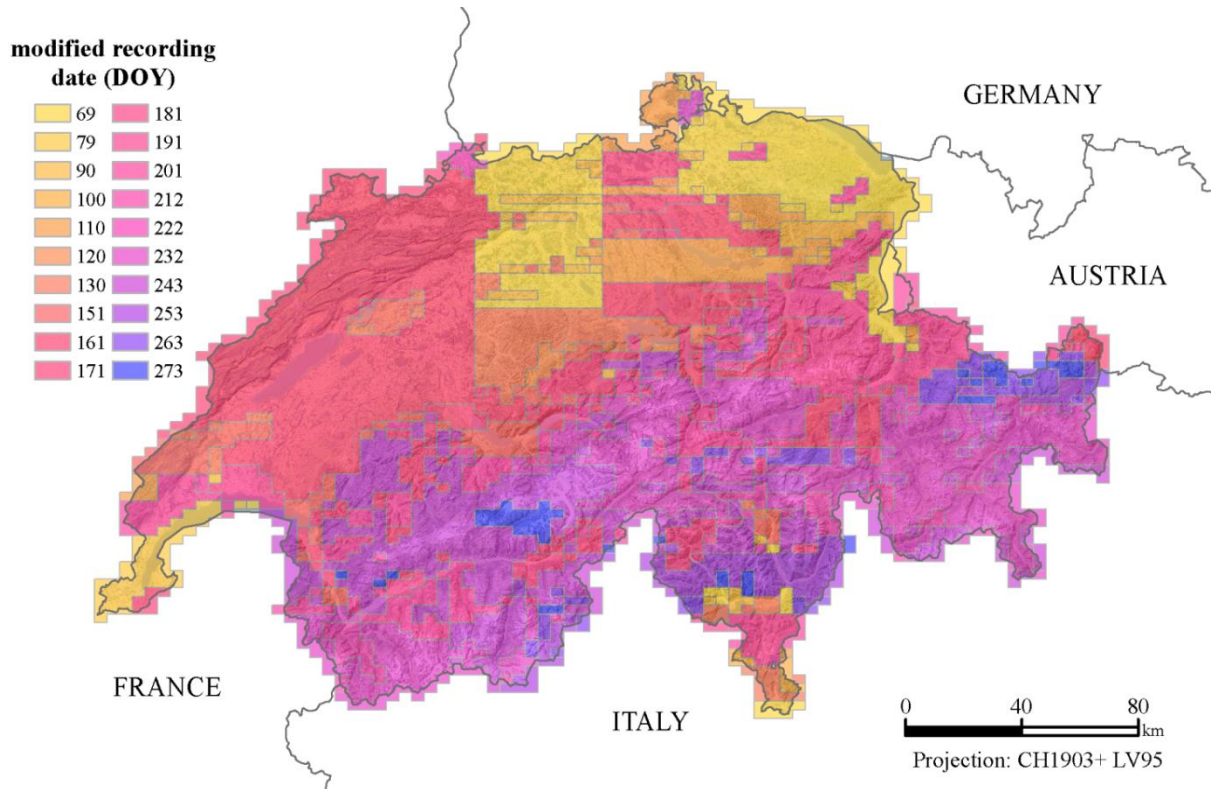


Fig. S4.2: Different recording dates for tiles of the Swissimage FCIR orthophoto product (DOY= day of the year).

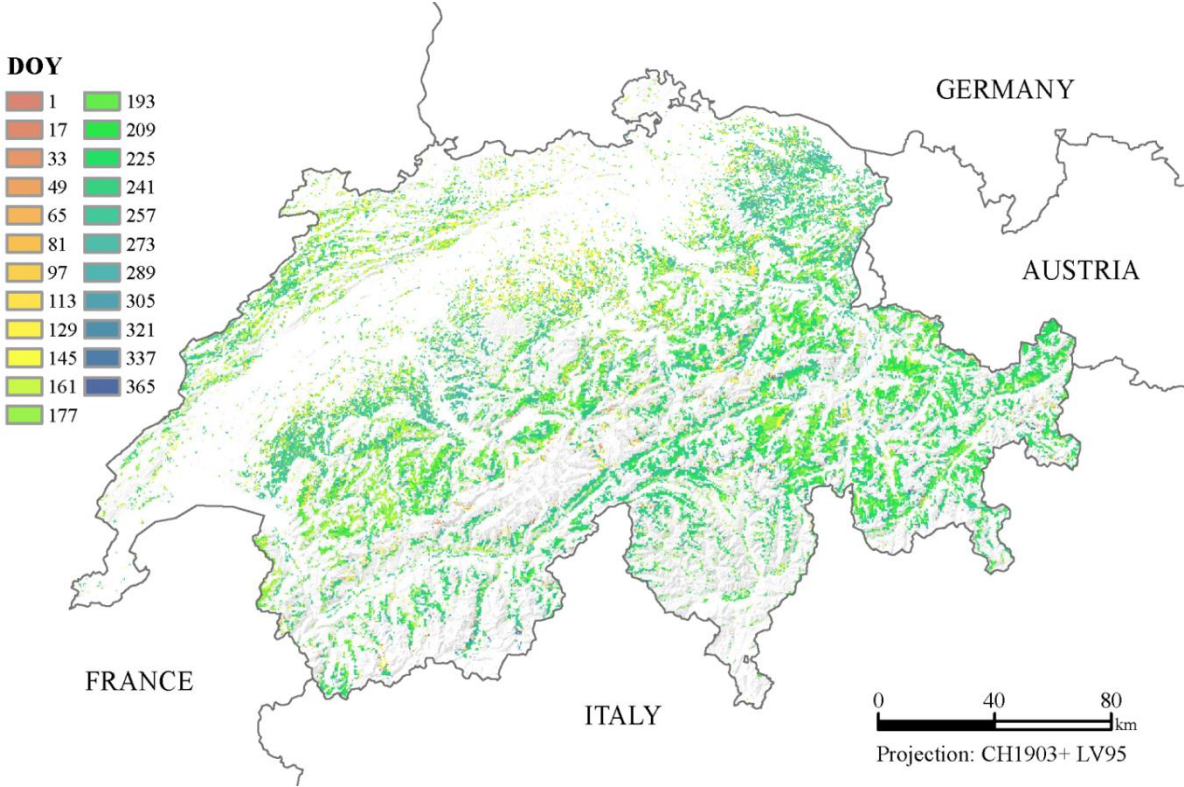


Fig. S4.3: Day of the year (DOY) with the maximum long-term NDVI (2005-2015) derived from MOD13Q1 data



Fig. S4.4: Map of Swiss Cantons without Geneva and Basel-Stadt due to marginal grassland fraction (SwissTopo 2017d)

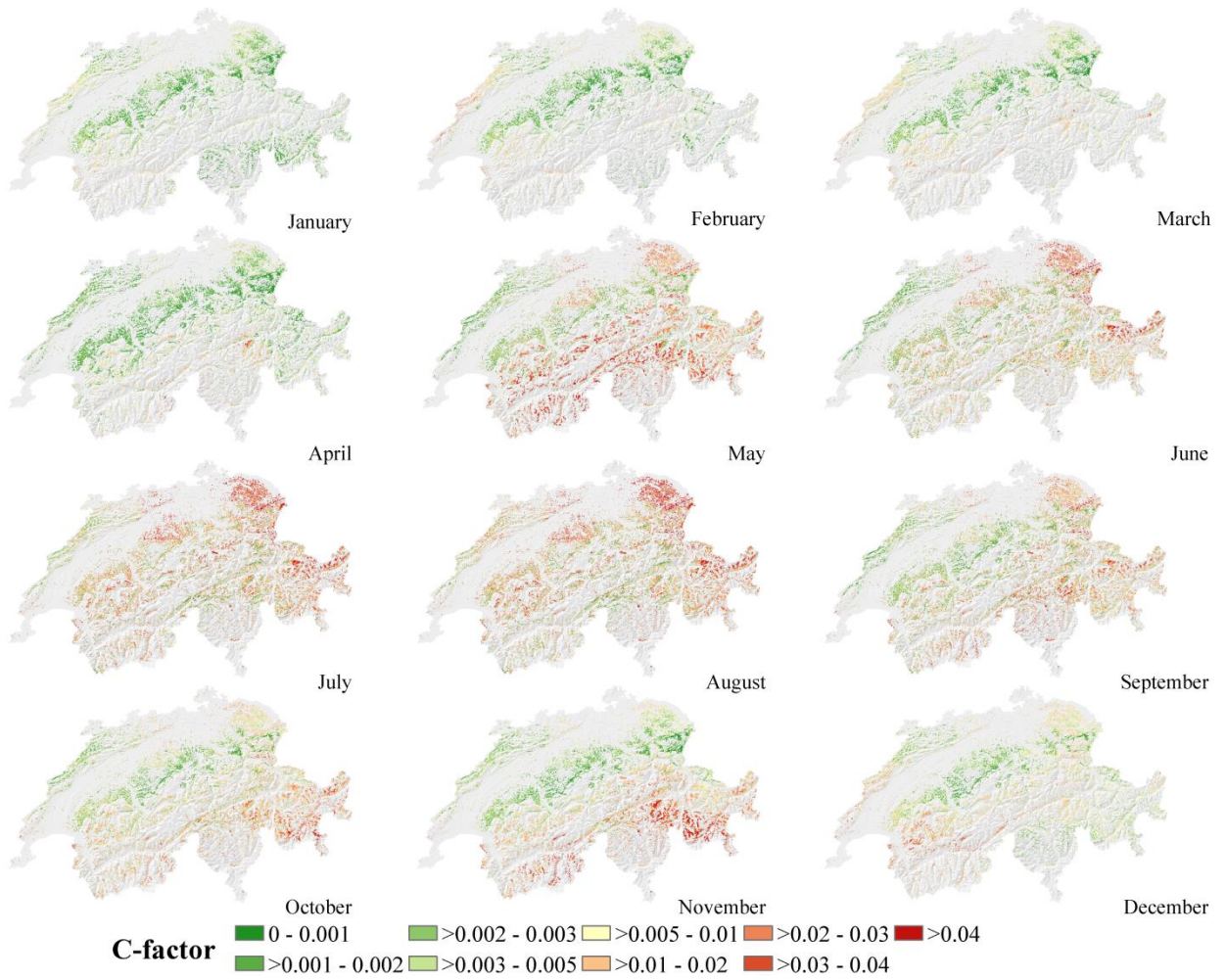
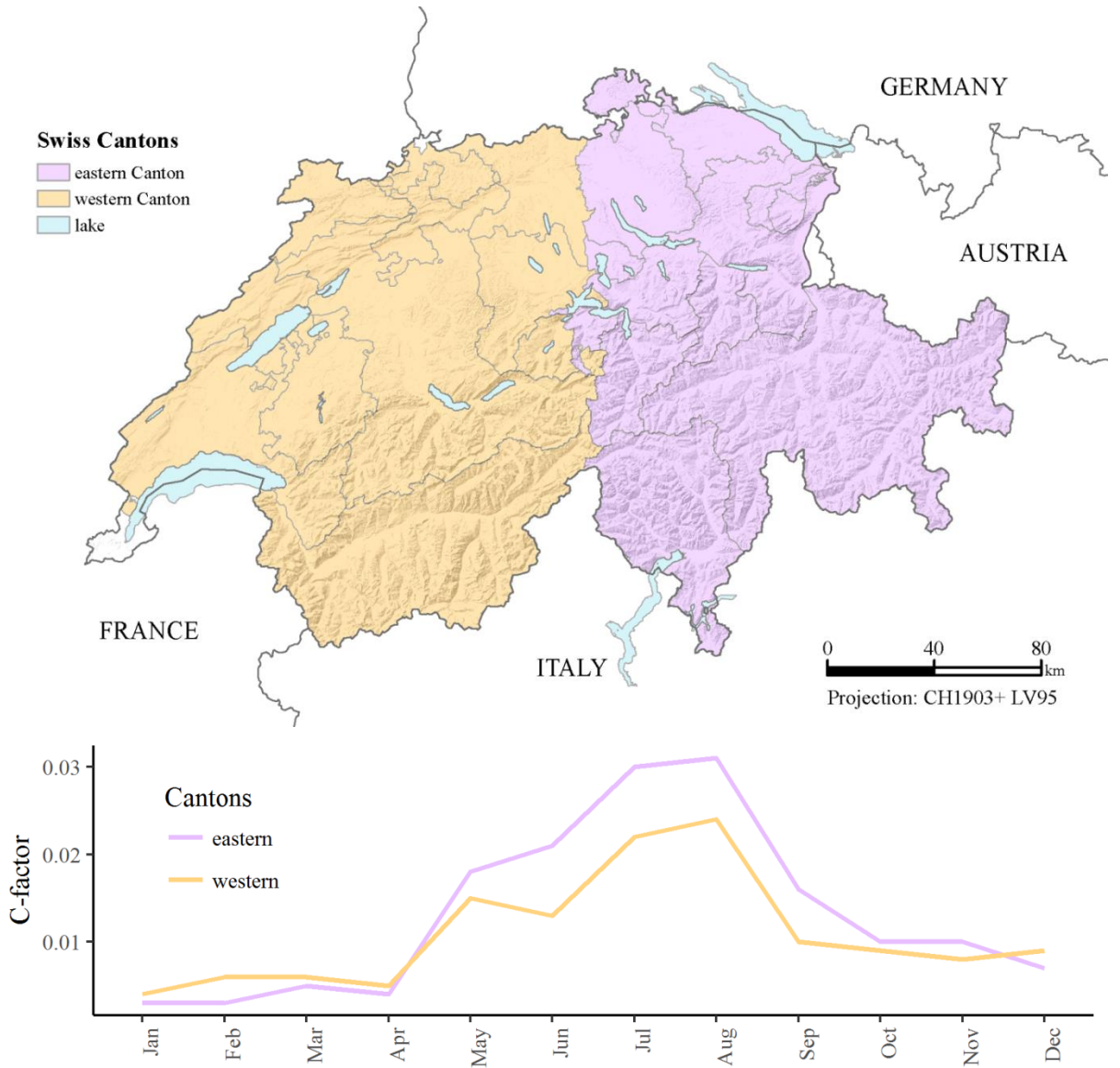


Fig. S4.5: Spatio-temporal variation of C-factors for Swiss grasslands per month (spat. res. 100 m)



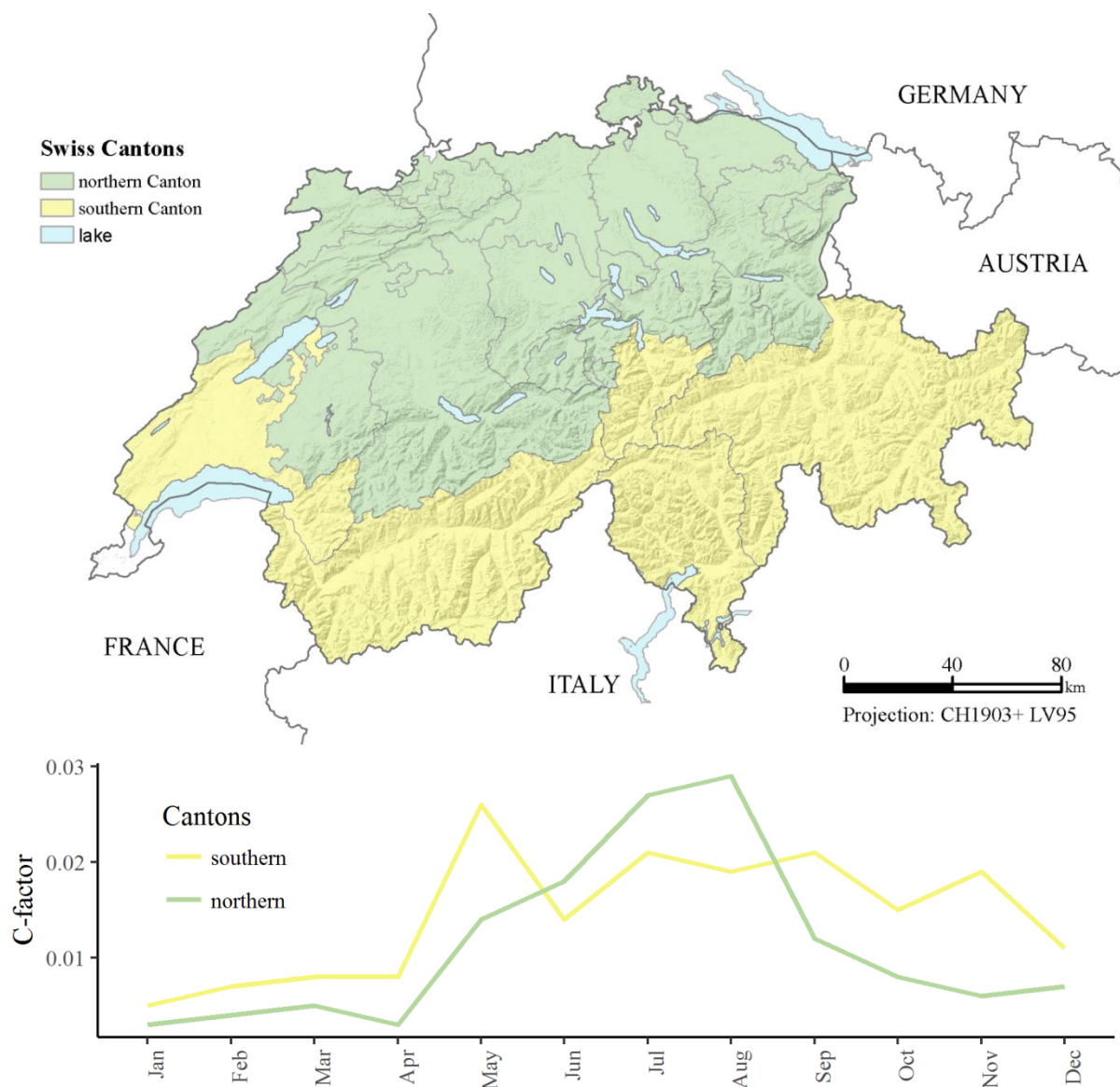


Fig. S4.6: Mean monthly C-factors for Cantons of western/ eastern and northern/ southern Switzerland (Note: cantons Basel-Stadt and Genève are not included due to marginal grassland extent)

Acknowledgments

I would like to express my sincere gratitude to my supervisors Prof. *Christine Alewell* and Dr. *Katrin Meusburger* for supporting me. The way, both guided me over the years was influenced by high professionalism combined with a friendly and respectful working environment. I will always consider you as a role model for a perfect scientist. Both supervisors gave me the opportunity to work together with international erosion experts and present our work at national and international conferences.

Thank you, Dr. *Julian Klaus*, for agreeing to be co-examiner of the thesis and showing your interest in my work.

I'm grateful for the amazing cooperation with the researchers of the Joint Research Centre of the European Commission in Ispra, Italy (*Panos Panagos, Cristiano Ballabio, Oihane Fernández-Ugalde, Alberto Orgiazzi, Emanuele Lugato, and Luca Montanarella*). The international exchange and collaboration widened my point of view and get me acquainted with the work on a political level.

Many credits go to the Federal Office for the Environment FOEN of Switzerland for financing the project. I'd like to thank *Corsin Lang* of the FOEN for supporting me in contract issues, data acquisition, evaluation of our ideas, and promotion of the project.

I honor the collaboration with the researchers, working on the erosion risk map 2 at the Centre of Development and Environment of the University Bern and the Federal Office for Agriculture (*Pascal Bircher, Volker Prasuhn, Hans-Peter Liniger, Hans Hurni, Chinwe Ifejika Speranza and Michael Zimmermann*). Thank you very much for the fruitful discussions.

My thanks go to the whole Environmental Geoscience group of the University Basel (*Axel Birkholz, Judith Kobler, Franz Conen, Daniela Kandl, Jen-How Huang, Sonja Paul, Martin Jiskra, Jan-Paul Krüger, Emiliano Stopelli, Laura Arata, Pranav Hirave, Claudia Mignani, Miriam Gross-Schmölders, Lauren Zweifel, and Lena Wohlgemuth*) but in particular to *Pasquale Borrelli* for the fruitful methodological discussions and *Stefan Osterwalder* for being the best office colleague I ever had. I acknowledge the support by all co-authors and students.

Still, without the support of my past colleagues and supervisors (*Jürgen Böhner, Jan Wehberg, Tomás de Figueiredo, Ulrich Kindermann, Olga Weigl*), I would not be at that point in my career.

Without my parents, this work would not be able for me. Thanks for believing in me all the time.

I like to thank *Sarah* for motivating me and being proud of my work. The present work would not be the same without your encouragement. *Hannah* and *Raya* ensured that I gained the necessary distance to work every day. Thanks for being my beloved daughters.

Curriculum Vitae

Simon Schmidt

Born on 29th of April 1989 in Weissenburg i. Bay., Germany

Address: Eickhorst 3, 29413 Dähre, Germany

Email: simon@simonschmidt.de Web: <http://www.simonschmidt.de>

-
- 2015 - 2019 **DOCTORAL STUDENT**
*Environmental Geosciences at the Department of Environmental Sciences,
University of Basel, Switzerland*
DOCTORAL THESIS: “Soil erosion risk map for Swiss grasslands –
A dynamic approach to model the spatio-temporal patterns of soil loss”
-
- 2011 - 2014 **MASTER OF SCIENCE IN PHYSICAL GEOGRAPHY**
University of Leipzig, Germany
Major in Physical Geography
Minor in Soil Science
M. SC. THESIS: „Entwicklung eines Winderosionsmodells zur potentiellen
Gefährdungsabschätzung des Bodenabtrags auf landwirtschaftlichen
Nutzflächen in Westsachsen“
-
- 2008 - 2011 **BACHELOR OF SCIENCE IN GEOGRAPHY**
University of Hamburg, Germany
Major in Geography
Minor in Soil Science
B. SC. THESIS: “Implikation der Waldkonversion für das
geomorphologische Prozessgefüge – eine GIS-gestützte Analyse der
räumlichen Verbreitung von Bodenerosion in Mato Grosso (Brasilien)“
-
- 1999 - 2008 **ABITUR**
Werner-von-Siemens Gymnasium Weissenburg i. Bay., Germany
-